United States
Environmental Protection
Agency

Office of Air and Radiation
Washington D.C. 20460

EPA 400/1-87/001G
December 1987

EPA

Assessing the Risks of Trace Gases That Can Modify the Stratosphere

Volume VII:
Technical Support Documentation
Atmospheric Science Papers

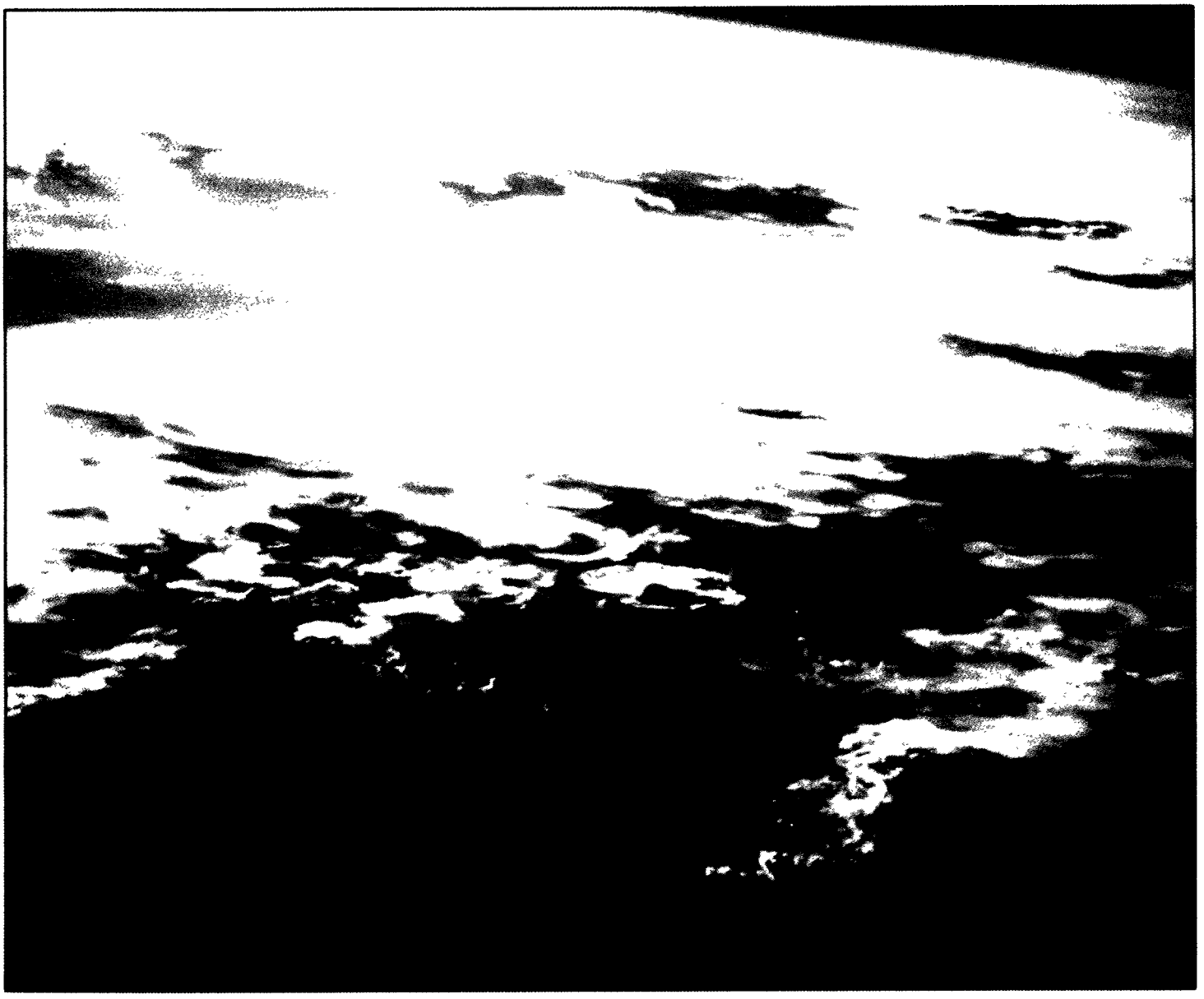

Assessing The Risks of Trace Gases That Can Modify The Stratosphere

Volume VII: Technical Support Documentation Atmospheric Science Papers

Senior Editor and Author: John S. Hoffman

Office of Air and Radiation
U.S. Environmental Protection Agency
Washington, D.C. 20460

December 1987

APPENDIX D

TABLE OF CONTENTS

JOURNAL OF GEOPHYSICAL RESEARCH, VOL. 91, NO. D7, PAGES 7853–7864, JUNE 20, 1986

Sensitivity of an Atmospheric Photochemistry Model to Chlorine Perturbations Including Consideration of Uncertainty Propagation

R. S. STOLARSKI

Atmospheric Chemistry and Dynamics Branch, NASA Goddard Space Flight Center, Greenbelt, Maryland

A. R. DOUGLASS

Applied Research Corporation, Landover, Maryland

Models of stratospheric photochemistry are generally tested by comparing their predictions for the composition of the present atmosphere with measurements of species concentrations. These models are then used to make predictions of the atmospheric sensitivity to perturbations. Here the problem of the sensitivity of such a model to chlorine perturbations ranging from the present influx of chlorine-containing compounds to several times that influx is addressed. The effects of uncertainties in input parameters, including reaction rate coefficients, cross sections, solar fluxes, and boundary conditions, are evaluated using a Monte Carlo method in which the values of the input parameters are randomly selected. Results are probability distributions for present atmospheric concentrations and for calculated perturbations due to chlorine from fluorocarbons. For more than 300 Monte Carlo runs the calculated ozone perturbation for continued emission of fluorocarbons at today's rates had a mean value of -6.2%, with a 1-sigma width of 5.5%. Using the same runs but only allowing the cases in which the calculated present atmosphere values of NO, NO_2, and ClO at 25 km altitude fell within the range of measurements yielded a mean ozone depletion of -3%, with a 1-sigma deviation of 2.2%. The model showed a nonlinear behavior as a function of added fluorocarbons. The mean of the Monte Carlo runs was less nonlinear than the model run using mean values of the input parameters.

1. INTRODUCTION

Stratospheric photochemical models have been used to attempt to predict the effects of changes in the rates at which various chemicals are added to the atmosphere. One problem that has received much attention is the effect on ozone of the addition of fluorocarbons 11 and 12 ($CFCl_3$ and CF_2Cl_2). Since first proposed by *Molina and Rowland* [1974], this effect has been evaluated by examining the response of one-dimensional and two-dimensional models to arbitrary increases in the input of fluorocarbons. Over about the last 7 years these evaluations have been made most frequently by determining the difference between the ozone calculated for an atmosphere without fluorocarbons and the ozone calculated in the steady state which would eventually be reached if fluorocarbon release were continued at the present rate. This present rate has remained relatively constant since about 1977 [*Alexander Grant and Company*, 1985]; however, some recent evaluations have suggested that future increases are probable [e.g., *Quinn et al.*, 1985].

The change in the column amount of ozone predicted by models has varied over the years from a decrease of nearly 20% to a decrease of only about 3% [see, for example, *World Meteorological Organization* (WMO), 1982, National Academy of Science, 1984]. The calculations have varied mainly because of new information on reaction rate coefficients and photodissociation cross sections which are input parameters to such models and, to a lesser extent, because of improvements in the physical and chemical details of the models. The current calculations, using the chemical reaction rate coefficients given by *DeMore et al.* [1985], yield results at the low end of this range; for example, the present model gives 5% depletion. Such relatively small calculated decreases are obtained not because the chlorine catalytic cycle has been found to be slow but because interference reactions of the nitrogen and hydrogen cycles with the chlorine cycle have been found to have greater significance than previously thought.

Recently, *Prather et al.* [1984] have pointed out that the capacity of these models to absorb chlorine without large changes in ozone is limited. When the total chlorine concentration becomes approximately equal to the total odd nitrogen concentration, the interference between these species saturates, and catalytic removal of ozone by chlorine again becomes the dominant effect. In fact, the added chlorine titrates nitric oxide via the reaction of NO with ClO, significantly increasing the efficiency of chlorine catalysis. Models thus show significant nonlinear response to added chlorine. In the present model a 5% decrease in ozone column is obtained for steady state emission of fluorocarbons at present rates, and nearly 50% reduction is obtained for 4 times the present emission rates. This type of effect is implied by the results of *Cicerone et al.* [1983], but their calculations were never carried beyond the present emission rates.

This paper considers the problem of the injection of large amounts of chlorine into a stratospheric photochemistry model. This problem is considered independent of consideration of whether such chlorine concentrations are likely to be reached in the future because the calculations reveal interesting information concerning the structure and limitations of the conceptual model of the stratospheric system. Specifically, the robustness of conclusions concerning the effects of large amounts of chlorine are tested by examining their sensitivity to variations in input data. The sensitivity is examined in two

Paper number 6D0166.
0148-0227/86/006D-0166$05.00

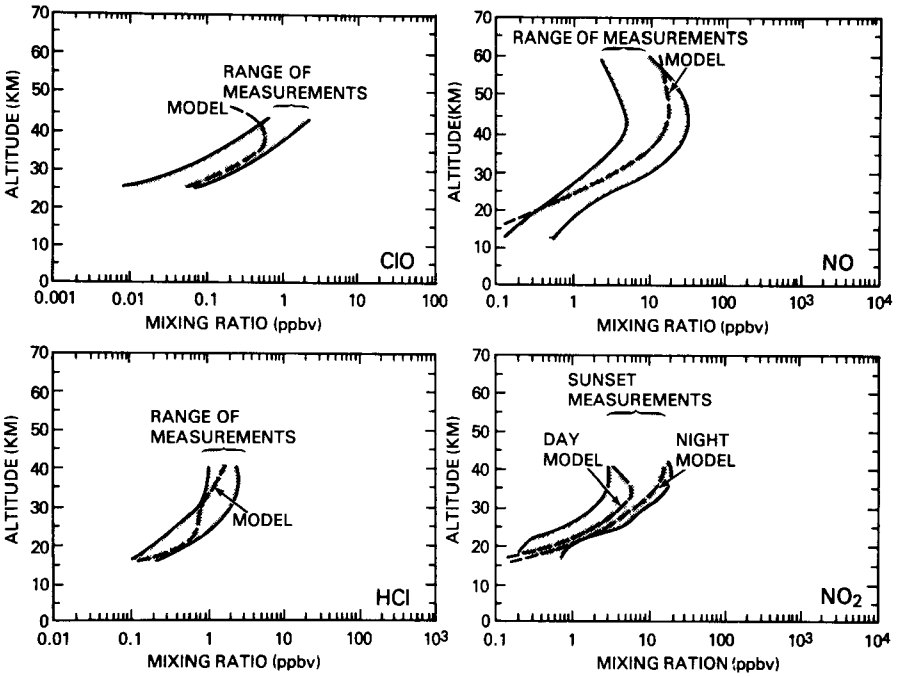

Fig. 1. Comparison of steady state model calculations of the present atmosphere for four species with the range of atmospheric measurements. Total chlorine for the model runs is 2.5 ppbv Total odd nitrogen peaked at 19 ppbv. The shaded areas indicate the range of measurements taken from *WMO* [1982] (Figures 1–96 for ClO, Figures 1–100 for HCl, Figures 1–62 for NO, and Figures 1–71 for NO_2).

ways. The first is to consider extreme values of some of the key rate coefficients which determine the NO_xClO_x interaction. The second is to employ the Monte Carlo method to propagate uncertainties in all of the rate coefficients, cross sections, solar flux values, and boundary conditions through the model calculation.

One-dimensional models have been notably successful in providing a first-order description of the processes governing stratospheric composition. Altitude profiles of the concentrations of species such as O_3, O, Cl, ClO, NO, NO_2, HNO_3, HCl, and OH have been measured and found to be in general agreement with calculations from one-dimensional models. When examined closely, however, a number of areas of disagreement are found. For instance, ozone in the upper stratosphere is consistently lower in the models (both one and two dimensional) than in the actual atmosphere. The upper stratosphere is a region in which these models should be a reasonable representation of stratospheric photochemistry and composition. This paper will reexamine some of these disagreements of models with the atmosphere, including the consideration of photochemical uncertainties. Model comparisons to data in the lower stratosphere will also be examined, along with the implications of these results on ozone perturbation calculations. This is a region in which there are known physical limitations to the one-dimensional model description of the atmosphere. These limitations do not, however, negate the basic photochemical conclusions of the model. It is not practical at present to do a full uncertainty propagation calculation in a multidimensional model. The present calculations will provide a useful guide in the interpretation of multidimensional model comparisons to data.

2. Base Case Calculation Using Current Chemistry

For the following calculations a one-dimensional photochemical steady state model is used. The domain runs from 0 to 60 km in 1.25-km intervals. Vertical transport is represented using a standard diffusive formulation; the diffusion coefficient has a minimum value of 5.4×10^3 cm^2 s^{-1} at 19 km and then increases with altitude to 2.4×10^4 cm^2 s^{-1} at 30 km and 3.3×10^4 cm^2 s^{-1} at 50 km. More than 30 chemical species are considered in the oxygen, nitrogen, hydrogen, and chlorine families as well as the methane oxidation chain. The model transports 15 species or families of species, with the rest assumed to be in photochemical steady state with the transported quantities. Photochemical steady state is achieved in the model by solving the continuity equation for each species or family in sequence, assuming previously calculated values for each of the other species. Iteration is then carried out until convergence is achieved such that the change in species between successive iterations is less than one part per thousand. The original model was described by *Rundel et al.* [1978] and updated by *Stolarski and Douglass* [1985]. Diurnal effects are considered by calculating daytime and nighttime values for diurnally varying species. Relatively simple assumptions are used, such as the instantaneous disappearance of O, $O(^1D)$, NO, OH, HO_2, and Cl at night. Special attention is paid to the conversion of ClO to $ClONO_2$ and NO_2 to N_2O_5 and vice versa through the diurnal cycle.

The rest of this section shows a few results from this basic model in order to demonstrate its behavior. First, the present atmosphere calculations will be examined, followed by consideration of a fluorocarbon perturbation that is constant at today's fluxes. Then the effect of larger amounts of chlorine is considered, and the nitric oxide titration effect is demonstrated. Finally, the effects of increasing nitrous oxide and methane are considered. The impact of uncertainties on these calculations is considered in the following sections.

The model present atmosphere is obtained using boundary conditions designed to give an odd chlorine (Cl_x) mixing ratio of 2.5 parts per billion by volume (ppbv) in the upper stratosphere. The only chlorine-containing source molecules injected

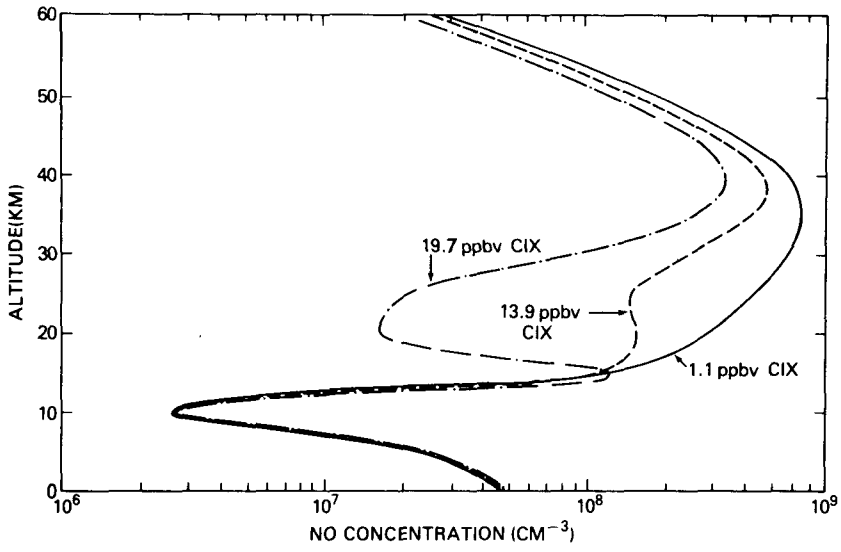

Fig. 2. Calculated NO concentration versus altitude for three values of total chlorine.

into the model are CH_3Cl, CCl_4, and the fluorocarbons 11 and 12 ($CFCl_3$ and CF_2Cl_2). The actual present atmosphere (1985) may contain as much as 3 ppbv of Cl_x. Many of the measurements with which the model will be compared were taken several years ago, however, and correspond to less than 2.5 ppbv of Cl_x. Figure 1 shows a comparison of calculated concentrations of four of the more important species, with the range of data given by *WMO* [1982]. Note that for the four species shown the model gives approximately the same concentrations as measured. A more detailed examination indicates a number of discrepancies. For instance, the model ClO profile is on the high side of the measurements up to about 35 km and then turns over to become smaller than measured values by about 40 km.

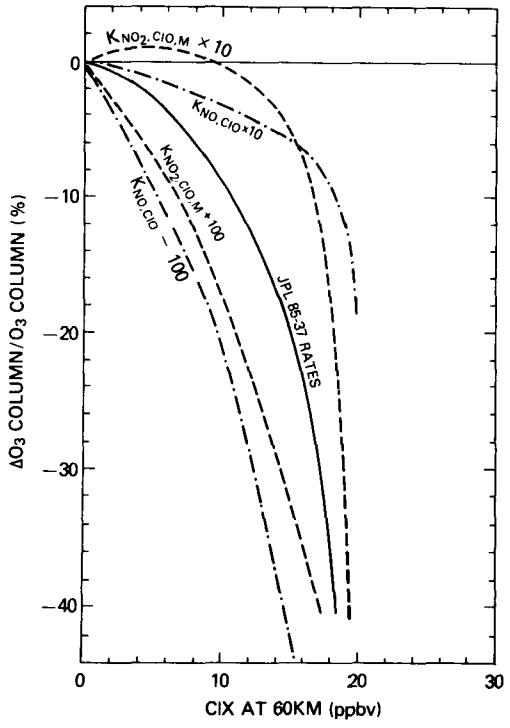

Fig. 3. Calculated ozone change versus total chlorine for arbitrary changes in key interference reactions. JPL 85-37 rates are from *DeMore et al.* [1985].

The HCl calculation lies within the range of measurements. The difference in shape between the calculation and the envelope of measurements should not be considered significant, as the measurements comprising the range show a number of different shapes.

The calculated NO profile is in the middle of the data envelope, except above the stratopause and near the tropopause. Both disagreements are traceable to model assumptions but should not significantly affect the perturbation calculations shown below. In the 50- to 60-km region, virtually all of the odd nitrogen is present as NO. Its concentration is controlled by the balance of transport from the source region below, with local loss following the photolysis of NO and upward transport to the sink region above 60 km. In this model the upward transport process is represented by an upward flux at the upper boundary that is related to the loss expected to take place in the mesosphere Because the odd nitrogen contribution to odd oxygen loss above 50 km is small, differences in the NO concentration here should not significantly affect the ozone balance. Near the tropopause, NO is substantially below measurements, while NO_2 is not. Again, this is a region where odd nitrogen processes make insignificant contributions to odd oxygen loss. In the middle and upper stratosphere, particularly in the altitude region where NO_x loss processes dominate ozone destruction, NO_2 daytime and nighttime calculations are near the middle of the range of measurements.

Many other examples could be considered to demonstrate

TABLE 1. Asymptotic Value of Total Chlorine, Cl_x, as a Function of the Release Rate of Fluorocarbons 11 and 12 in Factors Times the Present Rate

Factor Times Present Fluorocarbon Flux	Asymptotic Cl_x, ppbv
0	1.1
1.0	7.5
1.5	10.4
2.0	13 1
2.5	15.5
3.0	17.4
3.5	20.5

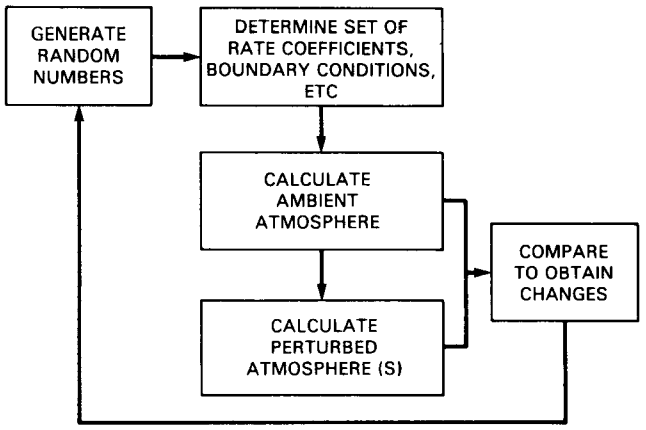

Fig. 4. Logical flow diagram for Monte Carlo calculation.

how this particular one-dimensional model compares with atmospheric data. The overall picture is similar to that produced by other one-dimensional models (see, for example, *Prather et al.* [1984]; *Wuebbles* [1983*a*]), that is, general agreement with measurements but many detailed differences. Comparison of model results with measurements will be considered in more detail below when the Monte Carlo uncertainty propagation results are discussed.

The model has been run for the fluorocarbon perturbation case, that is, comparison of the predicted steady-state atmosphere with today's emissions of fluorocarbons 11 and 12 to the predicted atmosphere with no fluorocarbons. This has been done for the idealized case in which the fluxes of other species, such as CH_4 and N_2O, are held constant. Because of the nonlinear response of the model for higher chlorine concentrations, similar to that shown by *Prather et al.* [1984], these calculations have been extended to consider the effects of constant fluorocarbon fluxes up to 3.5 times the present-day release rate. Even if growth to these levels proves unlikely, these results are instructive concerning the expected behavior of a chlorine-dominated atmosphere and the behavior during the transition to that atmosphere.

As in the work by *Prather et al.* [1984], a nonlinearity in ozone change as a function of chlorine added to the model was found. The calculated ozone depletion in the upper stratosphere was found to be relatively linear, while the lower stratosphere showed extreme nonlinear behavior. The lower stratospheric change is positive for small perturbations due to a near cancellation between the direct chlorine-catalyzed ozone loss and the combination of self-healing (more UV penetration causing increased production) and interference of Cl_x with the NO_x catalytic cycle. As Cl_x increases, the interference with NO_x increases to the point where the titration of NO takes place. This is illustrated in Figure 2, which shows the calculated NO concentration versus altitude for successively larger Cl_x values. At 120 ppbv of Cl_x, which is obtained at 3.5 times the present fluorocarbon flux, a significant bite has been taken out of the NO profile between 20 and 25 km. This occurs because the reaction $ClO + NO \rightarrow NO_2 + Cl$ takes over the conversion of NO to NO_2 and drives the NO to NO_2 ratio to small values. In this region the same reaction is the dominant path for conversion of ClO back to Cl. The catalytic path $ClO + O \rightarrow Cl + O_2$ is only a few percent of the conversion of ClO to Cl. When the titration of NO has occurred, the conversion of ClO to Cl slows down significantly because of the absence of NO. Thus less chlorine is available as Cl atoms for conversion to HCl. However, the rate of removal from the HCl reservoir remains high and is even slightly enhanced by an increase in OH. Thus the HCl reservoir begins to drain, and the chlorine chemistry of this part of the stratosphere becomes dominated by ClO and $ClONO_2$. The resulting increase in the ratio of ClO to Cl_x leads to efficient ozone destruction. When the Cl_x concentration approximately equals the odd nitrogen concentration (which peaks at 18.6 ppbv in this model), the ratio ClO/Cl_x increases dramatically from about 0.01 to 0.07, with a change of only a few ppbv in Cl_x. To demonstrate this dependence on the odd nitrogen level, a second case was run in which the odd nitrogen level was arbitrarily reduced to about 2 ppbv by reducing the N_2O flux into the atmosphere by a factor of 10. In this case, ClO/Cl_x increased rapidly at a much lower Cl_x concentration ($\sim$2 ppbv).

The above explanations suggest that the calculated large ozone changes due to adding 15–20 ppbv of Cl_x may be robust to changes in the chemical rate coefficient data. To test this assertion, runs of the model were made with arbitrary, large changes in the key NO_x-ClO_x interference reactions. Figure 3 shows the calculated column ozone change versus Cl_x for the base case and for cases in which the reaction rate coefficients for $ClO + NO \rightarrow Cl + NO_2$ and $ClO + NO_2 + M \rightarrow ClONO_2 + M$ were separately increased by a factor of 10 and decreased by a factor of 100. Note that decreasing either rate (by an amount that is tantamount to setting it to zero) causes the added chlorine to destroy ozone efficiently, so that a large, linear response is obtained. Increasing either rate causes NO_x-Cl_x coupling to be so efficient that chlorine has little effect on ozone until Cl_x is in the 15-20 ppbv range, and then the interference rapidly saturates and ozone responds strongly to only small amounts of additional chlorine. This result suggests that the conclusion that a large ozone depletion will be observed at 15-20 ppbv Cl_x is robust but is based on varying only one rate at a time. Results shown in section 3, from a Monte Carlo uncertainty propagation in which all rates are varied at the same time, demonstrate the limitations of this conclusion.

Indicated in Table 1 are the fluorocarbon fluxes necessary to obtain the given stratospheric Cl_x amounts for the present chemistry case. Note that as the ozone decreases, each increment of fluorocarbon flux is less efficient at producing Cl_x in the stratosphere. This is due to the increased ultraviolet solar radiation penetration, which leads to decreased fluorocarbon lifetimes and smaller atmospheric concentrations. Thus the effects of fluorocarbon release on stratospheric ozone are, in a sense, self-limiting. Unfortunately, to achieve this self-limitation, the fluorocarbons must reduce the ozone content of the atmosphere by a significant amount.

All of the above model runs have assumed changes in the fluorocarbon fluxes into the atmosphere with all other boundary fluxes held constant. This is certainly not the case in the real atmosphere where a number of other species, including CH_4 [*Blake et al.*, 1982; *Rasmussen and Khalil*, 1984], CO_2 [*Keeling et al.*, 1984], and N_2O [*Weiss*, 1981], are observed to be increasing. Furthermore, several others, including tropospheric O_3 [*Logan*, 1985], CO [*Khalil and Rasmussen*, 1984] and NO_x [*Crutzen and Gidel*, 1983], are strongly suspected to be increasing. Two of these, CH_4 and N_2O, will be considered to illustrate their possible interaction with the calculated chlorine effects. Increases in methane will tend to slow down the chlorine catalytic effects through conversion of active ClO_x to

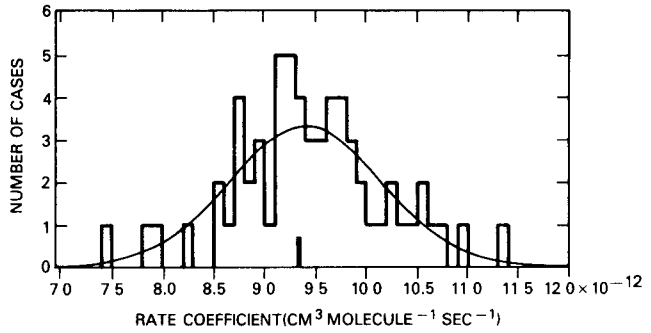

Fig. 5 Histogram of individual data points for the rate coefficient of $O + NO_2 \rightarrow O_2 + NO$. The distribution contains 62 data points with a mean of 9.45×10^{-12} cm^{-3} molecule^{-1} s^{-1} and a standard deviation of 0.74×10^{-12}. The smooth curve is a Gaussian with the above parameters.

the reservoir HCl. Nitrous oxide increases provide more NO_x to interfere with ClO_x catalysis through the $ClO + NO$ and $ClO + NO_2 + M$ reactions.

Because constant fluxes were assumed, as the stratospheric column of ozone begins to be depleted, more ultraviolet radiation penetrates to any given altitude and the loss rates for CH_4, N_2O, and other species are increased. This shortens their atmospheric residence time, resulting in a smaller abundance in steady state for the assumed (constant) flux. For a perturbation calculation with 3.5 times the present fluorocarbon flux, the steady state, ground-level mixing ratio of CH_4 is reduced from 1.6 to 0.82 ppmv and that of N_2O from 300 to 240 ppbv. To test the importance of changes in N_2O and CH_4, a few sensitivity tests were run with differing assumptions concerning changes in the fluxes of CH_4 and N_2O. At a fluorocarbon flux of 3.5 times the present level the CH_4 flux was increased by successively larger factors. At 1.5 times the CH_4 flux the ground-level concentration returned to a value slightly above the ambient 1.6 ppmv, and the ozone depletion was reduced from 40% to 30%. At double the CH_4 flux its concentration in steady state was 3.7 ppmv, and the ozone depletion was further reduced to 23%. If enough CH_4 were added, the recovery in the ozone perturbation would end because ozone depletion due to enhanced HO_x would begin to dominate. Increasing the N_2O flux shows a more dramatic effect. At 1.5 times the present flux the perturbation due to 3.5 times the present flux of fluorocarbons is reduced to 20%. At 2 times the N_2O flux the fluorocarbon perturbation has become 15%, but at higher N_2O fluxes, larger perturbations result due to NO_x effects on ozone.

3 Monte Carlo Calculations

The Monte Carlo method of uncertainty propagation has been used to examine the questions of comparison of calculated atmospheric concentrations with measurements and to determine their relationship to chlorine perturbations. The basic method was described by *Stolarski et al.* [1978]. That study is updated here by using the improved model described in the previous section, by using updated reaction rate and cross-section data, and by consideration of uncertainties both in the preexponential factor of rate coefficients and in the temperature dependence. It is shown that the uncertainty in the calculated ozone depletions may be reduced significantly by requiring that calculated values of key constituents fall within a range of values specified by measurements.

Figure 4 reviews schematically the Monte Carlo technique, as applied to this photochemical model. For calculation with the base case chemistry, reaction rate coefficients, absorption cross sections, solar fluxes, and boundary conditions are input to the model. These are used with the difference formulation of the constituent continuity equations to calculate an ambient atmosphere which approximates conditions previous to any fluorocarbon release. A series of perturbed atmospheres is then calculated for the particular set of changes being tested, in this case, increased levels of fluorocarbon fluxes. The results of each perturbed run are compared to the ambient case. For a Monte Carlo study one additional step is taken. A set of random numbers is generated, one for each input parameter to be varied. The estimated probability distributions are then used with each of these random numbers to pick a new value for each input parameters. These are used in the model to calculate an ambient atmosphere and a series of perturbed atmospheres. Then a new set of random numbers is generated, and a completely new set of input parameters is used in the model. In this way, distributions of calculated concentrations as well as perturbed concentrations and changes are accumulated.

A major advantage of the Monte Carlo method described above over more conventional one-dimensional models is illustrated in Figure 5. Shown is a histogram of all of the individual measurements of the room temperature rate coefficient of the reaction $O + NO_2 \rightarrow O_2 + NO$ by three different groups [*Bemand et al.*, 1974; *Slanger et al.*, 1973, *Davis et al.*, 1973]. These 62 data points form a distribution that is fit well by either a Gaussian or a log-Gaussian distribution with parameters given by *DeMore et al.* [1985]. These are a central value of 9.4×10^{-12} and a one-sigma uncertainty of $\pm 10\%$. Also shown in Figure 5 is a vertical line representing the mean value which is normally used in a photochemical model. This is not a complete representation of the known information on

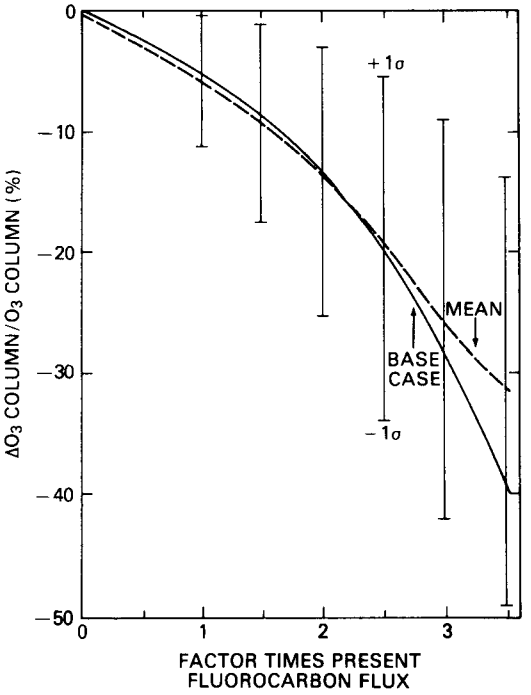

Fig. 6. Monte Carlo results for ozone change versus the factor times the present fluorocarbon fluxes Solid line is the base case, dashed line is the mean of the 329 cases. Vertical bars are the one-sigma uncertainty limits

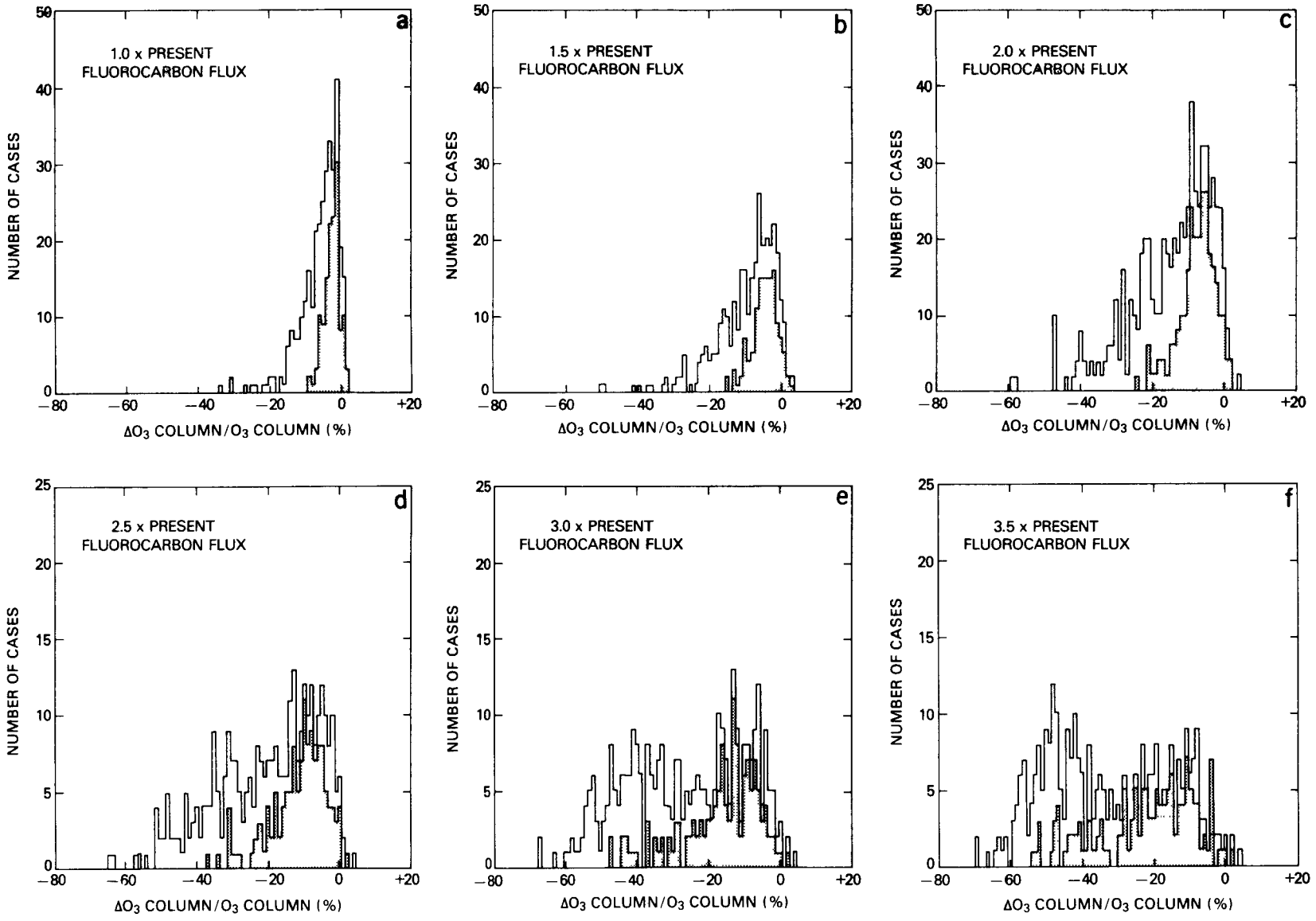

Fig 7. Frequency distributions for the calculated change in the column content of ozone for various values of the fluorocarbon flux. The shaded area shows the cases for which the NO, NO_2, and ClO concentrations all fell within the range of measurements at 25 km.

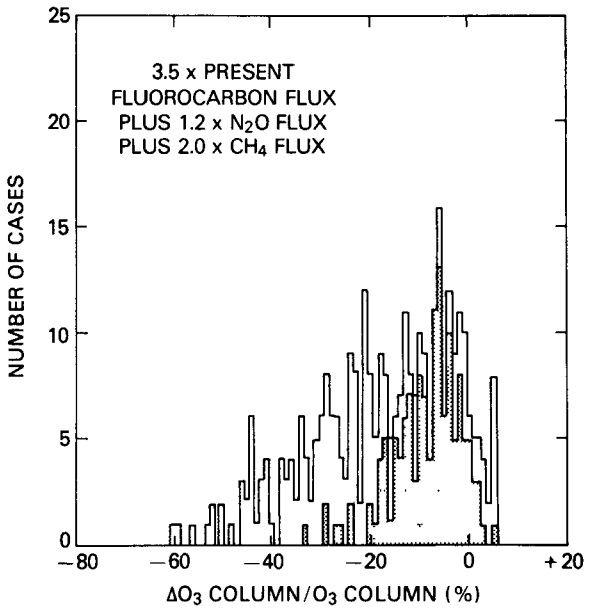

Fig. 8. Frequency distribution for the calculated change in the column content of ozone for 3.5 times the present fluorocarbon flux, 1.2 × N_2O flux, and 2.0 × CH_4 flux. The shaded area shows cases in which NO, NO_2, and ClO concentrations all fall within the range of measurements at 25 km.

this reaction. Using the Monte Carlo method, an approximation to the complete distribution is considered rather than a single value, and results should better reflect the status of knowledge concerning this rate coefficient. Of course, a well-measured reaction was chosen for this illustration. Other reactions have only been measured a few times (or only the mean of the actual runs were reported), and the measurements may disagree with one another by substantial amounts. For these cases it is not obvious how much improvement is obtained by attempting to represent an entire distribution.

The Monte Carlo technique was applied to the model described earlier to generate a total of 329 cases of varied inputs for calculation of the atmosphere without fluorocarbons, with enough fluorocarbons to give a reasonable steady state representation of the present atmosphere, and with the sequence of increasing fluorocarbon perturbations to investigate the model response to large chlorine amounts. Figure 6 shows the calculated change in the column content of ozone compared to the no-fluorocarbons case as a function of the injected fluorocarbon flux shown in units of the present flux of fluorocarbons 11 and 12 (PFF). The solid curve, labeled the base case, gives the result using the mean values for each input parameter. The dashed curve is the mean ozone depletion obtained from the 329 cases. The mean curve is significantly more linear than the base case curve. The mean perturbation calculated for the PFF is −6.2%, as opposed to −5.0% for the base case. At 3.5 times PFF the calculated mean perturbation is −31%, as opposed to −40% for the base case. The vertical ranges shown are the one-sigma variance of the calculated distribution of ozone change, but these are only a general guide to the width of the distributions because they are asymmetric. The distributions of calculated ozone changes are given in Figure 7; the shaded areas indicate the distributions which remain when the calculated concentrations in NO, NO_2, and ClO are required to fall within a range of values specified by measurements. This attempt to limit the uncertainty in the calculated ozone depletions is discussed at the end of this section. For the case of 1.0 times the PFF the cases ranged from an increase of slightly more than 2% to a decrease of 35%. The distribution is skewed, with the most probable value between −2 and −3%. Figures 7*a*–7*f* show the progression of distributions obtained as the fluorocarbon flux was increased. The mean increases as the flux increases, but the positive cases do not entirely disappear, even for the perturbation of 3.5 times the PFF. At 3.5 times PFF the distribution has a bimodal character with one group of cases having ozone changes between about −35 to −60% and with the other group of cases ranging from 0% to about −30%.

As in the previous section, these fluorocarbon flux changes have been made with all other boundary fluxes held constant. To illustrate the effects of uncertainties on increased interference with the chlorine cycle caused by increased CH_4 and N_2O, and the distribution of ozone column depletions at 3.5 PFF with 1.2 times the N_2O flux and 2.0 times the CH_4 flux is given in Figure 8. The mean ozone depletion in this case is smaller than for the 3.5 PFF case in which CH_4 and N_2O fluxes are held fixed, and the bimodal character apparent in Figure 7*f* is not observed.

In an effort to understand these distributions and to reduce the uncertainty in the calculated ozone depletions, comparisons have been made of measurements with calculated concentration distributions for the current atmosphere. The first comparison considers the well-known problem that the calculated ozone concentrations near the stratopause are tens of percent less than measurements (see, for example, *Butler* [1978] or *Solomon et al.* [1983]). In Figure 9 the probability distributions of calculated ozone concentrations at 50, 40, 30, and 20 km are compared to the 1-sigma variability ranges of data given by *Krueger and Minzner* [1976]; the Krueger-Minzner (KM) data are in close agreement with more recent satellite data [*McPeters et al.*, 1984]. Although there are cases which fall within the 1-sigma range of variability of the KM data at each altitude, there are no cases which fall within this range at all four altitudes. This suggests that the problem of disagreement between measured and calculated ozone is not likely to be solved within the ranges of current rates, cross sections, and solar fluxes. This is consistent with the results of *Froideveaux et al.* [1985]. There are only three cases which fall within 2-sigma variability of the KM data at all altitudes, and these cases were examined individually to search for common features. No obvious single variation in production, loss, or species concentration was found. A common characteristic was that all three of these cases resulted in small ozone depletions, less than 2% for 1 times PFF and less than 14% for 3.5 times PFF. A large number of cases were found to fall within 2.5-sigma variability, but these cases correspond to the full range of possible ozone reductions. It is concluded that conformity to the measured KM ozone profile is not a good criterion for reduction of the uncertainty in the calculated range of ozone depletions. This comparison does indicate that the disagreement between the measurements and calculated ozone concentrations at high altitude is with the overall shape of the ozone profile. This problem cannot be resolved by changes that will produce agreement at a single altitude.

Next, consider the comparison of the concentrations of some of the other minor species with measurements. Because local concentrations are more directly comparable to model output than are column abundances, comparisons are made with measurements at single altitudes. Although the physical

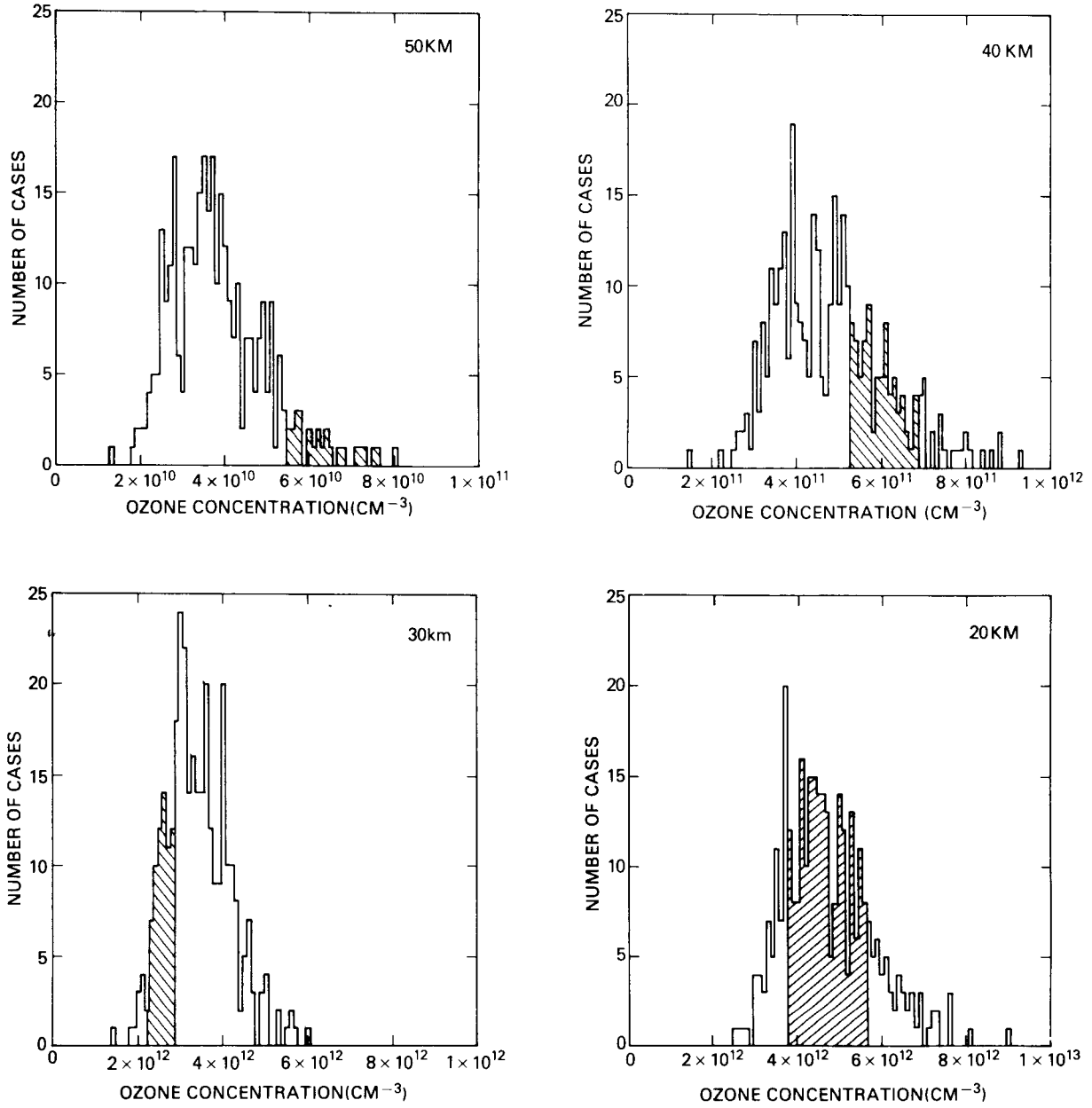

Fig. 9. Frequency distributions for the calculated ozone concentrations at 4 altitudes (*a*) 50 km, (*b*) 40 km, (*c*) 30 km, and (*d*) 20 km The shaded areas indicates the one-sigma variability range, as given in the Krueger-Minzner mid-latitude model which is based on rocket measurements.

representation of the dynamical processes near the ozone concentration peak is poor in one-dimensional models, the calculated ozone column changes are highly correlated with the local ozone changes at these altitudes. This is illustrated by Figure 10, a scatter plot of the local ozone change at 25 km versus the ozone column change for the perturbation caused by the PFF. The high degree of correlation indicates that the chemistry leading to local changes at 25 km should show a high correspondence with the calculated change in the column.

Figure 11 is a scatter plot of the diurnal average NO concentration versus the diurnal average NO_2 concentration, both at 25 km. Also shown are several lines of constant ratio of NO_2 to NO. There is a tendency for the cases to cluster about a ratio of approximately 4. This is an indication that many of the input parameters that are varied in the calculation tend to preserve the NO_2–NO ratio. There is also a spread about this ratio ranging from about 2 to 10, indicating that other input parameters tend to drive NO_2/NO from the mean ratio when they are varied. Also shown in Figure 11 are pairs of horizontal and vertical solid lines. These indicate the range of measurements as taken from *WMO* [1982]. These measurements have been adjusted to correspond approximately to diurnal average values for comparison to model results. The majority of the Monte Carlo cases fall within the box formed by the intersection of these lines. A number of cases fall outside the range of NO_2 measurements, some fall outside the range of NO measurements, and a few fall outside the range of both measurements.

The behavior of the ambient atmosphere concentrations resulting from the random input parameter variations is illustrated further in Figure 12, which is a scatter plot of the diurnal average NO concentration versus the diurnal average ClO concentration, both at 25 km. Again the points tend to lie

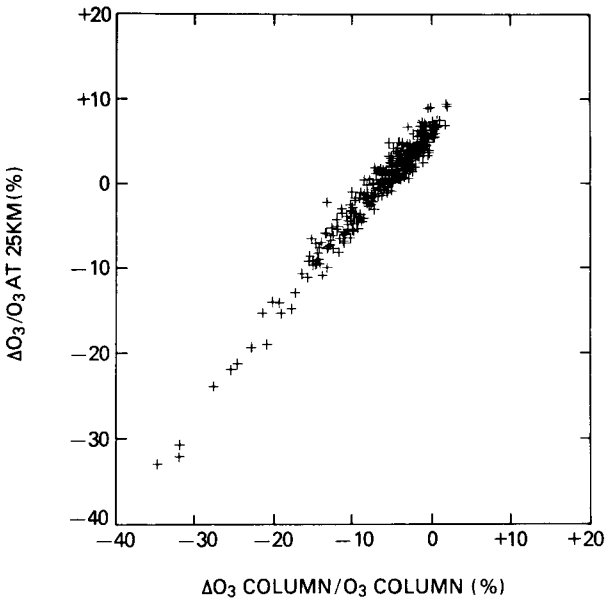

Fig. 10. Scatter plot of the change in the local ozone concentration at 25 km versus the change in the ozone column content; both changes are for a calculated perturbation due to addition of fluorocarbons at the present rate

along a line, this time the line of constant product NO $\times$ ClO = 1×10^{16} cm^{-6}. The solid lines are the range of measurements from *WMO* [1982]. The range for ClO is taken from measurements by Anderson and coworkers [*Weinstock et al.*, 1981], but the two largest measurements are eliminated from the range as they are many sigma from the mean. The range of measurements falls on the low side of the Monte Carlo cases. This was illustrated earlier in Figure 1, which compared the same measurements to the base case. Figure 13 shows the same type of scatter plot for HNO_3 versus NO.

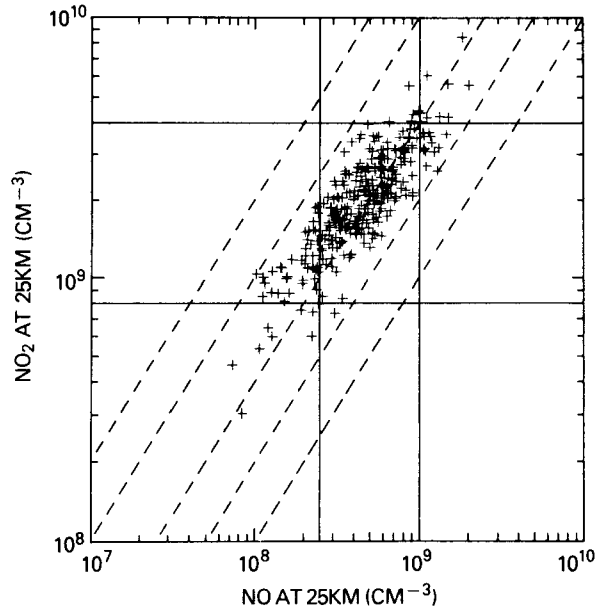

Fig 11. Scatter plot of the calculated ambient NO_2 concentration versus the calculated NO concentration, both diurnally averaged at 25 km. The dashed lines indicate the range of measurements for both species, as given by *WMO* [1982] The solid lines indicate constant values for the ratio NO_2/NO. Base case concentrations are NO_2 = 2.0×10^9 cm^{-3} and NO = 4.5×10^8 cm^{-3}

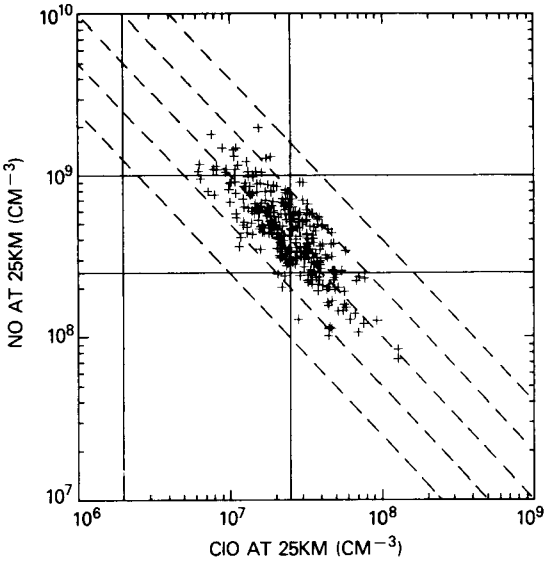

Fig. 12. Same as Figure 11 for NO versus ClO The solid lines indicate constant values for the product NO times ClO. Base case concentrations are NO = 4.5×10^8 cm^{-3} and ClO = 2.5×10^7 cm^{-3}.

Again, the data encompass the majority of the points as for NO versus NO_2. Figure 13 combined with Figure 11 demonstrates that in spite of the poor representation of the actual physical processes that control total odd nitrogen in the lower stratosphere, the individual odd nitrogen species concentrations are generally in good agreement with measurements. Even though the total odd nitrogen at 25 km agrees with measurements for the wrong reason (that is, vertical diffusion is not really the dominant transport mechanism), the above results demonstrate that the chemistry done with the odd nitrogen that is there conforms to atmospheric measurements within reasonable uncertainty.

The calculated ozone depletion due to increased emissions of fluorocarbons depends upon the calculated ambient concentrations of some species. Figure 14 is a scatter plot of the calculated ozone depletion for the present fluorocarbon flux case versus the calculated diurnal average NO concentration at 25 km for the present atmosphere. The crescent shape of the

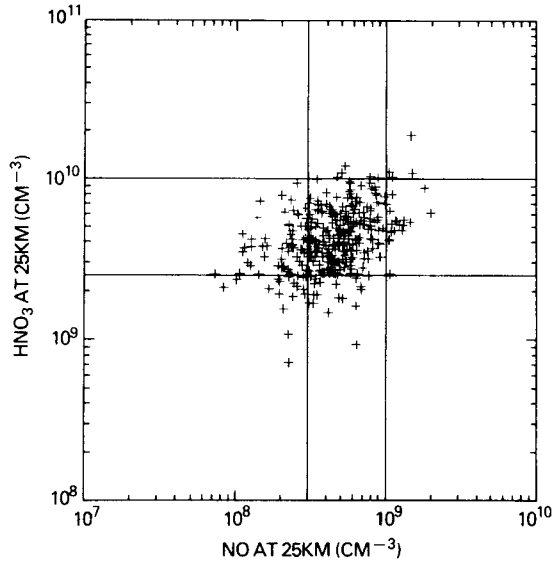

Fig 13 Same as Figure 11 for HNO_3 versus NO. Base case concentrations are HNO_3 = 4.4×10^9 cm^{-3} and NO = 4.5×10^8 cm^{-3}

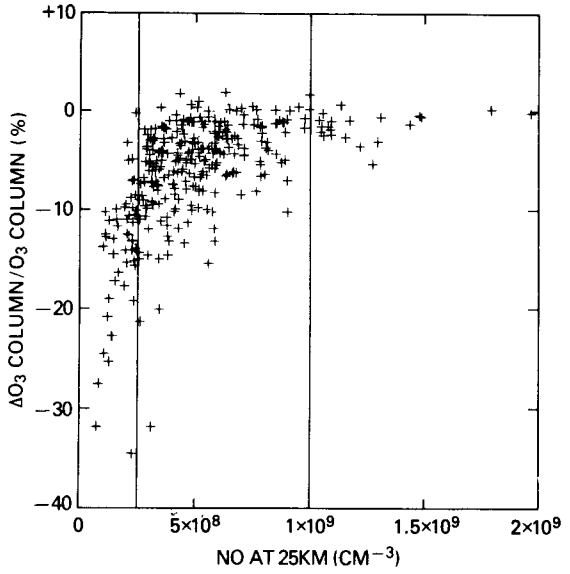

Fig. 14. Scatter plot of the calculated change in the ozone column for an injection of fluorocarbon at the present rate versus the calculated diurnal average concentration of NO at 25 km in the ambient atmosphere. The dashed lines indicate the range of measurements for NO, as given by *WMO* [1982]. Base case concentration for NO is 4.5×10^8 cm^{-3}.

distribution of points is typical of all the scatter plots of ozone change versus concentration of species in the nitrogen family. At low NO values a wide range of ozone changes is calculated, while at high NO values small ozone changes are always obtained. The solid lines, the range of measurements as before, indicate that both the lowest and highest NO concentrations are unacceptable. This removes a number of cases with small ozone depletion and most of the largest ozone depletion cases. Figure 15 shows the same type of plot for ClO. The correlation is quite high, with a correlation coefficient of −0.87. Because the model predictions of ClO tend to be on the high side of the measurements, the cases selected by agreement with ClO observations strongly favor the smaller ozone depletions. Because of the relationship between ClO and NO, about one-

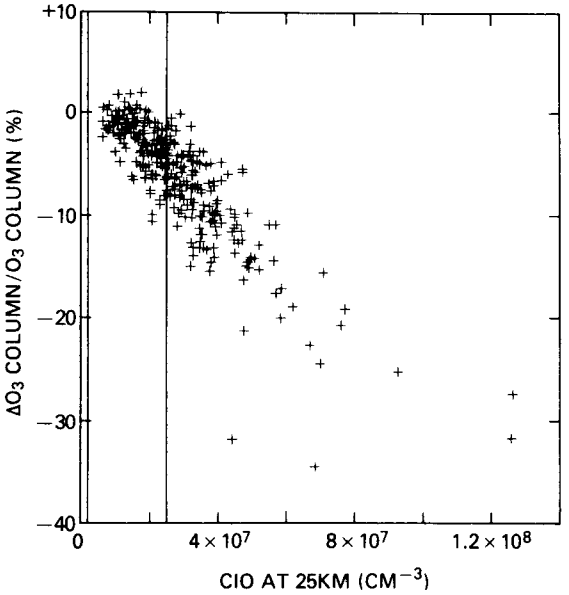

Fig. 15. Same as Figure 14 for ClO. Base case concentration for ClO is 2.5×10^7 cm^{-3}.

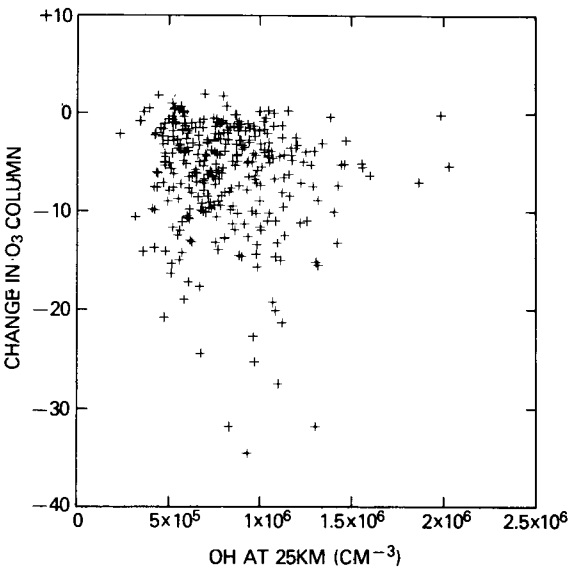

Fig. 16. Same as Figure 14 for OH. Base case concentration for OH is 7.6×10^5 cm^{-3}.

third of the cases in which ClO is larger than the range specified by measurements correspond to cases which NO is lower than its range of measurements. Some caution should be exercised in the interpretation of these screened results because the additional uncertainty due to the vertical transport coefficient was not considered. Its effect should be to broaden most of the probability distributions somewhat. The interrelationships between NO_x species, Cl_x species, and the calculated ozone depletions will be largely unaffected, and strong distortions of the mean values are not expected.

Another interesting correlation is that of ozone column change with the calculated OH concentration. Because of the critical role of OH in removal of chlorine from the reservoir HCl, its concentration is expected to play a crucial role in determining the catalytic efficiency of chlorine towards ozone. This has been emphasized by previous calculations [*WMO*, 1982; *Wuebbles*, 1983*a*, *b*]. However, the change in ozone column shows no significant correlation with the OH concentration at 25 km (correlation coefficient −0.11), as illustrated by Figure 16. The explanation of this result requires careful consideration of how the Monte Carlo calculations differ from the previous calculations. In earlier calculations, usually only a few rate coefficients were changed, and the changes have often been dominated by a single rate coefficient in the HO_x family. Thus the response to a change which caused increased HO_x concentrations would be an increase in ozone destruction by chlorine and a decrease in ozone destruction by NO_x. The present calculations change all of the rate coefficients and other input parameters for every case. The dominant changes are not necessarily directly in the HO_x family and affect other species as well as OH. For instance, a change that results in increased $O(^1D)$ will yield a higher OH concentration, which tends to give higher sensitivity toward chlorine. That same change will give high NO_x concentrations through the reaction of $O(^1D)$ with N_2O. Higher NO_x concentrations tend to interfere with chlorine catalysis of ozone destruction, counteracting the direct effect of HO_x. The overall result for the different combinations which produce variations in OH is the poor correlation of ozone depletion with ambient OH. Because of the poor correlation, no attempt has been

made to screen out ozone depletion cases by comparisons of measured with calculated OH.

It was found that of the 329 Monte Carlo cases, 125 had ambient concentrations of ClO, NO, and NO_2 that fall within their measurement ranges. These 125 cases have smaller mean ozone depletions for all levels of chlorine perturbation than do the full set. The distributions of ozone depletions are given by the shaded areas in Figure 7. At 1 times the PFF the distribution has a mean of -3.0% and a one-sigma standard deviation of 2.2%. None of the cases remaining have an ozone depletion greater than 10%. At 3.5 times PFF the calculated ozone change is $-23.9 \pm 13.6\%$. In this case the reduction in the mean resulted from the removal of more cases from the large-depletion part of the bimodal distribution than from the lower peak. Not all of the large-depletion cases were removed, however. The shaded area of Figure 8 shows the screened result for the 3.5 times PFF, 1.2 times the nitrous oxide flux, and 2.0 times the methane flux case. The result is now $-9.1 \pm 7.0\%$, and all cases above about a 30% depletion have been removed.

4. Summary and Conclusions

Using a one-dimensional stratospheric photochemical model, sensitivity studies in which key rate coefficients are changed by substantial amounts indicated that the calculated ozone depletions exhibit nonlinear behavior as the flux of chlorine-bearing compounds such as fluorocarbons is increased. This behavior is observed because as chlorine is increased the nitric oxide is titrated from the lower stratosphere, leaving chlorine to act upon ozone with little or no interference. Without the interference of odd nitrogen species, addition of chlorine results in large calculated ozone depletions as compared to the present atmosphere. Monte Carlo analysis, designed to explore the total extent of rate coefficient space, finds a much wider spread of potential conclusions concerning the impact of large chlorine amounts. The Monte Carlo calculation employs probability distributions for the values of parameters, such as reaction rate coefficients, cross sections, solar flux, and boundary conditions, and produces probability distributions for calculated concentrations and ozone changes. The ozone depletion due to fluorocarbon injection yields a skewed distribution for injection of the present fluorocarbon flux, with a mean calculated depletion of $-6.2\% \pm 5.5\%$ in the ozone column. This is compared to the calculation of -5.0% for the base case, using the central values of all the input parameters. The distribution moves toward higher ozone depletions as the fluorocarbon flux increases until at 3.5 PFF a double-peaked distribution is obtained, with peaks centered around -15 and -45% change in the ozone column. The mean is -31%, with a one-sigma standard deviation of $\pm 17\%$. This compares to the base case calculation of -40%.

Atmospheric measurements have been used in an effort to reduce the uncertainty in the calculated ozone depletions by considering only those Monte Carlo cases which fall within a range specified by the measurements. One such study concerned the ozone concentration profile itself. The upper stratospheric problem in which the model obtains lower ozone values than measurements was confirmed; however, a significant number of the Monte Carlo cases did overlap with the data. At 30 km the model tended to predict too much ozone, and while a significant number of cases again overlapped with data, no cases passed within the one-sigma variability limits of the data at both 30 and 50 km. When the variability limits were extended to two-sigma, only three cases passed this test. At 2.5 sigma, more than 40 cases passed, and these showed the entire range of possible ozone depletions, indicating that no reduction in the overall uncertainty could be obtained by requiring agreement of the calculated ozone profile with measurements.

A second data comparison was made for some of the minor constituents. Comparisons were made at 25 km because here the calculated local ozone depletion is best correlated with the calculated column ozone depletion. When the Monte Carlo cases were screened, such that only cases for which the calculated concentrations of NO, NO_2, and ClO at 25 km fell within the range of measurements, more than one-third of the cases remained. All cases remaining had a calculated ozone depletion of less than 10% for the PFF. The distribution was symmetric, with a mean of -3% and a standard deviation of $\pm 2.2\%$. Thus these measurements tend to select against the large ozone depletion cases. As the fluorocarbon flux was increased, there was also a tendency to select against high ozone depletion cases, but by 3.5 PFF a significant number of cases of large ozone depletion were obtained.

Although this study is only a beginning of what is possible in considering Monte Carlo results in the context of model-measurement intercomparisons, several tentative conclusions can be drawn:

1. It is possible to reduce the uncertainty in calculated ozone depletions by requiring calculated concentrations for key minor constituents to fall within the range specified by measurements.
2. Relatively low ozone depletions are associated with cases in which calculated concentrations in NO, NO_2, and ClO fall within the range specified by measurements.
3. For larger chlorine injection rates at least part of the bimodal nature of the ozone depletion prediction passes the minor constituent measurement test, thus retaining the possibility of large ozone depletions.
4. The problem of fitting ozone concentrations in the upper stratosphere is actually one of profile shape and simultaneously fitting in both the upper and middle stratosphere.
5. Conformity of the calculated ozone profile to measurements does not appear to be a good criterion for reduction of the uncertainty in the calculated range of ozone depletions.

Acknowledgments We wish to thank JoAnn Wadkins, a participant in the GISS summer fellowship program, for assistance in graphics and computations. We also appreciate the comments of two anonymous reviewers.

References

Alexander Grant and Company, Report to the Chemical Manufacturers Association, Washington, D. C., 1985.

Bemand, P. P., M A. A. Clyne, and R. T Watson, Atomic resonance fluorescence and mass spectrometry for measurements of the rate constant for elementary reactions· $O(^3P_J) + NO_2 \rightarrow NO + O_2$ and $NO + O_3 \rightarrow NO_2 + O_2$, *J. Chem. Soc. Faraday Trans. 2, 70*, 564–576, 1974.

Blake, D. R , E. W. Mayer, S. C Tyler, Y. Makide, D. C. Montague, and F S. Rowland, Global increase in atmospheric methane concentrations between 1978 and 1980, *Geophys. Res. Lett., 9*, 477–480, 1982.

Butler, D. M., The uncertainty in ozone calculations by a stratospheric photochemistry model, *Geophys. Res. Lett., 5*, 769–772, 1978.

Cicerone, R. J., S. Walters, and S. C. Liu, Nonlinear response of stratospheric ozone column to chlorine injections, *J. Geophys. Res., 88*, 3647–3661, 1983.

Crutzen, P. J., and L. T. Gidel, A two-dimensional photochemical

model of the atmosphere, 2, The tropospheric budgets of the anthropogenic chlorocarbons, CO, CH_4 CH_3 Cl, and the effect of various NO_x sources on tropospheric ozone, *J Geophys Res*, *88*, 6641–6661, 1983.

Davis, D D., J. T Herron, and R. E. Huie, Absolute rate constants for the reaction $O(^3P) + NO_2 \rightarrow NO + O_2$ over the temperature range 230–339K, *J. Chem. Phys*, *58*, 530–535, 1973.

DeMore, W. B., D M Golden, R F Hampson, M J Kurylo, C. J. Howard, J J. Margitan, M J. Molina, and A. R. Ravishankara, Chemical kinetics and photochemical data for use in stratospheric modeling, Evaluation Number 7, *JPL Publ., 85-37*, 1985.

Froidevaux, L., M. Allen, and Y L. Yung, A critical analysis of ClO + O_3 in the mid-latitude stratosphere, *J. Geophys Res.*, *90*, 12,999–13,029, 1985.

Keeling, C C., A F. Carter, and W G Mook, Seasonal, latitudinal, and secular variations in the abundance and isotopic ratios of atmospheric CO_2, 2, Results From oceanographic cruises in the tropical Pacific Ocean, *J. Geophys. Res., 89*, 4615–4628, 1984.

Khalil, M A. K, and R. A. Rasmussen, Carbon monoxide in the earth's atmosphere. Increasing trend, *Science, 224*, 54–56, 1984.

Krueger, A J., and R A Minzner, A mid-latitude ozone model for the 1976 U.S standard atmosphere, *J Geophys. Res*, *81*, 4477–4481, 1976.

Logan, J A., Tropospheric ozone: Seasonal behavior, trends, and anthropogenic influence, *J Geophys. Res., 90*, 10,463–10,482, 1985.

McPeters, R D, D. F Heath, and P K Bhartia, Average ozone profiles in 1979 from the Nimbus 7 SBUV instrument, *J. Geophys. Res*, *89*, 5199–5214, 1984.

Molina, M. J, and F. S. Rowland, Stratospheric sink for chlorofluoromethanes. Chlorine atom catalysed destruction of ozone, *Nature, 249*, 810, 1974

National Academy of Sciences, National Research Council, *Causes and Effects of Changes in Stratospheric Ozone· Update 1983*, National Academy Press, Washington, D C., 1984.

Prather, M. J., M B. McElroy, and S C. Wofsy, Reductions in ozone at high concentrations of stratospheric halogens, *Nature, 312*, 227–231, 1984.

Quinn, T. H., K. A. Wolf, W E. Mooz, J. K. Hammitt, T W. Chesnutt, and S. Sarma, Projected use, emissions and banks of potential ozone depleting substances, draft rep. *N-2282-EPA, Rand Corp.*, Santa Monica, Calif., 1985.

Rasmussen, R A., and M A K Khalil, Atmospheric methane in the recent and ancient atmospheres Concentrations, trends, and interhemispheric gradient, *J Geophys. Res*, *89*, 11,599–11,605, 1984

Rundel, R D, D M. Butler, and R S. Stolarski, Uncertainty propagation in a stratospheric model, 1, Development of a concise stratospheric model, *J. Geophys Res*, *83*, 3063–3073, 1978

Slanger, T. G., B J. Wood, and G. Black, investigation of the rate coefficient for $O(^3P) + NO_2 \rightarrow O_2 + NO$, *Int. J. Chem Kinet., 5*, 615–620, 1973

Solomon, S, D W Rusch, R J. Thomas, and R S Eckman, Comparison of mesospheric ozone abundances measured by the Solar Mesosphere Explorer and model calculations, *Geophys. Res Lett., 10*, 249–252, 1983.

Stolarski, R S., and A R. Douglass, Parameterization of the photochemistry of stratospheric ozone including catalytic loss processes, *J. Geophys Res*, *90*, 10,709–10,718, 1985.

Stolarski, R S, D. M Butler, and R D Rundel, Uncertainty propagation in a stratospheric model, 2, Monte Carlo analysis of imprecisions due to reaction rates, *J. Geophys Res., 83*, 3074–3078, 1978

Thompson, A M, and R. J Cicerone, Tropospheric CH_4, CO, and OH from 1850 to 1980, *Nature*, in press, 1986.

Weinstock, E M, M J Phillips, and J. G Anderson, In situ observations of ClO in the stratosphere A review of recent results, *J. Geophys Res*, *86*, 7273–7278, 1981.

Weiss, R. F, The temporal and spatial distribution of tropospheric nitrous oxide, *J Geophys. Res., 86*, 7185–7196, 1981.

World Meteorological Organization, The stratosphere 1981: Theory and measurement, *WMO Rep 11*, Geneva, Switzerland, 1982.

Wuebbles, D J, A theoretical analysis of past variations in global atmospheric composition and temperature structure, Lawrence Livermore *Lab Rep*, *UCRL 53423*, 1983*a*

Wuebbles, D J, Chlorocarbon emission scenarios Potential impact on stratospheric ozone, *J. Geophys Res*, *88*, 1433–1443, 1983*b*.

A. R Douglass, Applied Research Corporation, 8201 Corporate Drive, Landover, MD 20785.

R S Stolarski, Atmospheric Chemistry and Dynamics Branch, Code 616, NASA Goddard Space Flight Center, Greenbelt, MD 20771

(Received November 30, 1985,
revised March 18, 1986;
accepted March 19, 1986.)

UCRL- 95548
PREPRINT

OZONE PERTURBATIONS IN THE LLNL ONE-DIMENSIONAL MODEL - CALCULATED EFFECTS OF PROJECTED TRENDS IN CFC's, CH_4, CO_2, N_2O AND HALONS OVER 90 YEARS

Peter S. Connell
and
Donald J. Wuebbles

Prepared as a special report for the
Environmental Protection Agency

March 1986

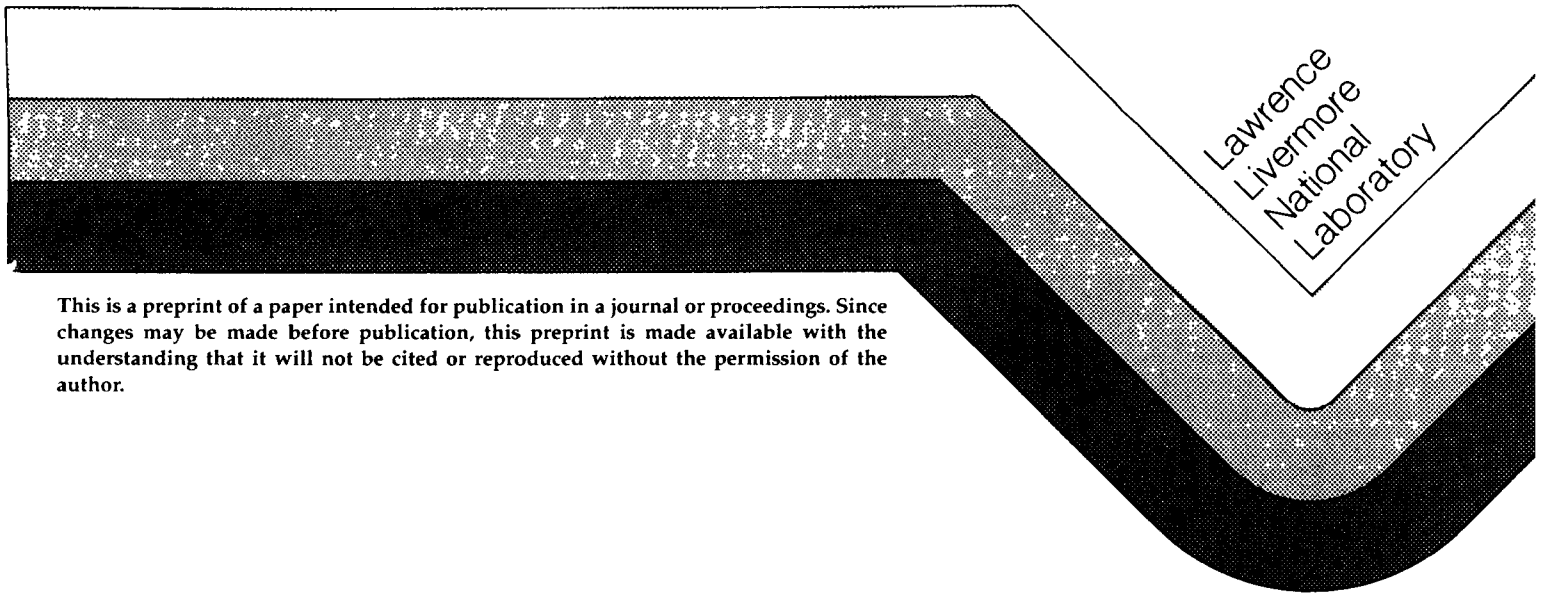

DISCLAIMER

I. INTRODUCTION

I.A The Nature of the Problem

Many processes in the earth's atmosphere and the earth's biosphere are closely connected. Mutual dependence is demonstrated in the biosphere's contribution to atmospheric composition (oxygen, carbon dioxide, nitrous oxide, methane, and methyl chloroform) as well as in the vital roles that atmospheric properties such as climate, weather, ultraviolet and infrared opacity and abundances of oxygen and carbon dioxide play in the maintenance of the biosphere. These interconnections would exist in the absence of man's intervention. In addition to 'natural' interactions of the atmosphere and biosphere, human activities can significantly alter properties of the atmosphere and by extension, conditions for life in the biosphere.

Human impacts on the atmosphere are of two major types. First, trace species of many types are directly emitted into the atmosphere as by-products of various activities, including transportation, combustion, energy production, refrigeration, plastic and polymer production and use, high-technology industry and personal hygiene. Second, methods of land development, agriculture and animal husbandry can affect the fluxes of naturally occurring atmospheric trace species. Atmospheric observations over the last 20 years have revealed dramatic increases in the trace abundances of man-made perhalogenated chlorocarbons and chlorofluorocarbons (CFC's). Observational evidence also shows enhancement in the abundances of naturally occurring species which are also directly emitted by society (e.g., CO_2, CH_4, CO), over the century time scale of industrialization and population growth. Enhancement (e.g., tropospheric ozone) or suppression (e.g., tropospheric HO, stratospheric ozone) of the abundance of naturally occurring atmospheric constituents that are photochemically produced may also be occurring (WMO, 1986). The atmospheric changes that can ensue from these perturbations include increased ultraviolet irradiance at the earth's surface, photochemical smog, reduced visibility, acid precipitation and perhaps changing climate.

An atmospheric response to anthropogenic emissions that was unexpected as recently as 1970 is the potential perturbation of the stratospheric ozone abundance. The diffuse layer of ozone (O_3) in the stratosphere (approximately 12–55 km above the surface) is chiefly responsible for controlling the intensity of solar ultraviolet radiation between the wavelengths of 210 and 320 nm penetrating the stratosphere and in particular the 280–320 nm radiation that reaches the ground. Such radiation is responsible for skeletal growth, vitamin D production, tanning and sunburn in man and exposure to it is correlated with various types of skin cancers. There are also diverse and often deleterious effects on plants and animals. Ozone, as well as several of the species with which it is photochemically connected, is also involved in the earth's radiation balance and thus climate.

The study reported here investigates the potential perturbation of stratospheric ozone on a global basis, in view of current and projected trends of increase in several anthropogenically-related atmospheric species. The authors of a recent review of the current state of knowledge of the stratosphere (WMO, 1986) have emphasized the wide range of uncertainties in both the projections of trends of trace species abundances and their potential effect on ozone in the troposphere and stratosphere. Several previous studies

(Brasseur et al., 1985; Callis et al., 1983; Owens et al., 1985; WMO, 1986; Wang et al., 1986; Wuebbles et al., 1983) have considered the effects on ozone of simultaneous trends of several important trace gases and have shown the inherent nonlinearity of ozone-controlling atmospheric dynamics and photochemistry. But these studies have not, in general, attempted to address the full range of trend possibilities. Our primary interest in this report is to investigate the extent of the effects of projection uncertainties and the nature of their coupling, chiefly with respect to relative changes in the vertically integrated ozone column. Special attention is given to considering trend projections over a range of uncertainty and to employing emission trends with economic bases, where appropriate. The choice of CFC trend projections is based on information provided by the EPA and the current study is also intended to support the possible development of an international protocol governing CFC production and release.

I.B Background

The existence of a layer of ozone in the upper atmosphere was first demonstrated by Hartley in 1881. To explain its origin, Chapman (1929) theorized that a region of enhanced ozone abundance would occur in an atmosphere of oxygen and nitrogen as a result of fission of the O=O bond in molecular oxygen by solar radiation. Observation of the abundance and behavior of stratospheric ozone continued in the early part of this century. As the kinetic parameters of the Chapman reactions were measured in the laboratory, it became clear that the actual situation was not completely explained by the reactions Chapman postulated to occur in an atmosphere in which atomic and molecular oxygen and ozone were the only reactive participants. In particular, the observed abundance was considerably less than predicted by the oxygen reactions, given the rate parameters for these reactions as measured in the laboratory. Additional ozone loss processes were inferred to exist.

Bates and Nicolet suggested in 1950 that cyclic processes were involved in the photochemistry of atmospheric water vapor. One generic example of a stratospheric cycle is

$$X + O_3 = XO + O_2 \qquad (1)$$
$$XO + O = X + O_2$$

The catalyst X is regenerated by the pair of reactions, while the process operates effectively to facilitate the net reaction

$$O + O_3 = 2O_2 \qquad (2)$$

Catalytic cycles of this type were discussed as important odd oxygen (O and O_3) loss mechanisms by Hampson (1964) and Crutzen (1970), who proposed HO and NO, respectively, as the catalyst X in the reactions above.

With this background, the potential for perturbation of the ozone amount by anthropogenic emissions was quickly realized (Johnston, 1971 and Crutzen, 1971). The emissions receiving the most attention from the standpoint of impacts on ozone have been: (1) in situ injection of NO_x and HO_x species by aircraft engines (CIAP, 1975; NRC, 1973), (2) increases in stratospheric NO_x abundance following indirectly from nitrogenous fertilizer production and usage (McElroy et al., 1977), (3) increases in the abundance of chlorine-containing radicals directly through solid rocket motor emissions or indirectly through

production and atmospheric release of chlorinated and brominated alkanes (Stolarski and Cicerone, 1974; Molina and Rowland, 1974; NASA, 1977; Wofsy et al., 1975), and (4) NO_x injections caused by large-weapon nuclear fireballs (NRC, 1975 and 1985).

Folk knowledge of the beneficial effects of human exposure to sunlight, and by inference the short wavelength ultraviolet tail of solar radiation, must predate modern science. Medical study of both beneficial and deleterious effects of sunlight in man began more than a century ago and the effects of exposure to ultraviolet radiation have been studied for more than fifty years. But it appears that the connection of varying effects of ultraviolet exposure specifically to consideration of ozone variability, rather than for example general latitude dependence or cloud and haze obscuration, arose only with the suspicion that anthropogenically-caused variability in ozone was possible. Knowledge of the effects of UVA (320–350 nm) and UVB (280–320 nm) exposure on man, vegetation and susceptible fauna has greatly increased in the last 15 years, although uncertainties in this area are still large.

While the potential for depletion of stratospheric ozone has been the major theme of stratospheric studies, it is now also understood that increased emissions of certain species could result in an increase in ozone abundance. Carbon dioxide, an active infrared absorber and emitter in the atmosphere, shows a well-documented increase in atmospheric concentration (Keeling et al., 1982). The stratospheric counterpart to warming of the surface/troposphere system by CO_2's infrared absorption properties is local stratospheric cooling by emission of infrared radiation to space. As increasing CO_2 cools the stratosphere, the efficiency of ozone-destroying catalytic cycles may be reduced (Luther et al., 1977) producing an increase in ozone. This effect connects the problem of the potential human perturbation of the climate (surface temperatures and tropospheric weather) with that of human perturbation of stratospheric ozone.

This connection is strengthened by the infrared radiative (climate) importance of ozone and several of the trace species mentioned above in consideration of ozone photochemistry. An increase in atmospheric CH_4, which appears well-documented over the last decade (WMO, 1986) and may date back a century (Stauffer et al., 1985), is expected to affect ozone in several ways. For example, stratospheric CH_4 is oxidized by HO producing H_2O and radicals (HOO and CH_3OO), which can produce ozone via reaction with NO. The water produced in CH_4 oxidation remains available as a source species for HO_x radicals. Methane also provides a stratospheric sink for Cl atoms, forming the less reactive species HCl. In addition, CH_4 has infrared radiative properties which make it and its observed increase currently important in the study of the perturbation of the earth's climate.

I.C Current Status of Research on Stratospheric Ozone

A continuing aspect of stratospheric ozone research is the identification of the complete set of participating species and significant kinetic processes. Recent advances in techniques for the study of reactions in the laboratory and improved detection and monitoring of stratospheric species from surface, balloon and satellite platforms have greatly expanded the set to be considered. More than 50 trace species have been identified in the laboratory as reactants and products of reactions of stratospheric importance and many of these species have been observed in the atmosphere.

The current picture of stratospheric photochemistry is conveniently discussed in terms of groupings or families of similar species, such as NO_x ($NO+NO_2$), NO_y ($NO_x + HNO_3 + HO_2NO_2 + NO_3 + 2^*N_2O_5 + HNO_2 + ClONO_2$) and ClO_x (Cl+ClO), which may include short-lived highly reactive radical molecules (those with unpaired electrons) or both radicals and longer-lived molecules such as HNO_3 or HCl. Other species such as HO_2NO_2 and $ClONO_2$ have been identified in the laboratory and have recently been tentatively observed in the stratosphere. These species fall between family groupings and represent important interconnections between catalytic cycles. Coupling the species involved in competing catalytic cycles can result in ozone perturbations that depend nonlinearly on emissions of anthropogenic trace species. Additionally, as a result of the range of temperature and ultraviolet intensity encountered as a function of altitude, different altitude regions are dominated by differing regimes of photochemical processes. Large sets of reactions are thus required to completely describe the processes controlling ozone chemistry as they are currently understood.

Two major current emphases in developing a coherent picture of stratospheric variables and properties are, first, understanding in terms of transport and photochemistry the observed distributions in space and time of ozone, temperature and the suite of other species and physical quantities that can be observed and, second, the detection of long-term trends in ozone abundance, temperature, source species such as chlorofluorocarbons and methane and perhaps even active radical species. One method of synthesizing the laboratory photochemical knowledge that has proved advantageous for comparison of theory to the atmosphere is the comprehensive photochemical/dynamics numerical model. Such models represent stratospheric processes in one, two or three spatial dimensions in either an equilibrium or time-dependent fashion. One- and two-dimensional models can contain essentially complete, known, laboratory-based photochemical reaction parameter sets. The results of these models (for example, vertical profiles of species concentrations or seasonal and latitudinal fields of abundance integrated vertically) can be compared to observations, with due regard given to the effects of assumptions made in reducing the dimensionality of the model. This diagnostic use of models can reveal inadequacies in the current understanding of photochemistry in the present atmosphere. Three-dimensional models, structured to give the best representation of atmospheric motions, are currently unable to include full elementary photochemistry because of available computational capabilities.

The effects of past or projected atmospheric perturbations can also be studied with these models. If all pertinent physical processes and photochemical kinetic parameters were known and included in the model, then prognoses of potential atmospheric perturbations could be produced by changing model boundary conditions, for example those representing projected emission trends. While comparison to the current atmosphere remains an important method of testing the correctness and completeness of models, it should be noted that prognostic applications of models can not necessarily be verified by acceptable diagnostic performance. That is, two models (differing for example in photochemical kinetic parameters) can achieve equivalent success in modeling current atmospheric observables but may predict widely diverging future changes in ozone for a proposed perturbation. These uncertainties arise from the restricted, if currently growing, cluster of stratospheric species that have actually been observed, the uncertainties in their quantitative observation, the lack of complete spatial and temporal coverage of the observations and the complexity of

the kinetic system. The confidence level for model predictions, then, is based somewhat subjectively on completeness and applicability of kinetic, radiative and dynamic model components as well as on diagnostic capabilities.

I.D The One-Dimensional Model

The chief variable in studying the biospheric impact of altered surface ultraviolet radiation in the UVB region is the optical thickness of the vertically integrated ozone column. As mentioned above, diverse photochemical behavior occurs in the atmosphere as a result of the altitude dependence of solar UV flux, temperature and distributions of long-lived source species. A model with at least one spatial dimension, the vertical, is required to investigate the dependence of the ozone column abundance on the various atmospheric variables.

Various one-dimensional (1-D) models have been used extensively since 1971 to study the photochemistry of the stratosphere. In general, these models account for homogeneous mono-, bi- and termolecular reactions, photolytic reactions, atmospheric mixing in the vertical, and various other physical processes. Current 1-D models usually include the complete set of significant stratospheric species and the kinetic parameters of their reactions, to the extent that laboratory and observational evidence is available. The intensity of visible and ultraviolet solar radiation is calculated as a function of altitude based on the model computed vertical profiles of the important absorbers O_3, O_2 and NO_2. The individual photolytic constants for each species are then calculated from the laboratory absorption spectra. Atmospheric dynamics and processes such as removal of species from the troposphere by precipitation and dry deposition are included as empirical parameterizations constrained by observations and understanding of the associated physics in the atmosphere. Some models also include the coupled calculation of the stratospheric temperature profile, which depends on solar absorption by ozone and infrared absorption and emission by CO_2, H_2O and O_3.

Because the concentrations of many source species are changing and future projection of source strengths are uncertain, even for industrially produced species like CFC-11 ($CFCl_3$), predictions for future changes in ozone can not at present be closely constrained. Investigating the possibilities requires model parameter studies with boundary conditions specified over the anticipated range of emission scenarios of the source species. One-dimensional models have been used for this purpose because they are much more conservative of computer resources than 2-D models, although attempts are being made at time-dependent integrations in two dimensions over several decades of model time. The results of a 1-D model can be considered to represent global or hemispheric average behavior for considerations of ozone change. They can give a global indication of the effects of perturbations taking into account the fine detail of photochemical interactions but are incapable of representing potentially significant variations with latitude or season. The results presented in this report will show the importance of including simultaneous perturbations of the various trace gas emissions in predicting future ozone change.

Some limitations and uncertainties are inherent in the 1-D model formulation. Latitudinal variation in the changing ozone column can not, of course, be considered. Preliminary study of CFC perturbations in 2-D models have shown a strong latitudinal dependence,

with ozone depletion occurring preferentially at middle and high latitudes. In addition, rates of reactions computed with global annual average concentrations will differ from the actual global average reaction rate for species that are correlated or anti-correlated in space or time. The effects of uncertainties in the numerical parameters of processes which are included can be estimated by various approaches, including Monte Carlo studies in which the parameters are allowed to vary according to the appropriate uncertainties (Stolarski and Douglass, 1986; Grant et al., 1986). Uncertainty caused by the neglect of important processes not yet identified can not be estimated, but has had a substantial impact in the past. The predicted response of the ozone total column to the given standard perturbation (usually constant CFC emissions at late 1970's levels) has varied significantly as new species and reactions have been introduced.

I.E Focus of This Report

We report here on the application of one numerical atmospheric model, the LLNL 1-D troposphere-stratosphere model, to the investigation of future response of ozone to anthropogenic emissions of chlorine- and bromine-containing alkanes (CFC's and Halons) against the background of simultaneously changing levels of CO_2, CH_4 and N_2O.[1] The atmospheric abundances of some industrially produced halocarbons are currently increasing at measurable rates, which, if projected to continue for decades, may reach a point of significant impact on ozone. Knowledge of the magnitude of the impact as a function of emissions projections is required to evaluate the effectiveness of measures which might be implemented to control the rate of release of these species to the atmosphere. The problem is considered in a globally averaged sense, with detailed consideration given to photochemical kinetics and radiative processes in the stratosphere. Lesser consideration is given to the model treatment of stratospheric motions and no attempt is made to address ozone changes over other dimensions and smaller spatial scales, i.e. latitudinal behavior.

Many of the trace atmospheric species that are changing in these scenarios, CFC-11 ($CFCl_3$), CFC-12 (CF_2Cl_2), N_2O, CH_4, CO_2, stratospheric O_3 and stratospheric water vapor, also contribute to the infrared radiative balance in the earth's atmosphere. The atmosphere can be assumed well-mixed from the surface over the altitude range that infrared absorption and emission by the long-lived species is important in determining surface temperature. Lacis and coworkers, using the NASA/Goddard Institute for Space Studies 1-D radiative convective model (Lacis et al., 1981 and Hansen et al., 1981), have parameterized the radiative contribution to the global average equilibrium change in surface air temperature arising from specified changes in surface mole fractions of CO_2, CH_4, N_2O, CFC-11 and CFC-12 and in the vertical profiles of ozone and stratospheric water vapor. The relationships derived do not include the effects of climate feedbacks on, for example, the hydrologic cycle. Rather the effects on surface temperature predicted by these relations represent only the pure radiative effect at equilibrium of the particular trace species considered. The effect of climate feedbacks can then be estimated from GCM simulations in which these are included. A recent NAS panel study (NRC, 1983), summarizing the

[1] The term halocarbon (or Halon) refers to organic species (in the chemical sense) containing one or more halogen atoms (F-, Cl-, Br- or I-). The term chloroflurocarbon (or CFC) usually refers to halogenated alkanes containing fluorine and chlorine atoms.

current state of knowledge, predicts a feedback amplification factor of 1.25 to 3.75 for the equilibrium doubled CO_2 radiatively forced surface temperature change of 1.2°C (without feedbacks), corresponding to a total temperature change of 1.5 to 4.5°C. Using these relationships and estimates of the climatic feedback factors, the emission scenarios, model-derived CFC and CH_4 mole fractions and calculated ozone and water vapor profiles, surface air temperature changes have been calculated for several of the scenarios. The timing of temperature increases depends on many factors whose discussion is beyond the scope of this report. As with the case of ozone perturbations, major uncertainties, such as the effect of the thermal inertia of the oceans, exist in applying both 1-D radiative convective and GCM models prognostically.

The connected issues of stratospheric photochemistry and global climate are considered as separate pieces in this report. A discussion of the overall impact of increasing trace gas abundances on climate and the biosphere is beyond the scope of this report.

The estimates of future surface emissions of the CFC's and other industrial halocarbons (sometimes termed a scenario) are pivotal to the prediction of ozone changes. Since this report focusses on ozone changes in the near future (defined in this report as the next 90 years) rather than the elucidation of stratospheric response to individual perturbants, we have adopted CFC scenarios based on the work of Quinn et al. (1985) and ICF, Inc. as communicated by the U.S. Environmental Protection Agency (S. Seidel, private communication). Scenarios with restricted CFC emissions representing the effects of possible policy decisions are also investigated to study the possibility of mitigating CFC impacts.

The projections of the various CFC and other halocarbon emissions are based on industry figures and estimates and can be checked against measured atmospheric abundance if the atmospheric lifetimes are known (Prinn et al., 1983). Projections of the future surface fluxes of other trace species which have a positive trend (CO_2, CH_4 and N_2O) are more difficult to define. First, the measurements of current trends can be subject to uncertainties resulting from a short time series of observations, problems of global representativeness in sampling, unusual events such as El Chichon/El Niño which perturb a monotonic trend or simply a small trend relative to the average atmospheric abundance. In addition, these species have multiple sources, both anthropogenic and natural, and the relationship of the fluxes to their controlling variables is in many cases uncertain. Finally, the magnitude or capacity of atmospheric sinks, and thus the atmospheric lifetime, can be uncertain.

For example in the case of CO_2, predictions of future abundance depend on our understanding of biospheric and oceanic uptake as well as factors determining energy demand and fossil fuel consumption. Trends in the rates of both surface emission and atmospheric destruction may be instrumental in affecting methane abundance. Projecting future methane concentrations depends on understanding surface emissions of CH_4 and CO and the atmospheric interactions of CH_4, CO and the observationally elusive tropospheric hydroxyl radical, HO, each of which affects the others. Assumptions made in predicting future levels of these species can impact the overall model behavior significantly, as will be shown in the discussion of results.

Several previous studies of ozone perturbation in response to trends in several species occurring simultaneously have been reported (Brasseur et al., 1985; Callis et al., 1983; Owens et al., 1985; WMO, 1986; Wang et al., 1986; Wuebbles et al., 1983). These studies

have been mainly directed toward understanding atmospheric processes and have employed simple constant or smooth growth projections for species such as the CFC's. In this study we consider the time evolution of the ozone response to econometrically derived CFC projections which may or may not be smooth and monotonic. We consider a wider range of possibilities, including large increases to the stratospheric Cl_z (= Cl + ClO + HCl + $ClONO_2$ + HOCl) abundance in the so-called chlorine catastrophe regime (Prather et al., 1984). We also investigate how individual uncertainties in the projection scenarios for each important trace species or species group (e.g., CFC's) combine to affect the calculated ozone change.

In the next section a brief description of the structure, geophysics and photochemical kinetics in the model is given, followed by a discussion of ozone-controlling mechanisms in the model stratosphere and previous results of ozone perturbations. Historical trends in important trace species concentrations and emissions and the model-derived impacts on ozone and temperature are discussed in Section III. Section IV presents the emissions projections used in the study, and Section V presents a detailed discussion of the model results for an intermediate reference case scenario. The sensitivity of the calculated ozone and temperature perturbations to scenario assumptions and regulatory possibilities is considered in Section VI.

II. THE LLNL ONE-DIMENSIONAL MODEL

The LLNL one-dimensional atmospheric model, used for this study of stratospheric ozone perturbation resulting from the changing abundances of several trace constituents, has been developed in over a decade of research. Improved solution techniques and new information arising from both atmospheric observation and laboratory investigations have been evaluated and incorporated into the model originally described by Chang et al. (1974). The emphasis in development has been on comprehensive and detailed representation of photochemical kinetic processes and on numerical accuracy, within the limitations of the reduced dimensionality for the treatment of atmospheric dynamics. More discussion can be found in Luther et al. (1979) and Wuebbles et al. (1983).

II.A Model Structure

The model atmosphere is divided into 44 vertical layers, extending from the surface to just above the stratopause (at about 56 km). The spatial (vertical) coordinate metric is the Naperian logarithm of the pressure, relative to the model's surface pressure. Some results in this report are presented on an approximate effective altitude scale, mapped from the pressure levels. The advantage of the pressure coordinate is simplification of the model coupling to the radiative submodel.

The chemical and physical processes determining the temporal variation in the concentration of the i^{th} atmospheric constituent, c_i, can be represented in mathematical form by a differential (continuity) equation,

$$\frac{\partial c_i}{\partial t} = \frac{\partial}{\partial z}\left[K_z(z)\rho\frac{\partial}{\partial z}(c_i/\rho)\right] + P_i(c) - L_i(c)c_i + S_i \qquad (3)$$

where t is time, z is altitude, $K_z(z)$ is the one-dimensional vertical diffusion coefficient, ρ is air density, $P_i(c)$ and $L_i(c)$ c_i are photochemical production and loss terms of constituent i, c_i represents the concentration and S_t represents any other sources or sinks. The vertical diffusion term is assumed to represent the global average of the net vertical transport flux.

Transport of atmospheric trace constituents in the 1-D model is an empirical representation which is not derived directly from observed atmospheric motions. Instead, the temporal and spatial distribution of various tracers is matched by adjusting the form of the effective diffusion constant K_z as a function of altitude. The tracers considered in establishing the K_z profile used here (Figure 1) include long-lived species (e.g., N_2O, CH_4, CFC-11, CFC-12 and CH_3Cl) and excess radioactive ^{14}C injected into the atmosphere by atmospheric nuclear testing.

The individual species conservation equations are solved simultaneously by means of a variable order multistep implicit method (Hindmarsh, 1976). The main advantage of this method is its ability to solve the coupled set of differential equations containing a wide range of characteristic times (stiffness) encountered in the chemical kinetic terms. The model time step is variable over orders of magnitude in order to assure both numerical accuracy and computational efficiency.

The boundary condition for individual species can be either fixed concentration or fixed flux at the surface and fixed flux at the upper boundary. The time dependent surface boundary conditions for the trace species which are the important source species considered in this report constitute the scenario of projected emissions and will be discussed below. Boundary conditions for other species can be found in Wuebbles (1981). The dry deposition and precipitatation scavenging parameterizations are also discussed there.

The stratospheric temperature is affected by absorption of solar radiation, chiefly by O_3 with a smaller contribution from NO_2, and by emission of infrared radiation to space by O_3, CO_2 and H_2O. In these calculations, the temperature profile is determined with a radiative transfer submodel assuming radiative equilibrium, that is a balance of the local heating from solar and infrared absorption and cooling from infrared emission (Luther et al., 1977; Wuebbles, 1983). Changes in the concentrations of the species involved in the radiative equilibrium as a result of photochemistry or transport can then affect the temperature distribution through the resulting changes in the solar heating or longwave cooling rates. Ozone solar heating rates are based on the results of Wang et al. (1982). Longwave cooling rates are taken from Ramanathan (1976) and Kiehl and Ramanathan (1983). The effect of temperature change on the transport parameterization is not easily included in a 1-D model and is not included in the current calculations. The temperature profile below 13 km in the model is specified according to the U.S. Standard Atmosphere (1976).

The effects of radiatively active trace species on the tropospheric and surface air temperatures cannot be calculated using the assumption of radiative equilibrium because of the importance of convective mixing and the hydrologic cycle in the troposphere. The trace species involved include the species mentioned previously as important in the stratosphere, as well as other species that absorb infrared radiation at wavelengths not otherwise absorbed by water or CO_2. These include N_2O, CFC-11 and CFC-12. The temperature in the troposphere can be calculated in models that include convective transport of heat. As

discussed above, the surface temperature changes calculated in this report are based on the parameterized results of such a model, and are not coupled to the transport-kinetics model.

II.B Model Photochemical Kinetics

Fifty-two species are included in the model. Oxygen (O_2) and CO_2 are assumed well-mixed throughout the atmosphere at specified abundances. Three of the minor constituents ($O(^1D)$, H and N) are assumed to be in instantaneous photochemical equilibrium, so that the effects of transport on their concentration profiles can be ignored. The remaining 47 species,

$O(^3P)$, O_3,
NO, NO_2, N_2O, HNO_3, HNO_4, HNO_2, NO_3, N_2O_5,
HO, HO_2, H_2O_2,H_2, H_2O,
Cl, ClO, HCl, HOCl, $ClONO_2$, $ClNO_2$,
CH_4, HCO, H2CO, CH_3, CH_3O_2, CH_3O, CO, CH_3OOH,
Br, BrO, HBr, HOBr, $BrONO_2$,
CH_3Cl, CCl_4, CF_3Cl (CFC-11), CF_2Cl_2 (CFC-12), CHF_2Cl (CFC-22), $CFCl_2CF_2Cl$ (CFC-113), (CF2Cl)2 (CFC-114), CF2ClCF3 (CFC-115), CH_3CCl3,
CH_3Br, CF_3Br (Halon 1301), CF_2BrCl (Halon 1211), and $C_2H_4Br_2$ (EDB),

are solved using Equation (3) for each species.

The 165 chemical and photolytic reactions contained in the model for this study are listed in Table 1. The kinetic rate parameters are based on the recommendations of the NASA Panel for Data Evaluation (JPL 83-62, 1983). Literature values are used for the few reactions for which recommendations were not made. We have chosen the recent experimental results of Smith et al. (1984) for the rate parameters of the reaction

$$HO + HNO_4 = H_2O + NO_2 + O_2, \tag{4}$$

while the NASA recommendation is derived from an average of this and earlier reported results. By analogy to the current recommendation for HO+HNO_3, we feel the Smith et al. value is more likely to be correct.

The solar flux, incident at the top of the atmosphere, used in the model is consistent with the recommendations made in WMO (1982). The solar zenith angle in the model is fixed at 30 degrees representing approximate global average conditions at equinox.

Photodissociation rate coefficients are computed at each vertical level and time step consistent with the specified solar conditions including the effect of multiple scattering and cloud cover (Luther et al., 1978) and the calculated distributions of the significant absorbers O_2, O_3 and NO_2. The absorption coefficients and product quantum yields used are discussed in Connell and Wuebbles (1983) for most of the species.

Many species concentrations as well as photodissociation rate constants have a diurnally varying component. The average rates for reactions involving these species are computed from consideration of the overlap of the curves of diurnal variability, which are

computed in a model including the full diurnal variation of insolation and are assumed to remain constant throughout a run.

II.C Ozone-Controlling Photochemistry in the Model

Ozone is the dominant component of the odd oxygen family, Ox, in the stratosphere, which also includes oxygen atoms in ground and excited states. Ozone and O atoms are rapidly interconverted by the reactions

$$O_3 + h\nu = O_2 + O \tag{5}$$
$$O + O_2 + M = O_3 + M, \quad M = N_2, O_2$$

and can be considered equivalent when calculating production and loss rates for ozone. Odd oxygen is formed primarily in the photolytic decomposition of molecular oxygen by solar radiation of wavelengths less than 242 nm,

$$0_2 + h\nu = 2\ O \tag{6}$$

with a maximum production rate around 40 km in the 1-D model, representing the maximum in the product of solar short wavelength UV flux and O_2 concentration. Ozone production in this region is largely balanced by local destruction processes, but some ozone is transported both up and down. The net source region for odd oxygen in the model atmosphere is between 25 and 35 km. The maximum ozone number density occurs at 23 km, where both local production and transport from above contribute. The maximum mole fraction of ozone occurs at 31 km.

Odd oxygen production by another path, requiring only near UV radiation which penetrates to the surface, also contributes to ozone abundance in the model's troposphere and lower stratosphere (0–16 km). In this region, the oxidation of methane produces peroxy radicals, CH_3OO and HOO, which can oxidize NO to NO_2. When the NO_2 is photolyzed

$$NO_2 + h\nu = NO + O \tag{7}$$

the oxygen atom produced combines with O_2 to form O_3. Nitric oxide is catalytic in this process but the CH_4 is consumed.

In contrast to the simple picture for odd oxygen production, odd oxygen loss occurs by many paths. The direct reaction of O with O_3, first proposed by Chapman (1930) to be important in the stratosphere, proceeds in the absence of trace catalytic species and increases in rate with altitude, as the O atom abundance increases. Other more important loss processes involve members of the NO_x, ClO_x, BrO_x and HO_x families in several catalytic cycles. Two major cycles are, schematically,

$$X + O_3 = XO + O_2 \tag{8}$$
$$XO + O_3 = X + 2O_2$$

and

$$X + O_3 = XO + O_2 \tag{9}$$
$$XO + O = X + O_2$$

where X in the first cycle can be HO and in the second cycle NO, H, HO, Cl or Br. Fluorine does not participate in catalytic photochemistry. Unlike the C-Cl or C-Br bonds, the C-F bond is sufficiently strong that F atoms can not be liberated by radiation reaching the stratosphere. Also the HF molecule is more stable than HCl or HBr, so that any atomic fluorine present is quickly tied up in the form HF. Other cycles of lesser importance can also be postulated involving species such as NO_3 and HOCl. The relative importance of these cycles in the model of the current atmosphere is discussed below.

The sources of these catalytically reactive trace species are the various long-lived surface emitted gases, N_2O, H_2O, CH_4 and perhalogenated Cl- and Br-containing alkanes. NO and HO are liberated from N_2O and H_2O, respectively, in the stratosphere by the reactions

$$N_2O + O(^1D) = 2\ NO \tag{10}$$

and

$$H_2O + O(^1D) = 2\ HO. \tag{11}$$

Methane can also react directly with $O(^1D)$ to form HO, as well as producing H_2O as an oxidation product. $O(^1D)$ is produced by photolysis of ozone at wavelengths less than about 315 nm. Chlorine and bromine are liberated from their respective sources by photolysis at mid and short UV wavelengths modeled as, for example

$$CFCl_3(CFC - 11) + h\nu = 3\ Cl. \tag{12}$$

Reaction (12) does not represent a true elementary photolytic process, but the set of reactions that liberate each Cl atom are assumed to be simple and rapid. The remaining fluorine-containing fragments are ignored for the reason mentioned above.

NO_x, ClO_x and BrO_x are eventually lost from the stratosphere by conversion to less reactive species which diffuse down into the troposphere where they are removed by wet and dry deposition processes. For NO_x, loss occurs chiefly through HNO_3, formed by the reaction

$$HO + NO_2 + M = HNO_3 + M. \tag{13}$$

For ClO_x and BrO_x, loss occurs through formation of HCl and HBr,

$$Cl + CH_4 = HCl + CH_3 \tag{14}$$

and

$$Br + HOO = HBr + O_2. \tag{15}$$

These loss processes depend on interactions of the various families and are an example of how changes in a given source species can affect several aspects of the photochemistry (e.g., increasing CH_4 will increase HO_x and decrease NO_x by producing more HNO_3). Bromine has been identified as a more efficient catalyst for odd oxygen loss than chlorine, even though the reaction of BrO with O atoms, the rate-determining step in the cycle,

is slower than the corresponding reaction of ClO. The greater efficiency for BrO_x cycles results from the inability of Br atoms to abstract hydrogen from CH_4 as well as the lesser stability of HBr than HCl with respect to photolysis and reaction with HO. BrO makes up a larger fraction of the total bromine available than does ClO of the total Cl_z. Future increase in the stratospheric bromine radical abundance will affect the chlorine chemistry through the reaction

$$BrO + ClO = Br + Cl + O_2. \tag{16}$$

Other interactions among families can also have significant impacts on the ozone-related photochemistry. Three examples of reactions that have caused changes in the theory of ozone depletion are

$$HOO + NO = HO + NO_2,$$

$$ClO + NO = Cl + NO_2, \tag{17}$$

and

$$ClO + NO_2 = ClONO_2.$$

Consideration of the first two reactions shows that they short circuit catalytic cycles for odd oxygen destruction for both families involved, effectively reducing the catalytic efficiencies. The discovery that the reaction of HOO with NO was substantially more rapid than previously thought (Howard and Evenson, 1977) greatly reduced the ozone depletion expected from supersonic transport NO_x emissions in models at that time. The third reaction serves to sequester some of the active radicals in both the NO_x and ClO_x into a less reactive form, making them unavailable for the catalytic destrcution of ozone. The reaction of BrO with ClO, cited earlier, completes an odd-oxygen catalytic loss cycle for both bromine and chlorine, increasing the efficiency of both in the lower stratosphere where O atom concentrations are low.

II.D Previous Ozone Perturbation Results

While the overall model structure has remained fairly constant since 1975, the set of species included and the kinetic parameters have changed continually as new information has become available. The result has been great variation in the predicted CFC impact at steady state on ozone column abundance. Figure 2 shows the evolution of computed results from a standard CFC surface flux assumed constant at levels characteristic of the mid or late 1970's. The ozone depletion calculations in this figure were made with CH_4, CO_2 and N_2O fixed at present day surface mole fractions and usually do not include the effects of temperature feedback.

From 1975 to 1981, calculated changes in the total ozone column resulting from the CFC perturbation at steady state varied from about -20% to about -4%. These variations in estimates can be traced primarily to three related sources. First, rate parameters for the reactions involving chlorine chemistry have changed, with conflicting impact on the sensitivity of ozone to chlorine perturbations. The experimental evidence for the higher of two measured rates of $ClONO_2$ formation had the greatest impact, reducing the efficiency of both Cl and NO_x perturbations and significantly reducing the depletion estimates. Second, the computed abundance of HO and the relative importance of NO_x cycles to odd

oxygen loss also contributed to the variation in the CFC-caused ozone perturbation. When higher HO abundance is calculated, Cl is freed more rapidly from the inactive form, HCl, so that changes that promote higher HO abundance increase CFC perturbations. Current models of photochemistry tend to produce lower HO concentrations than prior calculations, which are also consistent with available observational evidence. Third, models in which the importance of NO_x-based cycles is greater tend to exhibit smaller effects on ozone from CFC perturbations. The photochemical interactions of ClO_x and NO_x compensate increased ozone loss from ClO_x by reducing the efficiency of ozone loss through NO_x.

Perhaps the most significant recent change in stratospheric photochemical modelling incorporated into this study concerns the optical absorption properties of oxygen. The absorption cross sections of O_2 in the Herzberg continuum region between 195 and 242 nm have been reduced over the values previously employed in 1-D models, as a result of in situ stratospheric measurements of solar flux (Herman and Mentall, 1982; Frederick and Mentall, 1982) and subsequent laboratory reevaluation of O_2 absorption (Johnston et al., 1984; Cheung et al., 1984). Radiation in this wavelength region is thus allowed to penetrate more deeply, increasing the rate of photodissociation of species such as the CFC's, N_2O and HNO_3. The role of upper stratospheric ozone in controlling mid-stratospheric UV flux at these important wavelengths is also increased as the contribution of oxygen is decreased. The coupling of upper stratospheric ozone depletion to mid stratospheric photochemistry is thereby increased.

If CFC-11 and CFC-12 emissions are projected to be constant in the future, with other trace species boundary values fixed at current levels, the present model (Table 1) computes a 5.8% depletion of the vertically integrated ozone column abundance after 400 years (essentially the steady state value). Assumed emission rates are 264.5 million kg per year for CFC-11 and 412.2 million kg per year for CFC-12. Updating the model to the recommendations of JPL 85-37, for which the kinetic parameter changes are listed in Table 2, we calculate a depletion of 7% for slightly different constant emission rates of 309 for CFC-11 and 433 for CFC-12 in kg per year. (See WMO, 1986, for comparisons with other current models). The effect of these updated recommendations on the results of a multiple species scenario are discussed below. The calculated depletion is increased compared to the model used in this study.

III. THE CURRENT ATMOSPHERE

Any human activities that would significantly increase stratospheric abundances of HO_x, NO_x, ClO_x or BrO_x have the potential to bring about perturbation of stratospheric ozone. Various sources (e.g., stratospheric aircraft emissions of water and NO_x, use of fertilizers and solid propellant booster rockets) have been evaluated for their potential to increase the rate of the corresponding catalytic ozone destruction cycles (WMO, 1986; NRC, 1982). Increases in halocarbon emissions and the resultant stratospheric ClO_x enhancement are the subject of this report. However, given the photochemical complexities outlined above, even relatively small trends in source species, such as N_2O or CH_4, that may or may not be directly or indirectly anthropogenic, can affect ozone response to direct perturbations of other species (e.g., CFC's). For this reason, projected emissions and trends of all important source species must be considered as coupled in studying the ozone impact.

In this study we have investigated the effects of nonzero trends in CO_2, N_2O, CH_4 and Halons 1211 and 1301 (CF_2BrCl and CF3Br) on the ozone response to the central CFC perturbation. The halocarbons CFC-11, CFC-12, CCl4, CH_3CCl_3, CFC-22 and CFC-113 are considered in projecting future Cl emissions. There is strong observational evidence for continuing increasing trends for each of these species at present.

Two other species, CO and tropospheric NO_x, may be changing as a result of human activities with impacts on ozone and other species, but the observational cases for their trends are much weaker as is knowledge of source and sink strengths. There is some evidence that CO has shown an average annual increase of a few per cent over the last several years at Cape Meares, Oregon (Khalil and Rasmussen, 1984) and over 30 years in the Swiss Alps (Rinsland and Levine, 1985). Increases in tropospheric NO_x are probable as a result of combustion of fossil fuels in the developed world (Logan, 1983), biomass burning in tropical regions (Crutzen et al., 1979) and increasing air traffic (Liu et al., 1980; Wuebbles et al., 1983).

The reaction of CO with tropospheric HO is an important loss term for HO, which plays an important role in determining the lifetimes of many trace tropospheric constituents. An increase in CO leads directly to a decrease in tropospheric HO, all else being equal. CO oxidation can also contribute to ozone formation in the troposphere and the lowest part of the stratosphere, if sufficient NO_x is available. In the troposphere NO_x acts as a catalyst for ozone production, so that increases in NO_x emissions could increase the tropospheric contribution to the global ozone column, if the NO_x is dispersed into the global troposphere away from the localized source regions.

These species, CO and tropospheric NO_x, have been assumed in the present study to have no trends in source strengths; however, tropospheric concentration changes can occur as a result of changes following from other perturbers. Both of these species have relatively short atmospheric lifetimes and high variability, severely limiting the applicability of 1-D models in simulating their behavior. Additionally, for long-term projections only the effects of emissions occurring within the previous few years of the time of interest in the future would be significant. Anthropogenic emissions of CO and NO_x are, however, closely connected to processes, such as fossil fuel combustion, with evident long-term trends. Projecting the effects of these emissions ahead 90 years in a 1-D model on the basis of current knowledge would be very difficult, so the fluxes have been fixed at current levels (that is, the surface flux boundary condition that reproduces the current measured atmospheric abundance). Tropospheric ozone constitutes only about 15% of the total column, so that any errors introduced should be minor, at least for cases of significant stratospheric ozone perturbation. However, effects on surface air temperature from changing tropospheric ozone may be significant as a result of tropospheric ozone's greater role in infrared radiative transfer.

The potential for substantial stratospheric NO_x emissions from large commercial fleets of supersonic transports (SST's) operating at 17–20 km altitudes has also not been considered in this study. Because of the strong coupling of the NO_x and ClO_x cycles, SST emissions could significantly alter the response of ozone to CFC increases. The few Concorde SST's now flying should have an insignificant effect on the scenarios considered here.

III.A Historical Emissions

Scenarios projecting emissions into the future are started from a common initial condition of species concentration profiles, representing the 1985 atmosphere. These profiles are generated by integrating the time-dependent model over the past 135 years with historically based emission or concentration boundary conditions for the trace species CO_2, CH_4, N_2O, CFC-11, CFC-12, CCl_4, CH_3CCl3, CFC-22, CFC-113, and Halons 1211 and 1301. The initial conditions for the model integration of historical emissions are obtained from integrating the model to steady state with trace species concentrations fixed at preindustrial (1850) values, estimated either from direct or indirect observational evidence or by backward extrapolation of observed trends with knowledge of source and sink terms. The evidence, interpretations and current understanding of the reasons for trace species trends are developed more fully in WMO (1986). (See also Wuebbles et al., 1984, for specific background material used in the present study). The choice of 1850 as the start of a 135 year period to represent the period of anthropogenic perturbation of the atmosphere is loosely based on population growth and industrialization. Earlier start times for this period could have been chosen with little effect on the model results.

A good historical record is also available for CO_2 atmospheric abundances. CO_2 is essentially inert photochemically (though radiatively active) in the troposphere and stratosphere and the resulting long lifetime produces a well-mixed distribution with altitude over the domain of the model. It is cycled through the natural biosphere by respiration, biological decay and plant biomass production and is taken up by solution in the oceans, where it is used to produce skeletal materials by various organisms. A continuous record of the atmospheric mole fraction of CO_2 at Mauna Loa, Hawaii beginning in 1958 (Keeling et al., 1982) shows a continuing increase which appears to be the result of anthropogenic inputs from fossil fuel combustion and changes in land use (e.g., extensive biomass burning in clearing forest). Air occluded in the icepack in Greenland and at the South Pole during the 19th century has been obtained from stratigraphically dated ice cores and analyzed to contain around 280±10 ppm CO_2 (Oeschger et al., 1982). The current value of 345 ppm CO_2 in 1985 represents an increase of about 25% over the apparent preindustrial value. These data sets were combined with simple exponential best fits to produce the following piecewise continuous function:

$$CO_2(\text{mole fraction in ppmv}) = \left\{ \begin{array}{ll} 270.\ \exp[0.00141(t-1850)], & 1850 \le t < 1958 \\ 270. + 44.4\ \exp[0.019(t-1958)], & 1958 \le t \le 1985 \end{array} \right\} \quad (18)$$

Methane surface emissions appear to be primarily of biological origin, both natural and anthropogenically influenced (WMO, 1986). The relative importance of identified sources, including rice paddies, bogs, termites, biomass burning and cows, is in dispute, but the observed trend of increase appears largely reconcilable with population increase and accompanying changes in land use (Thompson and Cicerone, 1985; Levine et al., 1985). Continuous monitoring of CH_4 extends back to only 1977 and shows an increase of around 1% per year, averaged over the various available data sets (Blake et al., 1982; Rasmussen and Khalil, 1981). Sporadic direct CH_4 observations extend back to 1948 and ice core data are available for the pre- and early industrial period. A constant value of around

0.7 ppm on a volume basis is indicated by the ice core data that predates population and industry growth. Methane measured in more recently occluded air and a reanalysis of 1951 atmospheric spectra, giving a value of 1.14±0.08 ppm (Rinsland et al., 1985), are consistent with a long-term increase, reaching the present value of about 1.7 ppm. The historical trend used in this study, the following simple exponential fit for the surface CH_4 concentration based on the approximate average of the various data sets, was developed before firm ice core evidence was available and before the work of Rinsland and coworkers (1985):

$$CH_4(\text{mole fraction in ppmv}) = 1.0 + 0.65 \ \exp[0.035(t - 1980)]. \qquad (19)$$

The historical CH_4 changes used in this study (from about 1 ppm in 1850 to 1.28 ppm in 1951 to the present value) are smaller than those given in the more recent studies, but the effects on the 1985 initial condition atmosphere used for the projected emission studies should be small. Results on calculated surface temperature effects in the past reported below will, however, be somewhat underestimated.

Nitrous oxide is emitted as a byproduct of nitrification and denitrification by soil bacteria, but combustion processes appear also to contribute to global emissions (WMO, 1986). An extensive data set of surface tropospheric N_2O observations exists covering the last decade, showing an average annual increase of about 0.25% (Weiss, 1981). Air samples from 1961 and 1964, analyzed for N_2O, support this trend level back to that time. Weiss (1981) has proposed that the trend of increase results from fossil fuel combustion, such that the preindustrial concentration, about 285 ppb by volume, was about 5% lower than the current level of about 305 ppb. A preliminary analysis of ice core samples is now available which indicates a preindustrial value of around 275 ppb. The historical trend used here was developed on the basis of the discussion by Weiss, and is again represented by the following simple exponential expression for the surface concentration (or mixing ratio).

$$N_2O(\text{mole fraction in ppbv}) = 285. + 14.0 \ \exp \ [0.04(t - 1978)] \qquad (20)$$

The historical trends and model boundary conditions for the species discussed above are based on observations of surface atmospheric concentration or mixing ratio. While evidence of this sort is available for the industrially produced halocarbons (continuously since 1978 with various earlier measurements), estimates of historical surface emissions based on production data and estimates are also possible. These historical emission estimates (CMA, 1982 and OECD, 1981) are used in the model as boundary conditions for the chlorine-containing halocarbons other than the naturally produced species, CH_3Cl. CCl_4 emissions commence in about 1910, CFC-12 in the early 1930's, CFC-11 in the mid 1940's, CFC-22 and CH_3CCl_3 in about 1950 and CFC-113 in 1960. The emission profiles are characterized by initially steep rates of increase that decline as significant emissions levels are reached, roughly over the last 25 years. CFC-11 and CFC-12 are commercially attractive as refrigerants, blowing agents in foam and aerosol spray propellants. By the mid 1970's, use as aerosol propellants constituted about 60% of the total emissions (CMA, 1982), but since the restrictions on aerosol uses in 1978 and as a result of slowing global economic growth, net emission of chlorine in the form of long-lived industrial halocarbons has remained relatively constant. Nonaerosol uses have increased to 65% of total emissions, currently growing at an annual rate of about 6%. The observed atmospheric increases in

the chlorine-containing haloalkanes, with the possible exceptions of CFC-12 and CCl_4, can be more or less reconciled with industrial production inventories, considering the appropriate conditions for release of the individual species produced into the atmosphere. Eastern bloc emissions could account for the apparent discrepancies of production and atmospheric abundance increases.

Only recent atmospheric observations are available for the long-lived bromine species and industrial production in quantity has also commenced only recently. The small atmospheric mole fractions that are observed at present were included as boundary conditions for the last 35 years of the historical model integration to present. This assumption probably results in an overestimation of bromine abundance, but the present levels produce an insignificant impact on ozone.

III.B Effects of Historical Emission Trends and the 1985 Model Atmosphere

III.B.1 Historical ozone trends

Figure 3 shows the relative change in the vertically integrated column of ozone over the 135 year historical period considered in this study, an increase of 1.4%. The increase is mostly the result of the increases in CO_2 and CH_4 abundances. The actual long-term trend in the globally averaged vertically integrated ozone column is unknown; that is, the uncertainties in the accuracy of ozone monitoring over this period are much larger than any observed trend. The actual long-term behavior of stratospheric ozone has also been affected by factors and emission sources not included in this model (e.g., solar variability and the timing and magnitude of atmospheric nuclear testing). These effects and their impact are discussed in detail by Wuebbles (1983). The purpose here in the historical integration is to produce internally consistent initial conditions for the emissions projection model.

The evolution of the ozone profile referenced to the preindustrial (1850) profile over the historical integration is shown in Figures 4a and 4b. The small wiggles most evident in Figure 4a and other figures in this report at 13 and 34 km are computational artifacts of the temperature calculation and should be ignored. Absolute changes in the model ozone column are seen to be dominated by the methane-related ozone increase in the lower stratosphere (Figure 4a). A computed decreasing trend in the upper stratosphere appears in about 1960 as the Cl_z abundance first reaches a level of significance (Figure 4b). Whether these calculated upper stratospheric decreases have been observed is a topic of current study. A statistical study of the observations of the network of ground-based Umkehr ozone profile observing stations (Reinsel et al., 1984) has derived statistically significant linear trends in ozone abundance between 30 and 40 km. The derived negative trends of about 3% over the period 1970–1980 are consistent with the 1-D model results of Wang et al. (1986), which include factors such as the 11-year solar variability and atmospheric nuclear test series (Figure 5). Whether the short time record of the ozone-observing satellites is capable of yielding a statistically significant trend over their period of operation is a question complicated by instrument performance considerations.

III.B.2. Historical temperature trends

The radiative impacts at equilibrium that the changing trace gas abundances between preindustrial times and 1985 would have on surface temperature, as computed by the NASA/Goddard 1-D radiative-convective model, can be computed using the parameterizations briefly discussed above. The increase in CO_2 is responsible for around 70% of the calculated equilibrium surface temperature increase without feedbacks (referenced to 1985 in Figure 6) of 0.63°C between 1850 and 1985. The equilibrium surface air temperature increase of 0.79°C calculated by Ramanathan et al. (1985) for the preindustrial to 1980 time period with a full 1-D radiative-convective model is consistent with this value, if allowance is made for their treatment of relative humidity and surface air vs. surface temperature. Other trace species trends and the model calculated ozone and stratospheric water vapor profile changes contribute the remaining 30%, with the largest contribution from CH_4 (16%). These values are not intended to represent historical reality, since the realization of temperature change depends on many factors other than equilibrium radiative forcing, such as the thermal lag time of the oceans. At present, considering the current trends in the trace species, differential increase in CO_2 contributes about 50% to the total calculated surface temperature increase, CH_4 about 17% and the other trace species 32%. Thus, trace species other than CO_2 are increasing in relative importance.

III.B.3 1985 Atmosphere

The historical model integration discussed above provides a model representation of the current atmosphere that serves as the basis for the perturbation calculations. For a diagnostic study of the photochemistry of the present atmosphere, better results might be obtained by specifying variables, such as the temperature profile, to match representative present profiles. But since the focus of this study is on the calculation of ozone trends, the initial conditions (1985 atmosphere) are developed for self-consistency in the profiles of ozone, temperature and long-lived source species abundances. In this case, the absolute accuracy of model-predicted quantities such as the current ozone column is of lesser importance than the inclusion of important processes like temperature feedback. Further complications in comparing 1-D model species profiles to observations result from the large degree of latitudinal variability exhibited by many species, including ozone. Such variability can not be represented in a one-dimensional model. Although comparisons with the atmosphere should strictly be made only with globally averaged quantities, results of one-dimensional model are often compared with mid-latitude spring/fall observations. These comparisons should be considered essentially qualitative in nature since the 1-D model does not represent the atmosphere at any specific latitude. More details on comparisons of model results to observations are available in WMO (1982 and 1986), which contain extensive evaluations that include most observed species.

The 1985 vertical distribution of ozone produced by the model is compared in Figure 7 to a range of observed vertical ozone distributions taken from WMO (1982). In the upper stratosphere, where the rapidity of the photochemistry should diminish the effects of model inadequacies in atmospheric transport, ozone is underpredicted by 20–30%, an oft-noted discrepancy in the shape of the calculated ozone profile. The source of this problem, which is general among current one- and two-dimensional models, has not been identified,

although it seems to point to defects in the photochemical kinetics (Froidevaux et al., 1986). However, a Monte Carlo analysis of kinetic uncertainties in the model (Grant et al., 1986) generates a standard deviation of around 40% for upper stratospheric ozone abundance from the known kinetic uncertainties, so the model is not necessarily inconsistent with observed 40–50 km ozone abundances. In a similar study, Callis et al. (1985) noted that modifying the model chemistry within its uncertainties to better match satellite ozone observations produced other difficulties in comparison with the available satellite data.

The calculated profiles of N_2O, CH_4, H_2O, CFC-11 and CFC-12 are shown in Figures 8a–c. Also indicated are representative observational ranges from WMO (1982 and 1986) for N_2O, CH_4 and H_2O. Observational data for CFC-11 and CFC-12 were taken from Fabian (1986). All but CH_4 have relatively long lifetimes, 50 years or greater, and are well-mixed in the model troposphere. The calculated methane lifetime, 10 years, is also long enough to allow CH_4 to become well-mixed in the troposphere. Again with the exception of CH_4, the shapes of the curves in the mid- and upper stratosphere (the decrease in mole fraction) are controlled by the magnitude of the eddy diffusion coefficient assumed in the lower stratosphere and by the depth of penetration of short wavelength UV flux. Reaction with HO and Cl provide the stratospheric sink for CH_4. The K_z (diffusion or vertical transport coefficient) profile used is partly based on comparisons with observed N_2O and CH_4 profiles, so the agreement of the profiles of these species to observations is not completely independent of the model assumptions.

Model profiles of the abundances of several NO_z species are shown in Figures 9a and b. Profiles of ClO and HCl are shown in Figures 10a and b. In each case, the model values are not inconsistent with the available observations. As will be shown later, the ozone response to high ClO_x levels is sensitive to the mid-stratospheric total NO_z predicted by the model. The model employed here develops a maximum value of about 20 ppb of NO_z at 35 km. Several contributors to NO_z, including HNO_4, and N_2O_5, have not been observed quantitatively, although N_2O_5 was recently identified in spectra obtained from a shuttle experiment (Toon et al., 1986). A value around 18–23 ppb for total mid-stratospheric NO_z can be inferred from the measured species and calculated relative abundances for the others (WMO, 1986 and Callis et al., 1985 and 1986).

The computed 1985 stratospheric temperature profile is compared to the U.S. Standard Atmosphere (1976) profile in Figure 11. The increase in temperature with increasing altitude in the stratosphere results largely from the greater O_3 solar heating. Many of the reactions controlling ozone abundance in the stratosphere exhibit a temperature dependent rate constant, so that changes in the ozone profile and thus local temperature feed back into the loss terms in the continuity equation for O_3.

In the model of the 1985 atmosphere, NO_x is the dominant catalyst for odd oxygen destruction, accounting for 36% of stratospheric loss (Figure 12). Catalytic cycles involving HO_x and O_x reactions account for 27 and 14%, respectively, of stratospheric odd oxygen loss, occurring mostly in the upper stratosphere. HO_x increases in the lower stratosphere (for example as a result of CH_4 increase) actually increase ozone through interference with the distribution of species in the NO_z family. By shifting NO_z into the inactive HNO_3 form, NO_x catalytic rates are reduced. A similar effect follows from small ClO_x increases in the lower stratosphere, through formation of $ClONO_2$. HOO and ClO also

oxidize NO, interrupting the NO_x catalytic cycle and reducing its efficiency. This negative feedback depends on the net relative importance of NO_x-catalyzed ozone destruction. If stratospheric NO_x abundance were smaller, the compensating effects would also be smaller. This behavior can be seen in some of the results discussed below.

ClO_x has a share of 22% in ozone destruction in the 1985 model atmosphere. The total abundance of Cl-containing species in the model's upper stratosphere is 2.3 ppb. Bromine based catalytic cycles account for only 0.2% of the odd oxygen loss in 1985, occurring mostly between 20 and 30 km. Finally, about 1% of the stratospheric ozone production is transported downward across the tropopause, eventually to be lost by dry deposition at the model surface.

IV. PROJECTED EMISSIONS

In the discussion above, CFC-11 ($CFCl_3$), CFC-12 (CF_2Cl_2), CCl_4, CH_3CCl_3, CFC-22 ($CHFCl_2$), CFC-113 (CF_2CFCl_2), Halon 1211 (CF_2ClBr), Halon 1301 (CF_3Br), CH_4 and N_2O have been identified as significant or potentially significant sources for reactive photochemically-generated stratospheric species responsible for determining the loss rates for stratospheric odd oxygen and several are important in infrared radiative transfer. CO_2 is a direct participant in establishing both tropospheric and stratospheric temperature profiles and indirectly affects the kinetic rates of important stratospheric reactions. Additionally, atmospheric observations of the abundances of these compounds, available over periods of varying length, have demonstrated upward trends continuing to the present. Continuation of these observed trends for a period on the order of a century would result in a substantial increase in the abundance of stratospheric chlorine and increases in stratospheric water vapor, HO_y and NO_y. Future increases in source species are here projected for periods up to 90 years, using the LLNL time-dependent 1-D model to evaluate concomitant ozone and temperature changes.

IV.A Halocarbons

Projected production and release values are based on the analysis of Quinn et al. (1985) for most of the fluorocarbons and the Halons and work by ICF, Inc. (S. Seidel, private communication) for CFC-22 and in some cases for CFC-11 and CFC-12. The U.S. Environmental Protection Agency supplied a series of halocarbon scenarios interpolated across the range of possibilities developed in the original studies. It is important to note that RAND (Quinn et al., 1985) claims no a priori economic reasons to rank the RAND scenarios among themselves with respect to likelihood. The presumption is, however, that the range of scenarios covers a significant portion of the range of probable future emission curves, developed as they are from economic growth assumptions varying from purposefully pessimistic (slow growth of world economy) to purposefully optimistic (rapid growth of world economy). The range of halocarbon scenarios investigated in this study actually exceeds the range of the seven RAND scenarios. The authors of WMO (1986) rightly point out the extreme uncertainties incumbent on such predictions over periods extending to 90 years. A particular RAND scenario (Later Market Maturation Scenario VI) was picked by the EPA, in conjunction with projections for other species discussed below, as a reference scenario. This designation is not intended to imply anything about its probability within the full range of RAND scenarios or within the range of scenarios in this report.

For the major chlorofluorocarbons, CFC-11 and CFC-12, projections over 90 years were broken into three segments. For the period 1985 to 1990, extensive surveys, current market trends, industry projections and industry experts were consulted, with a concensus choice of an average annual trend of about 5%. Econometric analysis was applied to the period 1990 to 2040. From the historical behavior of the US CFC market, Quinn et al. (1985) derived elasticities as a function of stage of market growth. The elasticity is defined as the relative growth in CFC use for a 1% increase in GNP per capita. For example, the elasticity in the nonaerosol US market over recent years is about 3; that is, the production of CFC's to meet nonaerosol needs increased three times as fast as per capita GNP. Estimates of population and GNP growth for the various world regions were then combined with the life cycle model, involving assumptions concerning the stages of market maturity and the elasticities to produce estimates of annual growth worldwide. For the designated reference scenario, Quinn et al. (1985) estimated worldwide growth in the period 1990–2000 to average 5.0% annually for CFC-11 and 3.2% for CFC-12. Between 2000 and 2040 emissions were projected to increase 2.4% annually for both species. Emissions after 2040 were assumed to increase at an annual rate of 1.7%, based simply on projected growth in GNP per capita (unit elasticity). This reference case (Figure 13) is intended to represent healthy development of the CFC markets and approximates a 2.5% compounded annual increase in CFC-11 and CFC-12 emissions over the 90 year period considered, an increase of a factor of 9.2 over 1985 fluxes in 90 years. The exact figures used are compiled in Appendix A.

Information on CCl_4 (the CFC feedstock), the solvents CH_3CCl_3 and CFC-113, the mobile refrigerant CFC-22 and the fire extinguishents Halons 1211 and 1301 is scarcer and projections more difficult. Where sufficient information was available, elasticities were evaluated, otherwise unit elasticity was assumed. The annual percentage rates of increase used in the reference case were:

	Global Annual Rates of Change (%) Period of Analysis			
Species	1985–1990	1990–2000	2000–2040	2040-2075
CFC-113	3.9	6.7	1.9	1.6
CFC-22	9.5	6.6	3.5	1.9
CCl_4	4.1	1.9	1.7	1.6
CH_3CCl_3	2.2	2.2	1.9	1.6
1301	5.9	8.4	3.1	1.7
1211	6	8	2.8	1.7

Curves representing the assumptions for growth over the 90 year period are shown in Figure 14 for each of these species, and the emission rates are tabulated in Appendix A.

Among other scenarios, Quinn et al. (1985) also developed an alternative growth scenario for CFC-11 and CFC-12 (Figure 15a) using elasticities at the lower end of the expected range and using conservative assumptions about future CFC use in the various global regions. Elasticities of 0.5 for CFC-11 and CFC-12 in the developed nations and 1.0 in the Eastern Bloc and developing nations combine to produce a global average annual

growth in emissions that remains at about 1% over the entire 90 year period. Correspondingly conservative (slow growth) assumptions were made for the minor halocarbons; for example, CFC-113 was assumed replaced as a defluxing agent in electronics with other methods. Halon emissions in 1985 were arbitrarily halved, while the growth rates were assumed equal to those in the reference case. The global annual percentage rates of change were:

	Global Annual Rates of Change (%)			
Species	1985–1990	1990–2000	2000–2040	2040–2075
CFC-113	3.9	2.4	1.9	1.6
CFC-22	5.5	4.2	1.3	1.0
CCl_4	-15.0	1.9	1.7	1.6
CH_3CCl_3	2.2	2.2	1.9	1.6
1301	6.0	8.0	3.0	1.7
1211	6.0	8.0	3.0	1.7

These projections are shown in Figure 15b and tabulated in Appendix A.

An alternative high growth rate scenario (Figures 16a and b and Appendix A) was supplied by the EPA, adapted from exponential econometric fits for CFC-11 and CFC-12 elasticities, developed by ICF. Growth patterns for CFC-113 were based on projected expansion in degreasing and defluxing and exponential elasticity expressions for CFC-22. The rates of increase in this scenario are:

	Global Annual Rates of Change (%)			
Species	1985–1990	1990–2000	2000–2040	2040–2075
CFC-113	3.9	6.7	1.9	1.6
CFC-11	14.0	7.2	7.6	9.4
CFC-12	7.6	6.0	4.0	6.0
CFC-113	13.0	10.0	5.0	1.6
CFC-22	11.0	8.1	4.0	5.3
CCl_4	4.1	1.9	1.7	1.6
CH_3CCl_3	2.2	2.2	1.9	1.6
1301	6.0	8.0	3.1	1.7
1211	6.0	8.0	2.8	1.7

II.B Other Trace Species

Past increases in CO_2, CH_4 and N_2O, while generally correlated to increasing population and industrialization, involve biospheric and geophysical processes in major roles. For CO_2, emission increases have been projected based on predicted demand and availability of fossil fuels (Edmonds et al., 1984). An analytic fit to Edmond's midrange values was used in the reference scenario and for most other runs, as described by:

$$CO_2(\text{mole fraction in ppmv}) = 341.4 + 1.539(t - 1983)\exp[0.009173(t - 1983)] \quad (21)$$

and is approximately equivalent to a 0.74% annual growth rate, producing a 96% increase over 1985 levels in 2075. An alternate scenario expression was based on the Edmond's low growth case:

$$CO_2(\text{mole fraction in ppmv}) = 341.4 + 1.82(t - 1983)\exp[8.34 \times 10^{-5}(t - 1983)] \quad (22)$$

with a nearly linear increase of 1.82 ppm annually, giving 50% growth by 2075.

The justification for projecting a continuing increase in N_2O comes from the observation that the current annual abundance increase of 0.25% represents more than 30% of the current atmospheric sink for N_2O (WMO, 1986), so that the current source is substantially out of balance with the sink. The additional source is presumably of anthropogenic origin. A gradual increase in N_2O to a value around 30% higher than present levels is expected, even if the current source strength stays constant. The observational data do not show whether the current small abundance increase is linear or geometric, but the differences over the next 90 years between the two formulations are not great. Both approaches give around a 20% increase in 2075. We have projected an annual increase of 0.25% in the N_2O surface concentration.

Although no alternative scenarios were promulgated in this study for N_2O, several runs were made in which the stratospheric NO_z abundance, for which surface emissions of N_2O are the chief source, was artificially enhanced or suppressed. This was accomplished by altering the branching ratio for the reaction of N_2O with $O(^1D)$,

$$N_2O + O(^1D) = 2\ NO$$

$$N_2O + O(^1D) = N_2 + O_2. \tag{23}$$

Observational indications are that the NO_z value is known to perhaps $\pm$ 10%. The behavior of the model was investigated at values of 17.8 ppb and 22.2 ppb, compared to the value of 20 ppb generated by the standard model. An extreme value of 12.4 ppb of stratospheric NO_z was also investigated, representing a value in the range of the lowest of current theoretical models (WMO, 1986).

An argument similar to the N_2O discussion above can be made for CH_4 surface emissions. The current observed increase in CH_4 abundance exceeds the model's atmospheric sink term by about 20%, so that a continued increase over a few decades to a level 20% above current values would occur even if the surface flux were held constant at current levels. Several additional considerations are important in the case of CH_4, however. The 1951 to 1985 observations can be equally well reconciled with a linear increase as with a geometric increase, although for CH_4 the growth rate (between 1 and 2% annually) is large enough that substantial differences arise between the two extrapolations after 90 years. Also, while the lifetime of N_2O exceeds the 90 year period of interest, many lifetimes of CH_4 pass during the model simulation. Methane abundance toward the end of the run is almost entirely dependent on emissions occurring several decades into the future, greatly increasing potential uncertainties.

Finally, projections can be made on the basis of surface flux or surface concentration. Since the abundances of CH_4, CO and tropospheric HO are closely and mutually interdependent, specifying the CH_4 surface concentration trend effectively removes a feedback mechanism from the model, whereby an increasing CH_4 concentration will increase the CO concentration. In the absence of sufficient tropospheric NO_x, tropospheric ozone will be decreased. All of these factors tend to diminish tropospheric HO, which lengthens the lifetimes of CH_4 and CO. Atmospheric concentrations of CH_4 and CO would then be increased even with constant surface emissions, in a system of positive feedback. However, if sufficient NO_x is present in the troposphere, O_3 can be increased. This can increase

HO, which is also increased as a byproduct of CH_4 oxidation in the presence of NO_x. This potential negative feedback shortens the CH_4 lifetime and opposes the effect of increasing surface emissions on the CH_4 concentration. Other processes, such as the CO increase, would compete by tending to decrease HO. Such feedbacks are allowed to occur in the model if the CH_4 surface flux rather than the surface concentration is specified as a boundary condition. However, a complete and proper treatment of these feedbacks requires a representation of tropospheric processes that includes the effects of spatial and temporal variability (i.e., a 3-D model).

A difficulty arises, however, in determining how the surface emissions must have changed with time before the present and therefore in justifying any projection for the future. While it is clear that CH_4 emissions have increased from preindustrial times, the rate of increase that reproduces the observed concentration increase depends on CO, which is also affected by direct emissions and emissions of higher hydrocarbons (e.g., plant hydrocarbons), and surface emitted NO_x, for which trends are not available. In this report, we employed a variety of CH_4 boundary conditions, specifying annual percentage changes in either surface concentration or surface flux, which are summarized in Appendix A. Until better understanding of the CH_4 source distribution and sensitivities is developed, none of the scenarios developed can be considered more or less likely than the others. We note here that a compounded 1% annual increase, used as a concentration boundary condition in the reference case, produces a doubling in 70 years (2055) and an increase by a factor of 2.44 in 90 years (2075).

V. REFERENCE CASE

The development of the projected future emissions or abundances of the various trace source species has been discussed above. For the purposes of detailed discussion of model results, a reference case or multispecies scenario has been selected from the range of projected possibilities, as they are understood at present. Results of other scenarios and studies of model sensitivity to projections for individual species in the multispecies context are also discussed below and in the Appendices. The reference case should not be considered as "most likely" or a "best guess," but since it falls in the mid-range of scenarios considered, it is used below as a basis for a detailed analysis of model results.

V.A Ozone Changes

The change in the total column of ozone relative to the 1985 column for the reference scenario is given in Appendix B and Figure 17. It is striking that although this global and annual average estimate of ozone depletion reaches about 20% after 90 years, half of the depletion occurs in the last 15 years of the simulation. Depletion over the first 50 years is less than 5%. This very slow initial decrease results from both the mitigating effects of the concomitant increases in CH_4 and CO_2 and nonlinearity in the ozone response to Cl_z increase.

A more detailed view of the various factors affecting stratospheric ozone in the reference scenario is gained by considering changes in the ozone concentration profile as a function of time, as shown in Figures 18a and b. For approximately the first 30 years, ozone depletion above 30 km from the direct effect of increased ClO_x catalytic cycle activity is

roughly balanced by an ozone increase below 30 km. This increase results largely from three sources: increased odd oxygen production or 'self-healing', ClO_x interference with the NO_x catalytic processes and CH_4 oxidation, which produces ozone and HO_x, which interferes with the efficiency of NO_x cycles. The increased odd-oxygen production follows from the deeper penetration of solar UV at wavelengths below 242 nm, which is capable of dissociating O_2. Atmospheric transmittance is increased in this wavelength region by the decreased overhead burden of O_3, the chief atmospheric absorber at wavelengths above about 207 nm. The increase in ClO that follows increasing CFC emissions increases the rates of reaction with both NO and NO_2. The reaction with NO_2 to form $ClONO_2$ reduces the fraction of total stratospheric NO_z that is present in catalytically active forms. The reaction with NO reduces the efficiency of the chlorine cycle. Similarly, increases in HO and HO_2 reduce the catalytically active fraction of NO_z by forming HNO_3 and HNO_4.

At later times, as the Cl_z abundance equals and exceeds the NO_z abundance in the 25 km region, the ability of interactions among the radical families to mitigate the impact on ozone diminishes. Chlorine catalytic cycles displace NO_x cycles as the primary odd oxygen loss mechanism in the altitude region of the ozone peak and in the stratosphere as a whole.

The relative change in ozone with time is seen to reach a maximum around 40 km. Because the fraction of the ozone column in this region is small, the contribution of the change in this area to the total column change is also small. But the possibility of early detection of concentration changes at 40 km is much better than for detecting the expected changes in the total column. Expected capabilities in satellite observing platforms should be able to reveal ozone changes of 0.2% per year at 40 km over 5 to 10 years of operation at the 95% confidence level (WMO, 1986). Changes of this magnitude are predicted by the model within the next 20 years for most of the scenarios investigated.

The dashed line shown in Figure 17 is the result of a model run with the reference case scenario but with the kinetic and photochemical input parameters updated to the recommendations of JPL 85-37 (1985). The rate constants that were updated are listed in Table 2. Very small changes were also made to the incoming solar flux and to ozone absorption coefficients. The Herzberg continuum absorption of oxygen was also reduced slightly. The net effect of these changes was to significantly increase the magnitude of the calculated ozone column depletion throughout the 90 year integration for the reference case scenario, increasing the relative ozone change value from 20 to 32% after 90 years.

In general, the ozone column change in the model updated to JPL 85-37 recommendations is more linear with respect to time and increase in stratospheric Cl_z abundance than is the model used in this study. The importance of interactive effects between families of odd-oxygen loss catalysts seems to be reduced. Certainly this is the case for the odd hydrogen loss rate, which depends chiefly on reactions of HO with HNO_3 and HNO_4 in the pre-update model and more on the reaction of HO with HO_2 in the updated model. Changes were also made in the rates of important reactions in ClO_x chemistry, but a full interpretation of these results is beyond the scope of this study. While the quantitative aspects of this study are affected to some extent, the overall conclusions on the magnitude of uncertainties in the effects of scenario assumptions should not be heavily dependent on the use of the earlier model version.

V.B Temperature Changes

From the surface mole fraction values of CO_2, CH_4, N_2O, CFC-11 and CFC-12 as functions of time (Appendix C), model-derived profiles of O_3 and H_2O and the parameterized radiative response expressions, the change in equilibrium surface air temperature from the changed radiative forcing can be estimated. The calculated equilibrium increase, without feedbacks, reaches 1°C, for reference case trace species abundances in 2035, and 2.08°C for abundances projected for 2065. The calculated equilibrium surface temperature change is more linear with time and with increase in the radiative species abundances (Figure 19) than is the ozone response. About half of the increase is caused by CO_2 and 40% by the combined effects of increases in the other long-lived infrared absorbing species. The remaining 10% results from alteration of the O_3 and stratospheric water vapor profiles during the model calculation. The order of importance of the direct radiative effects, relative to the CO_2 effect, among the trace species other than CO_2 after 80 years is CFC-12 (35%), CFC-11 (22%), CH_4 (18%) and N_2O (7%). The change in stratospheric water vapor profile that results from the CH_4 increase accounts for 6% and the change in ozone profile that results from the combined effects of all the trace species trends contributes 10%.

The coefficient of sensitivity for surface temperature change at equilibrium to the radiative forcing of CO_2 assumed in the parameterization used here is very close to the 1.2°C change for doubled CO_2, quoted as the best representation of current knowledge (NRC, 1983). Considering the range, 1.25 to 3.75, of the feedback amplification factor for temperature changes from CO_2 radiative forcing in GCM models, the equilibrium surface temperature change could vary from 2.5 to 7°C in for trace species abundances reached in 2065 (dashed lines in Figure 19), if the climate system were at equilibrium with the radiative forcing. These estimates are based on simple multipliers which roughly represent the results of current climate models. Actual future changes in temperature will depend on the time response of the climate system, which is not considered here.

Again, as for the changes in ozone abundance, the upper stratospheric temperature changes are larger, with a decrease of 16°C at 40 km after 40 years and 37°C after 80 years (Figure 20).

VI. OTHER SCENARIOS AND SENSITIVITY TO ASSUMPTIONS

The results of the reference case scenario represent only one of the possible outcomes that could arise from different combinations of plausible assumptions of trends in source species. The sensitivity of the predicted ozone depletion (and surface temperature change) to the emissions assumptions must also be known to establish the uncertainty in the result, the range of possible outcomes and the feasibility of regulation. Several approaches to investigation of the model's sensitivity to the choice of scenario are possible. First, various alternative scenario assumptions can be made to test the effects of, for example, greater CFC production, regulatory production caps or declining methane, alone or in combination on ozone and temperature. For analyzing ozone change, a second approach is to calculate the ozone response to trends in individual perturbers and then to evaluate the magnitude of cross terms between simultaneous trends in a number of species. Results of applications of both approaches are discussed below.

VI.A Alternate Scenario Results

VI.A.1 Ozone

For a given multiple species coupled scenario, the nature of the ozone response will depend on the details of specified emission increases for the various source species, which determine chiefly whether odd oxygen loss will remain dominated by NO_x reactions or shift to control by ClO_x. In this study, 36 individual scenarios were investigated with the model, covering a range of time-dependent CFC growth rates in combination with several assumptions on CH_4, CO_2 and Br_x emission increases. The change in total column ozone for each of the 36 scenarios investigated is tabulated in Appendix B.

The ozone column responses to the EPA-supplied "high" and "low" CFC emission scenarios, described previously in the discussion of emission projections, are depicted in Figure 21; compare to the reference scenario case, Figure 17, which is intermediate in terms of CFC emissions. Assumed N_2O, CO_2 and CH_4 trends for Figure 21 are identical to the reference scenario. In the "high" case, CFC emissions increase so rapidly that trends in other species play a minor role in affecting the ozone change. The ozone column response with time is strongly nonlinear as a result of the exponential nature of the CFC increases. A depletion of 20% is reached after 35 years (2020) and 60% after 40 years (2025), by which time the validity of the model has probably broken down. The "low" case ozone response is also somewhat nonlinear with time, with an ozone depletion of 1.5% over the first 50 years and an additional 2.3% over the subsequent 40 years. Interaction among families and increases in N_2O, CO_2 and CH_4 with time are relatively more important in the "low" case, given the gradual CFC increase.

The range of calculated change in the ozone column for the full range of multispecies scenarios, with the exception of the run with very low NO_z, is indicated by the area between the dashed lines in Figure 21. For about the first 25 years, the spread, or the uncertainty arising from uncertain scenario projections is distributed about the reference case value by a few per cent, skewed somewhat toward larger depletion. Between 25 and 40 years from present, the scenarios with the largest increases in halocarbon emissions (chiefly emissions of CFC-11 and CFC-12) diverge quickly from the reference case to very large ozone depletions. The spread of results at 40 years varies from +0.46% to -66%, demonstrating the great importance of uncertainties in projections of future emissions and concentrations, as well as the potential for alleviation of ozone depletion by control measures.

The dotted curves in Figure 21 show the total column ozone changes calculated using the updated rate parameter recommendations of JPL 85-37 (1985) for scenarios 4 and 5, the "low" and "high" cases, respectively. The results are in both cases more negative, as was the reference case result. Because trace species other than the CFC's increase relatively more rapidly in the low CFC scenario 4 than in the high CFC sceanrio 5, interactions among catalytic cycles are more important in the low case than the high case, as mentioned above. The rate parameters recommended in JPL 85-37 tend collectively to reduce the efficiency of catalytic cycle interactions, so that the change in chemistry affects the low case more than the high case. The reference case, discussed above, falls in the middle in this respect.

Brasseur et al. (1985) used a 1-D radiative-convective model with photochemistry to study the change in the ozone column caused by a multispecies scenario with constant CFC emissions at current levels. They obtained an increase in the ozone column of about 3% over 90 years from the present. Although the details of the scenario assumptions differ, a similar run with the model used here produced a 1.5% increase. The scenario differences in the Brasseur et al. calculation, faster CH_4 growth, smaller CFC emissions and projected increase in tropospheric NO_x, would be expected to favor a larger ozone increase, so there appears to be essential agreement between the two models.

Calculated changes in local ozone concentration in the upper stratosphere are more closely grouped for the range of scenarios than are the changes in vertically integrated ozone column. All scenarios predict a significant decrease in upper stratospheric ozone (Figure 22), resulting from increased Cl_z abundance. Near 40 km after 20 years, the calculated decrease in local ozone abundance ranges from 10 to 30%. After 90 years, the calculated decrease at this pressure level varies from 26 to > 80%.

The impact of policy alternatives for the regulation of CFC emissions was also investigated using several CFC emissions growth scenarios supplied by EPA. The results are presented in Figure 23. Issues related to regulation include sensitivity of ozone changes to the timing, method and degree of regulation and to the nature of the unregulated scenario to which the results of regulation are compared. In the cases investigated in this report, regulatory delays of the order of 10 years had little impact on the final (90 year) outcomes. The choice of unregulated scenario and the degree of CFC emission restriction were of greater significance.

VI.A.1.a Effects of methane projections

Since the proximate causes of the observed methane increase are at present uncertain, several assumptions other than a continued 1% annual increase in CH_4 surface abundance were investigated for common CFC growth scenarios (the reference case already discussed and a case with 2.6% average annual CFC-11 and CFC-12 increase). Three scenarios, in which the CH_4 surface flux rather than the surface abundance was assumed to increase at various compound growth rates, were compared to the reference case assumption of a 1% annual concentration increase (Figure 24). Two additional scenarios, one assuming a geometric (compound annual) increase in CH_4 flux and one assuming a linear increase, but both corresponding to an initial annual concentration increase of 1.5%, were also investigated. Over the 90 year period the geometric scenario continues to produce the same CH_4 concentration growth rate, resulting in a 12% O_3 depletion after 90 years, while the linear case drops to an average 0.9% annual rate of CH_4 concentration increase and produces a 21% ozone column depletion. A third case of monotonic geometric flux increase that gives only a 0.4% concentration growth in the first few years results in an 18% ozone column depletion and a 90 year average annual CH_4 growth of 1.1%. These results show that substantial uncertainty in long term ozone depletion can arise even among monotonic CH_4 growth projections that would reproduce the currently observed surface concentration growth rate of 1%.

If the future of CH_4 surface emission is not monotonic growth, the uncertainty in ozone change from CH_4 projection assumptions increases. Four cases were compared, with a 1%

annual flux increase to 2010 followed by either (1) 1% annual decrease to 2030, then zero trend, (2) zero trend from 2010, (3) 1% annual increase to 2075 or (4) 2% annual increase to 2075. The ozone column depletion values range from 8% to 62% in 2075 (Figure 25). As expected, higher levels of methane corresponding to faster emission growth rates are associated with smaller ozone column depletions.

Model runs with "high" case CFC projections show that when Cl_z gets large rapidly, uncertainties arising from CH_4 projections shrink. Cases with methane increasing at 0.5%, 1% and 1.5% annually (Figure 26) differ only by a few years in reaching extremely large ozone depletions. Conversely, for the "low" CFC growth case, assuming a methane trend of 1.5% annually rather than 1% is sufficient to change the sign of the ozone column change. After 90 years, the ozone column has increased by 3.4% (Figure 27).

VI.A.1.b Effects of Halon emissions

The effect of the projected reference case growth in Halon emissions was investigated relative to scenario 1A, a case with mid-range CFC growth. Fixing the abundances of the bromine source species, Halons 1301 and 1211, at the current very small levels reduced the ozone impact of scenario 1A by a factor of about 0.8. The increases in the bromine source species projected here contribute between 4 and 5% to the ozone column decrease after 90 years (Figure 28). This nonnegligible contribution, despite the small projected emissions compared to CFC-11 and CFC-12 (about 1%), demonstrates the efficiency of BrO_x in catalyzing odd oxygen loss in the model.

VI.A.1.c Effect of CO_2 projection

The difference between the reference and alternative lower rates of CO_2 increase discussed previously is small enough over 90 years and the effects of other simultaneously varying species are large enough that the sensitivity of the ozone column change to the CO_2 scenario choice is small. The calculated depletion in the ozone column for both alternatives in a mid-range CFC scenario differs by only 1% in the 25% depletion calculated at 90 years from present.

VI.A.2 Effects of stratospheric NO_z abundance

The importance of the interactions between the various families of reactive particularly NO_x and ClO_x, has been discussed previously. For two model runs the branching ratio for NO production in the reaction of N_2O with $O(^1D)$ was modified to artificially enhance or suppress the mid-stratospheric abundance of NO_z by about 10%. This change affected the initial conditions generated by the integration of historical emissions as well as the integration of projected emissions, so that the change in ozone column from the CFC and other species perturbations can be directly compared. The expected behavior, NO_z's mitigating role in determining the efficiency of ClO_x catalytic ozone destruction, was observed in the results (Figure 29). At an NO_z value of 22.2 ppb, compared to the standard model's 20 ppb, the impact of a mid-range CFC emission case (2.6% average annual increase) on ozone is reduced from a depletion of 26% at 90 years to 15%. When NO_z is reduced to 17.8 ppb, the 2075 depletion is more than doubled to 42%.

No cases were run in which surface N_2O concentrations increased at other than 0.25% annually, but the effect of a larger positive trend would be to flatten the total column ozone depletion curve with time, depending on the rate of CFC increase. A faster initial N_2O increase would cause faster initial ozone depletion, through the direct effects of the NO_x catalytic cycle. Further into the scenario, when ClO_x catalytic destruction is dominant, increased N_2O produces increased stratospheric NO_x, with the effect, shown above, of reducing the ozone decrease for scenarios with CFC annual increases of around 2%.

VI.A.2 Temperature

The calculated changes in stratospheric temperature show a smaller spread with scenario than the calculated ozone changes. This follows from the dependence of the stratospheric radiative equilibrium temperature mostly on local ozone abundance and the CO_2 atmospheric mixing ratio. The narrower spread of the calculated upper stratospheric ozone change relative to the calculated total ozone column change and the relative certainty of CO_2 increase (0.5–0.6% per year) tend to produce a restricted range of temperature change (Figure 30). The alternate CO_2 scenarios differ by less than 5% in the calculated stratospheric temperature decrease at about 45 km in the case of mid-range growth in halocarbon emissions. The variation in local upper stratospheric ozone depletion among the various halocarbon scenarios has a larger effect on the calculated temperature change, producing a range of 18 to > 40°C decreases after 80 years at 45 km. Around 10°C of this decrease results from the CO_2 increase, ozone decrease accounting for the rest.

Calculated surface temperature changes also do not vary as widely with scenario as for the ozone column. Where the effect on the ozone column represents a precarious balance of competing effects (e.g., CH_4 increase and CFC increase) increases in the various radiatively active species all serve to warm the surface. Mid and upper stratospheric ozone, which is of major importance in controlling the ozone column change, plays only a minor role in affecting the surface temperature. The equilibrium temperature increases for the radiative forcings of several scenarios range from around 1.3 to 2.2°C for trace species abundances reached in 80 years and are shown in Figure 31. Incorporating the climate feedback amplification discussed above increases the surface temperature change and its range from 1.6 to 8.2°C.

The increase in CO_2 accounts for between 50 and 70% of the calculated temperature increase in all cases. The combined direct radiative effects of increases in CH_4, N_2O, CFC-11 and CFC-12 contribute between 25 and 40%, with an average over the scenarios of about 30%. The direct effects of CFC-12 and CH_4 usually dominate over those of N_2O and CFC-11. The changes in the ozone vertical profile and stratospheric water vapor profiles that are produced by the trends in the various source species account for the remaining 10% of the calculated equilibrium surface temperature increase.

VI.B Analysis of Ozone Sensitivities

In the model runs previously discussed, various combinations of two or three trend or abundance assumptions for CFC's, CH_4 and mid-stratospheric NO_z produced a range of ozone change from a small increase over the 90-year projection to remarkable decreases after only 35 years. The question therefore arises whether these results can be systematized, for

example by identification of a small number of controlling variables. Although it is just the purpose of the model to include the nonlinearities and couplings inherent in this complex problem, it may be possible to explain the major characteristics of the ozone predictions based on a small number of factors involving the scenario assumptions and model behavior.

As discussed previously, there are two major regimes in the response of the ozone column to coupled perturbations involving large increases in stratospheric chlorine abundance. For conditions in which the family of nitrogen oxide-based catalytic reaction cycles dominates photochemical destruction of odd oxygen, the terms important to consider include the direct effect of chlorine increases on upper stratospheric ozone, the effect of chlorine increases on the nitrogen oxide reactions and the effect of methane increases and temperature decreases on the NO_x and HO_x catalytic cycles. For the alternate regime in which ClO_x cycle rates exceed the NO_x rates, the effects of NO_x and HO_x (produced by CH_4) increases on the chlorine species and cycles are most important. The sensitivity of the ozone column to increases in given species can vary between the two regimes and can even change sign.

Figure 32 shows the time dependence of the ozone depletion for the reference case CFC trend projections, but with CO_2, N_2O and CH_4 held fixed at 1985 surface abundances A calculated ozone depletion of 54% is obtained at 90 years [2] compared to 20% in the multiple scenario reference case. However, ozone depletion at 50 years is only increased from 4.3% to about 7%, demonstrating the strong nonlinearity of the sensitivity of ozone to Clx abundance. In Figure 33, the percentage ozone depletion in the CFC-only case is plotted against the total abundance of chlorine-containing species at 55 km. A knee in sensitivity is observed, occurring at around 20 ppb and 20% column ozone depletion. For Cl_z increases from 1985 of less than 15 to 20 ppb (by volume) the relative ozone column depletion for a unit absolute increase in Cl_z is less than a fifth of the sensitivity for a unit Cl_z increase when the total Cl_z concentration exceeds about 20 ppb. A very similar curve, also shown in Figure 33, is obtained when the ozone depletion for the case of "high" CFC emission projections is plotted against absolute change in Cl_z rather than time. In this case, a change of 30 ppb in Cl_z is reached after only 40 years rather than the 90 years of the reference case, and the trends in the other species have not yet resulted in increases which could effectively mitigate a portion of the Cl_z impact.

The absolute ozone profile changes in the CFC-only reference case (Figure 34 compare to Figure 18a) show that the source of the nonlinearity lies in the region of the ozone maximum, 20 to 25 km, and is the result of the reactions

$$ClO + NO = Cl + NO_2 \tag{24}$$

and

$$ClO + NO_2 + M = ClONO_2 + M. \tag{25}$$

When the ClO abundance in the mid stratosphere reaches the point at which $ClONO_2$ is the dominant NO_z species and NO is substantially suppressed, significant amounts of NO and NO_2 are no longer available for reaction, and additional ClO introduced by increasing

[2] This depletion is past the point where the validity of the model structure, lacking feedback to the transport parameterization, is expected to hold.

emissions participates in catalytic cycles with enhanced efficiency in the region with the greatest potential for ozone loss. This effect has also been discussed by Stolarski and Douglass (1986), who term it a "titration" of NO by the reagent ClO.

From the above discussion, it appears that the degree of ozone depletion produced by increased CFC fluxes, in the absence of complicating nonzero trends for other species, does not depend on the rate of increase of the CFC flux (the scenario) within reasonable limits, but only on the absolute increase. This result is expected for the 1-D model for situations in which the odd-oxygen controlling photochemistry can come into equilibrium with slowly varying long-lived source species.

The time scales of photochemical processes vary widely for different constituents and altitudes and in comparison to transport time scales. For the CFC perturbations of interest the relevant time scale for the possible occurrence of biospheric effects is several decades up to about 100 years. A few decades are necessary to increase stratospheric chlorine levels to the point of observable impact on the total column abundance given current and projected emissions. Around a century is necessary to remove 63% of a chlorofluorocarbon such as CFC-11, once it has been released in the atmosphere. The time constants in the one-dimensional model range from the order of seconds for the fast upper stratospheric photochemistry to several years for establishing an equilibrium profile between the surface and the stratopause for a long-lived species like CFC-12, given a constant surface flux matched to the current atmospheric burden. The photochemical lifetime of ozone in the lower stratosphere can range up to a few months, comparable to transport time scales. Thus the 1-D ozone profile accommodates rapidly to Cl_z abundance changes at the possible rates of CFC increase.

The position of the knee in the $\delta\ (O_3)/\delta\ (Cl_z)$ relationship as a function of $\delta\ (Cl_z)$ is clearly one important aspect of analyzing ozone depletion. The Cl_z value at which this transition in sensitivity occurs depends on both the abundance of NO_z and the fractions of NO_z and Cl_z that are present as active NO_x and ClO_x radicals, respectively. The model's NO_z abundance, 20 ppb at 35 km, is a function of the distribution of solar UV radiation of wavelengths capable of photolyzing N_2O and the choice of the profile of the eddy diffusion constant. (A smaller contribution arises from in situ cosmic ray production of NO.) Observations also indicate a value around 20–25 ppb of NO_z in the mid stratosphere.

While the transition region for sensitivity to Cl_z perturbations in the CFC-only case occurs near 20 ppb, which is also the NO_z maximum abundance in the current ambient model, the position of the sensitivity transition as a function of Cl_z will vary with scenario. In the multiple species reference case (Figure 35), the position of the knee appears to have moved to a higher value of $\delta\ (Cl_z)$, somewhere around the 27 ppb endpoint of the scenario at 90 years. Also shown are the results of runs made with the reference CFC projections in conjunction with a 0.25% annual N_2O trend (and fixed methane flux) and separately with a 0.5% annual CH_4 trend (fixed N_2O abundance).

In the CFC/methane case, the proportion of ClO_x to total Cl_z has been reduced in comparison to the CFC-only cases (Figure 36) by the higher rate for the reaction

$$Cl + CH_4 = HCl + CH_3. \tag{26}$$

As the proportion of ClO to total Cl_z is reduced, a higher value of total Cl_z must be reached before the mid-stratospheric interaction with NO and NO_2 is saturated. This accounts for most of the mitigating effect of CH_4 increase on Cl_z-related ozone depletion, with some contribution coming from increased HO_x reducing the efficiency of NO_x photochemistry. The knee in sensitivity appears at about 23 ppb Cl_z.

In the CFC/N_2O case, the effect of the increasing N_2O on ozone actually reverses at about 55 years from present. Added N_2O increases mid-stratospheric NO_x and for small values of δ (Cl_z) NO_x remains the primary catalyst for odd oxygen loss, so the increased NO_x increases the calculated depletion. For larger values of δ (Cl_z), the interference of NO_x with ClO_x catalyzed ozone destruction is a bigger effect than the direct interaction of NO_x with O and O_3. Calculated ozone depletion is reduced from the CFC-only case because more NO_x is available to interfere. The position of the knee is extended to about 24 ppb in this scenario.

Figure 37 shows the relatively small effects of temperature feedback on the calculated ozone column change for the CFC-only reference case. As stratospheric ozone decreases, the local heating rate, dependent on absorption of solar radiation by ozone, also decreases. The radiative balance between local heating and local infrared cooling is tilted in favor of cooling, so the temperature drops. Catalytic cycles for odd oxygen loss become less effective at lower temperatures so the calculated depletion is somewhat smaller than in a fixed temperature stratosphere. For the reference case including the projected CO_2 increase, as well as the nonzero trends in the other source species, the resulting stratospheric temperature decreases appear more important in their effect on odd-oxygen loss rates. When the temperature profile is fixed, ozone column depletion increases by a factor of 1.5 compared to the case in which temperature feedback is allowed (also shown in Figure 37). While upper stratospheric temperature decrease represents a damped negative feedback when the temperature drop results from local ozone decrease, temperature decreases resulting from increasing CO_2 are effective in decreasing the local ozone loss rate irrespective of local changes in ozone or other species.

The combination of the CFC-only ozone response, the effect of CH_4 on ClO_x/Cl_z and the dependence of NO_x on N_2O emissions appears capable of explaining the overall response of the model to the variety of multiple species scenarios investigated in this study. Smaller contributions to ozone sensitivity are also made by CO_2 and BrO_x.

VII. SUMMARY AND CONCLUSIONS

A detailed description has been given above of the method and assumptions that have been used to generate the model-predicted time dependent ozone changes. Inference of actual changes in atmospheric ozone, trace species and temperature from the results of the present study must include proper treatment of the future behavior of the troposphere in view of possible trends in CO and NO_x, and the effects of uncertainties and imperfections in the model structure and assumptions. Uncertainties and errors in the model formulation include gross simplification of atmospheric dynamics and possible neglected or incorrect photochemistry.

We have shown that current uncertainties in the projection of trends of emissions of both the biogenic and industrially produced source species are sufficient to produce a

dramatic range of model-predicted ozone column changes over the next 30 to 90 years. The variables that appear to contribute most to the uncertainty in the calculated effect on ozone are the magnitude of the projected change in Cl_z abundance (projections of halocarbon emissions), the current stratospheric NO_x abundance and the lack of knowledge of the causes of the observed change in methane abundance, and thus the difficulty in predicting future changes. The timing of projected changes in the abundance or emissions of the various source species is also important. For example, rapid increases in CFC-11 and CFC-12 could overwhelm the mitigating effects of CH_4 and N_2O trends.

Another source of significant uncertainty is the model itself. Improvements in knowledge of photochemical kinetics and spectroscopy have resulted in the past in dramatic swings of predicted ozone change for a given simple CFC only scenario. Whether such major oscillations are now or will be damped in the future by the achievement of completeness and accuracy in the stratospheric kinetic data set is not clear, although the current situation is a substantial improvement over the state of knowledge only 10 years ago. Recent work with techniques such as Monte Carlo sampling uses kinetic uncertainties, based on the evaluation of random and systematic errors in laboratory studies, to estimate the approximate range of uncertainties in predictions of ozone depletion obtained within the model's existing framework. Two studies of this type show that the uncertainty limits are on the order of the ozone depletion estimates for Cl_z abundances reached by constant production at current levels.

Finally, the biospheric impacts of stratospheric ozone depletion and surface UV enhancement will depend strongly on latitude. The geometry of the earth's orbital inclination produces much smaller polar surface UV fluxes than are present in equatorial regions. The 1-D model results are quasi-global in nature, as has been discussed above, but the biospheric impact of ozone depletion clearly depends on latitude. Steady-state two-dimensional model results indicate substantial latitudinal dependence of the ozone change. The relative, but not absolute, impact in surface ultraviolet radiation is enhanced at high latitudes over the equatorial change both because of the greater ozone depletion calculated for high latitudes and because of the very small initial surface UV flux.

In summary, we have not attempted in this study to define the most probable future for the integrated ozone column. We have shown that many areas remain in which uncertainties could be reduced through better knowledge of atmospheric and biospheric processes as well as econometric forecasting. Improvement in the kinetic and photochemical data base and in model dimensionality and treatment of transport can also be profitably pursued. While the uncertainty of predictions plays a central role in this report, given the recent progress in all the areas of study listed above, a narrowing of uncertainties can confidently predicted.

ACKNOWLEDGMENTS

This work was performed under the auspices of the U.S. Department of Energy by Lawrence Livermore National Laboratory under Contract W-7405-Eng-48.

REFERENCES

Bates, D.R. and M. Nicolet, The photochemistry of atmospheric water vapor, *J. Geophys. Res., 55,* 301- , 1950.

Blake, D.R., E.W. Mayer, S.C. Tyler, Y. Makida, D.C. Montague and F.S. Rowland, Global increase in atmospheric methane concentrations between 1978 and 1980, *Geophys. Res. Lett., 9,* 477–480, 1982.

Brasseur, G., A. De Rudder and C. Tricot, Stratospheric response to chemical perturbations, *J. Atmos. Chem., 3,* 261–288, 1985.

CIAP (Climatic Impact Assessment Program), The stratosphere perturbed by propulsion effluents, CIAP Monograph III, U.S. Dept. of Transportation Report DOT-TST-75-53, 1975.

CMA (Chemical Manufacturers Association), World production and release of chlorofluorocarbons 11 and 12 through 1981, Report FPP 83-F, Washington, D.C., 1982.

Callis, L.B., M. Natarajan and R.E. Boughner, On the relationship between the greenhouse effect, atmospheric photochemistry and species distribution, *J. Geophys. Res., 88,* 1401–1426, 1983.

Callis, L.B., M. Natarajan and J.M. Russell III, Estimates of the stratospheric distributions of odd nitrogen from LIMS data, *Geophys. Res. Lett., 12,* 259–262, 1985.

Callis, L.B., M. Natarajan, R.E. Boughner, J.M. Russell III and J.D. Lambeth, Stratospheric photochemical studies using Nimbus 7 data 2. Development of inferred trace specie distributions, *J. Geophys. Res., 91,* 167–1197, 1986.

Chang, J.S., A.C. Hindmarsh and N.K. Madsen, Simulation of chemical kinetics transport in the stratosphere, Stiff Differential Systems, R.A. Willoughby, ed., Plenum, New York, 51–65, 1974.

Chapman, S., A theory of upper-atmospheric ozone, *Mem. Roy. Meteorol. Soc., 3,* 103- , 1930.

Cheung, A.S.C., K. Yoshino, W.H. Parkinson and D.E. Freeman, Herzberg continuum cross section of oxygen in the wavelength region 193.5–204.0 nm: New laboratory measurements and stratospheric implications, *Geophys. Res. Lett., 11,* 580–582, 1984.

Connell, P.S. and D.J. Wuebbles, "Summary of photochemical and radiative data used in the LLNL one-dimensional transport-kinetics model of the troposphere and stratosphere: 1982," Lawrence Livermore National Laboratory Report UCID-19557-82, 1983.

Crutzen, P.J., The influence of nitrogen oxides on the atmospheric ozone content, *Quart. J. Roy. Met. Soc., 96,* 320–325, 1970.

Crutzen, P.J., Ozone production rates in an oxygen-hydrogen-nitrogen oxide atmosphere, *J. Geophys. Res., 76,* 7311–7327, 1971.

Crutzen, P.J., L.E. Heidt, J.P. Krasnec, W.H. Pollock and W. Seiler, Biomass burning as a source of the atmospheric gases CO, H_2, N_2O, NO CH_3Cl and COS, *Nature, 282,* 253–256, 1979.

Delany, A.C., P.J. Crutzen, P. Haagensen, S. Walters and A.F. Warthourg, Photochemically produced ozone in the emission from large-scale tropical vegetation fires, *J. Geophys. Res., 90,* 2425–2429, 1985.

Edmonds, J.A., J. Reilly, J.R. Trabalka and D.E. Reichle, An analysis of possible future atmospheric retention of fossil fuel CO_2, U.S. Dept. of Energy Carbon Dioxide Research Division Technical Report , 1984.

Fabian, P., Halogenated hydrocarbons in the atmosphere, in The Handbook of Environmental Chemistry, Volume 4/Part A, O. Hutzinger, ed., Springer-Verlag, Berlin, pp. 24–51, 1986.

Frederick, J.E. and J.E. Mentall, Solar irradiance in the stratosphere: Implications for the Herzberg continuum absorption of O_2, *Geophys. Res. Lett., 9,* 461–464, 1982.

Grant, K.E., P.S. Connell and D.J. Wuebbles, "Monte Carlo uncertainty analysis of changes in atmospheric ozone concentrations from large trace gas perturbations," Lawrence Livermore National Laboratory Report UCRL-93375, 1986.

Hampson, J., Photochemical behavior of the ozone layer, Can. Armament Res. and Development Establishment, TN1627/64, 1964.

Hansen, J., D. Johnson, A. Lacis, S. Lebedeff, P. Lee, D. Rind and G. Russell, Climate impact of increasing atmospheric carbon dioxide, *Science, 213,* 957–966, 1981.

Herman, J.R. and J.E. Mentall, O_2 absorption cross sections (187–225 nm) from stratospheric solar flux measurements, *J. Geophys. Res., 87,* 8967–8975, 1982.

Hindmarsh, A.C., "Preliminary documentation of GEARBI: Solution of ODE systems with block-iterative treatment of the Jacobian," Lawrence Livermore National Laboratory Report UCID-30149, 1976.

Howard, C.J. and K.M. Evenson, Kinetics of the reaction of HO_2 with NO, *Geophys. Res. Lett., 4,* 437–440, 1977.

JPL (Jet Propulsion Laboratory) Publication 83-62, Chemical Kinetics and Photochemical Data for Use in Stratospheric Modeling, W.B. DeMore, ed., Pasadena, California, 1983.

JPL (Jet Propulsion Laboratory) Publication 85-37, Chemical Kinetics and Photochemical Data for Use in Stratospheric Modeling, W.B. DeMore, ed., Pasadena, California, 1985.

Johnston, H.S., Reduction of stratospheric ozone by nitrogen oxide catalysts from SST exhaust, *Science, 173,* 517–522, 1971.

Johnston, H.S., M. Paige and F. Yao, Oxygen absorption cross sections in the Herzberg continuum and between 206 and 327 K, *J. Geophys. Res., 89,* 11661–11665, 1984.

Keeling, C.D., R.B. Bacastow and T.P. Whorf, Measurements of the concentration of carbon dioxide at Mauna Loa Observatory, Hawaii, in Carbon Dioxide Review: 1982, W.C. Clark, ed., New York, 377–385, 1982.

Khalil, M.A.K. and R.A. Rasmussen, Carbon monoxide in the earth's atmosphere: Increasing trend, *Science, 224,* 54–56, 1984.

Kiehl, J.T. and V. Ramanathan, CO_2 radiative parameterization used in climate models: Comparison with narrow band models and with laboratory data, National Center for Atmospheric Research Report NCRA/0304/82-9, 1983.

Lacis, A., J. Hansen, P. Lee, T. Mitchell and S. Lebedeff, Greenhouse effect of trace gases, 1970–1980, *Geophys. Res. Lett., 8,* 1035–1038, 1981.

Levine, J.S., C.P. Rinsland and G.M. Tennille, The photochemistry of methane and carbon monoxide in the troposphere in 1950 and 1985, *Nature, 318,* 245–249, 1985.

Liu, S.C., D. Kley, M. McFarland, J.D. Mahlman and H. Levy II, On the origin of tropospheric ozone, *J. Geophys. Res., 85,* 7546–7552, 1980.

Logan, J.A., Nitrogen oxides in the troposphere: global and regional budgets, *J. Geophys. Res., 88,* 10785–10807, 1983.

Luther, F.M., D.J. Wuebbles and J.S. Chang, Temperature feedback in a stratospheric model, *J. Geophys. Res., 82,* 4935–4942, 1977.

Luther, F.M., D.J. Wuebbles, W.H. Duewer and J.S. Chang, Effect of multiple scattering on species concentrations and model sensitivity, *J. Geophys. Res., 83,* 3563–3570, 1978.

Luther, F.M., J.S. Chang, W.H. Duewer, J.E. Penner, R.L. Tarp and D.J. Wuebbles, Potential environmental effects of aircraft emissions, U.S. Dept. of Transportation Report FAA-EE-79-32, 1979.

McElroy, M.B., S.C. Wofsy and Y.L. Yung, The nitrogen cycle: Perturbations due to man and their impact on atmospheric N_2O and O_3, *Phil. Trans. Roy. Soc. London, B277,* 159–181, 1977.

Molina, M. and F.S. Rowland, Stratospheric sink for chlorofluoromethanes: Chlorine atom catalyzed destruction of ozone, *Nature, 249,* 810–812, 1974.

NASA (National Aeronautic and Space Administration) Reference Publication 1010, Chlorofluoromethanes and the Stratosphere, R.D. Hudson, ed., Washington, D.C., 1977.

NRC (National Research Council), Climatic Effects of Supersonic Flight, National Academy of Sciences, Washington, D.C., 1973.

NRC (National Research Council), Long-term Worldwide Effects of Multiple Nuclear Weapons Detonations, National Academy of Sciences, Washington, D.C., 1973.

NRC (National Research Council), Causes and Effects of Stratospheric Ozone Reduction. An Update, National Academy Press, Washington, D.C., 1982.

NRC (National Research Council), The Effects on the Atmoshere of a Major Nuclear Exchange, National Academy Press, Washington, D.C., 1985.

NRC (National Research Council), Changing Climate, Report of the Carbon Dioxide Assessment Committee, National Academy Press, Washington, D.C., 1983.

OECD (Organization for Economic Cooperation and Development), Scenarios for chlorofluorocarbons, ENV/CHEM/PJC/81.93, Paris, 1981.

Oeschger, H., B. Stauffer, A. Neftel, J. Schwander and R. Zumbrunn, Atmospheric CO_2 content in the past deduced from ice-core analyses, *Annals of Glaciology, 3,* 227–232, 1982.

Owens, A.J., C.H. Hales, D.L. Filkin, C. Miller and M.C. McFarland, Multiple scenario ozone change calculations: The subtractive perturbation approach, in Atmospheric Ozone, Proceedings of the Quadrennial Ozone Symposium, Halkidiki, Greece, C.S. Zerefos and A. Ghazi, eds., D. Reidel, Dordrecht, 82–86, 1985.

Prather, M.J., M.B. McElroy and S.C. Wofsy, Reductions in ozone at high concentrations of stratospheric halogens, *Nature, 312,* 227–231, 1984.

Prinn, R.G., P. Simmonds, R. Rasmussen, R. Rosen, F. Alyea, C. Cardelino, A. Crawford, D. Cunnold, P. Fraser and J. Lovelock, The Atmospheric Lifetime Experiment, 1: Introduction, instrumentation and overview, *J. Geophys. Res., 88,* 8353–8368, 1983.

Quinn, T.H., K.A. Wolf, W.E. Mooz, J.K. Hammitt, T.W. Chesnutt and S. Sarma, Projected use, emissions and banks of potential ozone depleting substances, RAND Report N-2282-EPA, 1986.

Ramanathan, V., Radiative transfer within the earth's troposphere and stratosphere: A simplified radiative-convective model, *J. Atmos. Sci., 33,* 1330–1346, 1976.

Ramanathan, V., R.J. Cicerone, H.B. Singh and J.T. Kiehl, Trace gas trends and their potential role in climate change, *J. Geophys. Res.,* 5547–5566, 1985.

Rasmussen, R.A. and M.A.K. Khalil, Atmospheric methane (CH_4): Trends and seasonal cycles, *J. Geophys. Res., 86,* 9826–9832, 1981.

Reinsel, G.C., G.C. Tiao, A.J. Miller, C.L. Mateer, J.J. Deluisi and J.E. Frederick, Analysis of upper stratospheric Umkehr ozone profile data for trends and the effects of stratospheric aerosols, *J. Geophys. Res., 89,* 4833–4840, 1984.

Rinsland, C.P. and J.S. Levine, Free tropospheric carbon monoxide concentrations in 1950 and 1951 deduced from infrared total column amount measurements, *Nature, 318,* 250–254, 1985.

Rinsland, C.P., J.S. Levine and T. Miles, Concentration of methane in the troposphere deduced from 1951 infrared solar spectra, *Nature, 318,* 245–249, 1985.

Smith, C.A., L.T. Molina, J.J. Lamb and M.J. Molina, , *Int. J. of Chem. Kin., 16,* 41- , 1984.

Stauffer, B., G. Fischer, A. Neftel and H. Oeschger, Increase of atmospheric methane recorded in Antarctic ice core, *Science, 229,* 1386–1388, 1985.

Stolarski, R.S. and R.J. Cicerone, Stratospheric chlorine: A possible sink for ozone, *Can. J. of Chem., 52,* 1610–1615, 1974.

Stolarski, R.S. and A.R. Douglass, Sensitivity of an atmospheric photochemistry model to chlorine perturbations including consideration of uncertainty propagation, *J. Geophys. Res.,* (in press), 1986.

Thompson, A.M. and R.J. Cicerone, Atmospheric CH_4, CO and OH from 1860 to 1985, *Nature, 321,* 148–150, 1986.

Toon, G.C., C.B. Farmer and R.H. Norton, Detection of stratospheric N_2O_5 by infrared remote sounding, *Nature, 319,* 570–571, 1986.

U.S. Standard Atmosphere, 1976, NOAA-S/T76-1562, Supt. of Documents, U.S. Government Printing Office, Washington, D.C., 1977.

WMO (World Meteorological Organization), The Stratosphere 1981: Theory and Measurements, WMO Global Ozone Research and Monitoring Project Report No. 11, 1982.

WMO (World Meteorological Organization), Atmospheric Ozone: Assessment of Our Understanding of the Processes Controlling its Present Distribution and Change, , 1986.

Wang, P.H., S.S. Hong, M.F. Wu and A. Deepak, A model study of the temporal and spatial variations of the zonally-averaged ozone heating rate, *J. Atmos. Sci., 39,* 1398–1409, 1982.

Wang, W-C., D.J. Wuebbles, W.M. Washington, R.G. Isaacs and G. Molnar, Trace gases and other potential perturbations to global climate, *Rev. of Geophys., 24,* 110–140, 1986.

Weiss, R.W., The temporal and spatial distribution of tropospheric nitrous oxide, *J. Geophys. Res., 86,* 7185–7195, 1981.

Wofsy, S.C., M.B. McElroy and Y.L. Yung, The chemistry of atmospheric bromine, *Geophys. Res. Lett., 2,* 215–218, 1975.

Wuebbles, D.J., "A theoretical analysis of the past variations in global atmospheric composition and temperature structure," Lawrence Livermore National Laboratory Report UCRL-53423, 1983.

Wuebbles, D.J., F.M. Luther and J.E. Penner, Effect of coupled anthropogenic perturbations on stratospheric ozone, *J. Geophys. Res., 88,* 1444–1456, 1983.

Wuebbles, D.J., M.C. MacCracken and F.M. Luther, A proposed reference set of scenarios for radiatively active atmospheric constituents, U.S. Dept. of Energy Carbon Dioxide Research Division Technical Report DOE/NBB-0066, 1984.

TABLE 1

Chemical kinetic rate coefficients[1]

$k = A * \exp (B / T)$

		A		B
1	$O + O_2 + M = O_3 + M$		S1	
2	$O + O_3 = 2\ O_2$	8.000E-12		-2.060E+03
3	$O(^1D) + M = O + M$	2.100E-11		9.500E+01
4	$O(^1D) + O_3 = 2\ O_2$	1.200E-10		0.
5	$O(^1D) + O_3 = O_2 + 2\ O$	1.200E-10		0.
6	$O_3 + NO = NO_2 + O_2$	1.800E-12		-1.370E+03
7	$O + NO_2 = NO + O_2$	9.300E-12		0.
8	$N_2O + O(1D) = N2 + O_2$	4.900E-11		0.
9	$N_2O + O(1D) = 2\ NO$	6.700E-11		0.
10	$N + O_2 = NO + O$	4.400E-12		-3.220E+03
11	$N + NO = N2 + O$	3.700E-11		0.
12	$N + NO_2 = N_2O + O$	3.000E-12		0.
13	$N2 + O(1D) + M = N_2O + M$		S4	
14	$NO + O + M = NO_2 + M$		S5	
15	$NO_2 + O_3 = NO_3 + O_2$	1.200E-13		-2.450E+03
16	$NO + NO_3 = 2\ NO_2$	3.000E-12		0.
17[2]	$NO_2 + O = NO + O_2$		S10	
18	$NO_2 + NO_3 = N_2O_5$		S11	
19	$N_2O_5 = NO_2 + NO_3$		S12	
20	$O + NO_3 = O_2 + NO_2$	1.000E-11		0.
21	$O(^1D) + H_2O = 2\ OH$	2.200E-10		0.
22	$H2 + O(^1D) = OH + H$	1.000E-10		0.
23	$O_3 + OH = HO_2 + O_2$	1.600E-12		-9.400E+02
24	$O + OH = O_2 + H$	2.200E-11		1.170E+02
25	$O_3 + HO_2 = OH + 2\ O_2$	1.400E-14		-5.800E+02
26	$O + HO_2 = OH + O_2$	3.000E-11		2.000E+02
27	$H + O_2 = HO_2$		S2	
28	$O_3 + H = OH + O_2$	1.400E-10		-4.700E+02
29	$HO_2 + HO_2 = H_2O_2 + O_2$		S27	
30	$HO_2 + HO_2 + H_2O = H_2O_2 + O_2 + H_2O$		S13	
31	$HO_2 + OH = H_2O + O_2$		S28	
32	$H_2O_2 + OH = H_2O + HO_2$	3.100E-12		-1.900E+02
33	$OH + OH = H_2O + O$	4.200E-12		-2.420E+02
34	$OH + OH = H_2O_2$		S6	
35	$H_2O_2 + O = OH + HO_2$	1.400E-12		-2.000E+03
36	$H2 + OH = H_2O + H$	6.100E-12		-2.030E+03
37	$H + HO_2 = H2 + O_2$	4.200E-11		-3.500E+02
38	$H + HO_2 = 2\ OH$	7.400E-11		0.

39	$OH + NO_2 = HNO_3$		S3	
40[2]	$OH + HNO_3 = H_2O + NO + O_2$	9.400E-15		7.780E+02
41[2]	$OH + HNO_3 = H_2O + NO_2 + O$	9.400E-15		7.780E+02
42	$NO + HO_2 = NO_2 + OH$	3.700E-12		2.400E+02
43	$N_2O_5 + H_2O = 2\ HNO_3$	5.000E-22		0.
44	$HO_2 + NO_2 = HNO_3$		S14	
45	$HNO_4 = HO_2 + NO_2$		S15	
46	$OH + HNO_4 = H_2O + NO_2 + O_2$	5.100E-13		6.900E+02
47	$O + HNO_4 = OH + NO_2 + O_2$	7.000E-11		-3.370E+03
48	$HONO + OH = H_2O + NO_2$	6.600E-12		0.
49	$OH + NO = HONO$		S18	
50	$CO + OH = H + CO_2$		S7	
51	$OH + CH_4 = CH_3 + H_2O$	2.400E-12		-1.710E+03
52	$O + CH_4 = CH_3 + OH$	3.500E-11		-4.550E+03
53	$O(^1D) + CH_4 = CH_2O + H2$	1.400E-11		0.
54	$O(^1D) + CH_4 = CH_3 + OH$	1.400E-10		0.
55	$Cl + CH_4 = CH_3 + HCl$	9.600E-12		-1.350E+03
56	$CH_3 + O = CH_2O + H$	1.100E-10		0.
57	$CH_3 + O_2 = CH_3O_2$		S16	
58	$CH_3O_2 + HO_2 = CH_3OOH + O_2$	7.700E-14		1.300E+03
59	$CH_3O_2 + O = CH_3O + O_2$	3.000E-11		0.
60	$CH_3O_2 + NO = CH_3O + NO_2$	4.200E-12		1.800E+02
61	$CH_3O + O_2 = CH_2O + HO_2$	1.200E-13		-1.350E+03
62	$OH + CH_2O = HCO + H_2O$	1.000E-11		0.
63	$O + CH_2O = HCO + OH$	3.000E-11		-1.550E+03
64	$Cl + CH_2O = HCl + HCO$	8.200E-11		-3.400E+01
65	$HCO + O_2 = CO + HO_2$	3.500E-12		1.400E+02
66	$OH + CH_3OOH = CH_3O_2 + H_2O$	5.900E-12		0.
67	$OH + CH_3OOH = CH_2O + H_2O + OH$	4.100E-12		0.
68	$CH_3Cl + Cl = HO_2 + CO + 2\ HCl$	3.400E-11		-1.260E+03
69	$CH_3Cl + OH = Cl + H_2O + HO_2$	1.800E-12		-1.112E+03
70	$Cl + O_3 = ClO + O_2$	2.800E-11		-2.570E+02
71	$ClO + O = Cl + O_2$	6.000E-11		-1.000E+02
72	$HCl + O(^1D) = Cl + OH$	1.400E-10		0.
73	$HCl + O = Cl + OH$	1.000E-11		-3.340E+03
74	$NO + ClO = NO_2 + Cl$	6.200E-12		2.940E+02
75	$ClO + NO_2 = ClONO_2$		S9	
76[2]	$ClONO_2 + O = ClO + NO + O_2$	3.000E-12		-8.080E+02
77[2]	$ClONO_2 + O = ClO + NO_2 + O$	3.000E-12		-8.080E+02
78[2]	$OH + ClONO_2 = HOCl + NO_2 + O$	1.200E-12		-3.330E+02
79[2]	$OH + ClONO_2 = HOCl + NO + O_2$	1.200E-12		-3.330E+02
80[2]	$Cl + ClONO_2 = 2\ Cl + NO2 + O$	6.800E-12		1.690E+02
81[2]	$Cl + ClONO_2 = 2\ Cl + NO + O_2$	6.800E-12		1.690E+02
82	$Cl + HNO_4 = HCl + NO_2 + O_2$	3.000E-12		-3.000E+02

83	$Cl + NO_2 = ClNO_2$		S8	
84	$OH + HCl = H_2O + Cl$	3.100E-12		-4.000E+02
85	$Cl + HO_2 = HCl + O_2$	1.800E-11		1.700E+02
86	$Cl + HO_2 = OH + ClO$	4.100E-11		-4.500E+02
87	$Cl + H2 = HCl + H$	3.700E-11		-2.300E+03
88	$Cl + H_2O_2 = HCl + HO_2$	1.100E-11		-9.800E+02
89	$Cl + HOCl = OH + 2\ Cl$	3.000E-12		-1.300E+02
90	$ClO + OH = HO_2 + Cl$	9.200E-12		6.600E+01
91	$ClO + HO_2 = O_2 + HOCl$	4.600E-13		7.100E+02
92	$O + HOCl + OH + ClO$	1.000E-11		-2.200E+03
93	$OH + HOCl = H_2O + ClO$	3.000E-12		-1.500E+02
94	$CH_3Br + OH = Br + H_2O$	6.100E-13		-8.250E+02
95	$C2H4Br_2 + OH = 2\ Br + H_2O$	7.300E-12		-1.000E+03
96	$Br + O_3 = BrO + O_2$	1.400E-11		-7.550E+02
97	$BrO + O = Br + O_2$	3.000E-11		0.
98	$BrO + BrO = 2\ Br + O_2$	1.140E-12		2.550E+02
99	$BrO + ClO = Br + Cl + O_2$	6.700E-12		0.
100	$BrO + NO = Br + NO_2$	8.700E-12		2.650E+02
101	$BrO + HO_2 = HOBr + O_2$	5.000E-12		0.
102	$BrO + OH = Br + HO_2$	1.200E-11		0.
103	$Br + HO_2 = HBr + O_2$	2.200E-13		0.
104	$Br + CH_2O = HBr + HCO$	1.700E-11		-8.000E+02
105	$OH + HBr = Br + H_2O$	8.000E-12		0.
106	$O + HBr = Br + OH$	6.600E-12		-1.540E+03
107	$BrO + NO_2 = BrONO_2$		S29	
108[3]	$CFCl_3 + O(^1D) = 3\ Cl$	2.300E-10		0.
109[3]	$CF_2Cl_2 + O(^1D) = 2\ Cl$	1.400E-10		0.
110[3]	$F13 + O(^1D) = Cl$	1.000E-10		0.
111[3]	$F112 + O(^1D) = 4\ Cl$	3.000E-10		0.
112[3]	$F113 + O(^1D) = 3\ Cl$	2.750E-10		0.
113[3]	$F114 + O(^1D) = 2\ Cl$	1.620E-10		0.
114[3]	$F115 + O(^1D) = Cl$	1.000E-10		0.
115[3]	$CCl_4 + O(^1D) = 4\ Cl$	3.300E-10		0.
116[3]	$OH + F142B = Cl$	1.500E-12		-1.800E+03
117[3]	$OH + CH_3CCl_3 = H_2O + 3\ Cl$	5.400E-12		-1.820E+03
118[3]	$OH + F21 = 2\ Cl$	8.900E-13		-1.013E+03
119[3]	$OH + F22 = Cl + H_2O$	7.800E-13		-1.530E+03

Photolytic processes:

1	$O_2 + hv = O + O$
2	$O_3 + hv = O + O_2$
3	$O_3 + hv = O(^1D) + O_2$

4	$NO_2 + hv = NO + O$
5	$N_2O + hv = N2 + O(^1D)$
6	$NO + hv = N + O$
7	$HNO_3 + hv = OH + NO_2$
8[2]	$N_2O_5 + hv = 2\ NO_2 + O$
9[2]	$N_2O_5 + hv = NO_2 + NO + O_2$
10	$NO_3 + hv = NO + O_2$
11	$NO_3 + hv = NO_2 + O$
12[2]	$HNO_4 + hv = OH + NO + O_2$
13[2]	$HNO_4 + hv = OH + NO_2 + O$
14	$HONO + hv = OH + NO$
15	$H_2O_2 + hv = 2\ OH$
16	$HO_2 + hv = OH + O$
17	$H_2O + hv = H + OH$
18[2]	$ClONO_2 + hv = Cl + NO + O_2$
19[2]	$ClONO_2 + hv = Cl + NO_2 + O$
20	$HCl + hv = H + Cl$
21	$ClO + hv = Cl + O$
22	$ClO + hv = Cl + O(^1D)$
23	$ClNO_2 + hv = Cl + NO_2$
24	$HOCl + hv = OH + Cl$
25	$CH_3OOH + hv = CH_3O + OH$
26	$CH_2O + hv = HCO + H$
27	$CH_2O + hv = CO + H2$
28	$CH_3Cl + hv = CH_3 + Cl$
29[3]	$CFCl_3 + hv = 3\ Cl$
30[3]	$CF_2Cl_2 + hv = 2\ Cl$
31[3]	$CCl_4 + hv = 4\ Cl$
32[3]	$CH_3CCl_3 + hv = 3\ Cl$
33[3]	$F21 + hv = 2\ Cl$
34[3]	$F13 + hv = Cl$
35[3]	$F112 + hv = 4\ Cl$
36[3]	$F142B + hv = Cl$
37[3]	$F113 + hv = 3\ Cl$
38[3]	$F114 + hv = 2\ Cl$
39[3]	$F115 + hv = Cl$
40[3]	$F22 + hv = Cl$
41	$CF3Br + hv = Br$
42[3]	$CF_2ClBr + hv = Br + Cl$
43	$BrO + hv = Br + O$
44	$HOBr + hv = Br + OH$
45[2]	$BrONO_2 + hv = Br + NO_2 + O$
46[2]	$BrONO_2 + hv = Br + NO + O_2$

Special kinetic rate expressions:

S1: $O + O_2 = O_3$
k=6.0E-34*M*(300/T)**2.3

S2: $H + O_2 = HO_2$
k=5.5E-32*M*(300/T)**1.6

S3: $OH + NO_2 = HNO_3$
k=(A/(1+A/B))*0.6**(1/(1+[log10(A/B)]**2))
A=2.6E-30*M*(300/T)**3.2
B=2.4E-11*(300/T)**1.3

S4: $N2 + O(^1D) = N_2O$
k=3.5E-37*M*(300/T)**0.6

S5: $NO + O = NO_2$
k=(A/(1+A/B))*0.6**(1/(1+[log10(A/B)]**2))
A=1.2E-31*M*(300/T)**1.8
B=3.0E-11*(300/T)**0.

S6: $OH + OH = H_2O_2$
k=(A/(1+A/B))*0.6**(1/(1+[log10(A/B)]**2))
A=6.9E-31*M*(300/T)**0.8
B=1.0E-11*(300/T)**1.0

S7: $CO + OH = H + CO_2$
k=1.50E-13*(1+M*2.40E-20)

S8: $Cl + NO_2 = ClNO_2$
k=(A/(1+A/B))*0.6**(1/(1+[log10(A/B)]**2))
A=1.6E-30*M*(300/T)**2.0
B=1.0E-10*(300/T)**1.0

S9: $ClO + NO_2 = ClONO_2$
k=(A/(1+A/B))*0.6**(1/(1+[log10(A/B)]**2))
A=1.8E-31*M*(300/T)**3.4
B=1.5E-11*(300/T)**1.9

S10: $NO_2 + O = NO + O_2$ (actual product NO_3, see note 2 above)
k=(A/(1+A/B))*0.6**(1/(1+[log10(A/B)]**2))
A=9.0E-32*M*(300/T)**2.0
B=2.2E-11*(300/T)**0.

S11: $NO_2 + NO_3 = N_2O_5$
k=(A/(1+A/B))*0.6**(1/(1+[log10(A/B)]**2))
A=2.0E-30*M*(300/T)**4.4
B=1.4E-12*(300/T)**0.5

S12: $N_2O_5 = NO_2 + NO_3$

k=(A/(1+A/B))*0.6**(1/(1+[log10(A/B)]**2))
A=1.88E-3*exp(-11001/T)*M*(300/T)**4.4
B=1.32E+15*exp(-11001/T)*(300/T)**0.5

S13: $HO_2 + HO_2 + H_2O = H_2O_2 + O_2 + H_2O$
k=1.77E-36*exp(4320/T)+M*1.31E-56*exp(4730/T)

S14: $HO_2 + NO_2 = HNO_4$
k=(A/(1+A/B))*0.6**(1/(1+[log10(A/B)]**2))
A=2.3E-31*M*(300/T)**4.6
B=4.2E-12*(300/T)**0.

S15: $HNO_4 = HO_2 + NO_2$
k=(A/(1+A/B))*0.6**(1/(1+[log10(A/B)]**2))
A=9.87E-5*exp(-10870/T)*M*(300/T)**4.6
B=1.8E+15*exp(-10870/T)*(300/T)**0.

S16: $CH_3 + O_2 = CH_3O_2$
k=(A/(1+A/B))*0.6**(1/(1+[log10(A/B)]**2))
A=2.2E-31*M*(300/T)**2.2
B=2.0E-12*(300/T)**1.7

S18: $OH + NO = HONO$
k=(A/(1+A/B))*0.6**(1/(1+[log10(A/B)]**2))
A=7.0E-31*M*(300/T)**2.6
B=1.5E-11*(300/T)**0.5

S27: $HO_2 + HO_2 = H_2O_2 + O_2$
k=2.3E-13*exp(590./T)+1.7E-33*M*exp(1000./T)

S28: $HO_2 + OH = H_2O + O_2$
k=7.0E-11+(1.57E-30)*M

S29: $BrO + NO_2 = BrONO_2$
k=(A/(1+A/B))*0.6**(1/(1+[log10(A/B)]**2))
A=5.0E-31*M*(300/T)**2.0
B=1.0E-11*(300/T)**1.0

---

1. JPL 83-82.
2. The primary reaction product NO_3 photolyzes quickly to form the products $NO_2 + O$ or $NO + O_2$. These products are included as primary products for computational reasons involving proper diurnal averaging and the branching ratio for NO_3 photolysis is included with the rate constant.
3. Not an elementary process.

TABLE 2

Changes to kinetic data set in 1985 update[1]

$k = A * \exp (B / T)$

		A		B
11	$N + NO = N2 + O$	3.400E-11		0.
14	$NO + O + M = NO_2 + M$		S5	
16	$NO + NO_3 = 2\ NO_2$	1.300E-11		2.500E+02
18	$NO_2 + NO_3 = N_2O_5$		S11	
31	$HO_2 + OH = H_2O + O_2$		S28	
38	$H + HO_2 = 2\ OH$	5.200E-11		5.000E+01
40[2]	$OH + HNO_3 = H_2O + NO + O_2$		S30	
41[2]	$OH + HNO_3 = H_2O + NO_2 + O$		S30	
44	$HO_2 + NO_2 = HNO_4$		S14	
46	$OH + HNO_4 = H_2O + NO_2 + O_2$	1.300E-12		3.800E+02
57	$CH_3 + O_2 = CH_3O_2$		S16	
61	$CH_3O + O_2 = CH_2O + HO_2$	8.400E-14		-1.200E+03
71	$ClO + O = Cl + O_2$	4.700E-11		-5.000E+01
72	$HCl + O(^1D) = Cl + OH$	1.500E-10		0.
84	$OH + HCl = H_2O + Cl$	2.600E-12		-3.500E+02
90	$ClO + OH = HO_2 + Cl$	1.000E-11		1.200E+02
99	$BrO + ClO = Br + Cl + O_2$	1.340E-11		0.
103	$Br + HO_2 = HBr + O_2$	8.000E-13		0.
105	$OH + HBr = Br + H_2O$	1.100E-11		0.

1. JPL 85-37.
2. See note 2 in Table 1.

Special kinetic expressions:

S5: $NO + O = NO_2$

```
k=(A/(1+A/B))*0.6**(1/(1+[log10(A/B)]**2))
A=9.0E-32*M*(300/T)**1.5
B=3.0E-11*(300/T)**0.
```

S11: $NO_2 + NO_3 = N_2O_5$

```
k=(A/(1+A/B))*0.6**(1/(1+[log10(A/B)]**2))
A=2.2E-30*M*(300/T)**4.4
B=1.5E-12*(300/T)**0.5
```

S14: $HO_2 + NO_2 = HNO_4$

```
k=(A/(1+A/B))*0.6**(1/(1+[log10(A/B)]**2))
A=2.0E-31*M*(300/T)**2.7
B=4.2E-12*(300/T)**2.0
```

S16: $CH_3 + O_2 = CH_3O_2$

k=(A/(1+A/B))*0.6**(1/(1+[log10(A/B)]**2))

A=4.5E-31*M*(300/T)**2.0

B=1.8E-12*(300/T)**1.7

S28: $HO_2 + OH = H_2O + O_2$

k=1.7E-11*exp(416/T)+3.0E-31*M*exp(500/T)

S30: $OH + HNO_3 = H_2O + NO_3$

k=7.2E-15*exp(785/T)+A/(1+A/B)

A=1.9E-33*M*exp(725/T)

B=4.1E-16*exp(1440/T)

APPENDIX A

EMISSION PROJECTIONS 1985-2075

CFC11 ($CFCl_3$) 10^6 kg/year

YEAR	A	1A[a]	4[b]	5[c]	B	C	12[d]	13	17
1985	325	325	324	594	354	490	325	325	325
1990	426	428	422	1184	464	845	348	427	426
1995	544	553	476	1486	559	1064	446	553	514
2000	699	717	522	2428	673	1626	598	684	578
2005	842	870	558	5456	761	3210	738	743	624
2010	986	1024	594	8485	849	4794	878	883	670
2015	1122	1173	626	17422	931	9328	1009	1014	689
2020	1263	1322	657	26358	1012	13862	1141	1146	708
2025	1411	1480	691	35841	1104	18679	1276	1280	717
2030	1559	1637	725	45323	1197	23496	1410	1415	717
2035	1730	1826	762	47660	1305	24757	1565	1570	717
2040	1900	2006	798	50009	1413	26018	1720	1725	717
2045	2106	2237	837	51790	1544	27020	1918	1922	717
2050	2313	2468	876	53570	1674	28021	2115	2120	717
2055	2528	2702	918	54795	1804	28743	2320	2324	717
2060	2744	2937	960	56020	1935	29464	2524	2529	717
2065	2976	3188	1006	57044	2077	30095	2741	2746	717
2070	3207	3440	1053	58068	2219	30726	2958	2962	717
2075	3456	3711	1104	69555	2373	36598	3190	3194	717

a. Also used in scenarios 2A, 6, 7, 8, 9, 14, 21, 22, 24, 25 and 27.

b. Also used in scenario 11.

c. Also used in scenarios 10 and 20.

d. Also used in scenario 26.

CFC11 ($CFCl_3$) 10^6 kg/year

YEAR	18	19	28	29	30[e]	31	D	E[f]	G
1985	324	325	326	326	283	217	325	107	107
1990	395	426	427	357	333	250	426	142	142
1995	443	540	545	444	400	283	544	181	164
2000	494	649	671	560	445	333	230	230	181
2005	532	728	765	642	454	379	282	282	194
2010	570	808	858	723	464	425	334	334	208
2015	588	856	915	838	464	500	384	384	219
2020	606	904	972	852	464	575	434	434	230
2025	610	928	1014	901	464	672	486	486	247
2030	615	955	1055	950	464	770	537	537	254

2035	616	986	1094	994	464	895	596	596	267
2040	616	1018	1133	1038	464	1019	654	654	280
2045	616	1039	1181	1095	464	1264	726	726	294
2050	616	1060	1229	1152	464	1410	797	797	308
2055	616	1064	1274	1203	464	1658	874	874	322
2060	616	1069	1320	1258	464	1905	952	952	337
2065	616	1069	1358	1304	464	2238	1034	1034	354
2070	616	1069	1397	1350	464	2570	1116	1116	370
2075	616	1069	1432	1391	464	2990	1203	1203	387

e. Also used in scenario 32.

f. Also used in scenario F.

CFC12 (CF_2Cl_2) 10^6 kg/year

YEAR	A	1A[a]	4[b]	5[c]	B	C	12[d]	13	17
1985	449	449	446	527	468	509	449	449	449
1990	528	528	519	772	547	674	387	528	528
1995	623	625	573	1042	623	857	427	625	594
2000	734	746	611	1406	701	1099	516	660	617
2005	844	870	647	1997	774	1349	606	619	631
2010	954	995	683	2587	847	1799	697	710	645
2015	1074	1130	723	3483	927	2306	792	805	650
2020	1193	1266	763	4378	1007	2814	887	900	656
2025	1331	1415	808	5219	1100	3305	990	1004	656
2030	1468	1564	853	6058	1192	3796	1094	1107	657
2035	1634	1742	902	6499	1304	4104	1212	1226	657
2040	1799	1919	951	6940	1416	4411	1331	1344	657
2045	1988	2131	1004	7299	1540	4687	1478	1491	657
2050	2177	2342	1058	7658	1663	4963	1624	1637	657
2055	2368	2556	1118	7890	1789	5175	1776	1788	657
2060	2559	2770	1177	8122	1914	5387	1927	1940	657
2065	2766	2998	1245	8278	2054	5571	2090	2103	657
2070	2972	3226	1312	8434	2193	5754	2253	2266	657
2075	3198	3472	1386	8547	2346	5927	2427	2440	657

a. Also used in scenarios 2A, 6, 7, 8, 9, 14, 21, 22, 24, 25 and 27.

b. Also used in scenario 11.

c. Also used in scenarios 10 and 20.

d. Also used in scenario 26.

CFC12 (CF_2Cl_2) 10^6 kg/year

YEAR	18	19	28	29	30[e]	31	D	E[f]	G
1985	446	449	445	450	421	330	449	227	226
1990	491	528	529	396	490	360	528	248	244
1995	519	622	624	430	638	421	623	290	267
2000	534	716	729	504	638	490	367	340	283
2005	544	787	808	550	638	564	406	391	300
2010	554	858	887	597	638	638	445	442	316
2015	559	915	956	636	638	724	498	496	334
2020	564	972	1024	676	638	810	551	551	352
2025	564	1009	1096	718	638	955	614	614	373
2030	565	1046	1167	761	638	1100	678	678	394
2035	565	1100	1232	802	638	1278	754	754	416
2040	565	1153	1296	856	638	1447	831	831	439
2045	565	1183	1350	908	638	1664	918	918	464

2050	565	1213	1404	959	638	1880	1005	1005	488
2055	565	1215	1458	1009	638	2170	1094	1094	514
2060	565	1217	1512	1059	638	2460	1184	1184	543
2065	565	1217	1555	1110	638	2843	1280	1280	574
2070	565	1217	1598	1161	638	3225	1376	1376	605
2075	565	1217	1643	1213	638	3690	1479	1479	639

e. Also used in scenario 32.

f. Also used in scenario F.

CCl_4 10^6 kg/year

YEAR	A[a]	1A[b]	4[c]	30[d]
1985	88	153	131	100
1990	90	188	41	100
1995	105	206	45	100
2000	125	226	49	100
2005	149	250	54	100
2010	173	275	59	100
2015	196	300	64	100
2020	219	325	70	100
2025	243	350	76	100
2030	260	384	83	100
2035	277	419	91	100
2040	295	454	99	100
2045	312	489	107	100
2050	329	524	115	100
2055	379	576	126	100
2060	429	628	137	100
2065	479	680	148	100
2070	529	732	160	100
2075	579	784	172	100

a. Also used in scenarios B, C, D, E and F.

b. Also used in scenarios 2A, 5-10, 12-14, 17-22 and 24-29.

c. Also used in scenarios 11 and G.

d. Also used in scenarios 31 and 32.

CH_3CCl_3 (methyl chloroform) 10^6 kg/year

YEAR	A[a]	1A[b]	30[c]
1985	510	510	500
1990	569	569	500
1995	635	634	500
2000	708	708	500
2005	793	793	500
2010	878	878	500
2015	964	963	500
2020	1050	1049	500
2025	1136	1135	500
2030	1257	1256	500
2035	1378	1377	500
2040	1500	1499	500
2045	1622	1621	500

2050	1744	1743	500
2055	1901	1922	500
2060	2058	2101	500
2065	2215	2280	500
2070	2372	2459	500
2075	2531	2638	500

a. Also used in scenarios B-F.

b. Also used in scenarios 2A, 4-14, 17-22, 24-29 and G.

c. Also used in scenarios 31 and 32.

CFC113 ($CF_2ClCFCl_2$) 106 kg/year

YEAR	A[a]	1A[b]	4[c]	30[d]	D	E[e]	G
1985	102	102	102	0	102	43	43
1990	131	142	142	0	131	53	53
1995	189	210	157	0	189	79	60
2000	274	277	180	0	104	104	68
2005	307	311	202	0	117	117	76
2010	341	344	224	0	129	129	84
2015	374	378	245	0	142	142	92
2020	408	411	267	0	154	154	100
2025	441	445	289	0	167	167	108
2030	489	493	320	0	185	185	120
2035	536	540	351	0	203	203	131
2040	584	588	381	0	220	220	143
2045	631	635	412	0	238	238	154
2050	679	683	443	0	256	256	166
2055	740	753	489	0	282	282	183
2060	800	823	534	0	309	309	200
2065	861	893	580	0	335	335	218
2070	921	963	625	0	362	362	235
2075	982	1033	671	0	3388	252	

a. Also used in scenarios B and C.

b. Also used in scenarios 2A, 5-10, 12-14, 17-22 and 24-29.

c. Also used in scenario 11.

d. Also used in scenarios 31 and 32.

e. Also used in scenario F.

CFC22 (CHF_2Cl) 10^6 kg/year

YEAR	1A[a]	4[b]	5[c]	30[d]
1984	52	54	59	0
1989	84	71	101	0
1994	122	89	156	0
1999	167	107	226	0
2004	221	127	321	0
2009	273	137	430	0
2014	332	148	564	0
2019	394	155	719	0
2024	463	163	900	0
2029	541	170	1028	0
2034	626	178	1130	0
2039	715	187	1218	0

2044	807	196	1287	0
2049	900	205	1339	0
2054	998	216	1380	0
2059	1097	226	1412	0
2064	1195	238	1438	0
2069	1292	250	1461	0
2074	1387	263	1480	0
2079	1495	276	1493	0

a. Also used in scenarios 2A, 6-9, 12-14, 17-19, 21, 22, 24-29 and A-F.

b. Also used in scenarios 11 and G.

c. Also used in scenarios 10 and 20.

d. Also used in scenarios 31 and 32.

HALON 1301 (CF_3Br) 10^6 kg/year

YEAR	A[a]	1A[b]	2A[c]	4[d]
1985	3	2	0	1
1990	4	3	0	2
1995	6	4	0	2
2000	9	6	0	3
2005	12	9	0	4
2010	15	12	0	5
2015	17	16	0	7
2020	20	19	0	9
2025	23	22	0	11
2030	25	25	0	12
2035	28	29	0	14
2040	30	32	0	16
2045	33	36	0	18
2050	35	39	0	20
2055	39	43	0	21
2060	43	47	0	23
2065	46	51	0	25
2070	50	55	0	27
2075	54	59	0	29

HALON 1211 (CF_2BrCl) 10^6 kg/year

YEAR	A[a]	1A[b]	2A[c]	4[d]
1985	1	0	0	0
1990	1	1	0	0
1995	1	1	0	0
2000	2	1	0	1
2005	2	1	0	1
2010	3	2	0	1
2015	3	3	0	2
2020	4	4	0	2
2025	5	5	0	2
2030	5	5	0	2
2035	5	6	0	3
2040	6	7	0	3
2045	6	8	0	4
2050	7	9	0	4
2055	7	9	0	4
2060	8	10	0	5
2065	9	11	0	5
2070	10	12	0	6
2075	11	13	0	7

a. Also used in scenarios B-F.

b. Also used in scenarios 5-10, 12-14, 17-22 and 26-29.

c. Also used in scenarios 24, 25 and 30-32.

d. Also used in scenarios 11 and G.

	CO_2 - surface mole fraction in ppm		CH_4 - surface mole fraction in ppm		
YEAR	A[a]	14	30[b]	A[b,c]	6
1985	344.5	345.0	348.6	1.756	1.756
1990	352.9	354.1	357.4	1.845	1.845
1995	362.0	363.3	366.4	1.939	1.892
2000	372.0	372.4	375.7	2.038	1.939
2005	382.8	381.5	385.2	2.142	1.988
2010	394.6	390.7	394.9	2.251	2.039
2015	407.4	399.8	404.8	2.366	2.090
2020	421.4	408.9	415.1	2.487	2.143
2025	436.4	418.1	425.6	2.614	2.197
2030	452.7	427.3	436.3	2.747	2.252
2035	470.3	436.5	447.3	2.887	2.309
2040	489.4	445.6	458.6	3.035	2.368
2045	509.9	454.8	470.2	3.189	2.427
2050	532.0	464.0	482.1	3.352	2.489
2055	555.9	473.2	494.2	3.523	2.551
2060	581.5	482.4	506.7	3.703	2.616
2065	609.1	491.7	519.5	3.892	2.682
2070	638.8	500.9	532.6	4.090	2.750
2075	670.7	510.1	546.1	4.299	2.819

a. Also used in all scenarios other than 14 and 30-32.

b. Also used in scenarios 1A, 2A, 4, 5, 12-14, 17-19, 21, 22, 24-26, 28-32, B-E and G.

c. Other scenarios used prescribed flux boundary conditions.

6: 1% increase per year to 1990, then 0.5% increase per year to 2075
7: 1% increase per year to 2010, then constant surface flux to 2075
8: 1% increase per year to 2010, then 2% increase per year to 2075
9 and 27: 1% increase per year to 2010, then -1% per year to 2030, then constant surface flux to 2075.
10: 0.5% increase per year
11 and 20: 1.5% increase per year
F: 1.25% increase per year.

N_2O - surface mole fraction in ppb.

YEAR	A[a]	30[b]
1985	303.1	304.0
1990	306.9	307.1
1995	310.8	310.1
2000	314.7	313.3
2005	318.6	316.4
2010	322.6	319.6
2015	326.7	322.8
2020	330.8	326.0
2025	334.9	329.3
2030	339.2	332.6
2035	343.4	336.0
2040	347.7	339.3
2045	352.1	342.7
2050	356.5	346.2
2055	361.0	349.6
2060	365.5	353.2
2065	370.1	356.7
2070	374.8	360.3
2075	379.5	363.9

a. Used in all scenarios other than 30-32.

b. Also used in scenarios 31 and 32.

REFERENCE CASE AND SCENARIO SENSITIVITY RUNS

	SCENARIO IDENTIFIER																	
YEAR	A	A[1]	1A	4	4[1]	B	C	5	5[1]	2A	6	7	8	9	10	11	14	20
1985	0.0	0.0	0.0	0.0	0.0	0.0	0.0	0.0	0.0	0.0	0.0	0.0	0.0	0.0	0.0	0.0	0.0	0.0
1990	-0.07	-0.16	-0.06	-0.07	-0.16	-0.09	-0.07	-0.10	-0.20	-0.06	-0.06	-0.04	-0.04	-0.04	-0.07	-0.02	-0.06	-0.05
1995	-0.18	-0.37	-0.21	-0.16	-0.34	-0.28	-0.18	-0.38	-0.66	-0.20	-0.22	-0.11	-0.11	-0.11	-0.33	-0.01	-0.19	-0.23
2000	-0.35	-0.66	-0.41	-0.27	-0.55	-0.62	-0.35	-0.91	-1.46	-0.37	-0.51	-0.24	-0.24	-0.24	-0.87	0.01	-0.40	-0.61
2005	-0.61	-1.06	-0.69	-0.40	-0.78	-1.18	-0.50	-1.82	-2.80	-0.63	-0.92	-0.45	-0.45	-0.45	-1.82	0.06	-0.70	-1.32
2010	-0.96	-1.61	-1.08	-0.55	-1.03	-2.21	-0.61	-3.66	-5.44	-0.95	-1.44	-0.75	-0.75	-0.75	-3.74	0.14	-1.12	-2.87
2015	-1.42	-2.31	-1.57	-0.71	-1.32	-4.05	-0.73	-7.47	-10.86	-1.35	-2.10	-1.19	-1.14	-1.21	-7.77	0.23	-1.66	-6.20
2020	-1.99	-3.17	-2.19	-0.88	-1.62	-7.76	-0.87	-19.54	-29.53	-1.84	-2.89	-1.81	-1.54	-1.93	-21.25	0.35	-2.32	16.07
2025	-2.65	-4.18	-2.91	-1.07	-1.95	-16.91	-1.05	-60.98	-62.75	-2.39	-3.82	-2.63	-1.96	-2.94	-65.71	0.48	-3.11	-55.82
2030	-3.42	-5.35	-3.75	-1.26	-2.31	-51.48	-1.27	-	-	-3.01	-4.89	-3.66	-2.39	-4.24	-79.06	0.65	-4.01	-72.44
2035	-4.30	-6.70	-4.73	-1.47	-2.69	-67.19	-1.53	-	-	-3.72	-6.13	-4.91	-2.83	-5.83	-85.68	0.83	-5.05	-79.00
2040	-5.29	-8.23	-5.85	-1.69	-3.11	-71.64	-1.84	-	-	-4.51	-7.59	-6.41	-3.30	-7.70	-	1.03	-6.23	-82.85
2045	-6.41	-9.99	-7.15	-1.94	-3.57	-73.69	-2.19	-	-	-5.42	-9.27	-8.22	-3.77	-9.89	-	1.28	-7.59	-
2050	-7.67	-12.01	-8.69	-2.19	-4.06	-74.72	-2.58	-	-	-6.46	-11.27	-10.42	-4.24	-12.56	-	1.59	-9.16	-
2055	-9.13	-14.35	-10.48	-2.46	-4.59	-75.35	-3.02	-	-	-7.68	-13.73	-13.20	-4.79	-16.00	-	1.92	-10.98	-
2060	-10.84	-17.19	-12.67	-2.76	-5.17	-75.78	-3.52	-	-	-9.18	-16.94	-16.96	-5.44	-20.92	-	2.27	-13.17	-
2065	-12.90	-20.75	-15.52	-3.09	-5.81	-	-4.09	-	-	-11.26	-21.57	-22.78	-6.22	-29.62	-	2.62	-15.88	-
2070	-15.58	-25.47	-19.64	-3.43	-6.52	-	-4.75	-	-	-14.70	-29.20	-33.53	-7.17	-45.79	-	2.98	-19.89	-
2075	-19.94	-31.79	-26.15	-3.76	-7.28	-	-5.47	-	-	-22.62	-39.80	-48.63	-8.34	-61.86	-	3.35	-25.08	-

1. Scenario run with kinetic and spectral parameters updated to recommendations of JPL 85-37.

MODEL PARAMETER SENSITIVITY RUNS AND BRASSEUR SCENARIOS

	SCENARIO IDENTIFIER																
	A[1]	21	22	24	25	26	27	28	29	30	31	32	A[2]	A[3]	A[4]	A[5]	A[6]
1985	0.0	0.0	0.0	0.0	0.0	0.0	0.0	0.0	0.0	0.0	0.0	0.0	0.0	0.0	0.0	0.0	0.0
1990	−0.23	−0.01	−0.13	−0.44	−0.14	−0.08	−0.06	−0.06	0.01	0.01	−0.00	−0.07	1.21	−0.27	−0.13	−0.12	−0.28
1995	−0.54	−0.08	−0.33	−0.99	−0.34	−0.22	−0.19	−0.18	−0.03	0.01	−0.08	−0.18	0.78	−0.59	−0.28	−0.23	−0.69
2000	−0.93	−0.20	−0.60	−1.67	−0.58	−0.44	−0.39	−0.33	−0.06	0.03	−0.18	−0.35	0.30	−0.97	−0.51	−0.39	−1.18
2005	−1.43	−0.40	−0.96	−2.54	−0.90	−0.75	−0.67	−0.53	−0.09	0.07	−0.31	−0.61	−0.27	−1.45	−0.86	−0.65	−1.76
2010	−2.06	−0.67	−1.43	−3.61	−1.32	−1.19	−1.03	−0.80	−0.12	0.11	−0.46	−0.96	−0.98	−2.05	−1.36	−1.02	−2.45
2015	−2.82	−1.03	−2.00	−4.91	−1.86	−1.82	−1.47	−1.13	−0.12	0.14	−0.64	−1.42	−1.84	−2.79	−2.01	−1.52	−3.25
2020	−3.74	−1.49	−2.67	−6.45	−2.52	−2.75	−1.98	−1.52	−0.10	0.15	−0.83	−1.99	−2.87	−3.67	−2.82	−2.15	−4.14
2025	−4.80	−2.03	−3.44	−8.29	−3.32	−4.00	−2.55	−1.97	−0.06	0.15	−1.03	−2.65	−4.07	−4.69	−3.80	−2.92	−5.14
2030	−6.02	−2.66	−4.32	−10.49	−4.24	−5.61	−3.18	−2.47	0.00	0.12	−1.24	−3.42	−5.47	−5.87	−4.95	−3.81	−6.24
2035	−7.41	−3.37	−5.31	−13.26	−5.31	−7.60	−3.86	−3.02	0.08	0.06	−1.47	−4.30	−7.12	−7.23	−6.30	−4.86	−7.44
2040	−8.98	−4.18	−6.47	−17.07	−6.56	−10.02	−4.59	−3.62	0.19	−0.05	−1.70	−5.29	−9.07	−8.82	−7.89	−6.09	−8.76
2045	−10.76	−5.10	−7.83	−23.46	−8.01	−13.02	−5.38	−4.28	0.33	−0.20	−1.95	−6.41	−11.44	−10.72	−9.81	−7.54	−10.22
2050	−12.79	−6.14	−9.49	−33.93	−9.70	−17.00	−6.23	−4.99	0.48	−0.41	−2.21	−7.67	−14.43	−13.07	−12.21	−9.30	−11.88
2055	−15.12	−7.33	−11.61	−41.62	−11.72	−23.04	−7.13	−5.75	0.65	−0.69	−2.48	−9.13	−18.36	−16.17	−15.42	−11.50	−13.80
2060	−17.84	−8.66	−14.69	−45.88	−14.21	−35.26	−8.11	−6.59	0.85	−1.06	−2.76	−10.84	−23.96	−20.99	−20.47	−14.52	−16.14
2065	−21.09	−10.26	−20.85	–	−17.40	–	−9.16	−7.51	1.06	−1.53	−3.06	−12.90	−32.38	−31.66	−32.17	−19.46	−19.27
2070	−24.94	−12.23	−31.37	–	−21.81	–	−10.29	−8.48	1.29	−2.09	−3.37	−15.58	−43.16	−46.61	−50.02	−30.38	−24.33
2075	−29.42	−14.81	–	–	−28.23	–	−11.53	−9.52	1.54	−2.76	−3.70	−19.28	−51.95	−54.36	−60.54	−43.80	−35.83

1. Scenario A run without temperature feedback calculation.
2. Scenario A including increasing trends only in CFC compounds, fixed CO_2, CH_4, N_2O and temperature profile.
3. As in note **2**, but with temperature feedback.
4. As in note 3, but with fixed CH_4 surface flux rather than fixed surface concentration.
5. As in note 3, but with 0.5% annual increase in CH_4 surface concentration.
6. As in note 3, but with 0.25% annual increase in N_2O surface concentration.

REGULATORY SENSITIVITY RUNS

YEAR	SCENARIO IDENTIFIER										
	12	13	17	18	19	28	29	D	E	F	G
1985	0.0	0.0	0.0	0.0	0.0	0.0	0.0	0.0	0.0	0.0	0.0
1990	-0.08	-0.08	-0.06	-0.06	-0.06	-0.06	0.01	-0.07	-0.06	-0.01	-0.06
1995	-0.19	-0.20	-0.19	-0.18	-0.19	-0.18	-0.03	-0.18	-0.07	0.05	-0.05
2000	-0.35	-0.40	-0.38	-0.35	-0.39	-0.33	-0.06	-0.35	-0.07	0.15	-0.01
2005	-0.57	-0.68	-0.63	-0.56	-0.66	-0.53	-0.09	-0.50	-0.10	0.25	0.04
2010	-0.86	-1.02	-0.93	-0.82	-1.01	-0.80	-0.12	-0.61	-0.16	0.34	0.10
2015	-1.25	-1.44	-1.27	-1.10	-1.43	-1.13	-0.12	-0.73	-0.27	0.40	0.16
2020	-1.74	-1.94	-1.66	-1.43	-1.91	-1.52	-0.10	-0.87	-0.42	0.44	0.21
2025	-2.33	-2.52	-2.07	-1.78	-2.45	-1.97	-0.06	-1.05	-0.61	0.46	0.26
2030	-3.01	-3.21	-2.50	-2.15	-3.04	-2.47	0.00	-1.27	-0.84	0.46	0.31
2035	-3.79	-3.99	-2.95	-2.55	-3.66	-3.02	0.08	-1.53	-1.12	0.44	0.35
2040	-4.70	-4.90	-3.42	-2.97	-4.32	-3.62	0.19	-1.84	-1.45	0.40	0.37
2045	-5.73	-5.92	-3.92	-3.41	-5.04	-4.28	0.33	-2.19	-1.82	0.33	0.39
2050	-6.90	-7.11	-4.43	-3.88	-5.79	-4.99	0.48	-2.58	-2.23	0.24	0.40
2055	-8.26	-8.47	-4.97	-4.37	-6.58	-5.75	0.65	-3.02	-2.68	0.17	0.40
2060	-9.86	-10.07	-5.53	-4.89	-7.41	-6.59	0.85	-3.52	-3.20	0.09	0.39
2065	-11.71	-11.95	-6.14	-5.45	-8.29	-7.51	1.06	-4.09	-3.79	-0.03	0.36
2070	-13.80	-14.29	-6.78	-6.06	-9.18	-8.48	1.29	-4.75	-4.46	-0.21	0.31
2075	-17.17	-17.33	-7.43	-6.67	-10.13	-9.52	1.54	-5.47	-5.20	-0.43	0.24

APPENDIX C

Surface mole fractions in Reference Run (Scenario A)

YEAR	F11	F12	CCl_4	CH_3CCl_3	F113	F22	1301	1211	CH_4	NO_z
				ppb				ppt	ppm	ppb@35
1985	0.209	0.378	0.161	0.137	0.032	0.044	0.	0.	1.755	19.9
1990	0.274	0.481	0.166	0.168	0.048	0.059	1.40	0.32	1.84	
1995	0.358	0.601	0.173	0.197	0.070	0.080	3.23	0.54	1.940	
2000	0.465	0.741	0.182	0.226	0.101	0.109	5.93	0.84	2.038	
2005	0.596	0.904	0.194	0.257	0.140	0.148	9.63	1.31	2.143	
2010	0.749	1.071	0.211	0.290	0.182	0.196	14.26	1.83	2.251	
2015	0.922	1.291	0.230	0.325	0.228	0.251	19.74	2.38	2.367	
2020	1.113	1.517	0.252	0.361	0.275	0.314	26.1	2.95	2.487	
2025	1.322	1.765	0.277	0.398	0.325	0.386	33.2	3.53	2.614	
2030	1.547	2.037	0.304	0.438	0.379	0.467	41.0	4.09	2.747	21.4
2035	1.790	2.335	0.331	0.483	0.437	0.559	49.2	4.59	2.888	
2040	2.051	2.662	0.360	0.532	0.498	0.660	58.1	5.04	3.035	
2045	2.332	3.019	0.389	0.582	0.563	0.770	67.3	5.46	3.189	
2050	2.636	3.407	0.419	0.633	0.631	0.888	77.0	5.85	3.351	
2055	2.961	3.826	0.452	0.688	0.703	1.013	87.3	6.26	3.523	
2060	3.304	4.272	0.490	0.746	0.779	1.145	98.5	6.74	3.703	
2065	3.665	4.751	0.534	0.807	0.859	1.282	110.4	7.26	3.892	
2070	4.040	5.253	0.583	0.866	0.943	1.421	123.0	7.77	4.091	
2075	4.425	5.785	0.634	0.919	1.027	1.558	136.1	8.20	4.298	23.6

Note: Surface mole fractions for N_2O and CO_2 are specified as boundary conditions and are found in Appendix A.

Figures

1. LLNL 1-D eddy diffusion coefficient profile.
2. Historical record of calculated ozone depletion at steady state for constant current CFC emission fluxes.
3. Calculated ozone column change, 1850-1985, referenced to 1985 model calculated column.
4. Selected vertical profiles of local ozone change, 1850-1985: (a) Absolute concentration change, (b) Relative change.
5. Comparison of model results of Wang et al (1986) to statistically derived decadal trend of local ozone from the Umkehr observational network, 1970-1980 (from WMO, 1986).
6. Calculated direct radiative equilibrium surface temperature change, 1850-1985. Short dashed line is CO_2 contribution, long dashed line is CO_2+CH_4 contribution.
7. 1985 ozone vertical profile compared to observations.
8. 1985 vertical mole fraction profiles compared to observations: (a) N_2O, (b) CH_4 and H_2O, (c) CFC11 and CFC12.
9. 1985 vertical mole fraction profiles compared to observations: (a) NO and NO_2, (b) HNO_3, $ClONO_2$ and HNO_4.
10. 1985 vertical mole fraction profiles compared to observations: (a) ClO, (b) HCl.
11. 1985 vertical temperature profile compared to US Standard Atmosphere (1976).
12. Rates of odd oxygen production and loss terms by family as a function of altitude.
13. Reference case CFC11 and CFC12 projected emissions.
14. Reference case projected emissions of other halocarbons.
15. Low case projected halocarbon emissions: (a) CFC11 and CFC12 and (b) other halocarbons.
16. High case projected halocarbon emissions: (a) CFC11 and CFC12 and (b) other halocarbons.
17. Reference case column ozone change vs. time (solid line) and reference case emissions with updated chemistry (dashed line).
18. Selected profiles of local ozone concentration change from reference case: (a) absolute concentration change and (b) relative change.
19. Increase in equilibrium radiative surface temperature with time for the reference case (solid line) and including climate feedback amplification (dashed lines).
20. Selected profiles of stratospheric temperature change from reference case.
21. High and low case column ozone changes with time (solid lines) and range of ozone change over all scenarios (dashed lines).
22. Relative change in local ozone abundance at 40 km from selected scenarios.

23. Total column ozone change with time for selected regulatory scenarios.

24. Total column ozone change with time for scenarios with monotonic methane surface flux boundary conditions (dashed lines) compared to the reference case (solid line).

25. Total column ozone change with time for scenarios with variable methane surface flux boundary conditions (dashed lines) compared to reference cases with specified concentration CH_4 boundary conditions (solid line).

26. Total column ozone change with time for high case CFC emissions and alternative methane scenarios 5, 10, 20.

27. Total column ozone change with time for low case CFC emissions and alternative methane scenarios 4 and 11.

28. Total column ozone change with time for alternative Halon emission scenarios 1A and 2A.

29. Total column ozone change with time for scenarios with varying NO_y abundances (1A, 21, 22).

30. Changes in calculated local temperature at 45 km for several scenarios.

31. Radiative calculated changes in equilibrium surface temperature for several scenarios (solid lines) and maximum and minimum changes with time in surface temperature including climate feedback amplification.

32. Total column ozone change with time for reference case CFC-only scenario compared to full reference case.

33. Relative change in total column ozone vs. change in Cl_z mole fraction for CFC-only reference case (solid line) and high case (scenario 5, dashed line).

34. Profiles of local ozone concentration change at selected times for CFC-only case.

35. Total column ozone change vs. upper stratospheric Cl_z abundance for reference case and CFC-only case (solid lines) and for a CFC/CH_4 (long dash) and CFC/N_2O case (short dash).

36. Vertical profiles of ClO/Cl_z for 1985 atmosphere (dotted line) CFC-only reference case (solid line) and CFC/methane case (dashed line).

37. Total column ozone change with time for CFC-only reference case with and without temperature feedback and complete reference case with and without temperature feedback.

Figure 1

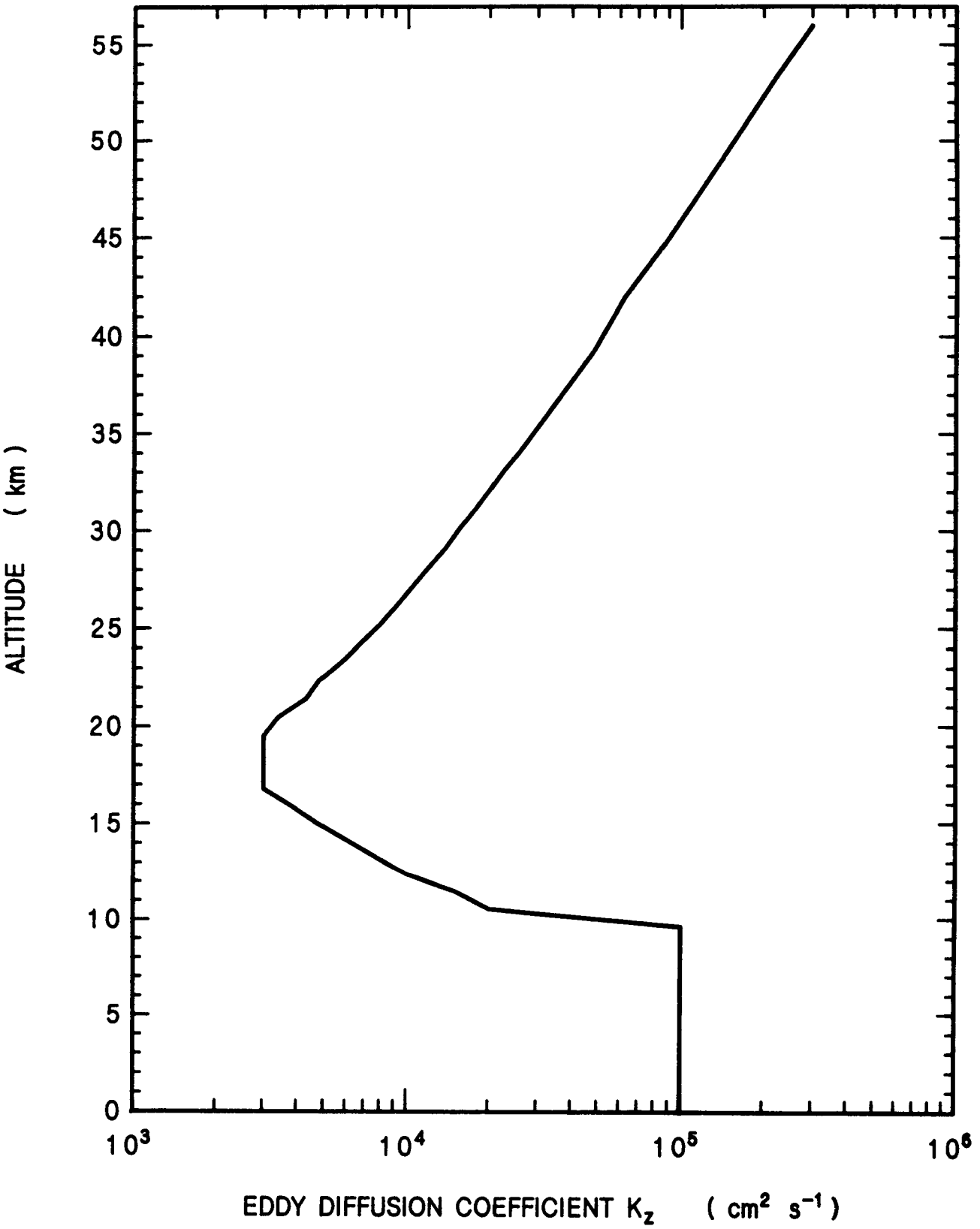
55
50
45
40
35
30
25
20
15
10
5
0
ALTITUDE (km)
10^3
10^4
10^5
10^6
EDDY DIFFUSION COEFFICIENT K_z (cm^2 s^{-1})

Figure 2

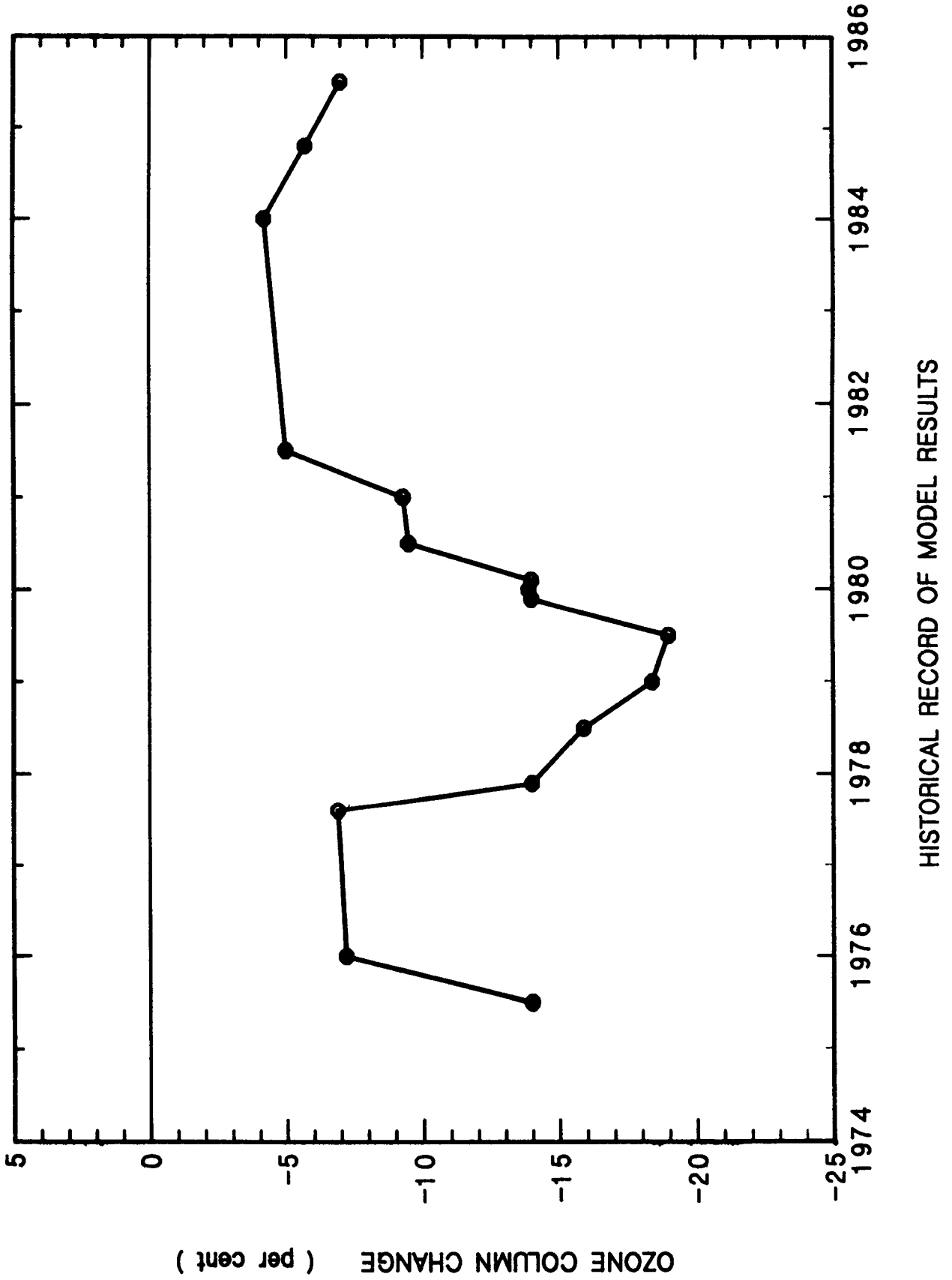
HISTORICAL RECORD OF MODEL RESULTS
OZONE COLUMN CHANGE (per cent)
5
0
-5
-10
-15
-20
-25
1974
1976
1978
1980
1982
1984
1986

Figure 3

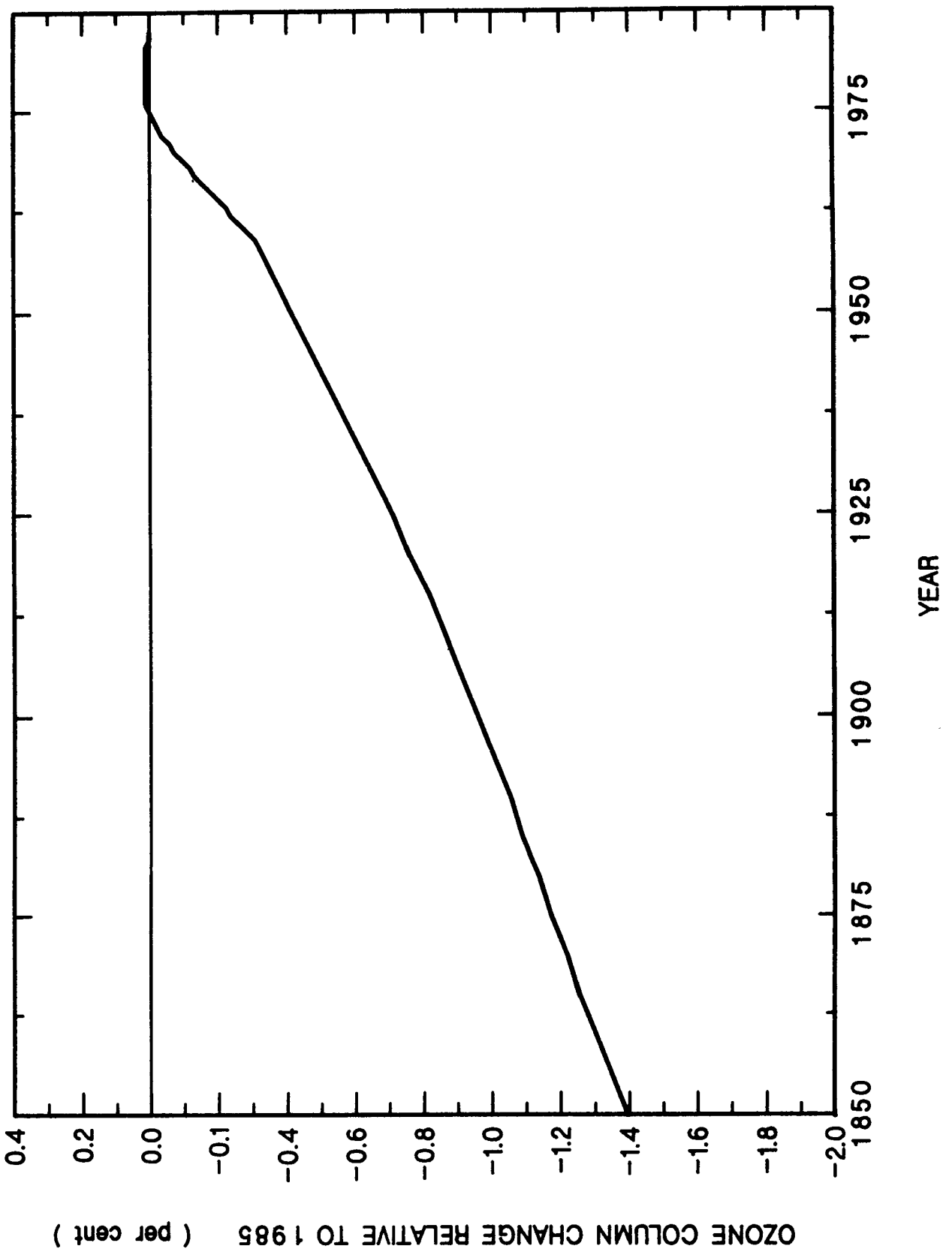
0.4
0.2
0.0
-0.1
-0.4
-0.6
-0.8
-1.0
-1.2
-1.4
-1.6
-1.8
-2.0
1850
1875
1900
1925
1950
1975
YEAR
OZONE COLUMN CHANGE RELATIVE TO 1985 (per cent)

Figure 4 a

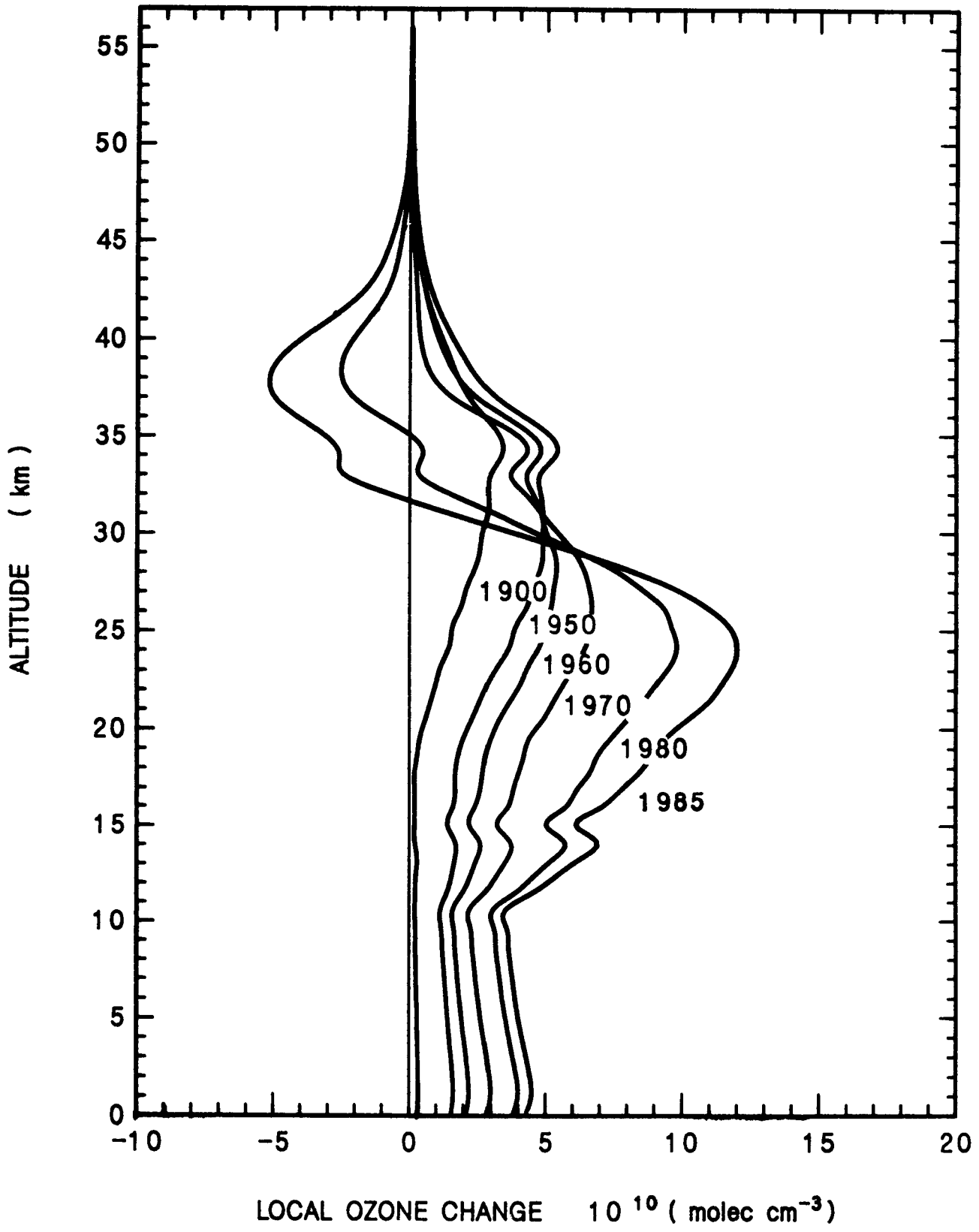
55
50
45
40
35
30
25
20
15
10
5
0
ALTITUDE (km)
-10
-5
0
5
10
15
20
1900
1950
1960
1970
1980
1985
LOCAL OZONE CHANGE 10 10 (molec cm-3)

Figure 4b

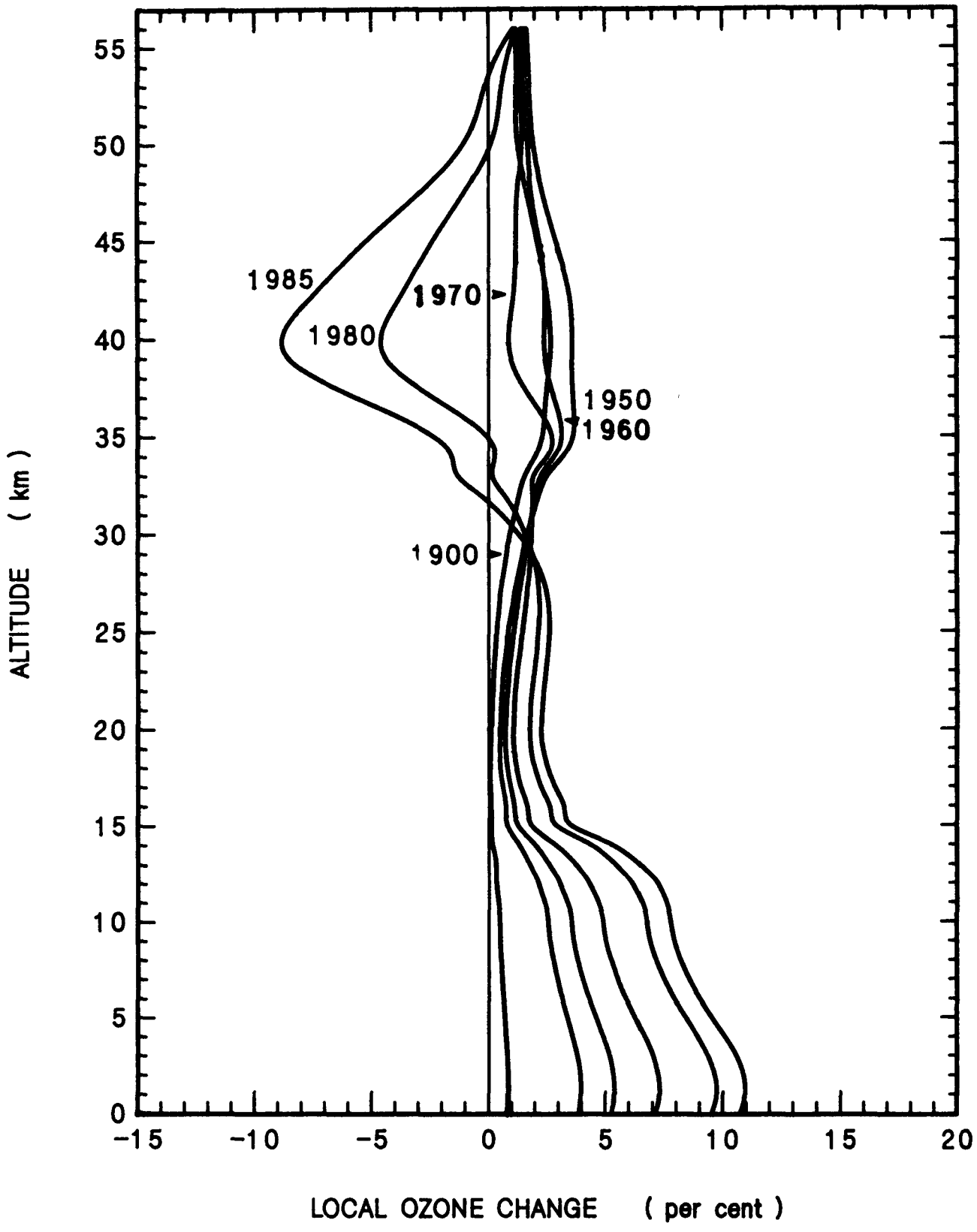
55
50
45
40
35
30
25
20
15
10
5
0
ALTITUDE (km)
1985
1980
1970
1950
1960
1900
-15
-10
-5
0
5
10
15
20
LOCAL OZONE CHANGE (per cent)

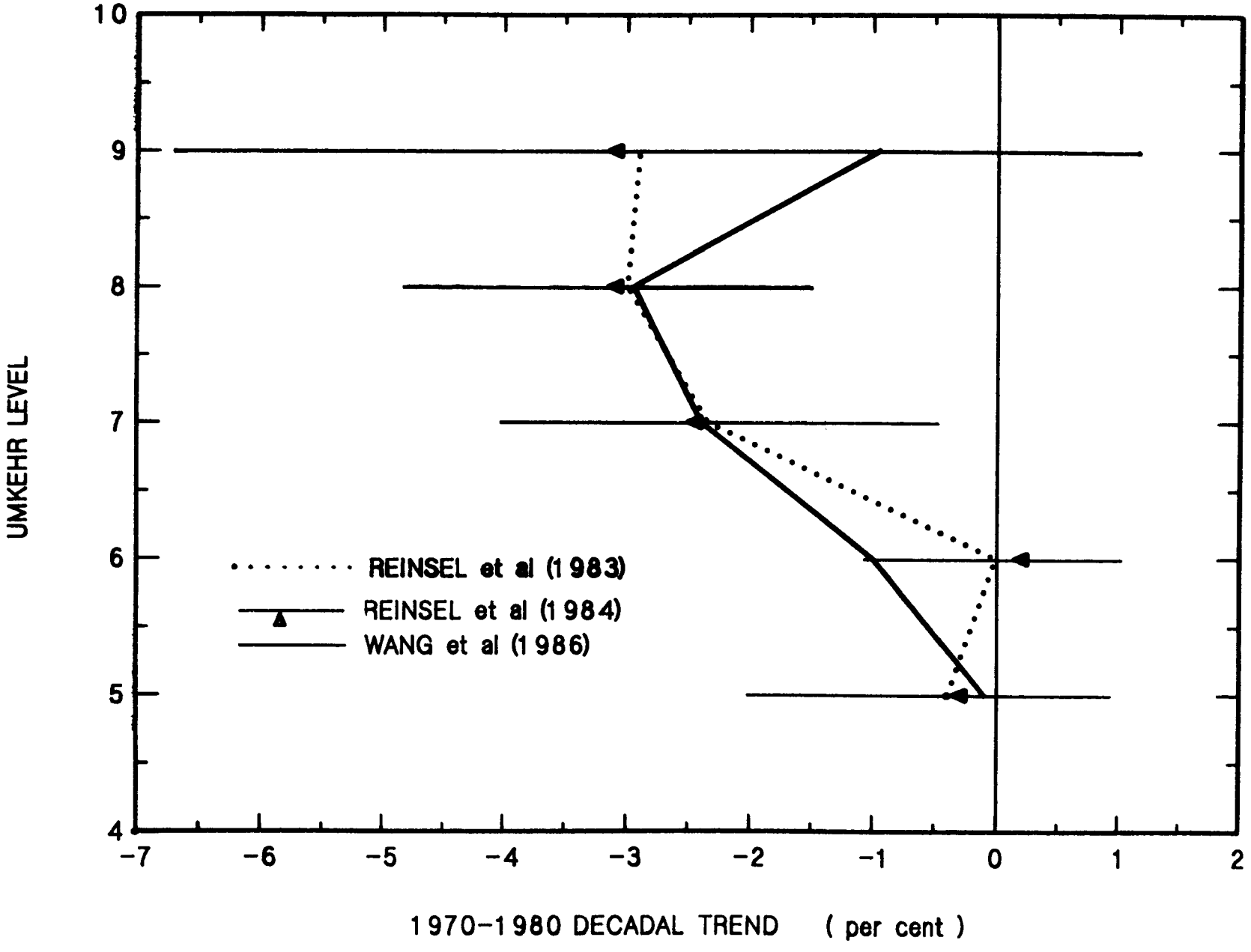
10
9
8
7
6
5
4
UMKEHR LEVEL
REINSEL et al (1983)
REINSEL et al (1984)
WANG et al (1986)
-7
-6
-5
-4
-3
-2
-1
0
1
2
1970-1980 DECADAL TREND (per cent)

Figure 5

Figure 6

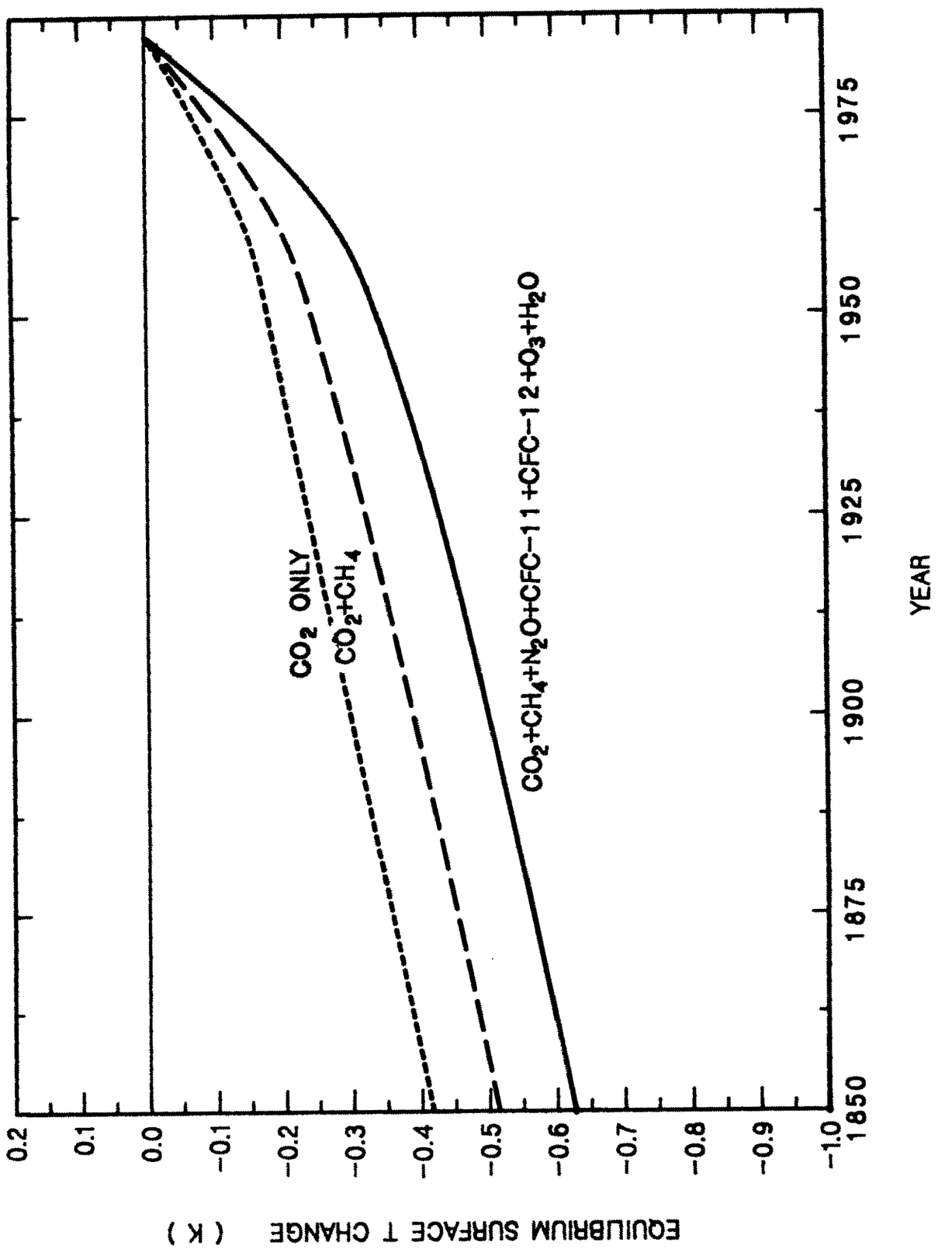
CO_2 ONLY
CO_2+CH_4
CO_2+CH_4+N_2O+CFC-11+CFC-12+O_3+H_2O
EQUILIBRIUM SURFACE T CHANGE (K)
0.2
0.1
0.0
−0.1
−0.2
−0.3
−0.4
−0.5
−0.6
−0.7
−0.8
−0.9
−1.0
1850
1875
1900
1925
1950
1975
YEAR

Figure 7

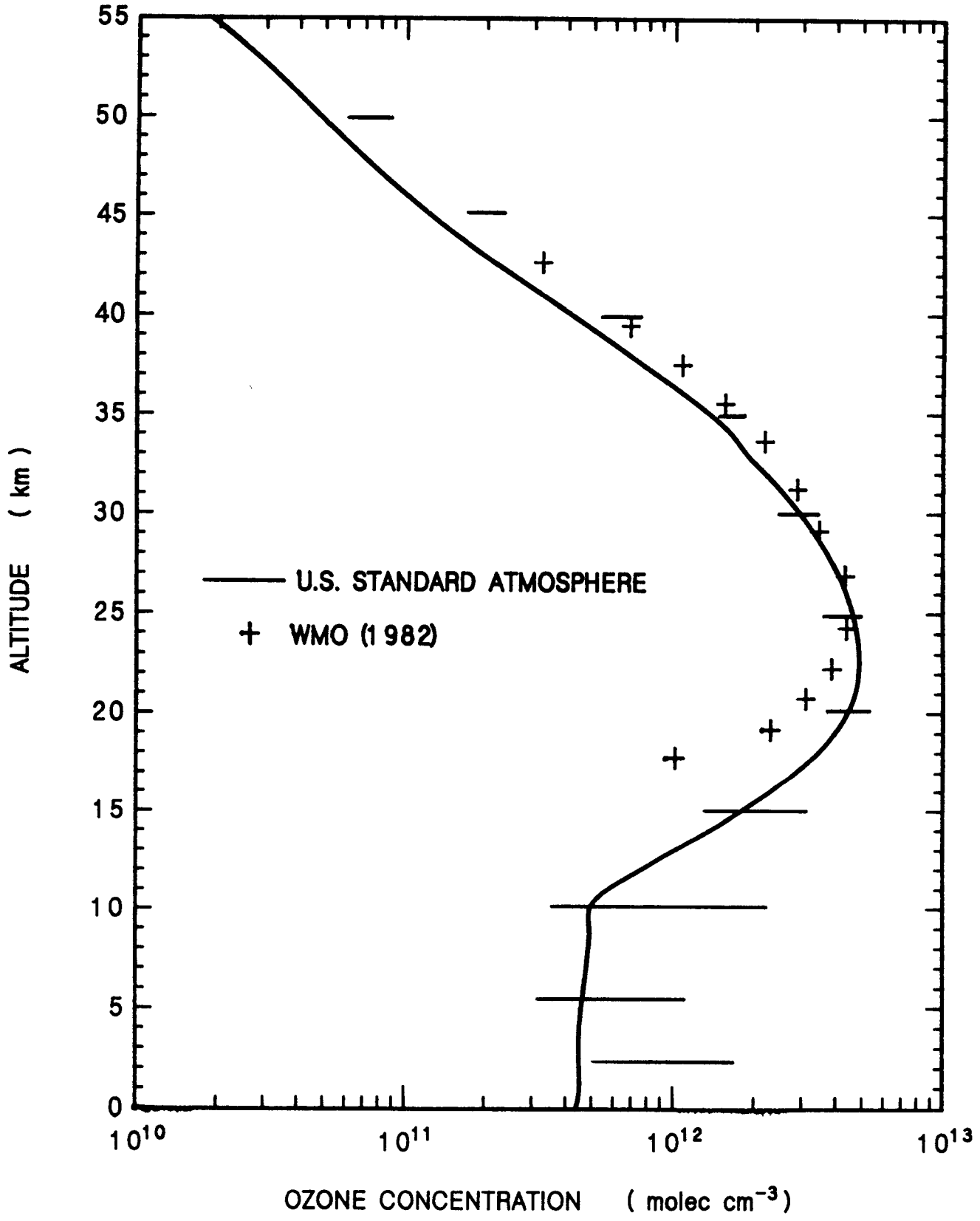
55
50
45
40
35
30
25
20
15
10
5
0
ALTITUDE (km)
U.S. STANDARD ATMOSPHERE
WMO (1982)
10^{10}
10^{11}
10^{12}
10^{13}
OZONE CONCENTRATION (molec cm^{-3})

Figure 8a

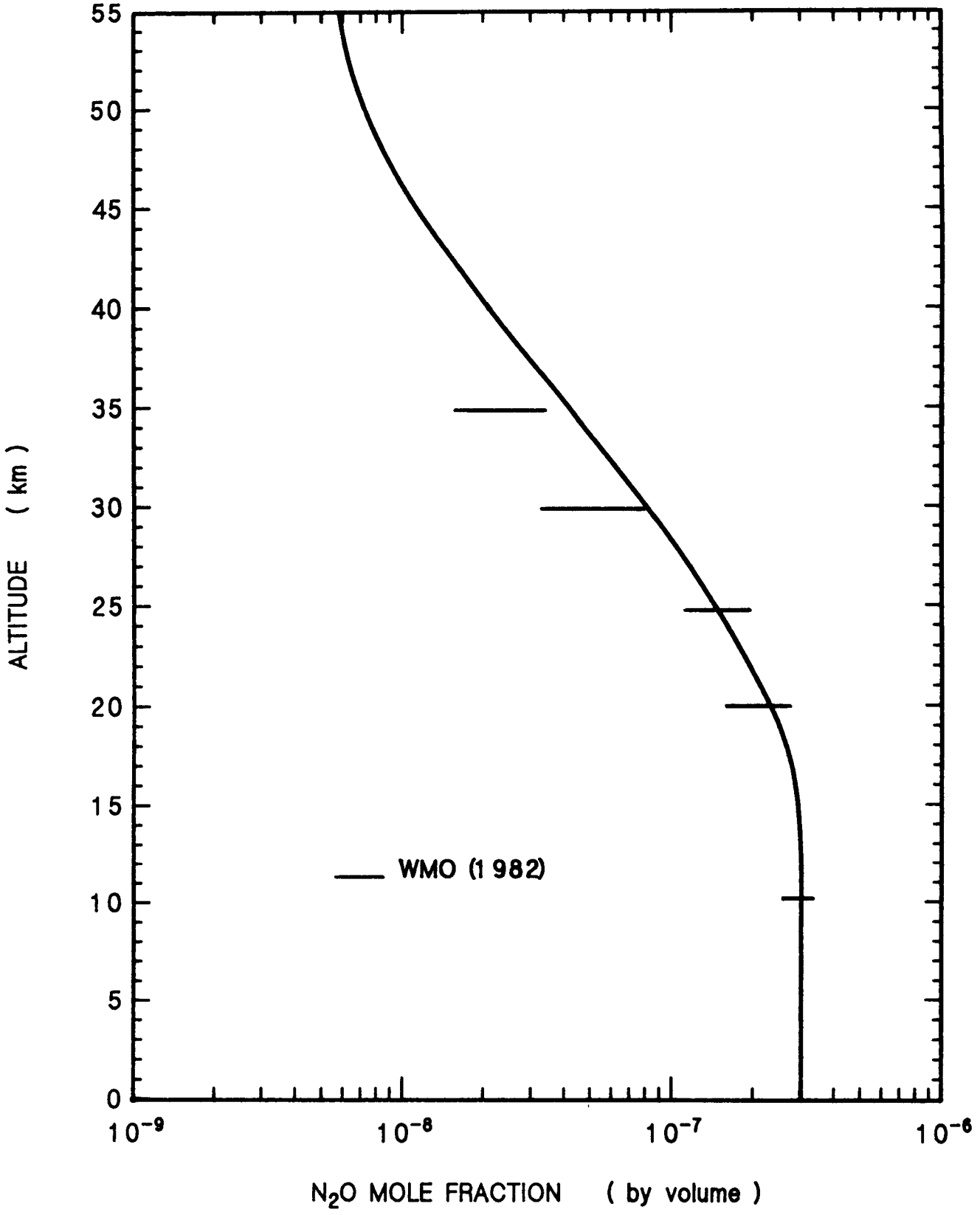
55
50
45
40
35
30
25
20
15
10
5
0
ALTITUDE (km)
WMO (1 982)
10^{-9}
10^{-8}
10^{-7}
10^{-6}
N_2O MOLE FRACTION (by volume)

Figure 8b

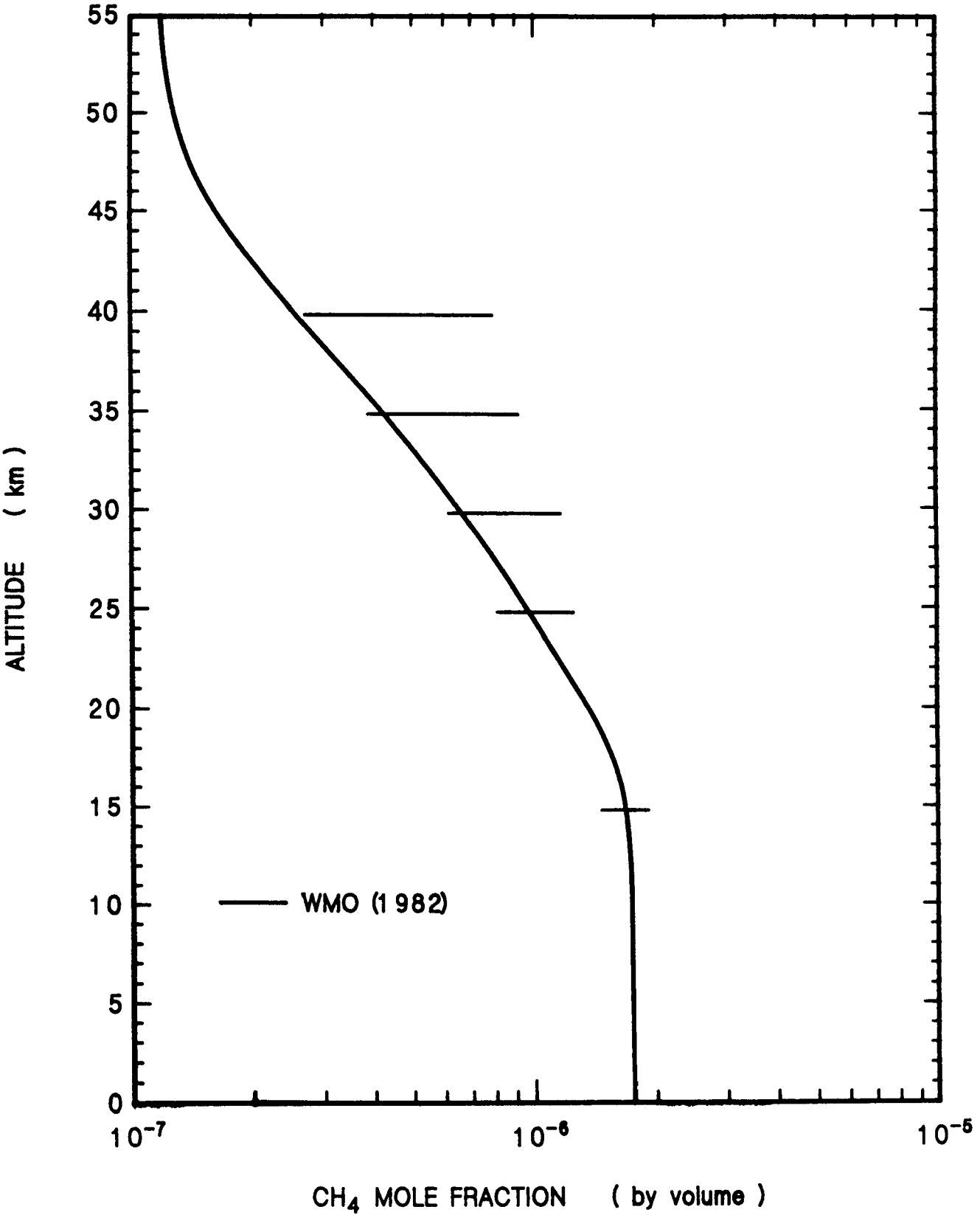
55
50
45
40
35
30
25
20
15
10
5
0
ALTITUDE (km)
WMO (1982)
10^{-7}
10^{-6}
10^{-5}
CH_4 MOLE FRACTION (by volume)

Figure 8c

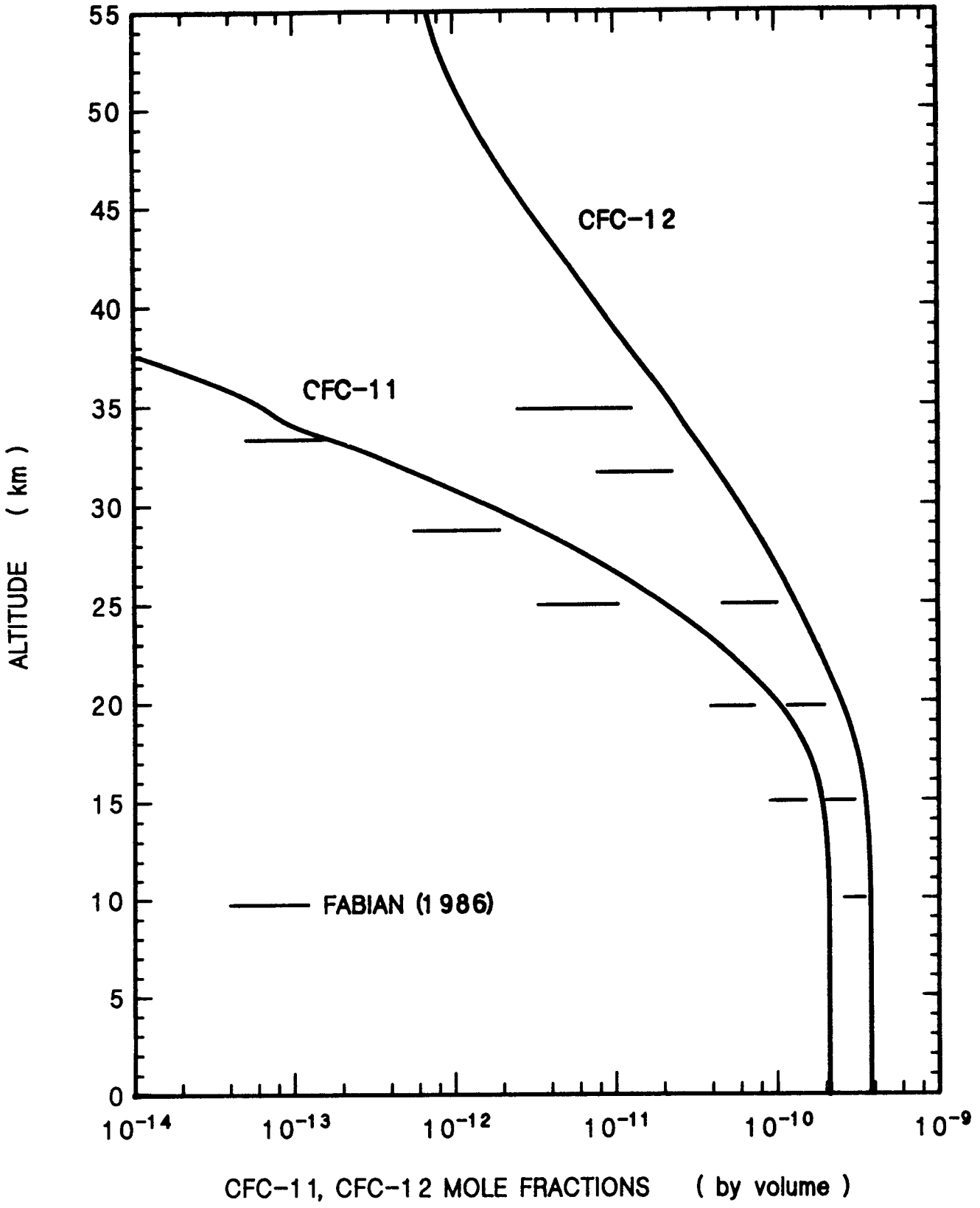
55
50
45
40
35
30
25
20
15
10
5
0
ALTITUDE (km)
CFC-12
CFC-11
FABIAN (1986)
10^{-14}
10^{-13}
10^{-12}
10^{-11}
10^{-10}
10^{-9}
CFC-11, CFC-12 MOLE FRACTIONS (by volume)

Figure 9a

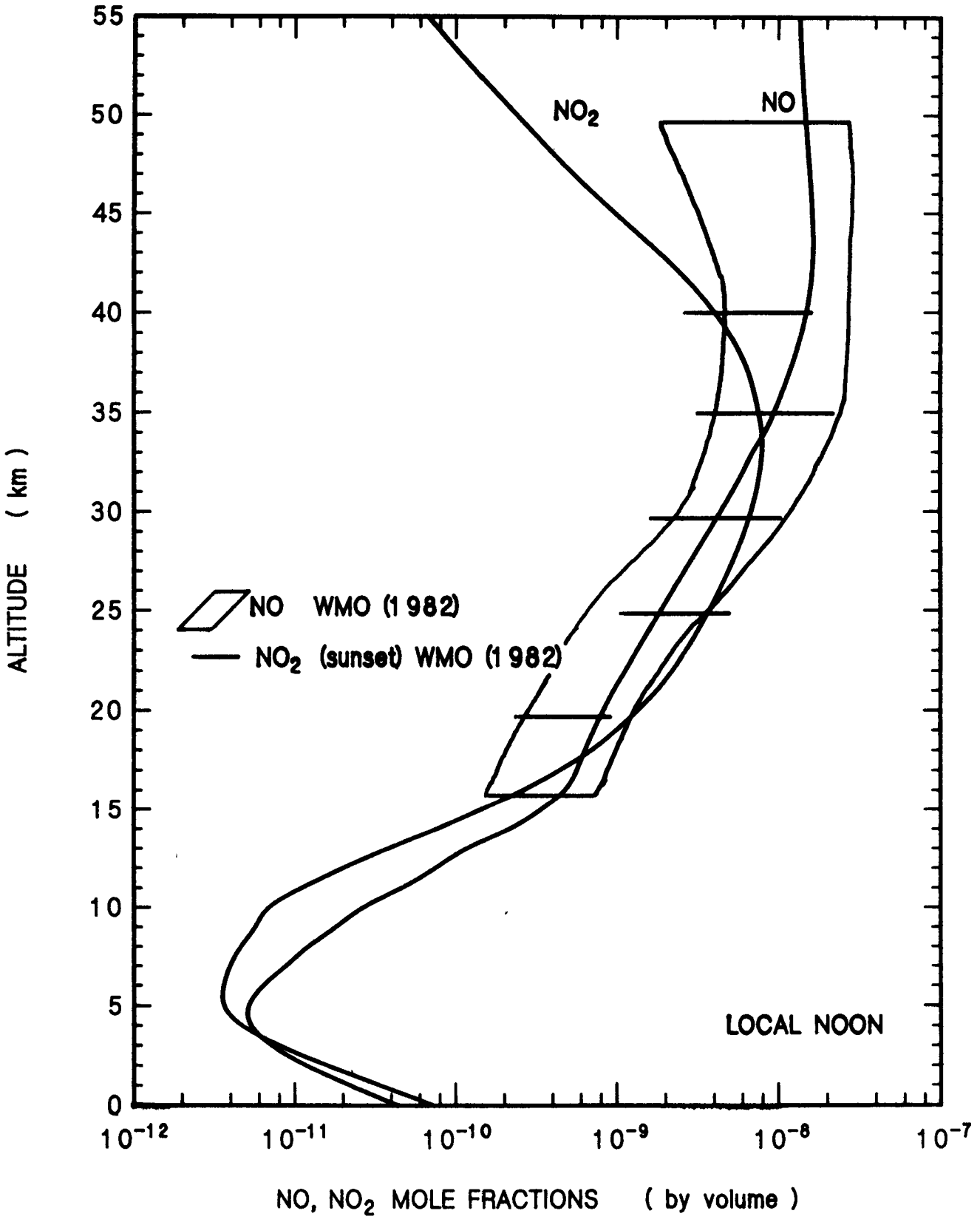
55
50
45
40
35
30
25
20
15
10
5
0
ALTITUDE (km)
NO_2
NO
NO WMO (1982)
NO_2 (sunset) WMO (1982)
LOCAL NOON
10^{-12}
10^{-11}
10^{-10}
10^{-9}
10^{-8}
10^{-7}
NO, NO_2 MOLE FRACTIONS (by volume)

Figure 9b

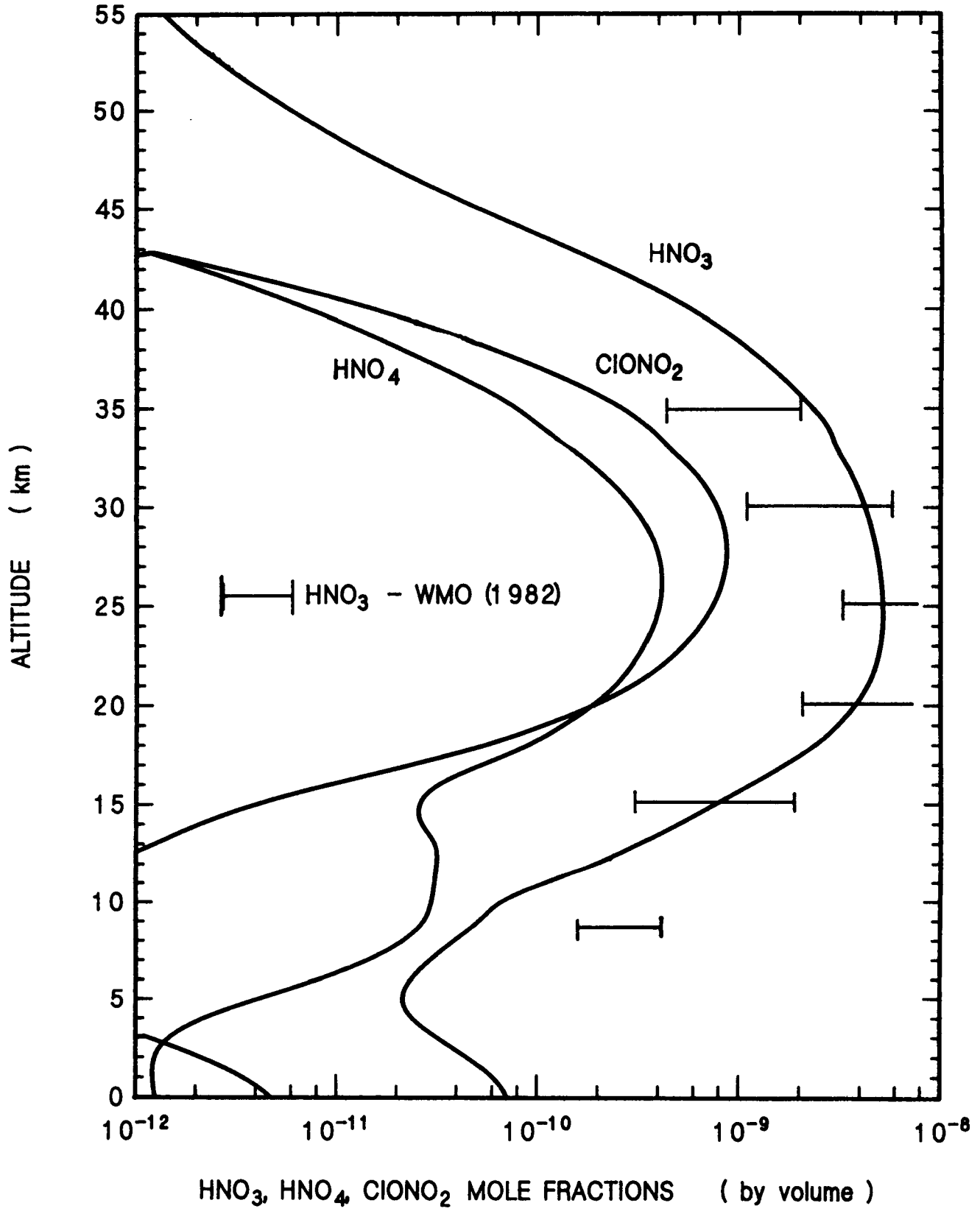
55
50
45
40
35
30
25
20
15
10
5
0
ALTITUDE (km)
HNO3
HNO4
ClONO2
HNO3 - WMO (1982)
10-12
10-11
10-10
10-9
10-8
HNO3, HNO4, ClONO2 MOLE FRACTIONS (by volume)

Figure 10a

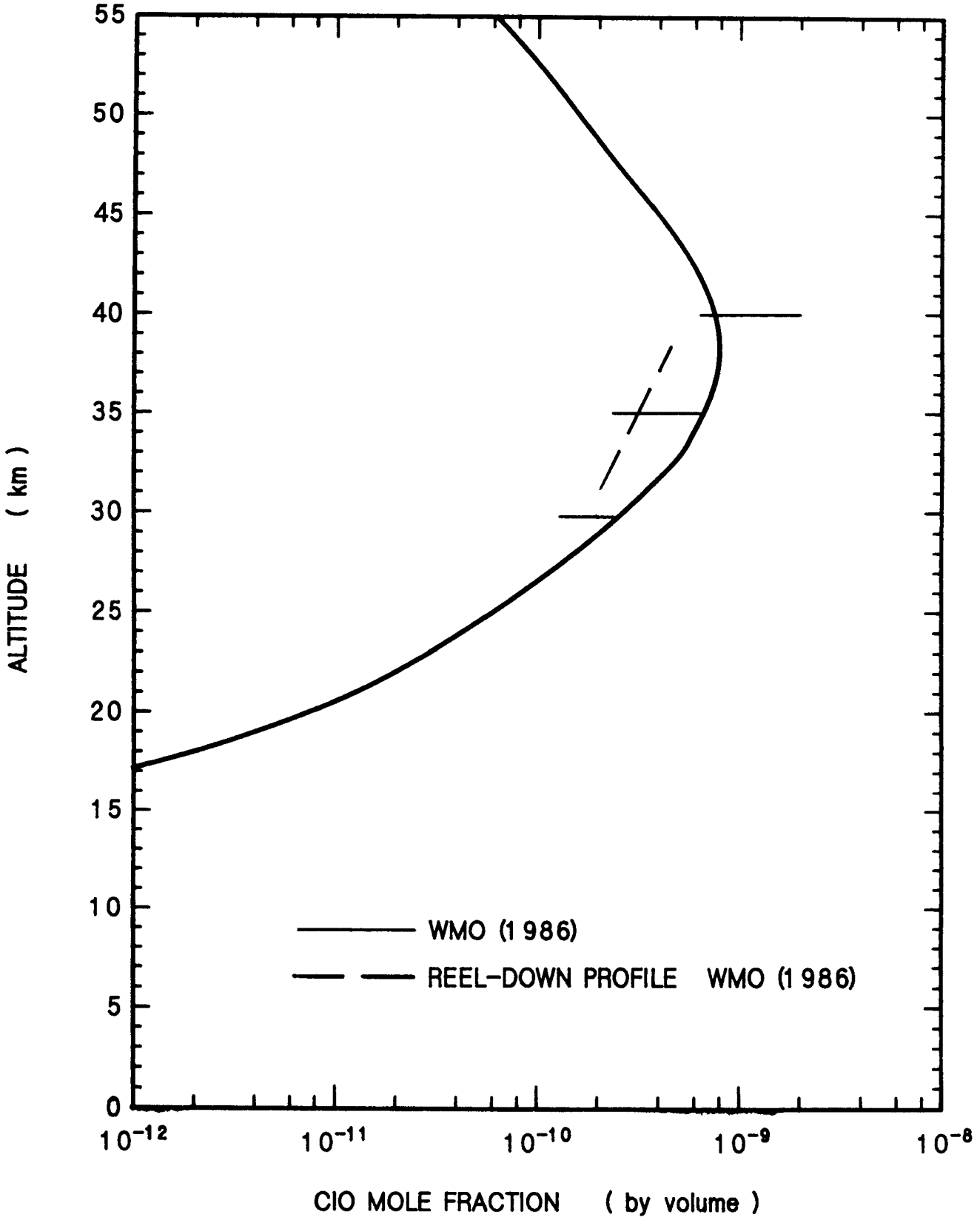
55
50
45
40
35
30
25
20
15
10
5
0
ALTITUDE (km)
WMO (1986)
REEL-DOWN PROFILE WMO (1986)
10^{-12}
10^{-11}
10^{-10}
10^{-9}
10^{-8}
ClO MOLE FRACTION (by volume)

Figure 10b

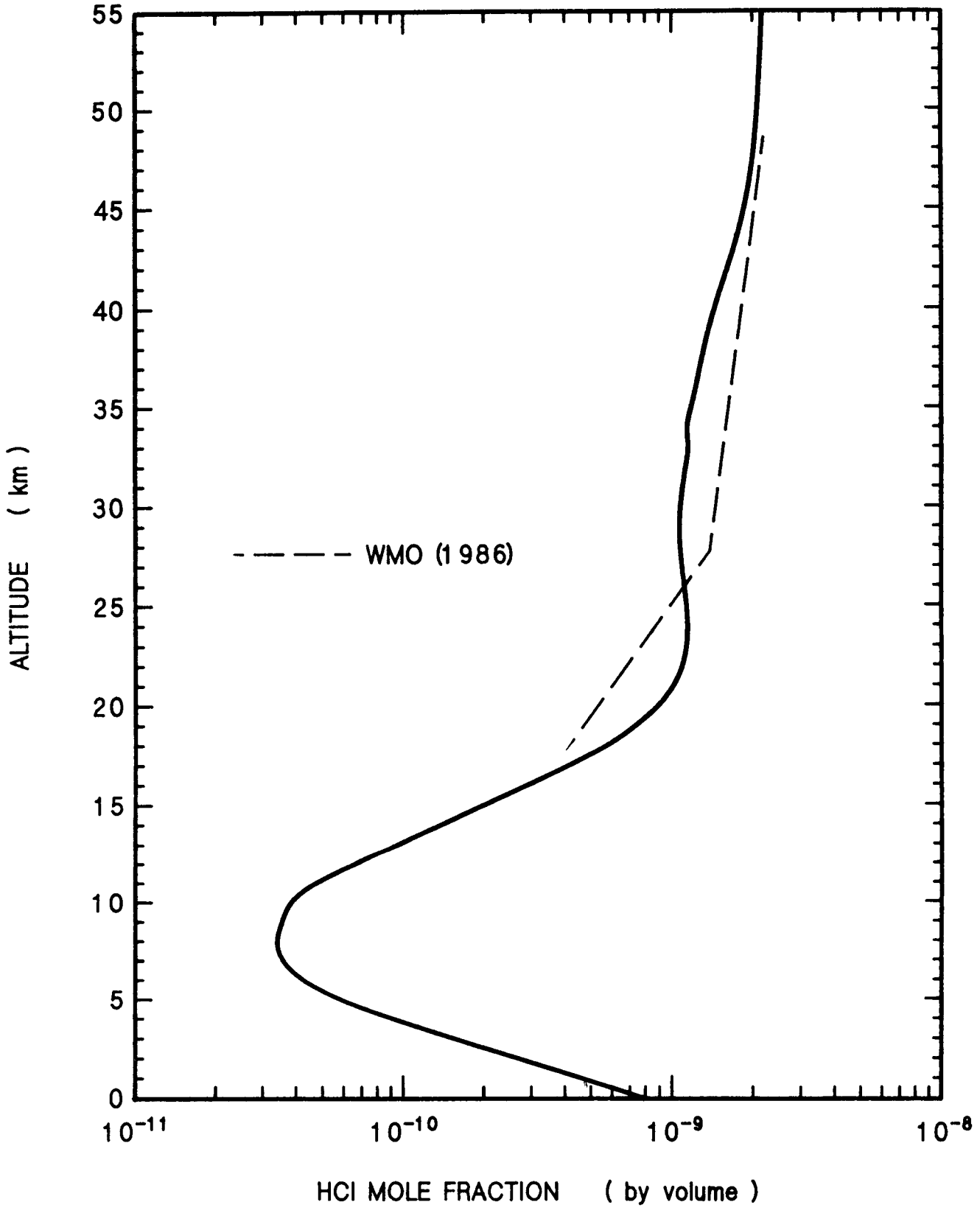
55
50
45
40
35
30
25
20
15
10
5
0
ALTITUDE (km)
WMO (1986)
10^{-11}
10^{-10}
10^{-9}
10^{-8}
HCl MOLE FRACTION (by volume)

Figure 11

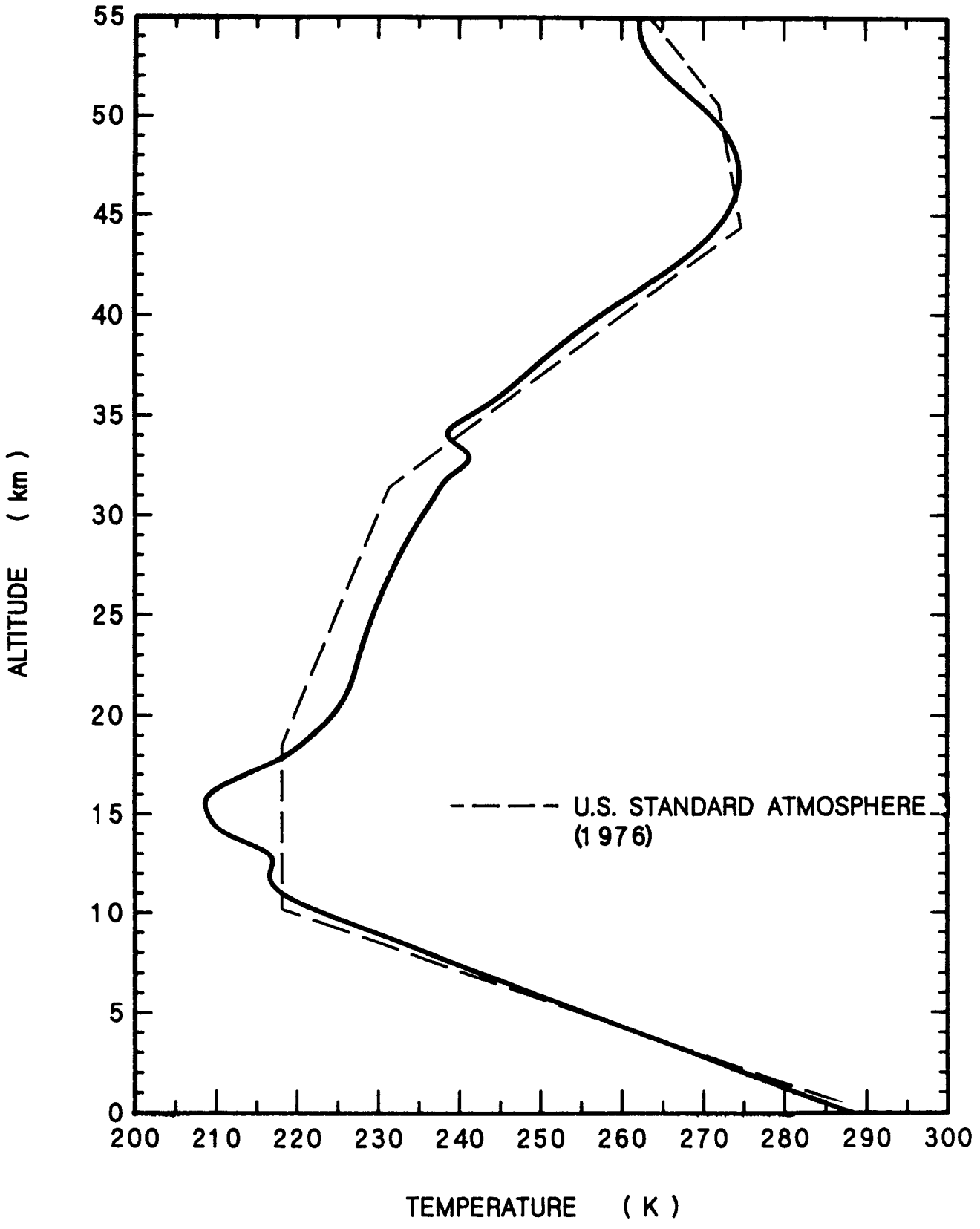
55
50
45
40
35
30
25
20
15
10
5
0
ALTITUDE (km)
200 210 220 230 240 250 260 270 280 290 300
TEMPERATURE (K)
U.S. STANDARD ATMOSPHERE
(1976)

Figure 12

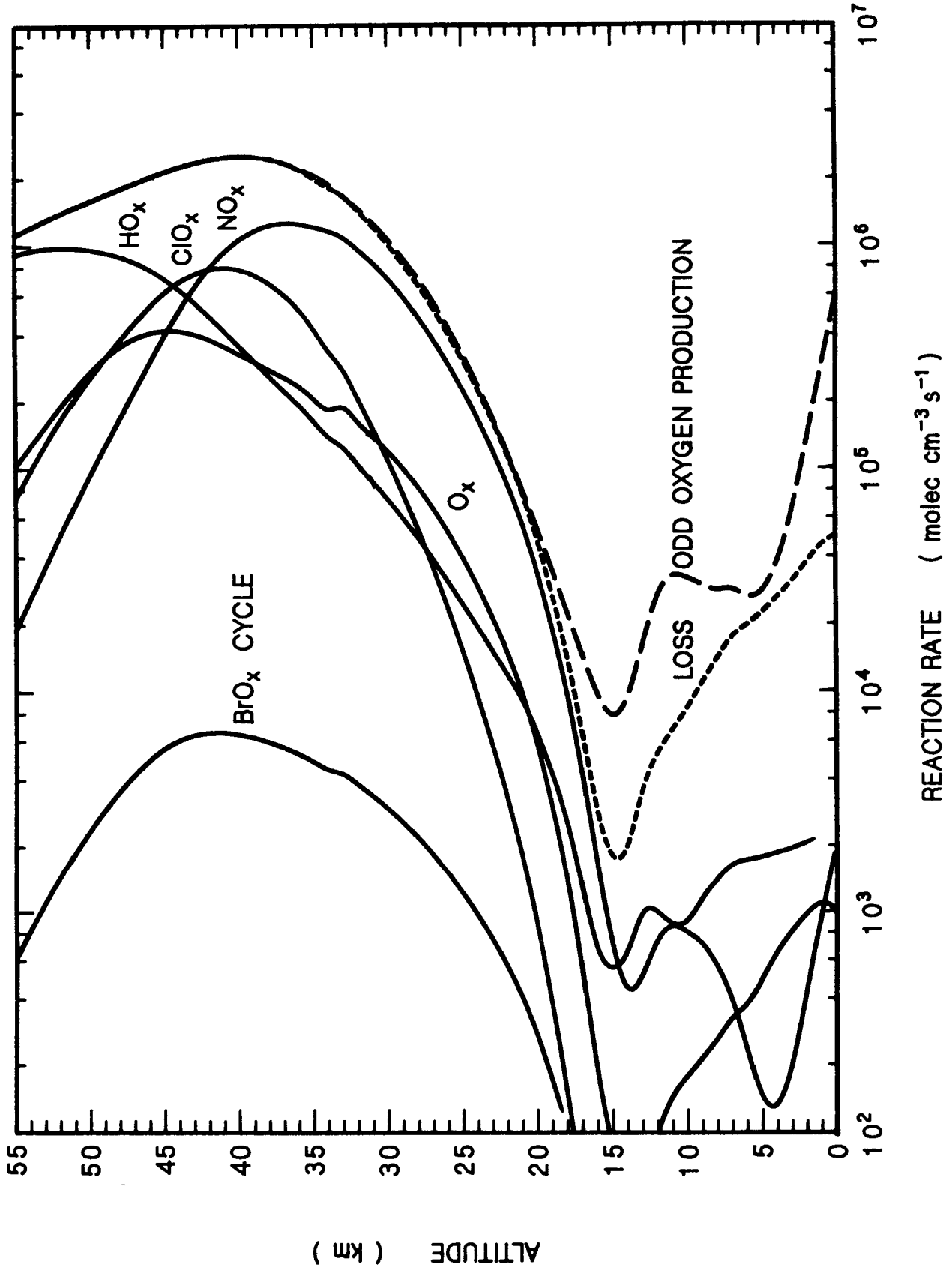
ALTITUDE (km)
55
50
45
40
35
30
25
20
15
10
5
0
REACTION RATE (molec cm^{-3} s^{-1})
10^2
10^3
10^4
10^5
10^6
10^7
HO_x
ClO_x
NO_x
O_x
BrO_x CYCLE
ODD OXYGEN PRODUCTION
LOSS

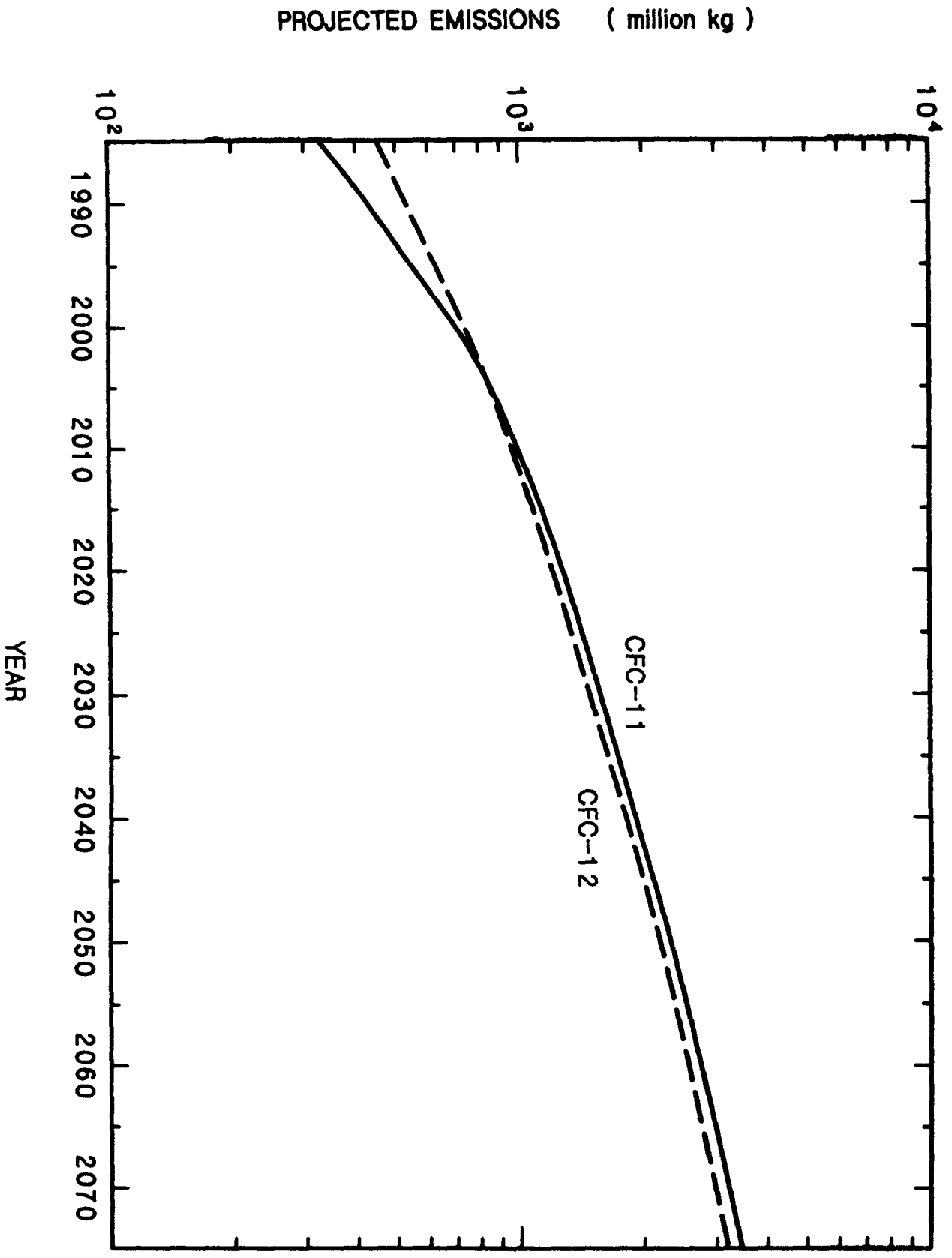
PROJECTED EMISSIONS (million kg)
10^2
10^3
10^4
1990
2000
2010
2020
2030
2040
2050
2060
2070
YEAR
CFC-11
CFC-12

Figure 13

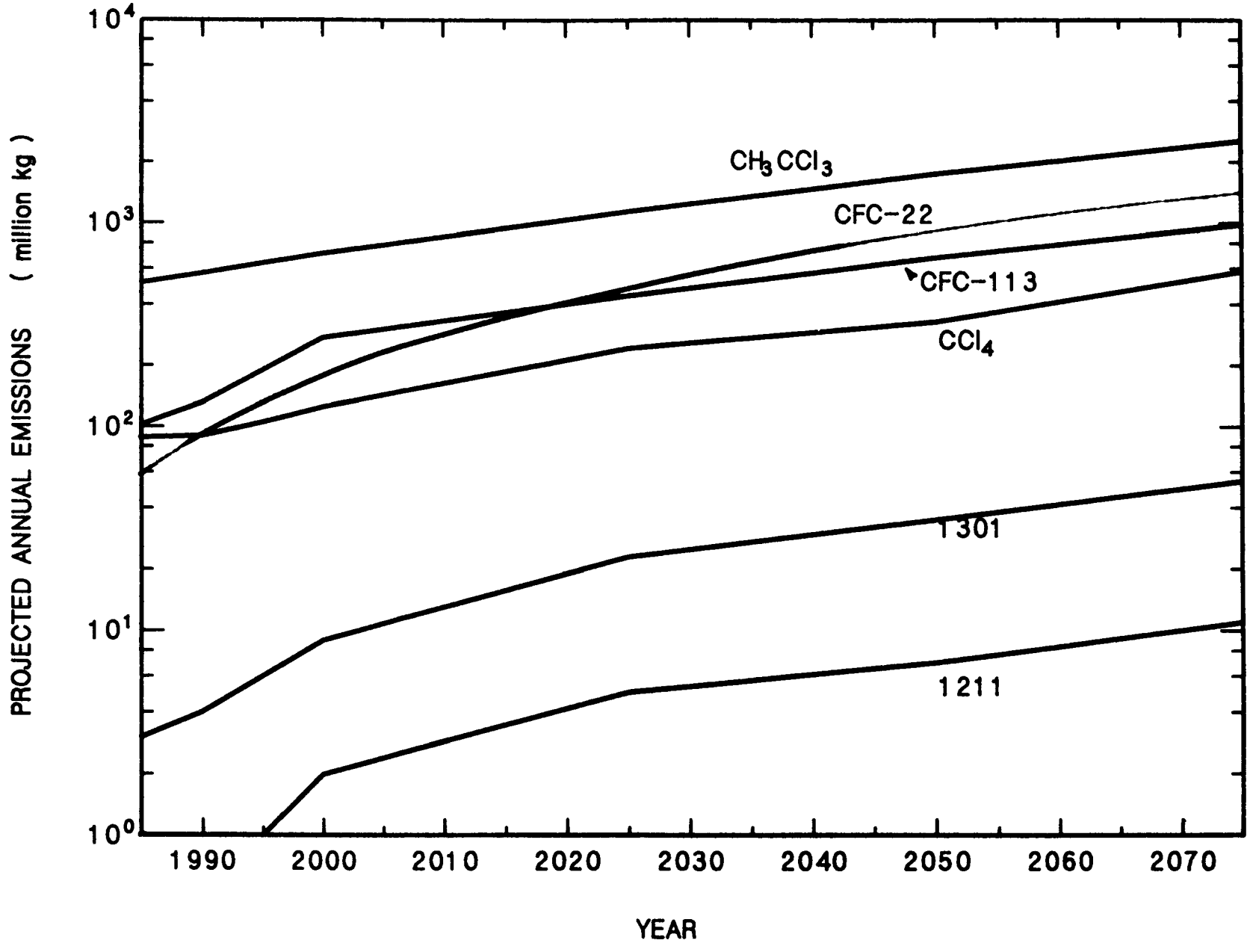
PROJECTED ANNUAL EMISSIONS (million kg)
10^4
10^3
10^2
10^1
10^0
CH_3CCl_3
CFC-22
CFC-113
CCl_4
1301
1211
1990
2000
2010
2020
2030
2040
2050
2060
2070
YEAR

Figure 14

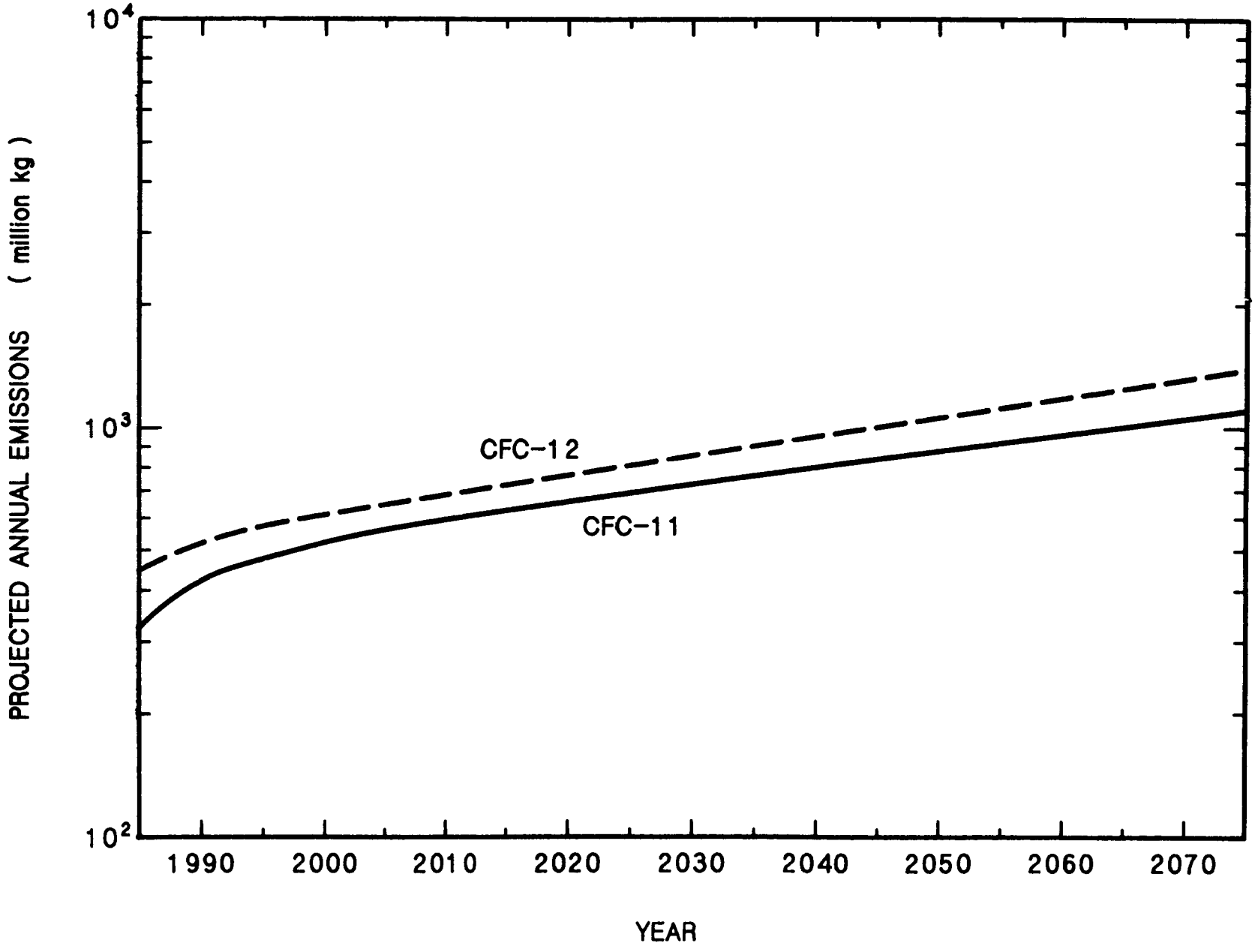
PROJECTED ANNUAL EMISSIONS (million kg)
10^4
10^3
10^2
CFC-12
CFC-11
1990
2000
2010
2020
2030
2040
2050
2060
2070
YEAR

Figure 15a

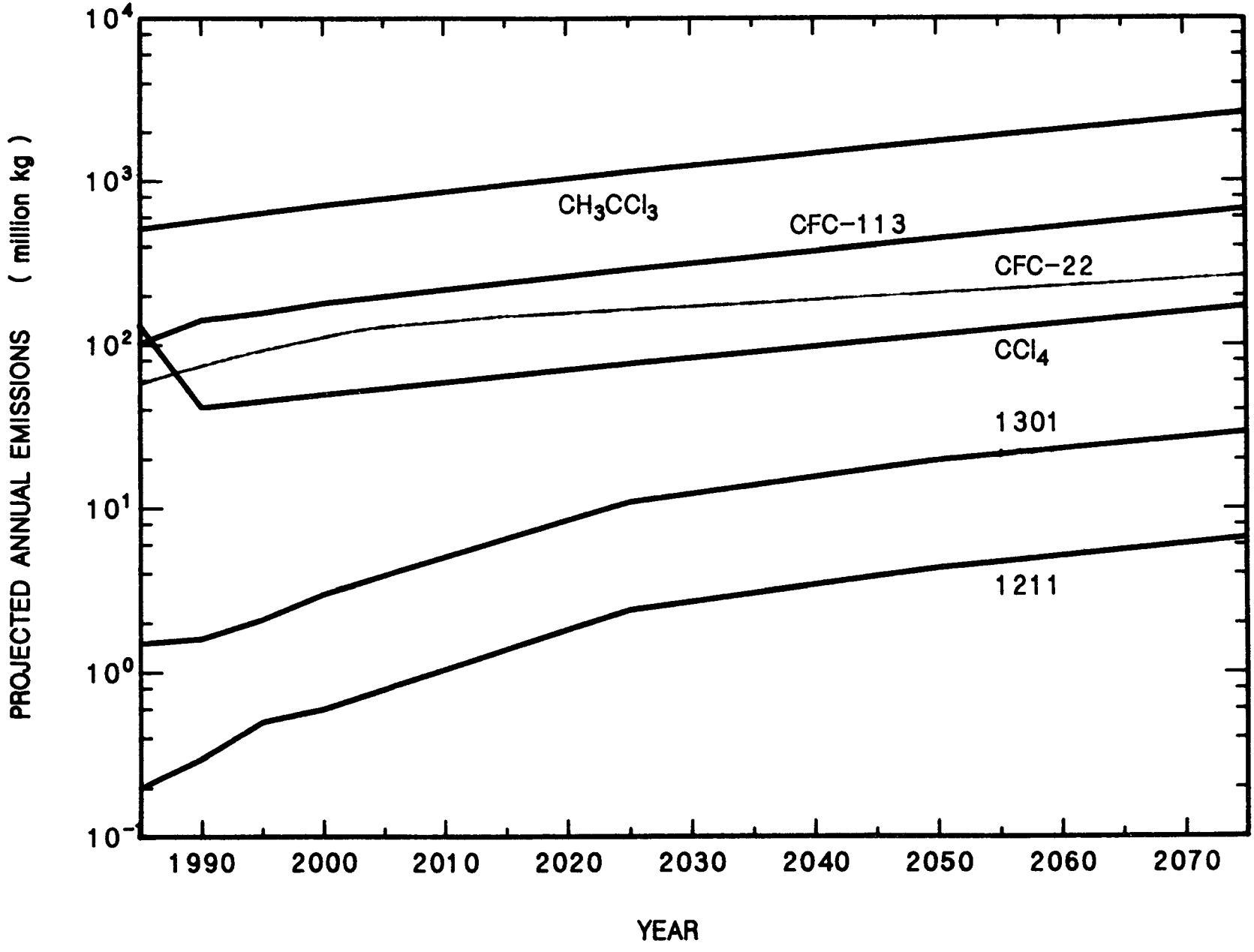
PROJECTED ANNUAL EMISSIONS (million kg)
10^4
10^3
10^2
10^1
10^0
10^{-1}
CH_3CCl_3
CFC-113
CFC-22
CCl_4
1301
1211
1990
2000
2010
2020
2030
2040
2050
2060
2070
YEAR

Figure 15b

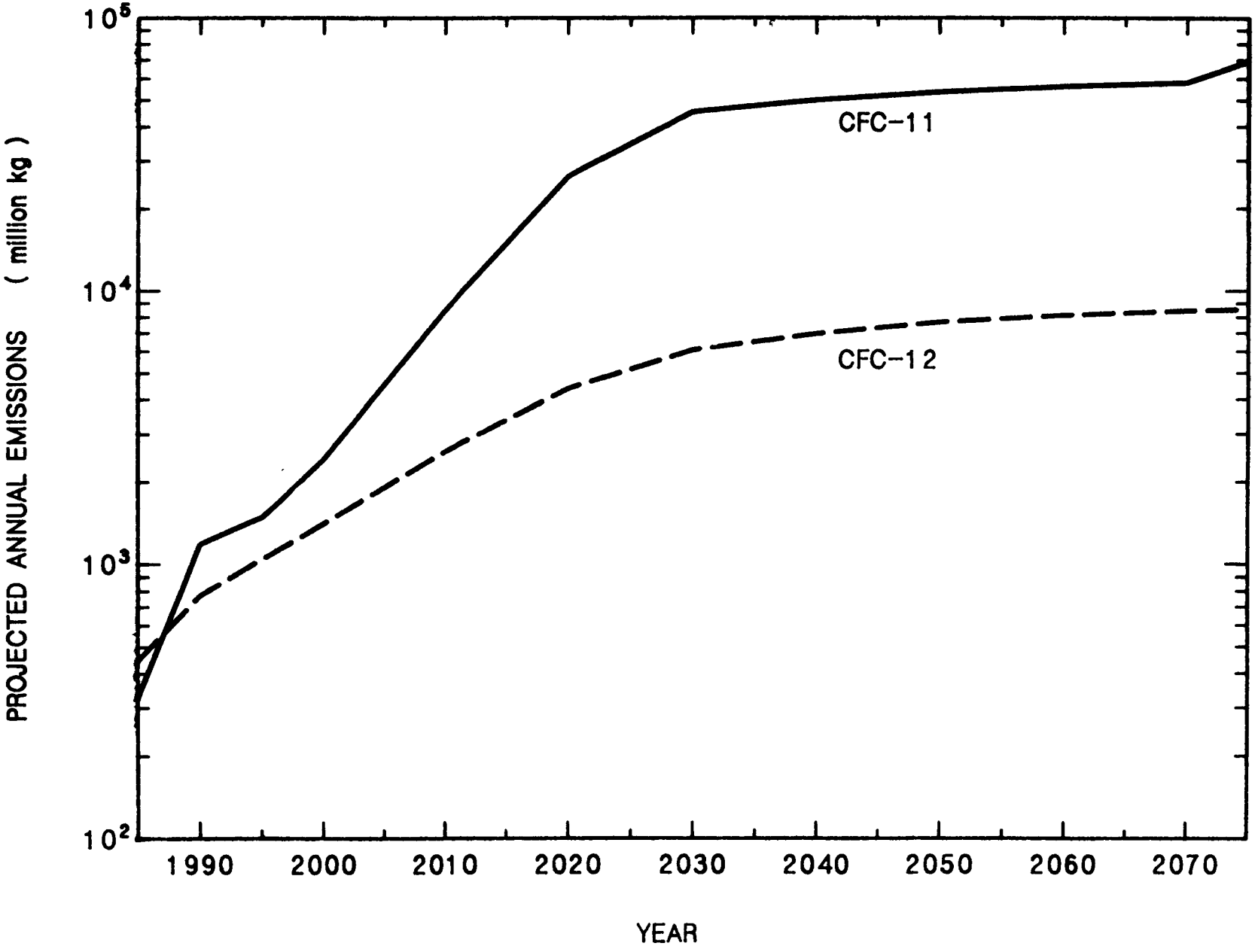
PROJECTED ANNUAL EMISSIONS (million kg)
10^5
10^4
10^3
10^2
CFC-11
CFC-12
1990
2000
2010
2020
2030
2040
2050
2060
2070
YEAR

Figure 16a

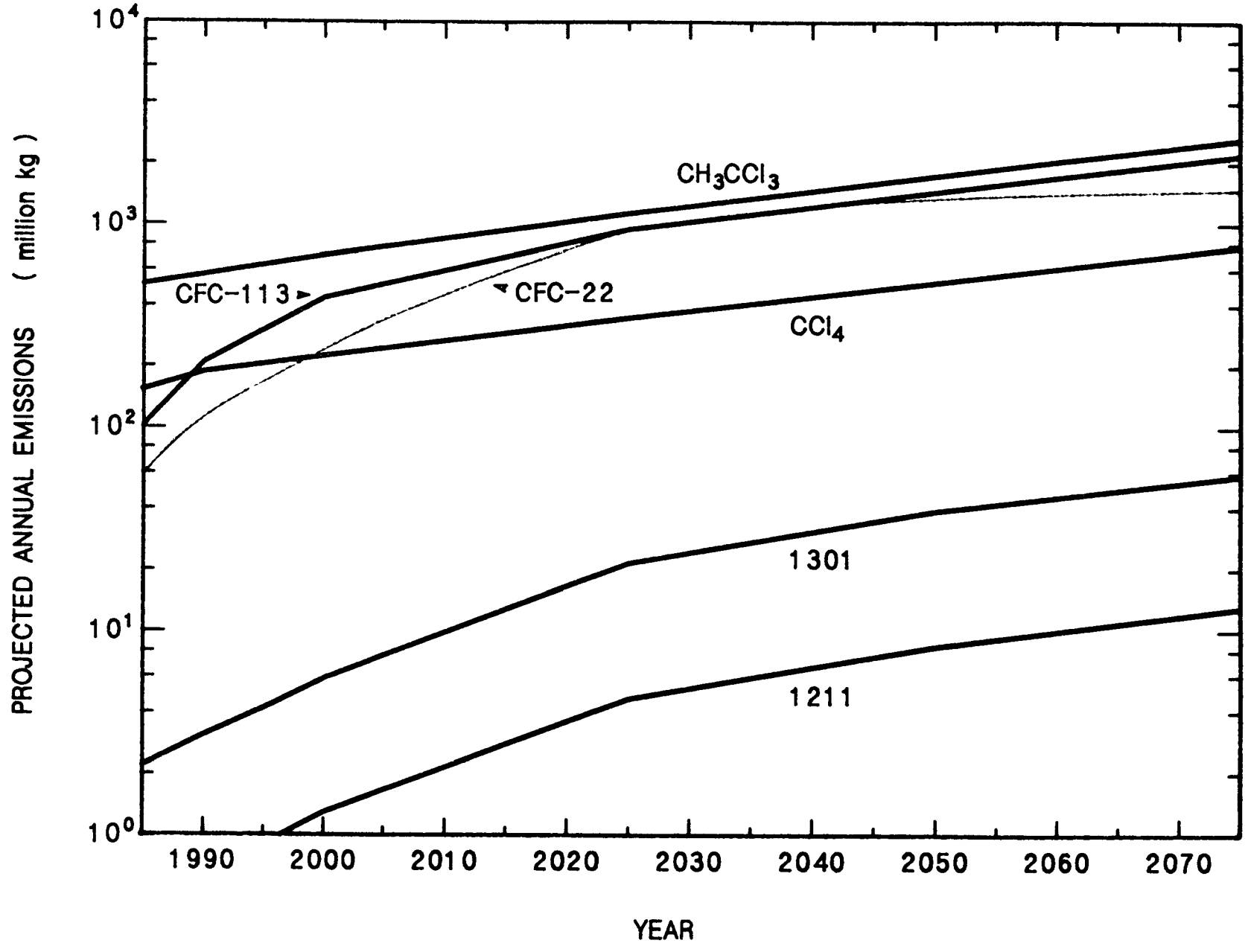
PROJECTED ANNUAL EMISSIONS (million kg)
10^4
10^3
10^2
10^1
10^0
CH_3CCl_3
CFC-113
CFC-22
CCl_4
1301
1211
1990
2000
2010
2020
2030
2040
2050
2060
2070
YEAR

Figure 16b

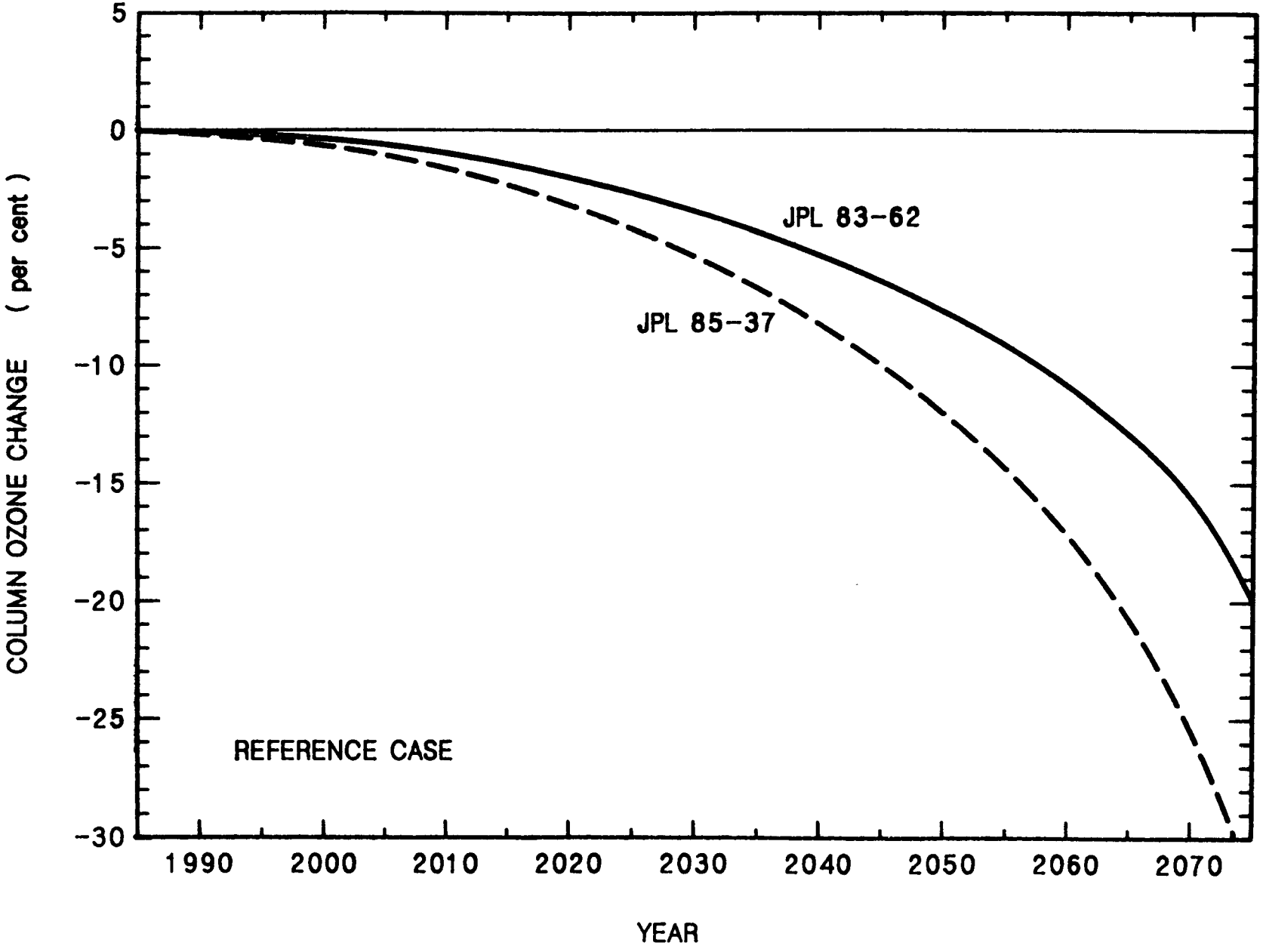
5
0
-5
-10
-15
-20
-25
-30
COLUMN OZONE CHANGE (per cent)
JPL 83-62
JPL 85-37
REFERENCE CASE
1990
2000
2010
2020
2030
2040
2050
2060
2070
YEAR

Figure 17

Figure 18a

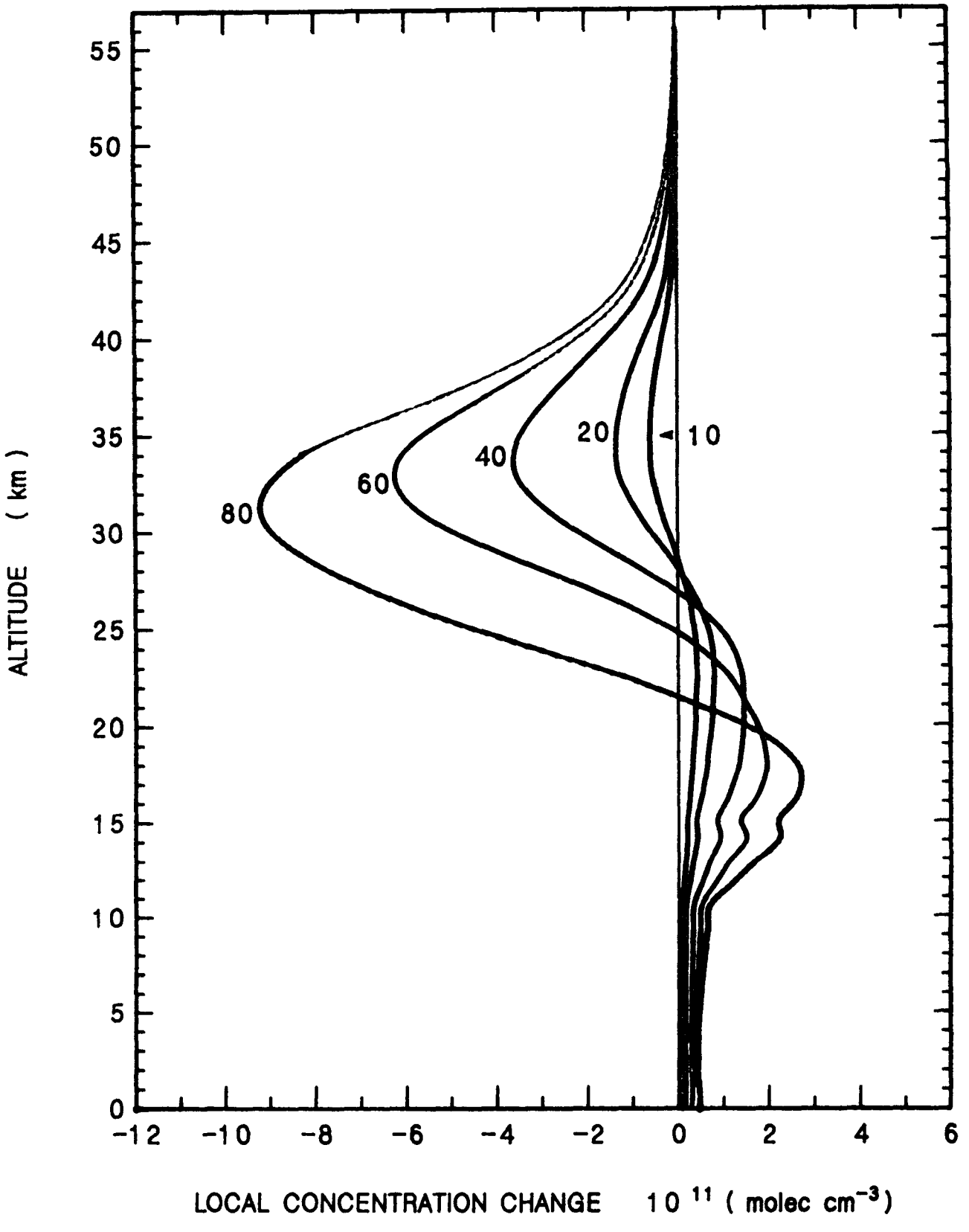
ALTITUDE (km)
55
50
45
40
35
30
25
20
15
10
5
0
-12
-10
-8
-6
-4
-2
0
2
4
6
80
60
40
20
10
LOCAL CONCENTRATION CHANGE 10 11 (molec cm-3)

Figure 18b

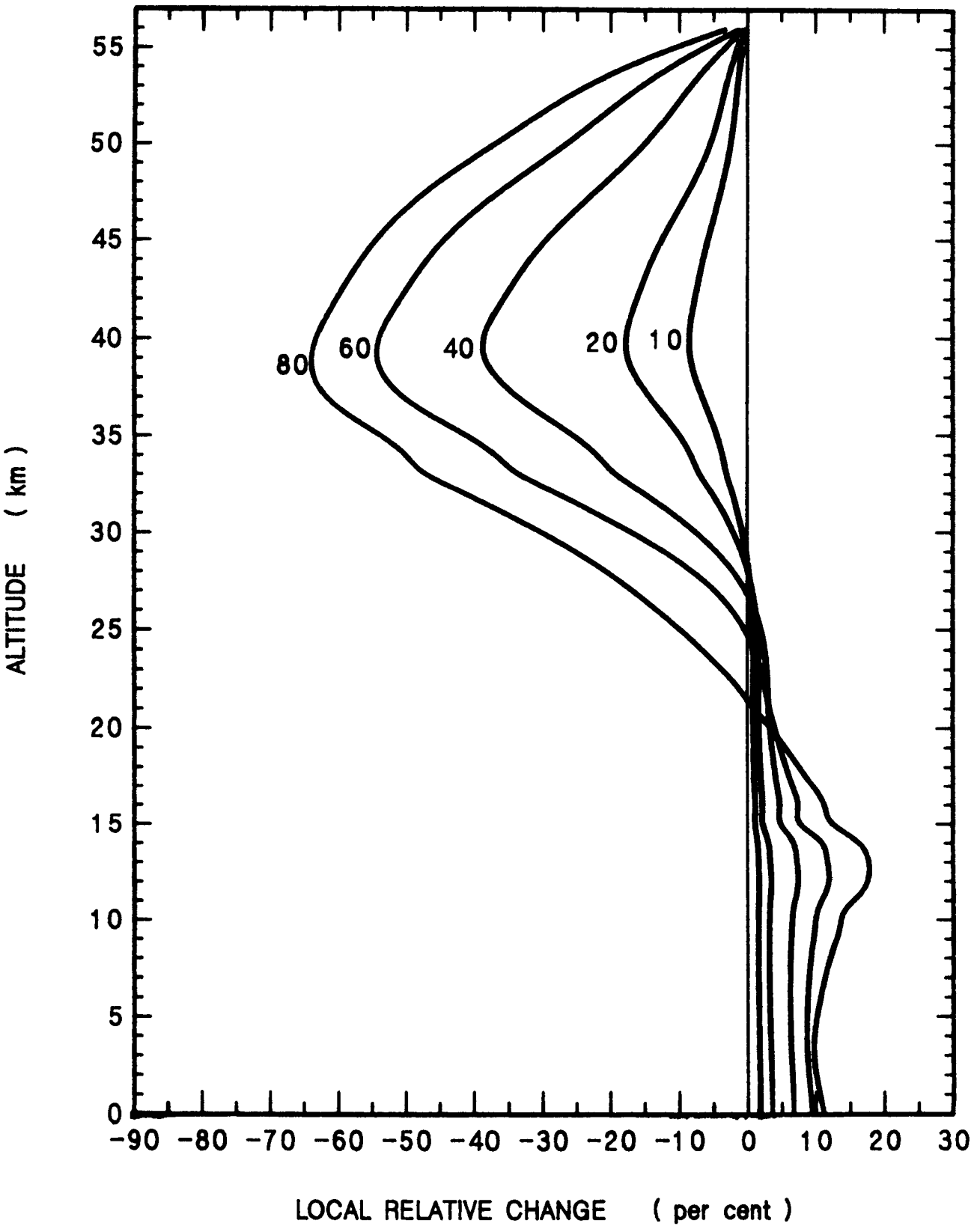
55
50
45
40
35
30
25
20
15
10
5
0
ALTITUDE (km)
80
60
40
20
10
-90 -80 -70 -60 -50 -40 -30 -20 -10 0 10 20 30
LOCAL RELATIVE CHANGE (per cent)

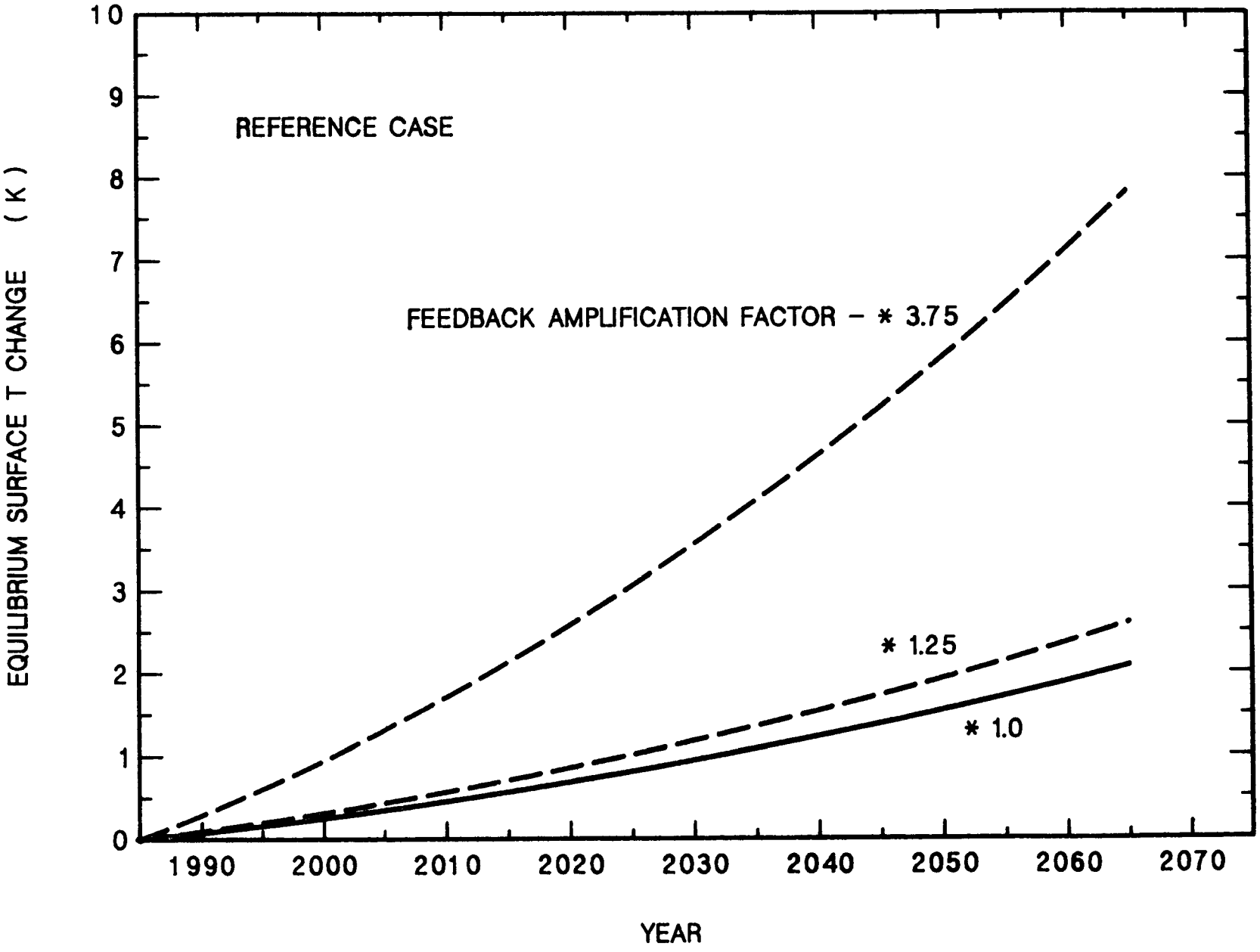
EQUILIBRIUM SURFACE T CHANGE (K)
10
9
8
7
6
5
4
3
2
1
0
REFERENCE CASE
FEEDBACK AMPLIFICATION FACTOR – * 3.75
* 1.25
* 1.0
1990
2000
2010
2020
2030
2040
2050
2060
2070
YEAR

Figure 19

Figure 20

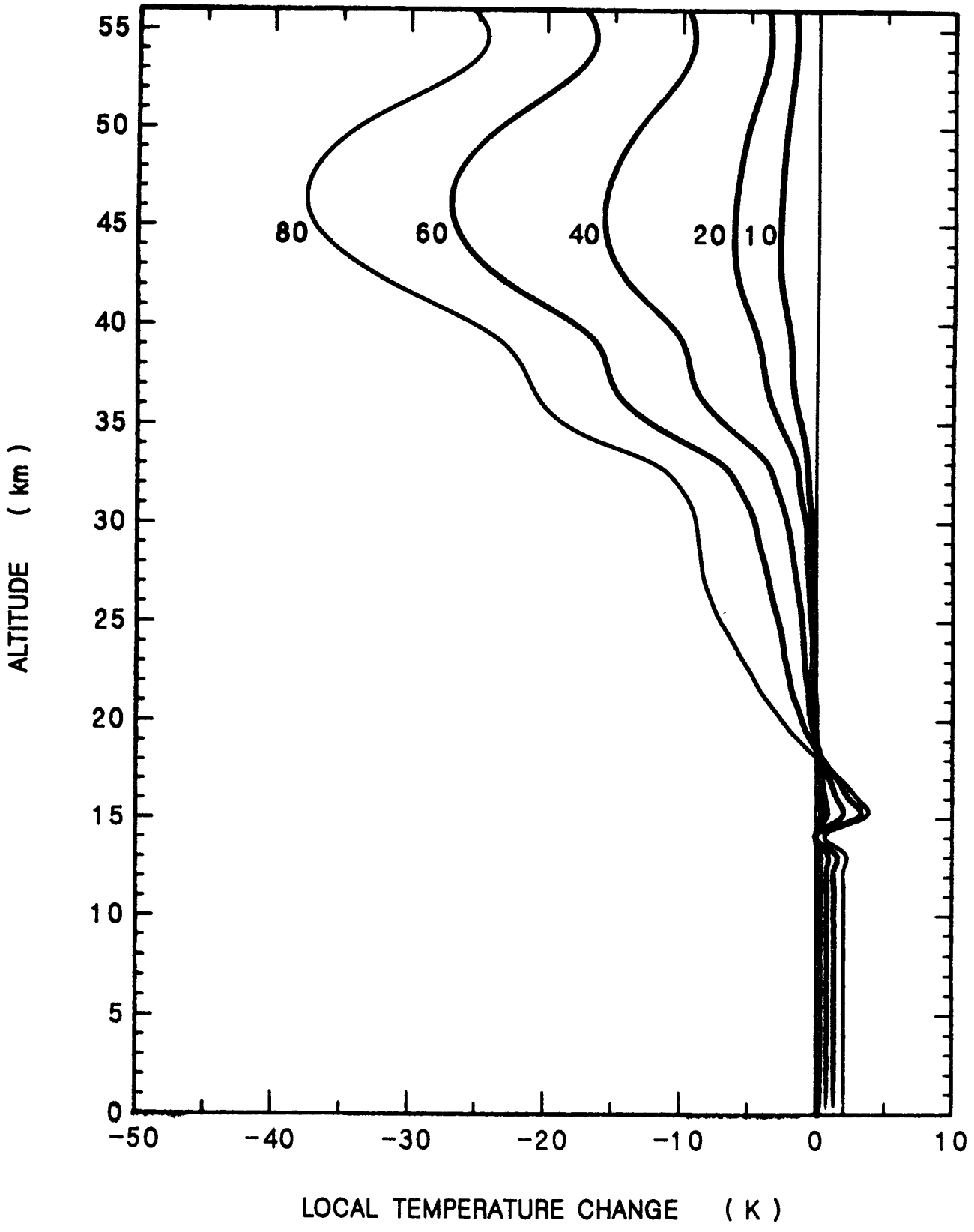
55
50
45
40
35
30
25
20
15
10
5
0
80
60
40
20
10
ALTITUDE (km)
-50
-40
-30
-20
-10
0
10
LOCAL TEMPERATURE CHANGE (K)

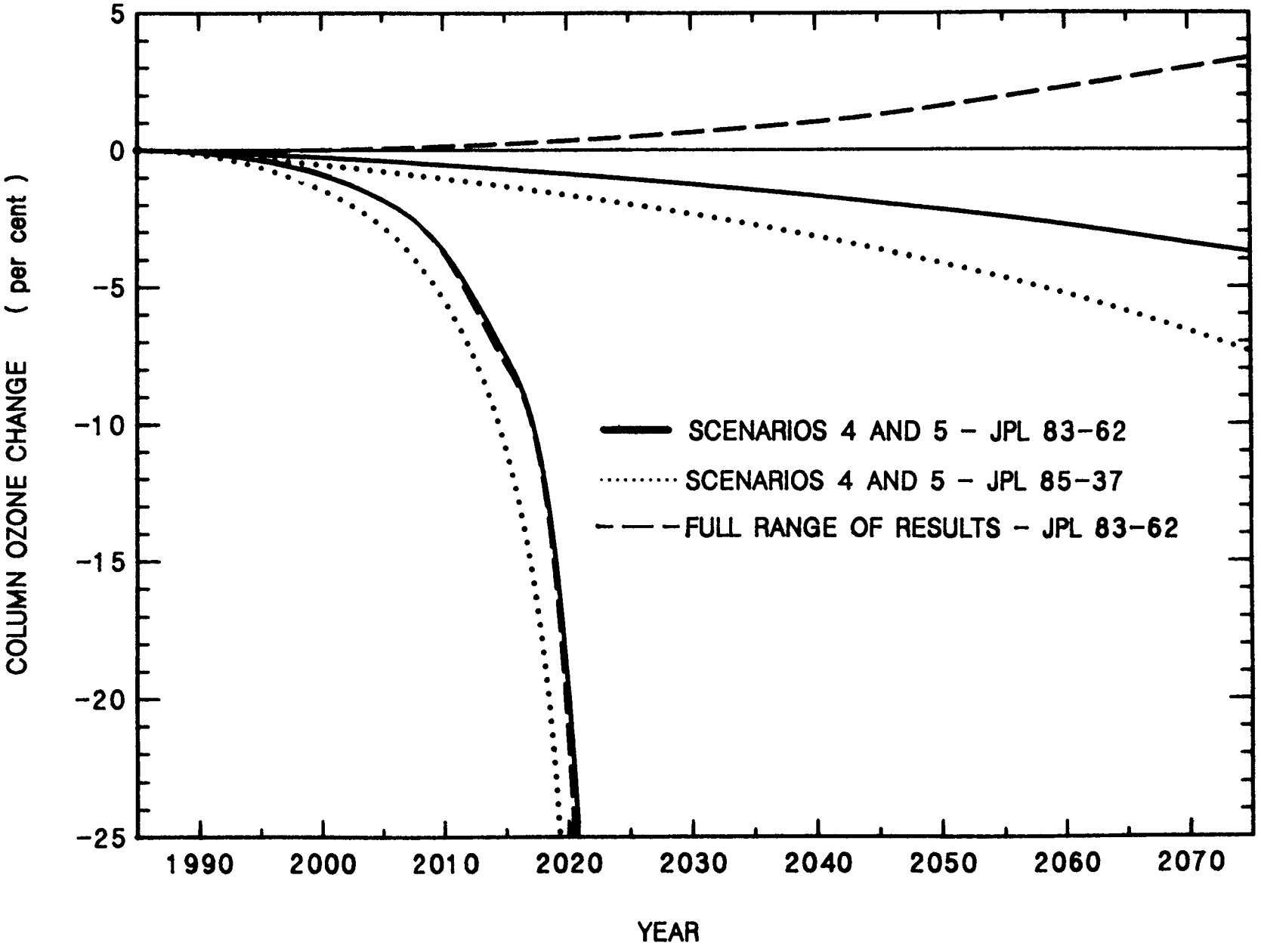
5
0
-5
-10
-15
-20
-25
COLUMN OZONE CHANGE (per cent)
1990
2000
2010
2020
2030
2040
2050
2060
2070
YEAR
SCENARIOS 4 AND 5 - JPL 83-62
SCENARIOS 4 AND 5 - JPL 85-37
FULL RANGE OF RESULTS - JPL 83-62

Figure 21

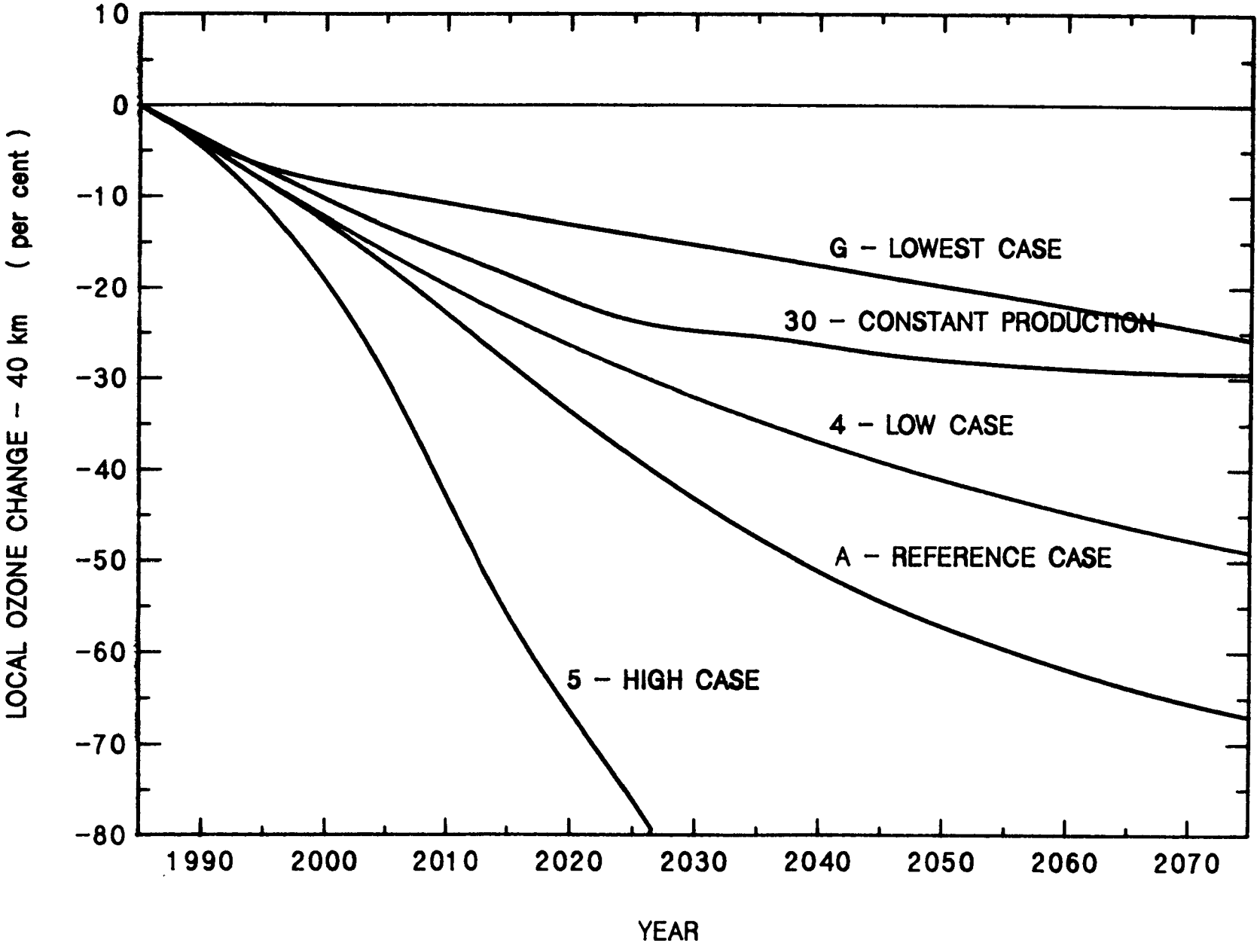
10
0
-10
-20
-30
-40
-50
-60
-70
-80
LOCAL OZONE CHANGE - 40 km (per cent)
1990
2000
2010
2020
2030
2040
2050
2060
2070
YEAR
G - LOWEST CASE
30 - CONSTANT PRODUCTION
4 - LOW CASE
A - REFERENCE CASE
5 - HIGH CASE

Figure 22

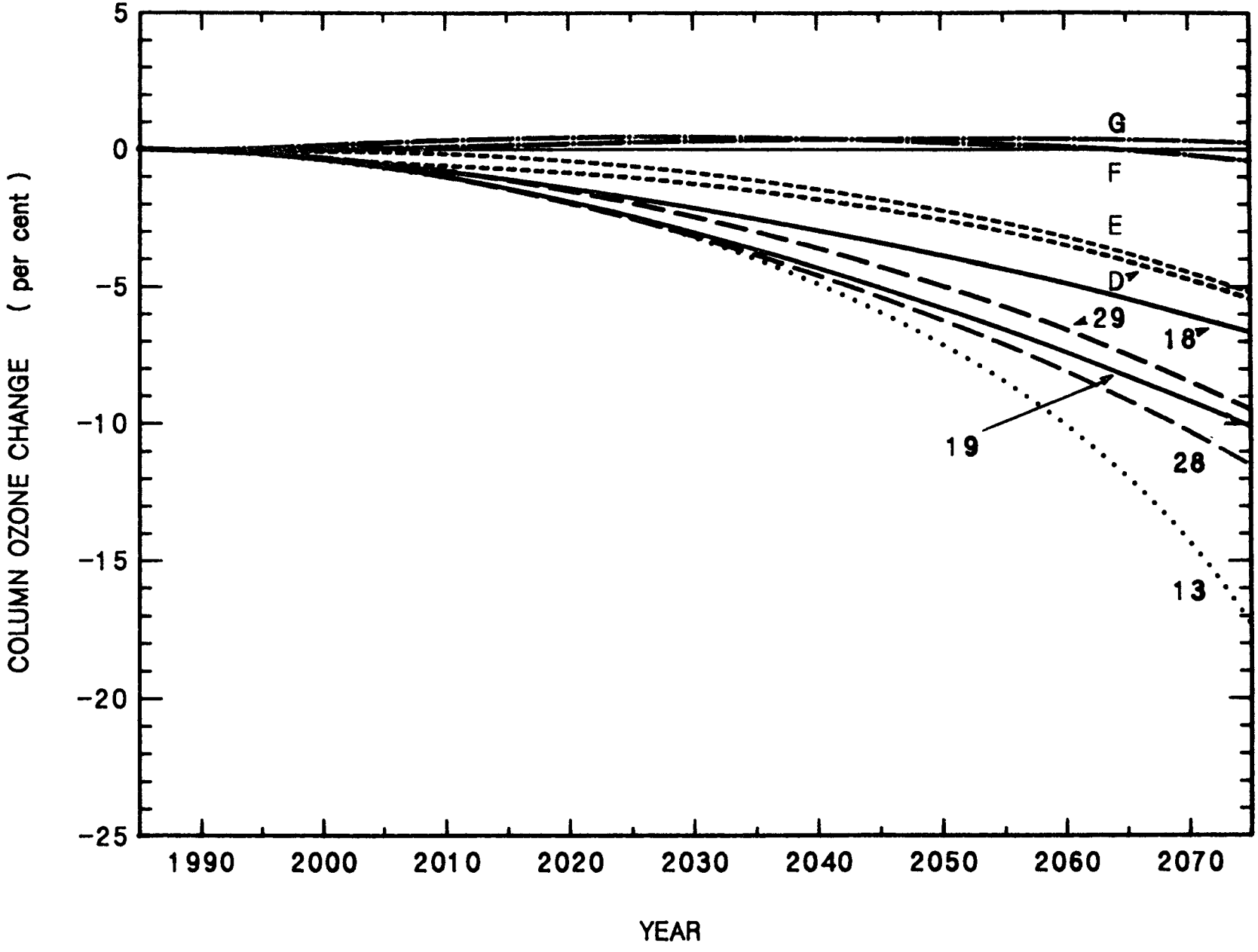
5
0
-5
-10
-15
-20
-25
COLUMN OZONE CHANGE (per cent)
1990
2000
2010
2020
2030
2040
2050
2060
2070
YEAR
G
F
E
D
29
18
19
28
13

Figure 23

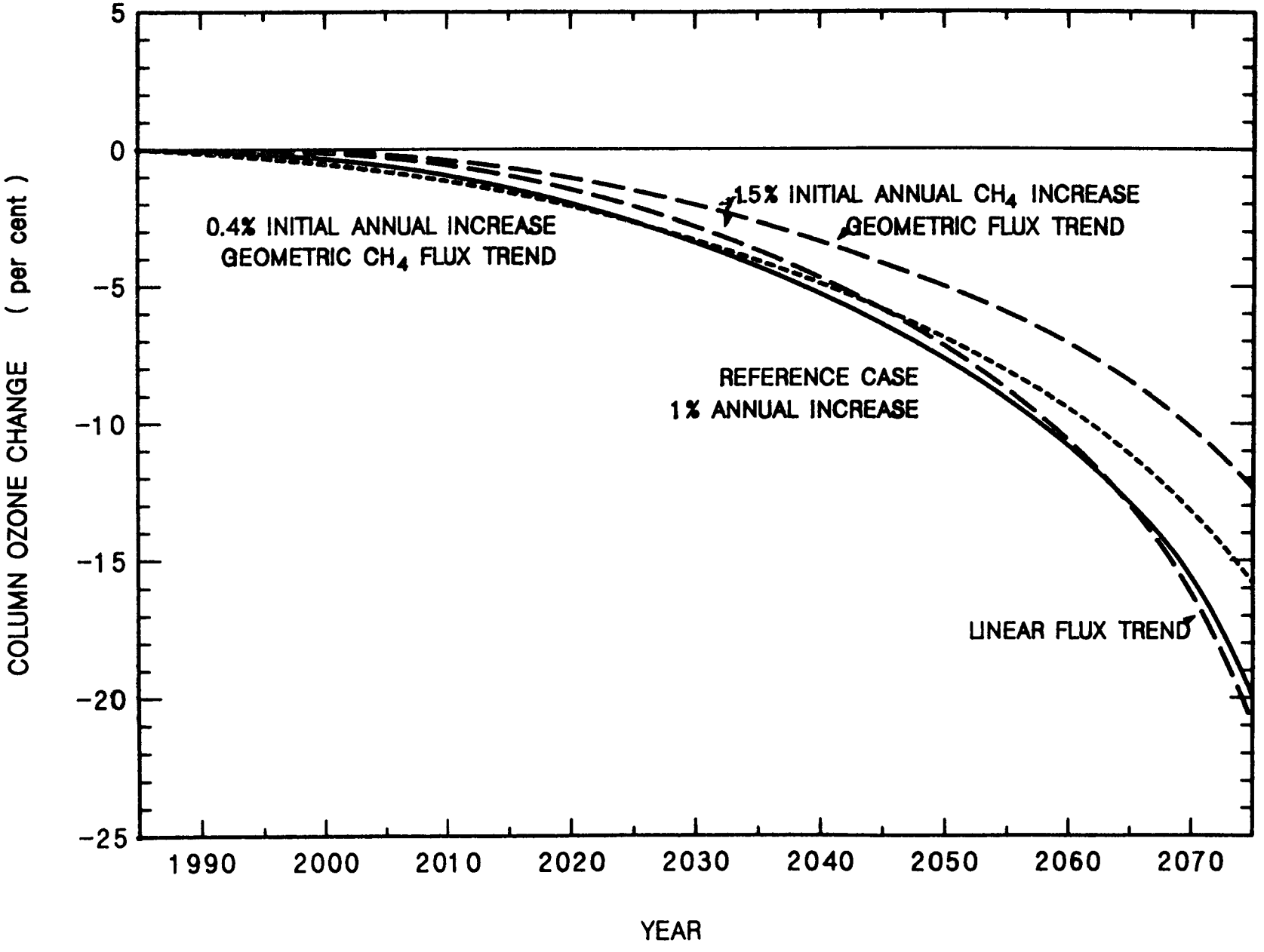
5
0
-5
-10
-15
-20
-25
1990
2000
2010
2020
2030
2040
2050
2060
2070
COLUMN OZONE CHANGE (per cent)
YEAR
0.4% INITIAL ANNUAL INCREASE
GEOMETRIC CH_4 FLUX TREND
1.5% INITIAL ANNUAL CH_4 INCREASE
GEOMETRIC FLUX TREND
REFERENCE CASE
1% ANNUAL INCREASE
LINEAR FLUX TREND

Figure 24

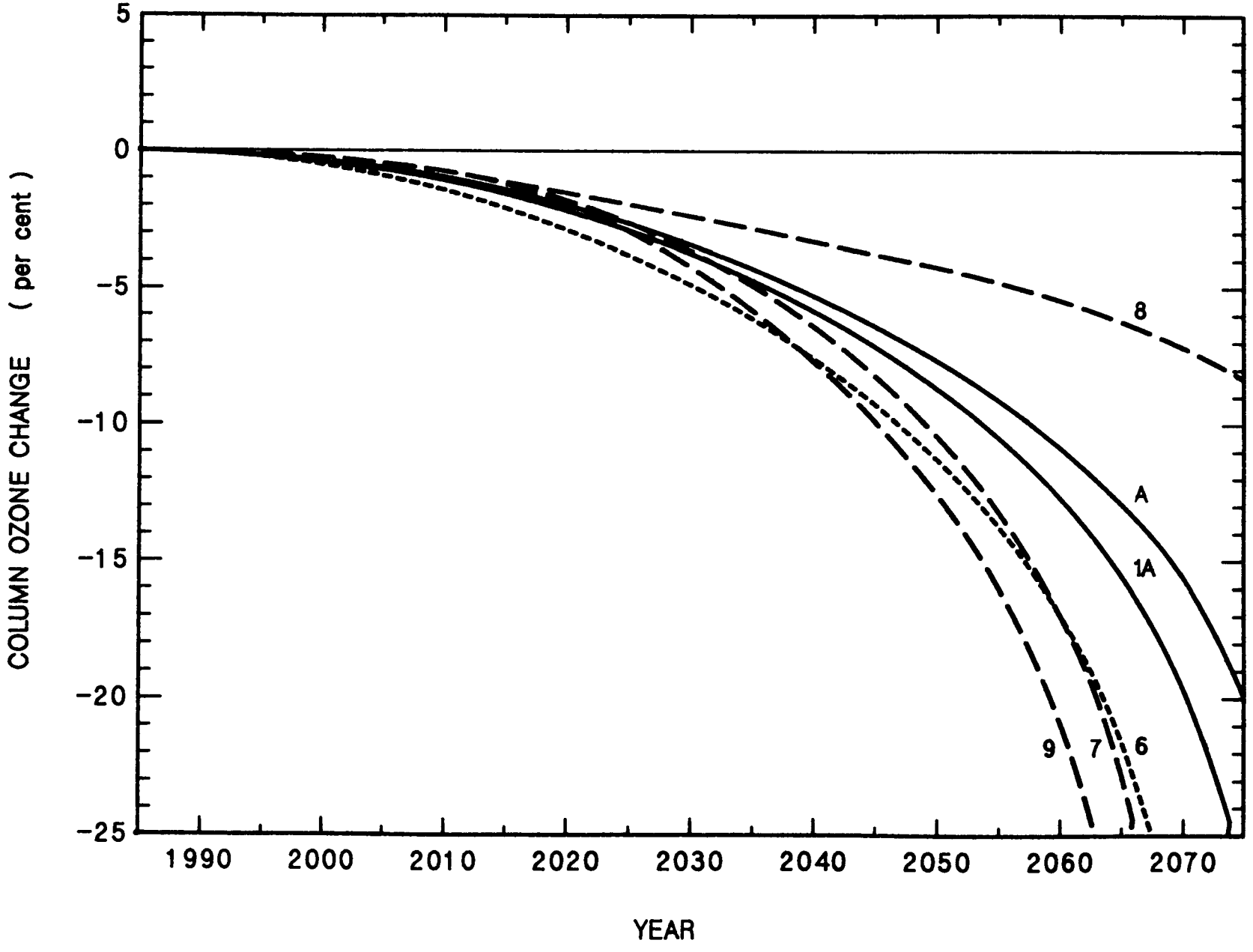
5
0
-5
-10
-15
-20
-25
COLUMN OZONE CHANGE (per cent)
1990
2000
2010
2020
2030
2040
2050
2060
2070
YEAR
8
A
1A
9
7
6

Figure 25

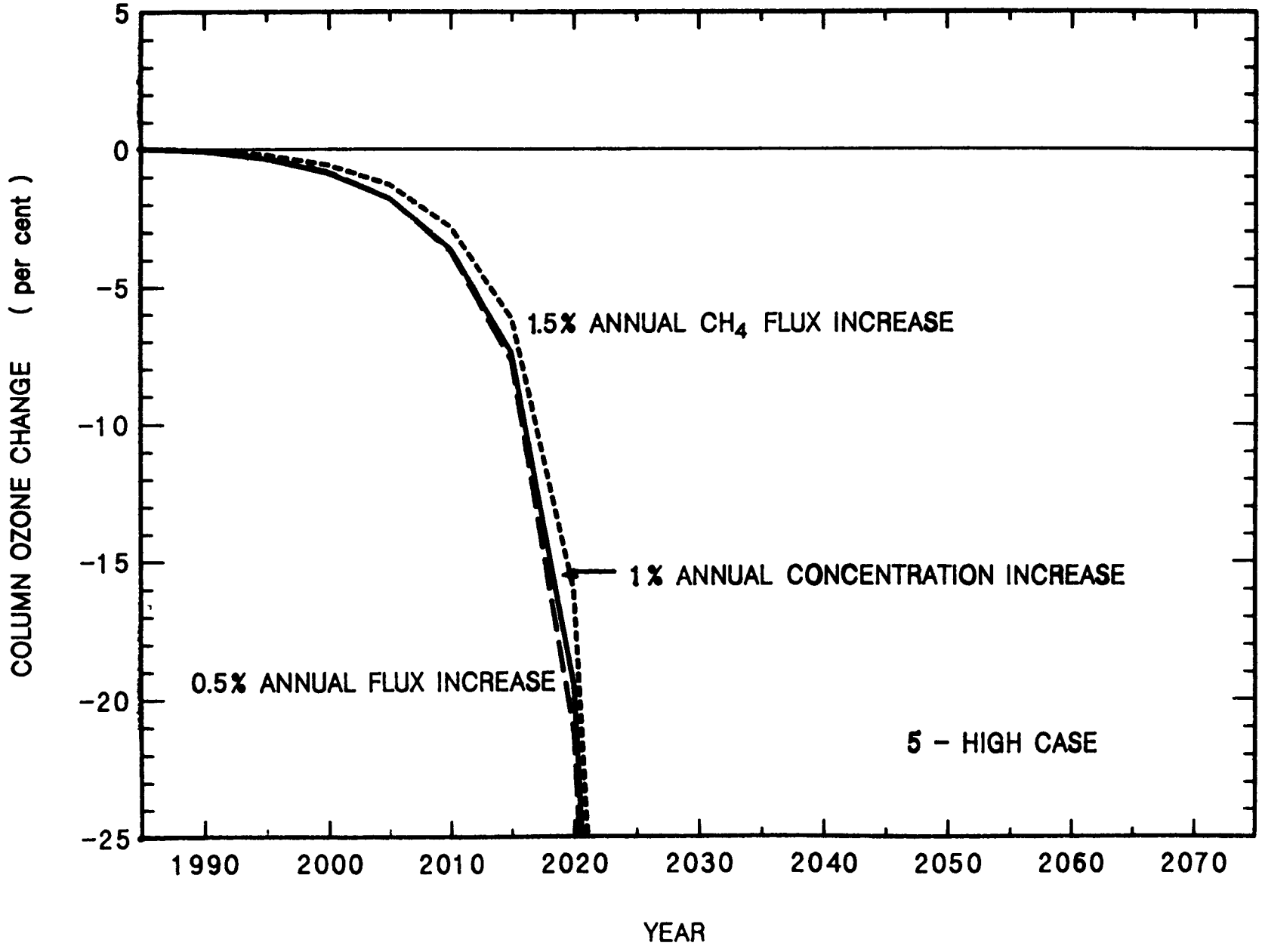
5
0
-5
-10
-15
-20
-25
COLUMN OZONE CHANGE (per cent)
1.5% ANNUAL CH_4 FLUX INCREASE
1% ANNUAL CONCENTRATION INCREASE
0.5% ANNUAL FLUX INCREASE
5 - HIGH CASE
1990
2000
2010
2020
2030
2040
2050
2060
2070
YEAR

Figure 26

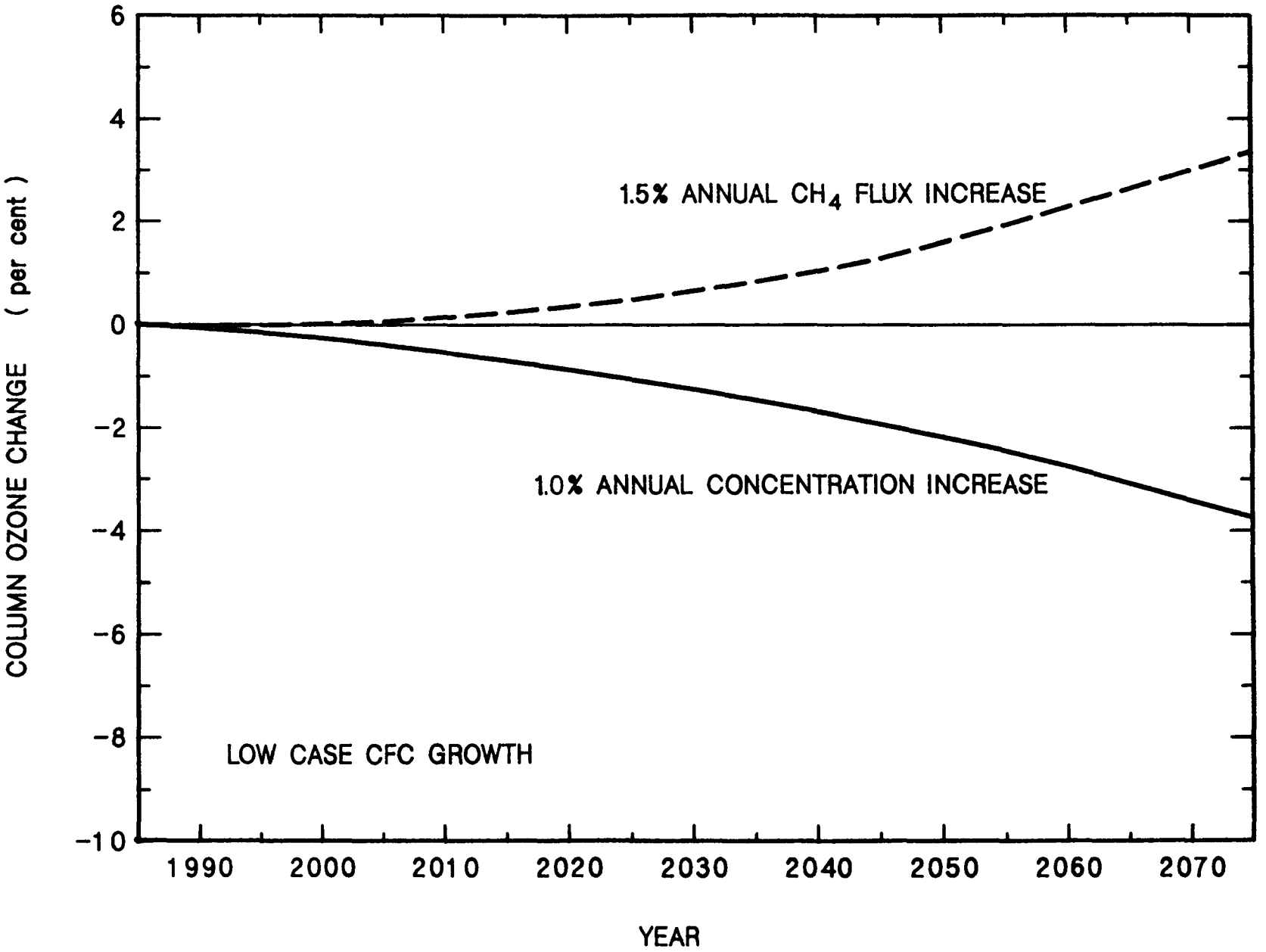
6
4
2
0
-2
-4
-6
-8
-10
1990
2000
2010
2020
2030
2040
2050
2060
2070
COLUMN OZONE CHANGE (per cent)
YEAR
1.5% ANNUAL CH_4 FLUX INCREASE
1.0% ANNUAL CONCENTRATION INCREASE
LOW CASE CFC GROWTH

Figure 27

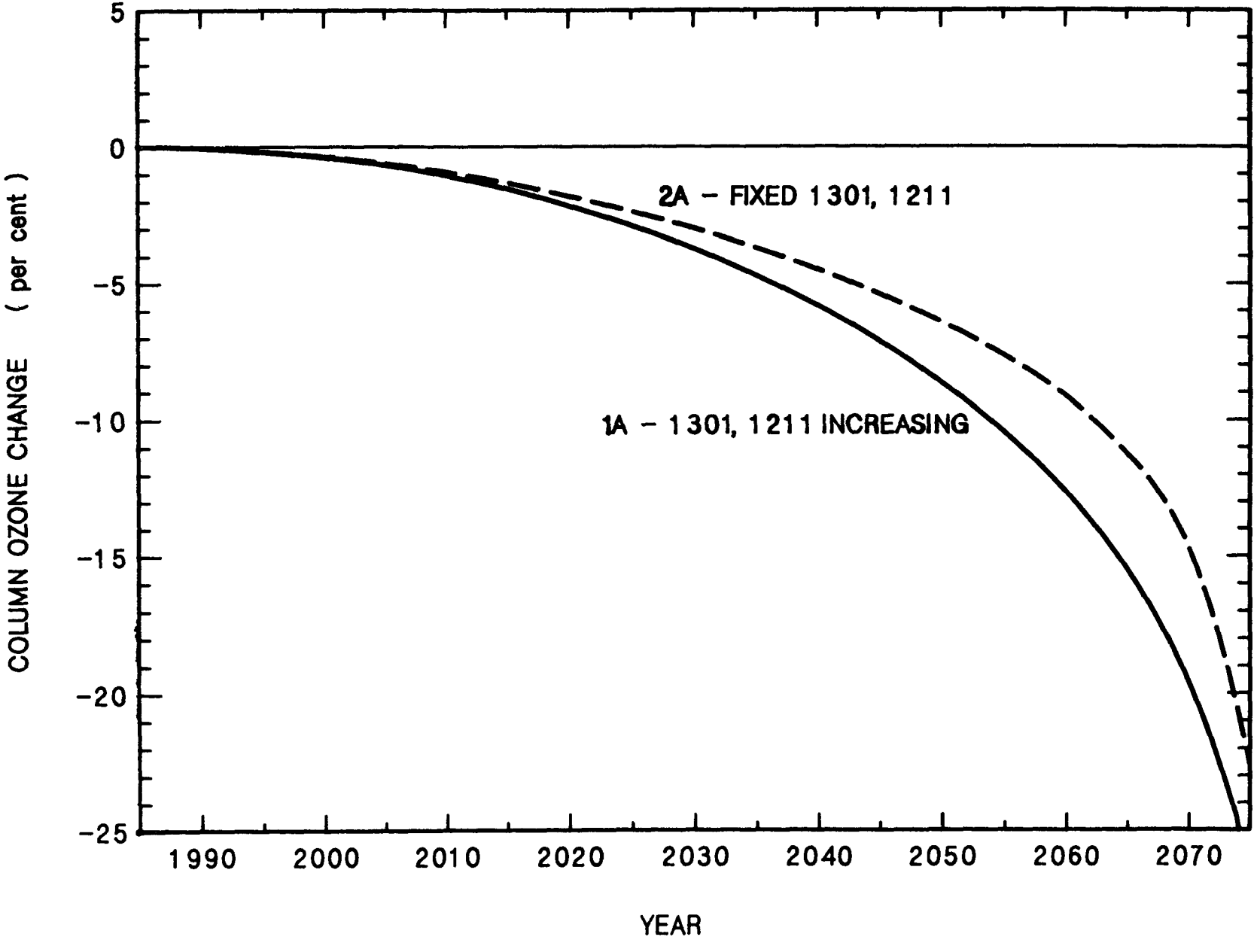
5
0
-5
-10
-15
-20
-25
COLUMN OZONE CHANGE (per cent)
2A - FIXED 1301, 1211
1A - 1301, 1211 INCREASING
1990
2000
2010
2020
2030
2040
2050
2060
2070
YEAR

Figure 28

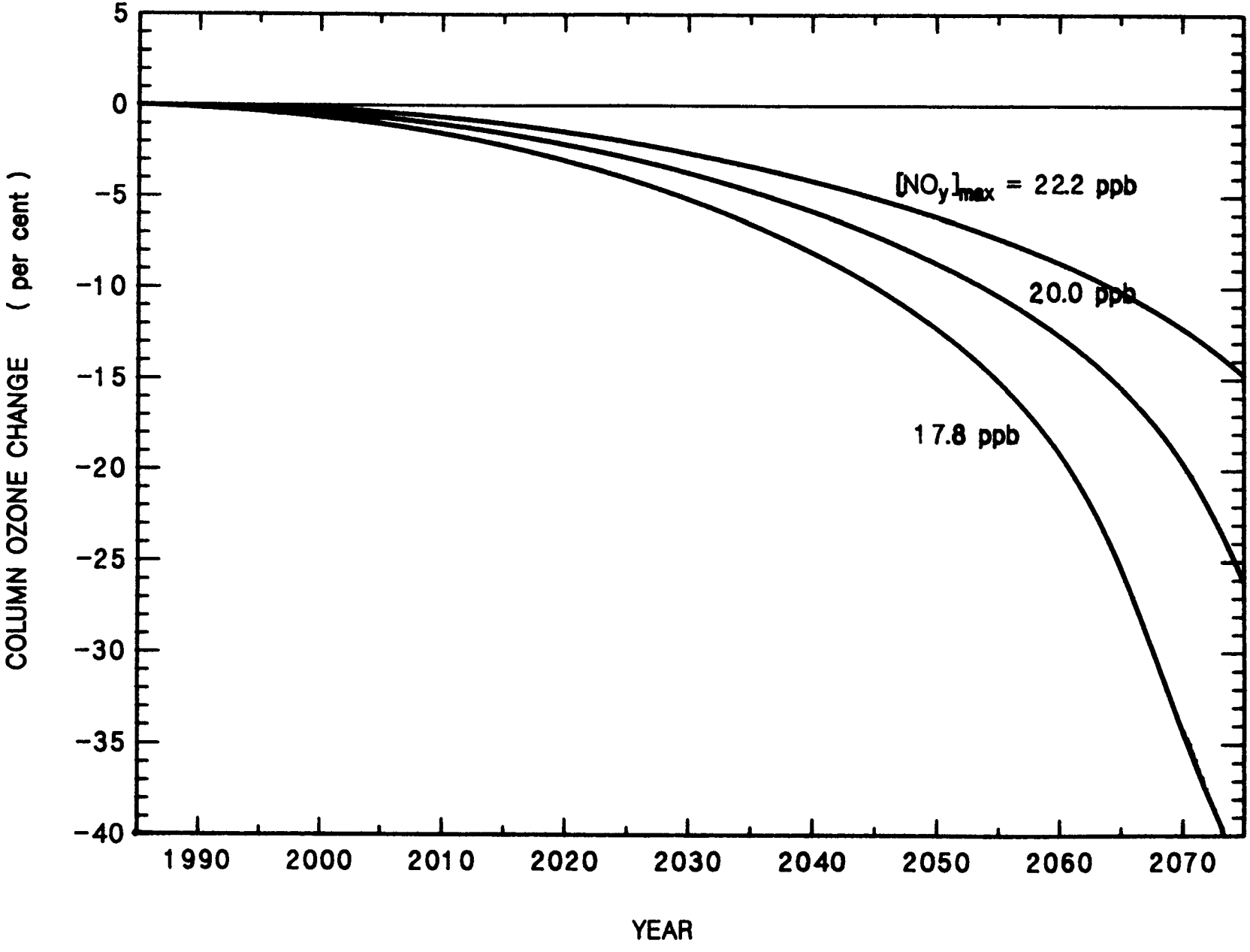
5
0
-5
-10
-15
-20
-25
-30
-35
-40
COLUMN OZONE CHANGE (per cent)
1990
2000
2010
2020
2030
2040
2050
2060
2070
YEAR
[NOy]max = 22.2 ppb
20.0 ppb
17.8 ppb

Figure 29

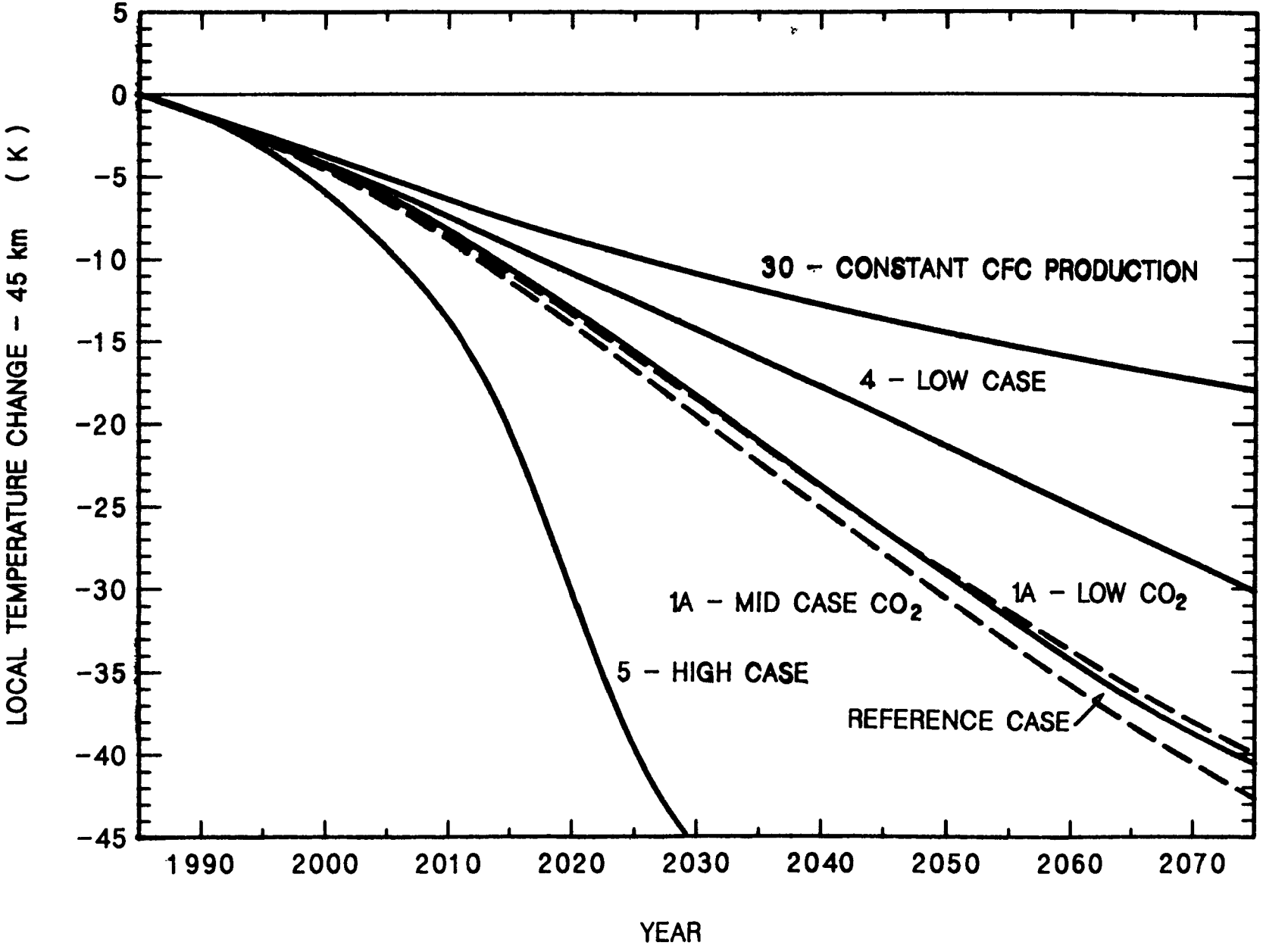
LOCAL TEMPERATURE CHANGE - 45 km (K)
5
0
-5
-10
-15
-20
-25
-30
-35
-40
-45
1990
2000
2010
2020
2030
2040
2050
2060
2070
YEAR
30 - CONSTANT CFC PRODUCTION
4 - LOW CASE
1A - MID CASE CO_2
1A - LOW CO_2
5 - HIGH CASE
REFERENCE CASE

Figure 30

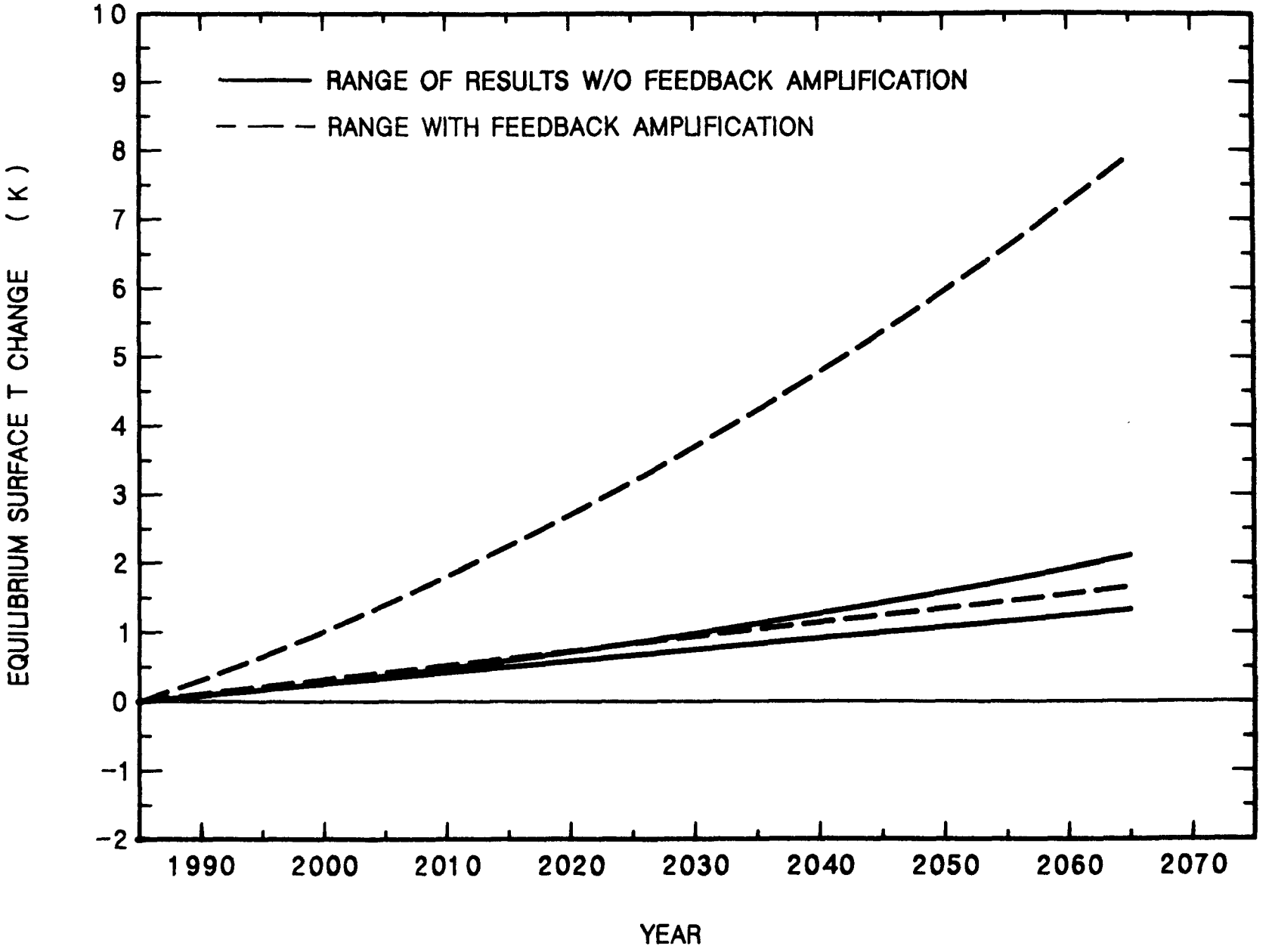
RANGE OF RESULTS W/O FEEDBACK AMPLIFICATION
RANGE WITH FEEDBACK AMPLIFICATION
EQUILIBRIUM SURFACE T CHANGE (K)
YEAR
10
9
8
7
6
5
4
3
2
1
0
-1
-2
1990
2000
2010
2020
2030
2040
2050
2060
2070

Figure 31

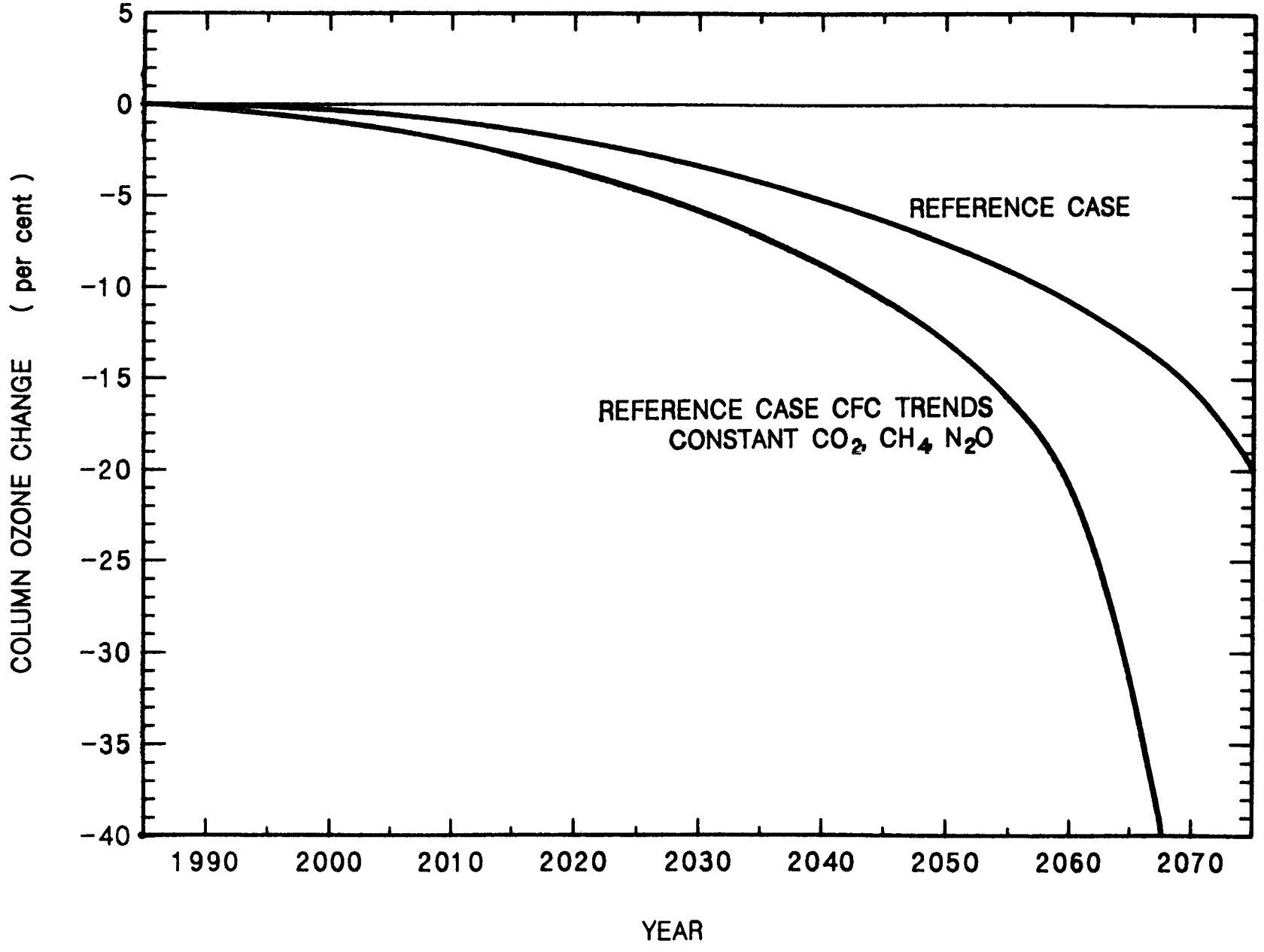
5
0
-5
-10
-15
-20
-25
-30
-35
-40
COLUMN OZONE CHANGE (per cent)
1990
2000
2010
2020
2030
2040
2050
2060
2070
YEAR
REFERENCE CASE
REFERENCE CASE CFC TRENDS
CONSTANT CO_2, CH_4 N_2O

Figure 32

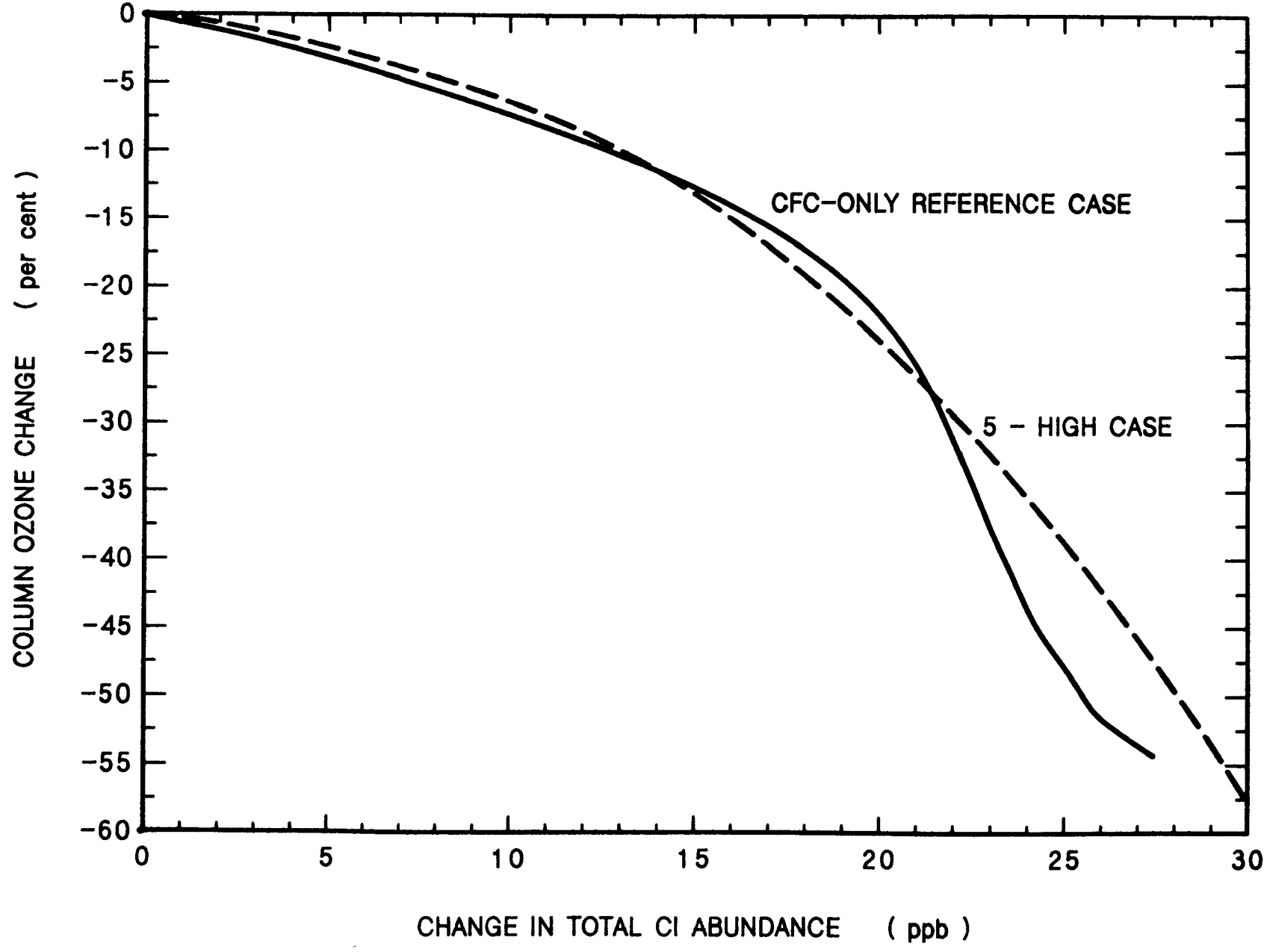
COLUMN OZONE CHANGE (per cent)
0
-5
-10
-15
-20
-25
-30
-35
-40
-45
-50
-55
-60
0
5
10
15
20
25
30
CHANGE IN TOTAL Cl ABUNDANCE (ppb)
CFC-ONLY REFERENCE CASE
5 - HIGH CASE

Figure 33

Figure 34

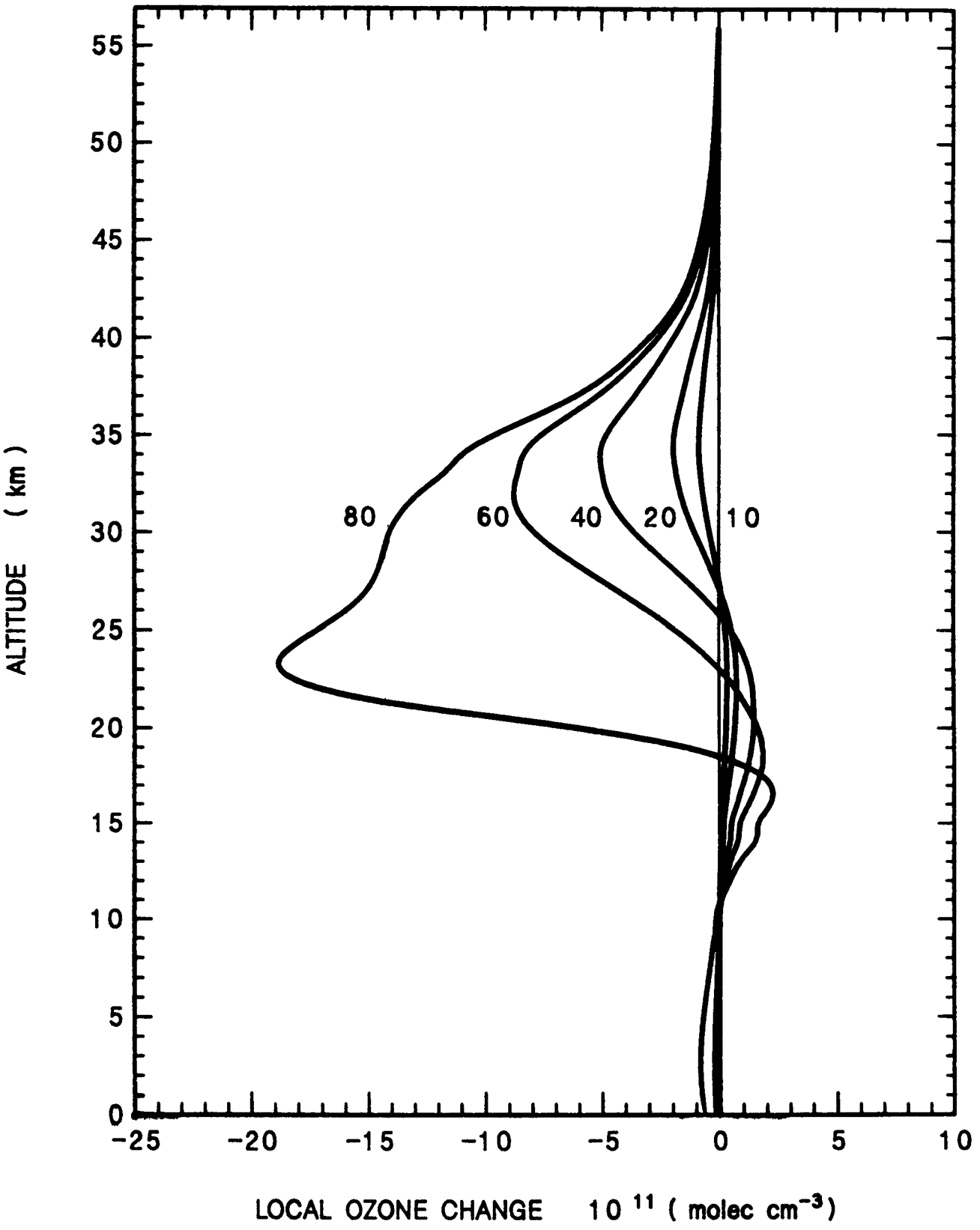
ALTITUDE (km)
55
50
45
40
35
30
25
20
15
10
5
0
80
60
40
20
10
-25
-20
-15
-10
-5
0
5
10
LOCAL OZONE CHANGE 10 11 (molec cm-3)

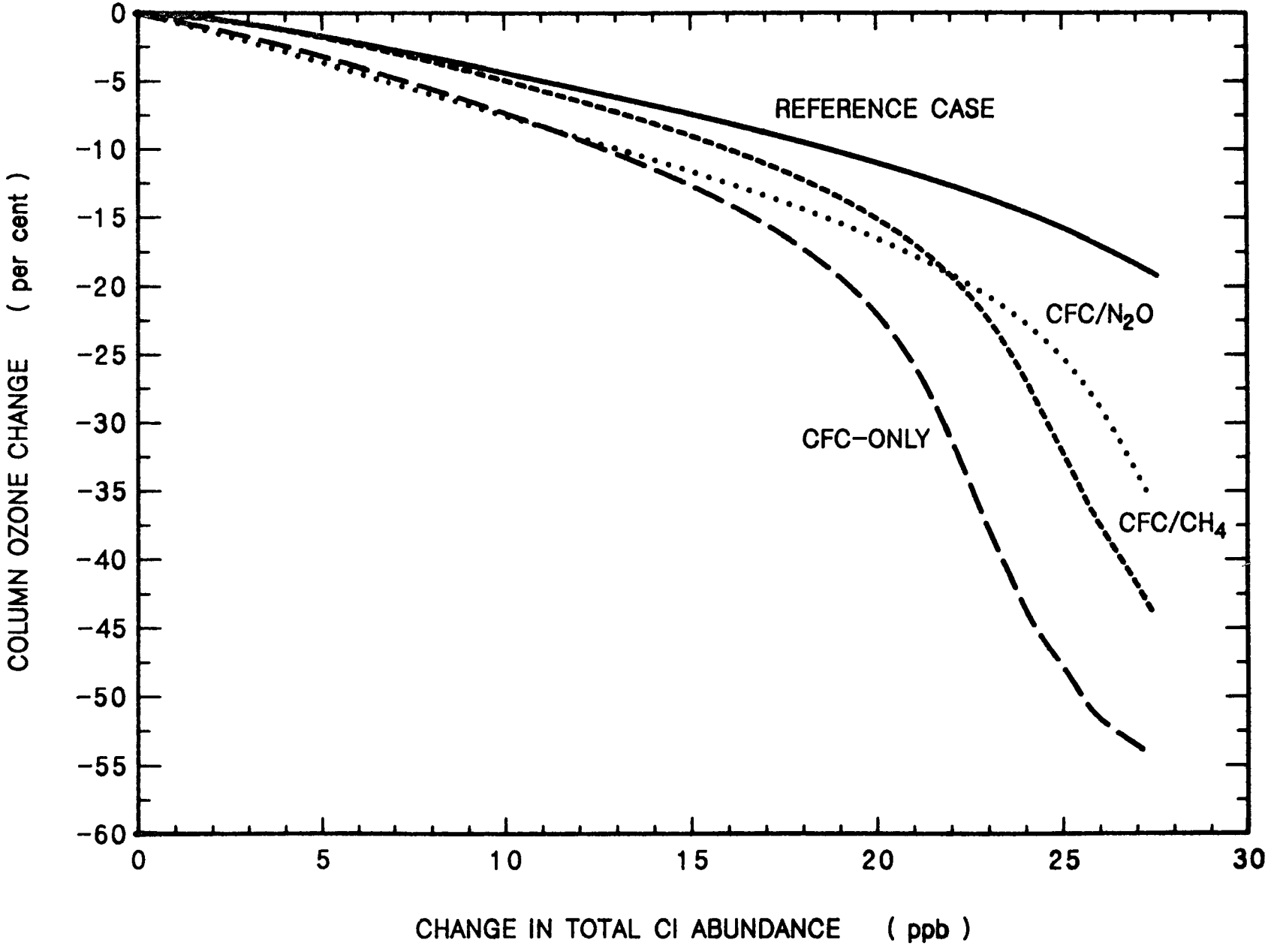
0
-5
-10
-15
-20
-25
-30
-35
-40
-45
-50
-55
-60
COLUMN OZONE CHANGE (per cent)
0
5
10
15
20
25
30
CHANGE IN TOTAL Cl ABUNDANCE (ppb)
REFERENCE CASE
CFC/N_2O
CFC-ONLY
CFC/CH_4

Figure 35

Figure 36

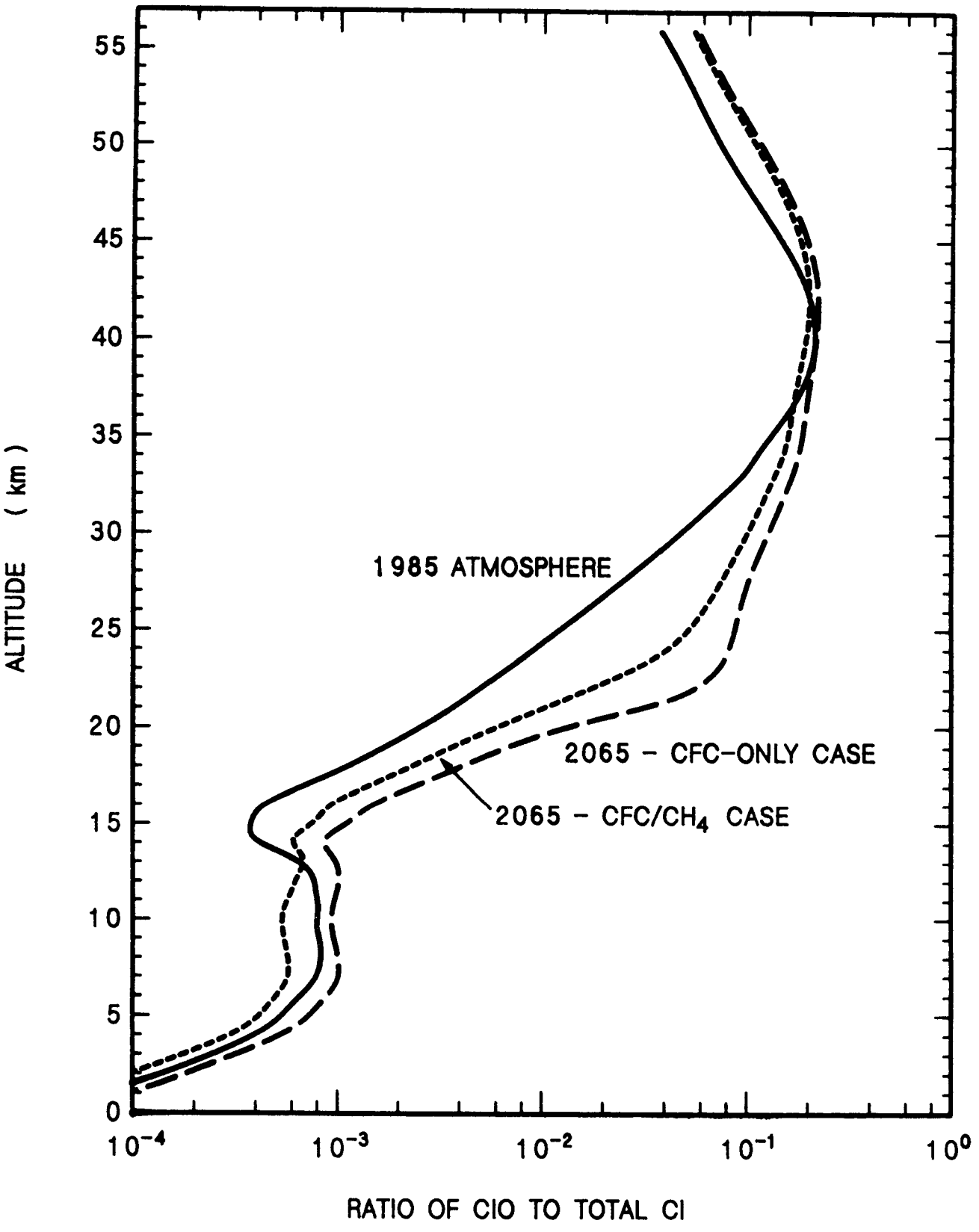
55
50
45
40
35
30
25
20
15
10
5
0
ALTITUDE (km)
1985 ATMOSPHERE
2065 - CFC-ONLY CASE
2065 - CFC/CH4 CASE
10-4
10-3
10-2
10-1
100
RATIO OF ClO TO TOTAL Cl

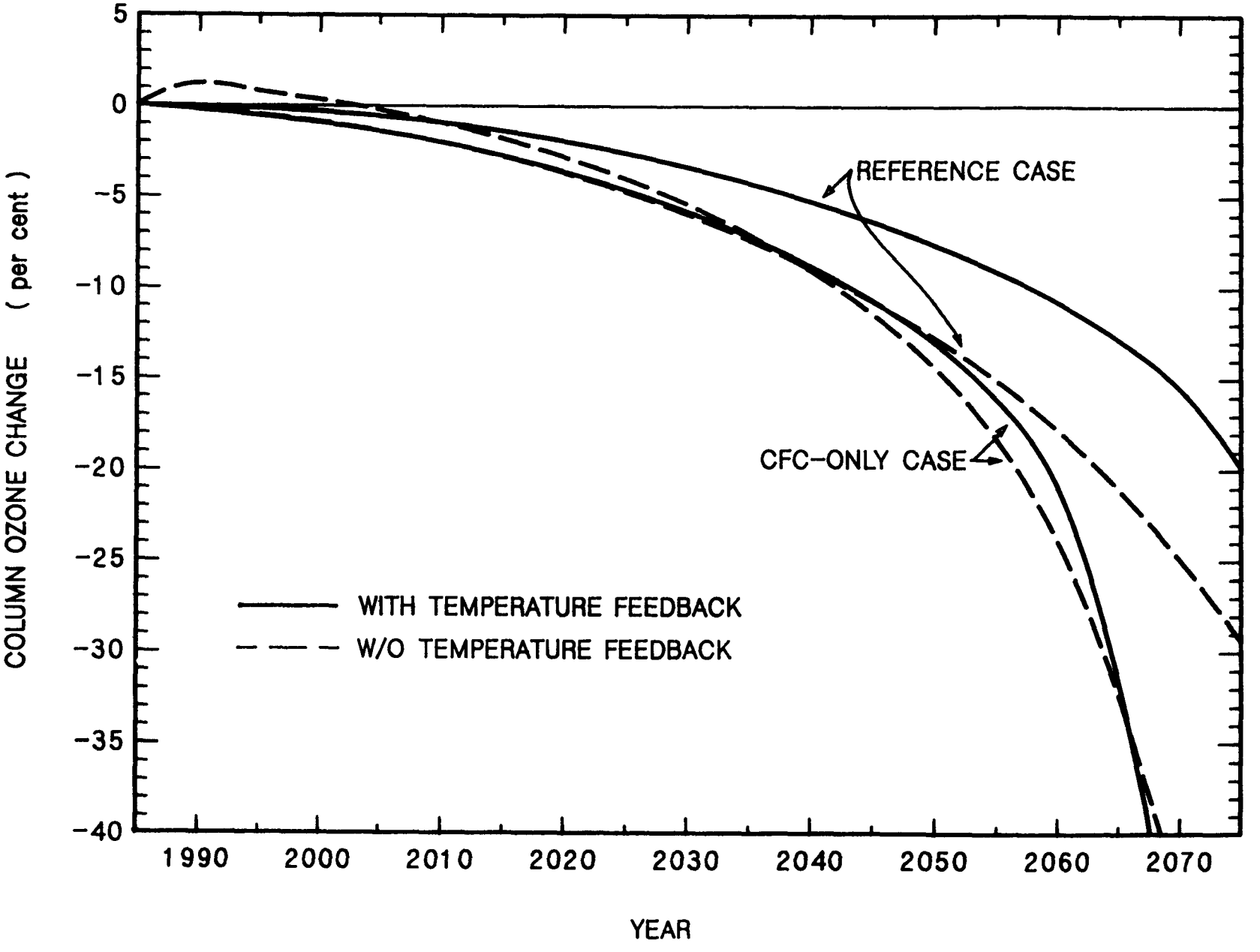
5
0
-5
-10
-15
-20
-25
-30
-35
-40
COLUMN OZONE CHANGE (per cent)
1990
2000
2010
2020
2030
2040
2050
2060
2070
YEAR
REFERENCE CASE
CFC-ONLY CASE
WITH TEMPERATURE FEEDBACK
W/O TEMPERATURE FEEDBACK

Figure 37

UCRL- 93375
PREPRINT

MONTE CARLO UNCERTAINTY ANALYSIS OF STRATOSPHERIC OZONE IN AMBIENT AND PERTURBED ATMOSPHERES

Keith E. Grant
Peter S. Connell
Donald J. Wuebbles

This paper was prepared for submittal to
Journal of Geophysical Research

July 1986

Lawrence Livermore National Laboratory

UCRL-93375

Monte Carlo Uncertainty Analysis of Stratospheric Ozone in Ambient and Perturbed Atmospheres

Keith E. Grant
Peter S. Connell
Donald J. Wuebbles

Lawrence Livermore National Laboratory,
Livermore, Ca 94550

Abstract

In recent years, numerous modeling studies have been directed toward assessment of the potential threat to the stratospheric ozone layer from anthropogenic trace gas perturbations. Interest is growing in the application of models as tools in assessing the potential biological, economic, and climatic consequences of possible future perturbations in the concentrations of trace gases. Uncertainties in model predictions arise from the inherent uncertainties in model representations of various physical and chemical processes, including kinetic rate coefficients, photolysis rates, transport, boundary conditions, and other physical parameters as well as uncertainties in the future rates of emissions of trace gases. In this paper we apply the Monte Carlo uncertainty analysis approach to this problem to examine the effects of these uncertainties on model predictions of trace gas concentrations.

Using the LLNL 1-D transport-kinetics model of the troposphere and stratosphere, we examine the extent to which uncertainties in rate parameters might be sufficient to account for the well-known problem of model underprediction of O_3 in the upper stratosphere. No single mechanism for increasing O_3 was apparent. Eight cases (of a set of 100 runs) were considered that satisfy the criteria that the profiles of $C\ell O$, NO, NO_2, and HNO_3 be consistent with observations. For each of these cases, the O_2 photolysis rate at 45 km was greater than that for the baseline case and significant decreases in effectiveness occurred in one or more of the major odd-nitrogen, odd-chlorine, or odd-hydrogen loss mechanisms. We also investigated the probability distribution of the change in O_3 for a

possible future chemically perturbed atmosphere. Using best-estimate rate parameters, a total column O_3 change of -7.7% was determined. With recommended uncertainties applied to all rate and photolysis parameters, we obtained a standard deviation about the baseline case of ±6.4% for 100 Monte Carlo runs. When the uncertainty of each of the parameters was set to 10%, this standard deviation was reduced to ±3.8%. We conclude that, without addition of other criteria, substantial prediction uncertainties will remain even when random and systematic errors in rate constant measurements approach their practical minimums. Because of significant skewness, baseline values with standard deviations are insufficient to adequately characterize the probability distributions of trace gas concentrations that we obtained via the Monte Carlo uncertainty technique.

Introduction

Numerous modeling studies have been directed toward assessment of the potential impact on ozone from anthropogenic perturbations to trace gas concentrations. For the last decade, the greatest concern has been focused on effects of increases in the concentrations of chlorofluorocarbons (CFCs) (NRC, 1979; WMO, 1981, 1986; Wuebbles, 1983a). More recently, the importance of coupling mechanisms between increases in CFC concentrations and perturbations to other traces gases such as CO_2, CH_4, and N_2O has been recognized (Wuebbles et al., 1983).

Considerable use is being made of models as tools in assessing the chemical and climatic consequences of possible future perturbations of trace gas concentrations. These models generally use as input scenarios for the projected changes in trace species concentrations or emissions. Such model applications are often precursors to the assessment of potential biological and economic consequences resulting from these scenarios. They are also important input to the development of corresponding regulatory and other planning strategies. It is crucial that these model results include analyses of uncertainty limits and probability distributions for predicted trace gas concentrations. This study is a response to this need. We use the LLNL 1-D transport-kinetics model combined with Monte Carlo parameter variation to obtain information on the uncertainties in model predictions for concentrations of ozone and other trace atmospheric species.

Uncertainties in model predictions for concentrations of ozone and other chemical species arise from the inherent uncertainties in measurements of chemical rate coefficients and photolysis rates, representation of transport processes, boundary conditions, and other physical parameters used within a model. Most past model uncertainty studies have individually varied each of a limited set of such parameters. This produced an estimate of the sensitivity of the model to each parameter varied. These sensitivities, along with the actual uncertainties of the parameters, were then combined into a cumulative model uncertainty (Butler, 1978a, 1978b; Smith, 1978; NRC, 1979). This approach has the advantage of producing uncertainties for a small, carefully selected set of parameters without requiring great expenditures of computer time. Moreover, the sensitivity of a model to an individual parameter is immediately and uniquely available, without the use of elaborate retrieval techniques or additional a priori information. On the other hand, this approach unavoidably neglects contributions to the predicted uncertainties from parameters not in the (necessarily small) selected set, does not allow for coupling between parameter uncertainties, and yields little information about nonlinearity in model response to changes in parameters.

A number of these shortcomings can be overcome by the use of the Monte Carlo sampling approach to model uncertainty analysis. Monte Carlo sampling, when applied to atmospheric transport-kinetics models, allows many kinetic rate constants, photolysis rates, boundary conditions, and transport parameters to be varied simultaneously. Specifically, for each Monte Carlo run, each parameter of interest is varied as a function of both the estimated uncertainty of the parameter and of a random number drawn from a pre-determined probability distribution. This technique has the immediate advantage, as compared with individual parameter variation, of automatically including effects of coupling between parameters. Moreover, by sampling each parameter over a wide range of

values, effects of nonlinear model response are also included. Use of systematic sampling techniques in the choice of random numbers combined with a sufficiently large number of model executions assures that each model parameter is sampled over its entire physically reasonable range. This, in turn, assures that a well-defined distribution of values for each model output is produced.

The power of this method does not come free of practical difficulties. As with other techniques for uncertainty analysis, implementation of the Monte Carlo sampling technique initially requires determining both physically reasonable parameter uncertainty magnitudes and functional forms. Moreover, with Monte Carlo techniques, one or more suitable probability distributions must be selected as a basis for random sampling. Additionally, because multiple parameters are being simultaneously varied, it can be desirable or necessary to specify covariances between selected uncertainties (Iman et al., 1981, 1984; Gardner et al., 1981).

Application of the Monte Carlo technique requires a number of model runs sufficient to obtain adequate statistical precision in the probability distributions of trace gas concentrations. The specific number of runs required depends greatly on the model, the sampling technique, and the statistical acceptance test used. For instance, we used the relatively sophisticated Latin Hypercube Sampling (LHS) method to reduce the number of runs required to obtain a given variance. Even with this method, the LLNL 1-D model required a minimum of 100 runs to reduce the estimated error in the mean variance (about the baseline value) of the percent change in total column ozone to 26%. Without the use of LHS, ten times as many runs could have been required (Gardner and Trabalka, 1985).

Even using LHS, this represents a considerable expenditure of computer time even for simple well-behaved scenarios run without time-dependence or temperature feedback. The addition of time-dependence and temperature feedback or the selection of especially difficult chemical scenarios would further increase modelling costs. For a time-dependent run, results would be produced at a number of prechosen times during the run, rather than just at the end of the run after species concentrations have reached steadystate. This will greatly increase the quantity of raw data produced and the associated computer costs. For a run with temperature feedback, the effects of changing concentrations of radiatively active trace species are used to calculate a new temperature profile. The changing temperature profile changes kinetic rate coefficients which in turn changes species concentrations. This iterative calculation would directly increase the computer time required.

In analyzing Monte Carlo uncertainty runs, we also face the ancillary problems of storing and processing the large quantities of data produced. These problems would also be proportionately greater for time-dependent Monte Carlo analyses. To avoid the necessity of redoing entire sets of runs, careful prior consideration is required in selecting which data from each separate model run are to be saved. This must usually be a small subset of the normal model results and diagnostics produced for single runs. The selection and extraction of desired information from this quantity of data is generally nontrivial.

Because of the costs of computer time and difficulties of analysis, previous applications of Monte Carlo sampling to atmospheric transport-kinetics problems have utilized models in which the number of independent species, reactions, and layers has been substantially reduced from state-of-the-art models (Stolarski et al., 1978; Stolarski and Douglass, 1986;

Natarajan et al., 1986). By contrast, the LLNL 1-D model used for this study has not undergone such simplification. However, to minimize costs and data handling difficulties in doing our initial Monte Carlo studies described below, we have chosen to investigate the behavior of the LLNL 1-D model for calculations of the atmosphere under steady state conditions. We used the U.S. Standard Atmosphere temperature profile (1976). Model determined atmospheres were calculated for three different conditions: a reference atmosphere without chlorofluorocarbons (CFCs), an ambient atmosphere with current levels of CFCs, and a perturbed atmosphere with larger trace gas concentrations. The information gain per model run was increased by use of a variance reducing sampling scheme known as Latin Hypercube Sampling which is also described below.

Model Description

The LLNL 1-D model (Wuebbles, 1983b) is a coupled transport and kinetics model of the troposphere and stratosphere. It calculates the concentration profiles of 40 chemical species using 130 chemical reactions and 46 photodissociation processes. The model atmosphere, extending from the ground to the stratopause, is divided into 44 vertical levels. The vertical coordinate system used within the model is the natural logarithm of the pressure relative to the surface pressure. The boundary conditions for individual species are either fixed concentrations or fluxes at the surface and prescribed flux conditions at the upper boundary.

Three of the minor constituents, $O(^1D)$, H, and N, are assumed to be in instantaneous equilibrium. Each of the other 37 species [$O(^3P)$, O_3, NO, NO_2, N_2O, HNO_3, OH, HO_2, H_2O_2, $C\ell$, $C\ell ONO_2$, $C\ell O$, $C\ell NO_2$, $HC\ell$, NO_3, N_2O_5, HONO, HNO_4, $HOC\ell$, HCO, CH_2O, CH_3, CH_3OOH, CH_3O, CH_4, H_2, CO, H_2O, $CH_3C\ell$, $CC\ell_4$, $CH_3CC\ell_3$, CFC-11 ($CFC\ell_3$), CFC-12 ($CF_2C\ell_2$), CFC-22 ($CHF_2C\ell$), CFC-113 ($CFC\ell_2CF_2C\ell$), CFC-114 ($CF_2C\ell CF_2C\ell$) and CFC-115 ($CF_2C\ell CF_3$)] has its concentration calculated at each of the 44 levels each time step using a variable order multistep implicit method suitable for stiff systems of ordinary differential equations. Photodissociation rate coefficients, computed at each altitude and each time step, are consistent with all species distributions and the specified solar conditions. Also included are the effects of multiple scattering (Luther et al., 1978). The chemical rates and photodissociation cross-sections are essentially those recommended by DeMore et al. (1985). The vertical transport of atmospheric trace constituents in the 1-D model does not utilize atmospheric motion directly, but is rather based on an eddy-diffusion formulation, with diffusion coefficients, K_z, derived from longitudinally and latitudinally averaged observations of the vertical distributions of selected tracers (Wuebbles, 1983b).

The model normally runs in a time-dependent diurnally-averaged mode, with averaging factors predetermined by a special version of the model designed to run over a diurnal cycle. With constant surface boundary conditions for long lived gases, the model can be run to steady state in a computationally efficient manner.

Monte Carlo Sampling Implementation

The efficiency of a Monte Carlo sampling method can be defined as the reduction in the variance of the mean of an output result for a given number of model runs. This is essentially a measure of the information gain per run. Under this definition, simple

random sampling has been found to be much less efficient than more systematic sampling methods (Hammersly and Handscomb, 1965; Gardner et al., 1981, 1985). Realizing that cost effective implementation was a highly important consideration with a complex transport-kinetics model, a particularly effective variance reducing scheme known as Latin Hypercube Sampling (LHS) was utilized (McKay et al. 1979; Iman et al. 1981, 1984). Using this method, normally distributed random sampling sets based on the number of samples to be generated (NS) and the maximum number of parameters to be varied (NP) were created prior to model execution. For the studies reported here, values of 50 and 500 were used for NS and NP, respectively.

To create a Latin Hypercube Sample set, the cumulative probability distribution between 0.001 and 0.999 for each parameter was divided into NS equal intervals. For a normal distribution, this truncated probability range corresponds to limiting sampling to within ± 3.09 standard deviations of the baseline case. NP random permutations of the integers from 1 to NS were then formed, thus creating an NS by NP matrix. Each of the NS rows of this matrix constitutes a sampling vector that randomly selected a single interval from the probability distributions of each of the NP parameters to be varied.

This combination process insures that over the complete set of NS sample vectors, the total allowed range of each of the NP parameters is sampled, with each of the NS probability intervals for a given parameter being used exactly once. Because of these features, for relatively small sampling sets (e.g., 50 to 100 samples), LHS yields much more representative approximate distributions than would have been expected with simple random sampling. This results in reduced variance among the result means and distributions obtained using successive sampling sets. It has been found that using LHS can reduce the number of runs required to obtain a given variance by a factor of 10 compared with simple random sampling (Gardner et al., 1985). Moreover, this is accomplished without biasing the expected means or distributions. In this initial study, specification of covariance between parameters (e.g. between the preexponential and exponential factors of a kinetic rate constat) was not attempted. LHS sampling readily lends itself to such covariance specifications, however (Iman and Conover, 1982; Iman et al., 1984), and utilization of this feature along with implementation of more extensive checking for fortuitous covariances are planned for future studies.

To complete the generation of a sample set, a random probability was uniformly chosen within each interval selected. Thus,

$$P = P_i(1 - u) + P_{i+1}u$$

where P_i and P_{i+1} are the probabilities at the lower and upper limits of a cumulative probability interval and u is a uniform random number such that $0 \leq u < 1$. Finally, the NP separate probabilities of a sample set were converted into coordinates using an inverse cumulative normal transformation (cf. Iman and Shortencarier, 1984).

A Monte Carlo version of the LLNL 1-D transport-kinetics model was then created with calculations of reaction rates and photolysis rates modified to include variation of rates based on the current sample vector and uncertainty factors for each rate constant (DeMore et al., 1985). For this initial study, transport coefficients and boundary conditions were not varied.

Variation of rate constants was complicated by the existence of several special forms involving multiple parameters (DeMore et al. 1985). In varying chemical rate constants, nonexponential factors were generally varied log-normally, while factors within exponents were varied normally. For example, for the standard Arrhenius equation,

$$k_0 = Ae^{-E/RT},$$

the varied form became

$$k = k_O(\Delta A)^{\alpha} e^{\beta(\Delta E/RT)|1-T/298|}$$

where ΔA and ΔE are uncertainties in A and E/RT as given in DeMore et al. (1985). α and β are normally distributed random numbers from a LHS set.

To vary photolysis rates, absorption cross-sections for O_2, O_3 and NO_2 were first varied in the calculation of atmospheric transmission. This was implemented using a broad wavelength band formulation (Table 1) for these cross-section uncertainties. We felt this to be a reasonable approach since bin-by-bin uncertainties were not available and since measurements yield absorption coefficients that are highly correlated within bands. These varied cross-sections were then used in calculating the wavelength and altitude dependent solar flux, thereby affecting all other photolysis rates. An additional non-wavelength dependent variation of all other absorption cross-sections (DeMore et al., 1985) was then included in calculating the photolysis rate for individual processes. In all cases, variations were selected from a log-normal distribution.

The Ambient Atmosphere: Model Results versus Observations

One dimensional models utilizing recommended photochemical rate parameters have consistently been found to underpredict O_3 in the upper stratosphere by about 20% to 50%, in spite of simultaneously favorable comparisons with in situ and remote-sensing observations of key radicals thought to catalyze O_3 destruction (Butler, 1978a; Wuebbles, 1983b; Froidevaux et al., 1985; Natarajan et al., 1986). This disagreement is not yet understood and continues to be an incentive for further investigation.

Incomplete understanding of the present stratospheric photochemistry is related both to uncertainties in laboratory measurements of reaction parameters and in observations of concentrations of key species. There may also be significant species or reactions missing in the postulated photochemical mechanism. Ozone concentrations in the upper stratosphere are primarily determined by photochemical processes; transport processes are relatively unimportant in this region. However, O_3 concentrations are determined by many competing photochemical processes and catalytic cycles in the upper stratosphere and are not dominated by any single process or species. Important processes include direct production and destruction of odd-oxygen ($O_x = O_3 + O(^3P) + O(^1D)$), interconversion between odd-oxygen species, and catalytic destruction of odd-oxygen involving odd-hydrogen (HO_x), odd-nitrogen (NO_x), and odd-chlorine ($C\ell O_x$).

Froidevaux et al. (1985) investigated the feasibility of correcting the ozone underprediction problem by varying individual photochemical reaction rates by factors of two. Their results appear to rule out the possibility of making one or two large adjustments to the current photochemical scheme to fit O_3 observations in the upper stratosphere.

Natarajan et al. (1986) used Nimbus 7 data, giving simultaneous measurements of O_3, H_2O, HNO_3, NO_2, CH_4, and temperature to check the consistency of the theoretical O_3 photochemistry. They utilized a zero-dimensional model incorporating relevant chemistry simplified to remove pre-specified or unimportant (in the upper stratosphere) reactions. Using available measurements and recommended photochemical rate data, they found that their model underpredicted upper stratospheric O_3 by 15-32%. Using Monte Carlo sensitivity analysis on this model, they concluded that the 1σ uncertainty limits of the observed O_3 are outside the range of the uncertainty bands for the calculated O_3. However, by varying six rate coefficients to the limits of their uncertainties, they were able to obtain much better agreement without creating other discrepancies.

Stolarski et al. (1978) and Stolarski and Douglass (1986) have compared the distributions obtained via Monte Carlo uncertainty techniques with observations for O_3, NO, NO_2, $C\ell O$, and OH. Stolarski and Douglass (1986) found that, out of 329 Monte Carlo runs, none would satisfy the 1σ limits of O_3 measurements at 20, 30, 40, and 50 km simultaneously. For three cases which fell within the 2σ limits, they did not find any obvious single variation in production, loss, or species variation that produces this result.

To further examine the extent to which uncertainties in current best estimates of chemical kinetic and photolysis rate parameters are able to explain the upper stratosphere O_3 discrepancy, we compared the results of our Monte Carlo runs with sample case selection criteria derived from observations (Table 2). The set of runs we used for this comparison was based on an ambient 1985 atmosphere with 2.5 ppb $C\ell X$. The criteria we used were chosen to select runs within the 2σ limits for O_3 (U.S. Std. Atmos., 1976) in the upper stratosphere that were still consistent with O_3 limits at other altitudes and with $C\ell O$, NO, NO_2, and HNO_3 observations (WMO, 1981; Austin et al., 1986) at several altitudes. The choice of species for comparison was based on the availability of stratospheric data, as well as on their importance to determining O_3 concentrations.

Previously, investigations of this discrepancy involved either varying a very limited set of rate parameters or using simpler models than the LLNL 1-D model. The few studies that have attempted to derive selection criteria based on comparison of model results with observations have looked at fewer species and/or fewer altitudes.

Selection criteria were used at 25 km, 35 km, and 45 km where sufficient data were available. For $C\ell O$ and NO_2 the data used did not extend to 45 km (WMO, 1981), therefore 40 km values were used instead. Likewise, for HNO_3, only 25 km and 35 km values were used. Except where otherwise noted, the envelopes of the measurements were used as the constraining criteria. For $C\ell O$, the two July profiles of Anderson et al. (1980) lying outside the envelope of other measurements were not included in determining the constraints. To be consistent with measurement data, diurnally averaged concentrations output from the 1-D model were converted to noon values, except for NO_2 concentrations, which were converted to sunset values. Conversion factors were obtained from a diurnal baseline case run of the 1-D model.

Of the 100 runs analyzed, 31 runs satisfied the O_3 criteria at 45 km (Table 2). When criteria for 25 km and 35 km were included, this was reduced to 15 runs. Twenty-four runs were found to satisfy the criteria for $C\ell O$, NO, NO_2, and HNO_3 without O_3 criteria. When all the above criteria were combined, only eight runs survived. Thus, while individual

criteria can be met with relative ease, the number of ways in which multiple criteria can be met is much more limited.

Following initial formulation of observational criteria, several individual criteria were reevaluated from the standpoint of the severity of the effect of applying each criterion versus its uncertainty. We originally assumed an observed upper limit for HNO_3 at 35 km of 2.6 ppbv (WMO, 1981). This constraint lies near the median of the Monte Carlo distribution obtained for HNO_3 and will thus very strongly effect case selection. This situation is clearly visible in the scatter diagram of percent change in O_3 versus ambient concentration of HNO_3 presented in Figure 1. Based on mean seasonal range concentrations from more recent midlatitude LIMS (Limb Infrared Monitor of the Stratosphere) satellite data (Austin et al., 1986), we felt justified in adjusting this limit upwards to 3.7 ppbv. The effects are minimal of including the constraints for HNO_3 with those for $C\ell O$, NO, and NO_2. As shown in Table 3, the use of HNO_3 criteria reduces the number of cases surviving criteria, other than those for O_3, from 32 to 24. When the O_3 criteria are included, the HNO_3 criteria reduce the number of surviving cases from nine to eight. In either instance, the addition of HNO_3 criteria does not change the minimums or maximums for percent O_3 depletion and only slightly affects the means and standard deviations.

Case selection was found to be highly sensitive to the upper limit $C\ell O$ constraint at 25 km. A value of 0.08 ppbv was used for this constraint. If this criterion were reduced (semi-abstractly) to as low as 0.056 ppbv, the baseline case and four of the eight cases previously satisfying all criteria would have been eliminated. This sensitivity can be seen in the scatter diagram of percent change in O_3 versus ambient concentration of $C\ell O$ shown in Figure 2. As shown in that figure, the $C\ell O$ concentrations at 25 km are densely scattered between 0.03 to 0.10 ppbv. Any change to a criterion lying within this range thus has the potential of strongly affecting the final result of a multiple criteria selection process. This derived sensitivity to $C\ell O$ upper limits is illustrative of the sensitivity produced when one attempts to simultaneously apply a number of constraints - we caution that such comparisons require careful analysis of the criteria used. Our judgment, that the potential elimination of half of the otherwise surviving cases plus the baseline case was a more severe result than justified by the relevant measurement uncertainties, is an indication of the considerations that arise in choosing constraints. In this case, we felt the higher value was sufficiently consistent with observations to merit its use.

It would be desirable to retrieve the sensitivity of the model to variation of individual parameters from the results of a series of Monte Carlo runs in which multiple parameters have been varied simultaneously. This would allow direct comparison with the results of sensitivity studies in which only one parameter is varied at a time. However, such a retrieval will generally require sophisticated techniques embodying substantial a priori knowledge of the general nature of the expected results. This difficulty arises both from the nonlinearity of model response to parameter variation and from the ill-posed nature of such inversion problems (Twomey, 1977; Menke, 1984). Without sufficient constraints on the general nature of the retrieval, numerically correct but physically meaningless model sensitivity coefficients will result. These coefficients would likely show little consistency between different sets of Monte Carlo runs.

For this initial study, we avoided the difficulties of doing a complete inversion by only analyzing the production and loss mechanisms for a very small set of reactions already known to be important in determining O_3 at 45 km. We manually compared the importance of each of these mechanisms for each of the eight cases satisfying all trace gas criteria. In future studies, our intent is to incorporate such a priori knowledge of reaction importance into an inversion scheme that can be applied to a much larger set of Monte Carlo runs.

For these eight cases, an analysis was made of O_2 photolysis rates versus major O_3 loss rates at 45 km (Table 4). No single mechanism was found that increased O_3 at 45 km while maintaining agreement with other criteria. This is consistent with the sensitivity studies of Froidevaux et al. (1985) and the Monte Carlo results of Stolarski and Douglass (1986).

In all of the eight retained cases, the O_2 photolysis rate at 45 km (and rate of O_3 loss) and column O_3 above 45 km were greater than that for the baseline case. In seven of these cases, the relaxation constant for loss of O_3 (loss rate divided by the O_3 concentration) summed over all pathways was less than that for the baseline case. Case 11 was unique in having a larger relaxation constant, but this case was also found to be the only retained case to have a total column O_3 amount below the 2σ limit of the observed variability for the 30° latitude zonal mean as reviewed in MAP (1985). All cases except for case 85 had a reduced relaxation constant for the HO_x cycle. This case displayed compensating moderate decreases in both the NO_x and $C\ell O$ cycles. Case 26 was notable both for having the O_2 photolysis rate closest to that for the baseline case and for having a relaxation constant for the $C\ell O$ cycle about half of that for the baseline case. Cases 26 and 85 were also the only two of the eight retained cases to survive the $HC\ell$ criteria discussed below.

Although models are known to underpredict $HC\ell$ compared to observations in the middle stratosphere (WMO, 1986), the eight cases surviving these previous criteria were further subjected to observational criteria for $HC\ell$ at 25 km and 35 km. The required data were taken from the suggested mean $HC\ell$ vertical profile and 3σ error limits presented in WMO (1981). A detailed look at the results is instructive in interpreting this type of analysis (Table 5). While six of the eight cases previously retained were eliminated, elimination of case 11 was borderline. An increase in the upper limit at 25 km from 1.23×10^9 to 1.25×10^9 molecules cm^{-3} would have retained it. Cases were eliminated either because they were too high at 25 km or too low at 35 km. None of the eliminated cases violated more than one constraint, however. Half of the six eliminated cases would have been retained if the upper limit at 25 km was increased by 11.4% and the lower limit at 35 km was decreased by 6.2%. To have retained all cases would have required changing the limits by 26.0% and -6.5%, respectively.

Predictions for The Chemically Perturbed Atmosphere

Comparison of model calculations for the ambient atmosphere with actual measurements is extremely important for gaining understanding of model behavior and for further refining current models. However, substantial motivation exists for modeling the potential effects of possible future concentrations of trace species. Accordingly, we calculated the

distribution of the percent change in O_3 for a possible future chemically perturbed atmosphere relative to a reference atmosphere. Our perturbed atmosphere corresponded to 15 ppbv CℓX, 1.25 $\times$ the present concentration of N_2O, and twice the present concentration of CH_4. The reference atmosphere was without chlorofluorocarbon (CFC) emissions with present concentrations of N_2O and CH_4.

To calculate this distribution, we executed a series of 100 Monte Carlo runs and a baseline run for each of the reference and perturbed atmospheres, using the same sequence of random perturbations to model parameters previously used for the ambient atmosphere. This sampling produced a series of paired runs from which O_3 probability distributions were derived for the column total and several selected altitudes. These distributions are shown in Figures 3 and 4. The corresponding probability distributions for the percentage change of O_3 were then produced by calculating the percent changes for each pair of runs having the same random sampling (Figure 5).

Using recommended rate parameter constants (DeMore et al. 1985), we determined a total column O_3 change of -7.7% for the chemically perturbed atmosphere relative to the reference atmosphere (Table 6). With recommended uncertainties applied to all rate and photolysis parameters, we obtained a standard deviation about the baseline case of $\pm$6.4% for 100 Monte Carlo runs.

The distributions for percent change in O_3 obtained when all uncertainties were reduced to an assumed minimum laboratory measurement error of 10% are shown in Figure 6. To facilitate comparison, the same set of random samplings and the same altitudes were used as for Figures 3-5. This modification reduced the standard deviation for change in total column O_3 to $\pm$3.8%. On the positive side, the relative uncertainty overall for the model is less than that assumed for the individual parameters. However, we conclude that significant uncertainties will still remain in model predictions for trace gas concentrations in the stratosphere, even if minimum likely measurement uncertainties of 10% are eventually obtained for all kinetic rate constant parameters and photolysis rates.

For the distributions obtained using both the recommended and 10% uncertainties, the predicted uncertainties in percent change of ozone were found to be roughly constant with altitude. This constancy is also evident from the profiles of the baseline value and standard deviation for percent change of O_3 for both sets of uncertainties, as shown in Figure 7. The baseline concentration and standard deviation profiles for O_3 in the reference atmosphere are shown in Figure 8. It is apparent from this figure that the largest absolute uncertainties in ozone concentrations were found to be near 25 km where the ozone concentration is largest. As seen from the altitude profile of the moment coefficient of skewness for percent change of O_3 in Figure 9, the shape of the these distributions is a strong function of altitude. At individual altitudes, the distributions were found to be skewed opposite to the calculated baseline changes as can be seen from Figures 7 and 9. Thus, at 25 km a small baseline increase with negative skewness was calculated, while at 40 km a large baseline decrease with positive skewness was obtained. However, the larger absolute O_3 concentrations and uncertainties in the lower stratosphere result in a baseline total column O_3 decrease with a distribution skewed toward even greater decreases.

Probability distributions obtained for the ambient atmosphere concentrations (at 25 km, 32 km and 40 km) and column total amounts of CℓO, OH, and NO_y are presented in

Figures 10-12. As was the case for ozone concentrations and percent change, the distributions for these trace species are asymmetrical, with the shape of the each distribution being a function of altitude.

We have noted the presence of significant skewness in most of the probability distributions presented in this study. Additionally, the baseline results and the means of the distributions obtained are not coincident. Stolarski and Douglass (1986) have observed that, as a function of increasing CFC source fluxes, the mean O_3 percent decrease behaves more linearly than the baseline percent decrease. This implies that the shape of the distribution is itself a function of the magnitude of the CFC perturbation. Because of these considerations, we conclude that baseline values with standard deviations are generally insufficient to adequately characterize the probability distributions of trace gas concentrations. This conclusion would appear to hold both for column total amounts and for concentrations at individual altitudes in the stratosphere.

The effects of case selection criteria applied to results for the ambient atmosphere on the corresponding results for percent change in O_3 were also investigated. The means, standard deviations, and extrema for this result for sets of Monte Carlo samples obtained by applying individual and combined selection criteria are shown in Table 3. For the 24 cases subjected to all criteria except O_3 concentrations, the minimum and maximum percentage O_3 changes are nearly equidistant from the mean. This implies that this subdistribution is much less skewed than the 100 case parent distribution. A reduction of skewness when observational constraints are applied was also observed by Stolarski and Douglass (1986). This effect is mainly attributable to removal of cases with very large percentage decreases of O_3 by the criteria applied for concentrations of $C\ell O$, as seen in Table 3.

The eight cases surviving all criteria given in Table 2 had the same extrema and essentially the same mean as the 24 cases subjected to all criteria except O_3 criteria. The standard deviation was larger than for the 24 case set, but not by more than would be expected by a factor of three reduction in the number of retained cases.

We also compared predictions for percent change in total column O_3 with mixing ratios of HNO_3, $C\ell O$, OH, and NO_y for the ambient atmosphere (2.5 ppbv $C\ell X$). The comparisons are presented as scatter diagrams in Figures 1, 2, 13, and 14. No clear relationship was evident between column O_3 and concentration of HNO_3 at 35 km (Figure 1) or between between column O_3 and the concentration of OH at 25 km (Figure 13). Johnston (1984) had suggested a correlation between concentration of OH and column O_3 percent change (all else being equal, which it is not). Our results as presented in Figures 2 and 14 indicate a strong negative relationship with C ℓO at 25 km and a weak positive relationship with NO_y at 35 km.

Conclusions

In this study, we have used the LLNL 1-D transport-kinetics model combined with Monte Carlo parameter variation to obtain information on the uncertainties in model predictions for concentrations of ozone and other trace atmospheric species. We have implemented the Monte Carlo uncertainty technique using a variance reducing technique called Latin Hypercube Sampling. This technique greatly reduces the number of runs

required to obtain a given variance in the mean value of a model prediction such as percent change in ozone.

Significant uncertainties in O_3 depletion were found in the upper stratosphere where the chemistry is generally considered to be understood. Current models of stratospheric photochemistry and transport commonly underpredict O_3 abundance by 20% in this region. The extent to which this discrepancy is consistent with current uncertainties in rate parameters and rates of photolysis processes has been open to question. Of the Monte Carlo runs we made for the ambient atmosphere, fully 30% yielded sufficiently large concentrations of O_3 at 45 km to be within the 2σ limits of O_3 measurements. However, this does not immediately imply that a set of rate constants can be found that would increase upper stratospheric O_3 predictions by 20% without unrealistically perturbing concentration profiles of O_3 or other trace species.

To further investigate this question, observational constraints for O_3, $C\ell O$, NO, NO_2, and HNO_3 were applied to 100 Monte Carlo runs based on an ambient atmosphere with 2.5 ppbv $C\ell X$. For the 8 cases surviving all criteria, no single mechanism was found that increased O_3 at 45 km while maintaining agreement with other criteria. In all of the retained cases, however, the O_2 photolysis rate at 45 km (and rate of O_3 loss) and column O_3 above 45 km were greater than that for the baseline case. Seven of the eight cases had total relaxation constants for O_3 loss less than that for the baseline case while simultaneously having greater O_2 photolysis rates. The one case where this was not true was sufficiently low in total column O_3 to have been discarded. These results would indicate that while an increase in O_3 production is helpful in obtaining increased O_3 in the upper stratosphere, it is not sufficient without net decreases in loss mechanisms.

A total column O_3 change of -7.7% was found for a possible future chemically perturbed atmosphere relative to a reference atmosphere. The perturbed atmosphere had 15 ppbv $C\ell X$, 1.25 $\times$ the present concentration of N_2O, and twice the present concentration of CH_4. The reference atmosphere was without CFC emissions and had present concentrations of N_2O and CH_4. Using recommended values for the uncertainties in kinetic rate constants and photolysis processes, a standard deviation of $\pm 6.4\%$ was obtained. The predicted uncertainties were found to be roughly constant with altitude. The largest absolute uncertainties in O_3 were found, however, near 25 km where the O_3 concentration is largest.

When all uncertainties were reduced to 10%, the standard deviation of column O_3 percent change was reduced to $\pm 3.8\%$. A similar reduction was found for the altitude profile. We conclude that, even if laboratory measurements of rate constants eventually achieve a practical minimum uncertainty of 10%, significant uncertainty will still remain in model predictions for stratospheric O_3 concentrations and total column amounts.

At individual altitudes, the distributions for percent O_3 change were found to be skewed opposite to the calculated baseline change. Thus, at 25 km a small increase with negative skewness was calculated, while at 40 km a large decrease with positive skewness was obtained. However, the much larger absolute O_3 concentration and uncertainty in the lower stratosphere resulted in a baseline total column O_3 decrease with a distribution skewed toward even greater decreases. Because of this skewness, it is apparent that baseline values with simple symmetrical error limits are not sufficient to categorize the uncertainties in stratospheric trace gas concentrations.

The effects of case selection criteria applied to results for the ambient atmosphere on the corresponding results for percent change in O_3 were also investigated. A reduction of skewness, attributable to removal of cases with very large percentage decreases of O_3, was obtained by the application of criteria for concentrations of $C\ell O$. In combination with other trace gas criteria that slightly truncated the upper limits of predicted O_3 change, the mean change in O_3 was reduced from -8.6% to -6.8%. Although the standard deviation per se did not decrease greatly from that for all cases, this is mainly due to the large reduction in the number of cases retained. In actuality, the distribution obtained with all criteria applied is much narrower.

We also compared predictions for percent change in total column O_3 with mixing ratios of HNO_3, $C\ell O$, OH, and NO_y for the ambient atmosphere (2.5 ppbv $C\ell X$). No clear relationship was evident between column O_3 and concentration of HNO_3 at 35 km or between between column O_3 and concentration of OH at 25 km. Our results indicate a strong negative relationship with $C\ell O$ at 25 km and a weak positive relationship with NO_y at 35 km.

Acknowledgements

This research was supported in part by the NASA Upper Atmospheric Research Program and by the Department of Energy Carbon Dioxide Research Program.

This work was performed under the auspices of the U.S. Department of Energy by the Lawrence Livermore National Laboratory under Contract W-7405-Eng-48.

List of Tables

Table 1: Absorption cross-section uncertainty factors for O_2, O_3, and NO_2 used in solar flux calculations

O_2 (General)	±1.4
O_2 (Schumann-Runge)	±1.4
O_2 (Herzberg)	-1.1, +1.5
O_3	±1.1
NO_2	±1.25

Table 2: Observational selection criteria used for Monte Carlo run comparisons. All values are for noon except those for NO_2 which are sunset values. All values are given in ppbv except those for O_3 which are in molecules cm^{-3}. Altitudes shown are on the model log-pressure grid and differ slightly from actual physical altitudes which are shown in parentheses.

Species	25 km	35 km	40 km	45 km
	(24.2)	(33.6)	(38.6)	(43.9)
O_3	3.29-5.69(12)	1.11-2.23(12)	—	1.80- 3.76(11)
$C\ell O$	0.008-0.08	0.15-7.0	0.4-1.5	—
NO	0.74-2.9	3.7-21	—	4.4-31
NO_2	0.66-5.8	2.8-22	2.6-18	—
HNO_3	2.7-12	0.31-3.7	—	—

Table 3: Means, standard deviations, and extrema of percent change in O_3 for the chemically perturbed atmosphere relative to the no-CFC reference atmosphere for sample sets meeting O_3, individual trace gases other than O_3, and combined selection criteria applied to the ambient (2.5 ppb $C\ell X$) atmosphere. Except where noted, selection criteria were applied at all altitudes for which concentrations were given in Table 2.

Set Criteria	N	Mean	Std. Dev.	Minimum	Maximum
None	100	-8.6	6.4	-31.6	1.56
O_3 at 45 km	31	-10.9	8.0	-31.6	0.35
O_3	15	-10.9	9.0	-29.9	0.35
$C\ell O$	53	-5.5	3.4	-13.9	1.56
NO	84	-8.1	6.0	-31.6	1.56
NO_2	81	-9.8	6.4	-31.6	0.35
HNO_3	64	-9.1	6.2	-31.6	1.29
All but HNO_3 and O_3	32	-6.4	3.2	-13.9	0.35
All but O_3	24	-6.9	3.3	-13.9	0.35
O_3 at 45 km & other trace gases	13	-7.0	4.0	-13.9	0.35
All but HNO_3	9	-7.0	4.9	-13.9	0.35
All criteria	8	-6.8	5.2	-13.9	0.35

Table 4: Comparison of relaxation constants for O_3 production and major loss mechanisms at 45 km for random samples meeting combined O_3 and other trace gas selection criteria. O_2 photodissociation rates are given in units of 10^6 molecules cm^{-3} sec^{-1}. All other quantities are O_3 loss relaxation constants given as percentages of the total loss relaxation constant of 2.87×10^{-5} for the basecase. Each loss cycle is listed by its rate limiting step.

	Case Number								
Reaction	Base	11	26	55	75	77	78	85	95
O_2 + hv	2.23	3.49	2.25	2.35	2.72	3.20	2.57	2.60	3.87
Total loss	100	111	82.6	83.9	96.2	88.6	94.0	97.1	84.4
$O + O_3$	15.7	28.9	20.3	18.2	15.7	24.8	16.3	13.6	17.7
$NO_2 + O$	19.0	23.1	20.7	11.8	24.3	16.1	19.5	15.4	14.8
$HO_2 + O$	26.9	24.2	19.1	23.9	19.4	18.8	24.6	30.5	13.9
$H + O_3$	2.8	2.2	3.2	2.9	2.3	3.8	2.3	7.3	2.9
$C\ell O + O$	34.8	32.1	17.7	26.4	33.6	24.5	30.4	29.7	34.4

Table 5: Comparison of $HC\ell$ 3σ criteria (WMO, 1981) with model baseline run and cases satisfying previous observation criteria. Values shown (molecules cm^{-3}) that conflict with the criteria are shown in **boldface**.

Case No.	25 km	35 km
3σ range	4.9-12.3(8)	2.6-5.8(8)
base	1.05(9)	2.83(8)
11	**1.24(9)**	3.08(8)
26	9.25(8)	3.10(8)
55	**1.43(9)**	3.68(8)
75	1.16(9)	**2.43(8)**
77	**1.55(9)**	3.99(8)
78	8.34(8)	**2.45(8)**
85	1.10(9)	3.44(8)
95	**1.36(9)**	3.53(8)

Table 6: Statistical moments for percent change in O_3 (perturbed atmosphere relative to the reference) obtained for 100 model runs (10% uncertainty results in parenthesis). The standard deviations and moments of skewness are taken about the baseline values not about the mean values.

Altitude km	Unvaried % Change	Standard Deviation	Moment of Skewness
Column Total	-7.7	6.4 (3.8)	-1.8 (-1.4)
25	+0.5	8.0 (4.3)	-2.5 (-1.3)
32	-22.1	10.3 (5.9)	+0.005 (-0.4)
40	-69.1	9.3 (3.8)	+1.7 (+0.8)

List of Figures

Bibliography

Anderson, J.G., H.J. Grassl, R.E. Shetter, and J.J. Margitan, "Stratospheric Free Chlorine Measured by Balloon-Borne in situ Resonance Fluorescence", *J. Geophys. Res., 85,* 2869-2887, 1980.

Austin, J., R.R. Garcia, J.M. Russell III, S. Solomon, and A.F. Tuck, "On the Atmospheric Photochemistry of Nitric Acid", *J. Geophys. Res., 91 (D5),* 5477-5485, 1986.

Butler, D.M., "The Uncertainty in Ozone Calculations by a Stratospheric Photochemical Model", *Geophys. Res. Lett., 5,* 769-772, 1978a.

Butler, Dixon, M., "Input Sensitivity Study of a Stratospheric Photochemistry Model", *Pageoph, 117,* 430-435, 1978b.

DeMore, W.B., J.J. Margitan, M.J. Molina, R.T. Watson, D.M. Golden, R.F. Hampson, M.J. Kurylo, C.J. Howard, and A.R. Ravishankara, Chemical Kinetics and Photochemical Data for Use in Stratospheric Modeling – Evaluation Number 7, Publ. 85-37, Jet Propul. Lab., Pasadena, Calif., 1985.

Froidevaux, Lucien, Mark Allen, and Yuk L. Yung, "A Critical Analysis of ClO and O3 in the Mid-Latitude Stratosphere", *J. Geophys. Res., 90* (D7), 12,999-13,029, 1985.

Gardner, R.H., R.V. O'Neill, J.B. Mankin, and J.H. Carnery, "A Comparison of Sensitivity Analysis and Error Analysis Based on a Stream Ecosystem Model", *Ecological Modelling, 12,* 173-190, 1981.

Gardner, R.H. and J.R. Trabalka, Methods of Uncertainty Analysis for a Global Carbon Dioxide Model, DOE/OR/21400-4, U.S. Dept. of Energy, 1985, Available from NTIS.

Hammersley, J.M. and D.C. Handscomb, Monte Carlo Methods, Chapman and Hall, London, 1964.

Iman, Ronald L., Jon C. Helton, and James E. Campbell, "An Approach to Sensitivity Analysis of Computer Models: Part I – Introduction, Input Variable Selection and Preliminary Variable Assessment", *J. Quality Tech., 13 (3),* 174-183, 1981.

Iman, R.L. and W.J. Conover, "A Distribution-Free Approach to Inducing Rank Correlation Among Input Variables", Commun. Stat., B11(3), 311-334, 1982.

Iman, Ronald L., and Michael J. Shortencarier, A FORTRAN 77 Program and User's Guide for the Generation of Latin Hypercube and Random Samples for use with Computer Models, SAND83-2365, Sandia National Laboratories, Albuquerque, New Mexico, 1984.

Johnston, Harold S., "Human Effects on the Global Atmosphere", *Ann. Rev. Phys. Chem., 35,* 481-505, 1984.

Luther F.M., D.J. Wuebbles, W.H. Duewer, and J.S. Chang, "Effect of Multiple Scattering on Species Concentrations and Model Sensitivity", *J. Geophys. Res., 83,* 3563-3570, 1978.

MAP (Middle Atmosphere Program), "Atmospheric Structure and its Variation in the Region 20 to 120 km – Draft of a New Reference Middle Atmosphere", Handbook for Map, vol. 16, 1985.

McKay, M.D., R.J. Beckman, and W.J. Conover, "A Comparison of Three Methods for Selecting Values of Input Variables in the Analysis of Output from a Computer Code", *Technometrics, 21 (2)*, 239-245, 1979.

Menke, William, Geophysical Data Analysis: Discrete Inverse Theory, Academic Press, San Francisco, 1984.

Natarajan, Murali, Linwood B. Callis, Robert E. Boughner, James M. Russell III, and James D. Lambeth, "Stratospheric Photochemical Studies Using Nimbus 7 Data - 1. Ozone Photochemistry", *J. Geophys. Res., 91 (D7)*, 1153-1166, 1986.

NRC (National Research Council Panel on Stratospheric Chemistry and Transport), Stratospheric Ozone Depletion by Halocarbons: Chemistry and Transport, National Academy of Sciences, 1979.

Smith, W.S., "Uncertainties in Evaluated Atmospheric Rate Constants", WMO Symposium on Geophysical Aspects and Consequences of Changes in the Composition of the Stratosphere, WMO No. 511, Toronto, Canada, 37-46, 1978.

Stolarski, R.S., D.M. Butler, and R.D. Rundel, "Uncertainty Propagation in a Stratospheric Model - 2. Monte Carlo Analysis of Imprecisions Due to Reaction Rates", *J. Geophys. Res., 83* (C6), 3074- 3078, 1978.

Stolarski, R.S., and A.R. Douglass, "Sensitivity of an Atmospheric Photochemistry Model to Chlorine Perturbations Including Consideration of Uncertainty Propagation", *J. Geophys. Res.*, 1986 (in press).

Twomey, S., Introduction to the Mathematics of Inversion in Remote Sensing and Indirect Measurements, Elsevier, New York, 1977.

U.S. Standard Atmosphere, 1976, NOAA-S/T 76-1562, 1976.

WMO (World Meteorological Organization), The Stratosphere 1981 - Theory and Measurements, WMO Ozone Research and Monitoring Project Report No. 11, May 1981.

WMO (World Meteorological Organization), Atmospheric Ozone 1985: Assessment of Our Understanding of the Processes Controlling its Present Distribution and Change, WMO Global Ozone Research and Monitoring Project Report No. 16, 1986.

Wuebbles, D.J., "Chlorocarbons Emission Scenarios: Potential Impact on Stratospheric Ozone", *J. Geophys. Res., 88* (c2),1433-1443, 1983a.

Wuebbles, Donald J., A Theoretical Analysis of the Past Variations in Global Atmospheric Composition and Temperature Structure, UCRL-53423 (Ph.D Thesis), Lawrence Livermore National Laboratory, 1983b.

Wuebbles, D.J., F.M. Luther, and J.E. Penner, "Effect of Coupled Anthropogenic Perturbations on Stratospheric Ozone", *J. Geophys. Res., 88* (c2), 1444-1456, 1983.

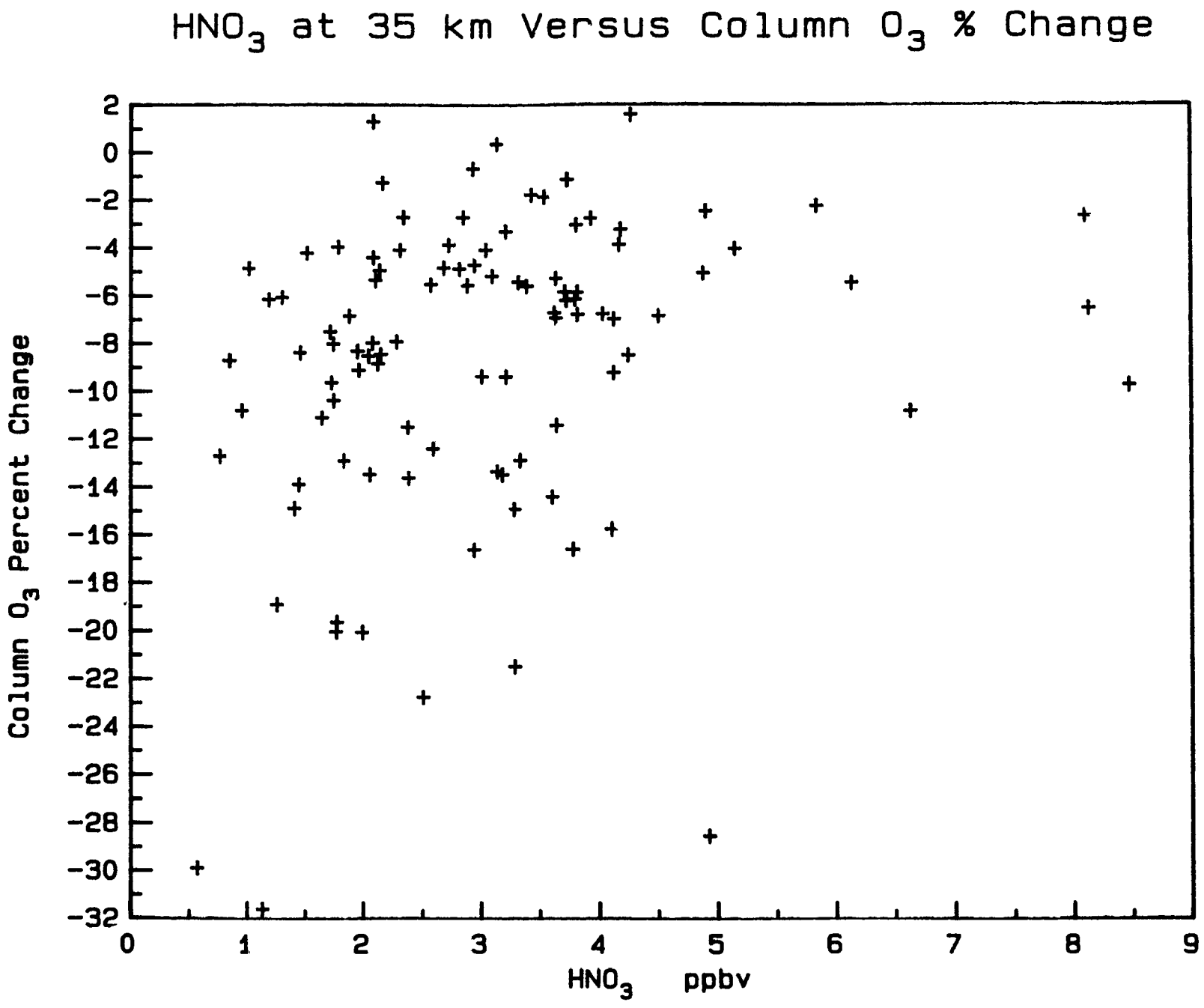
HNO3 at 35 km Versus Column O3 % Change
Column O3 Percent Change
2
0
-2
-4
-6
-8
-10
-12
-14
-16
-18
-20
-22
-24
-26
-28
-30
-32
0
1
2
3
4
5
6
7
8
9
HNO3 ppbv

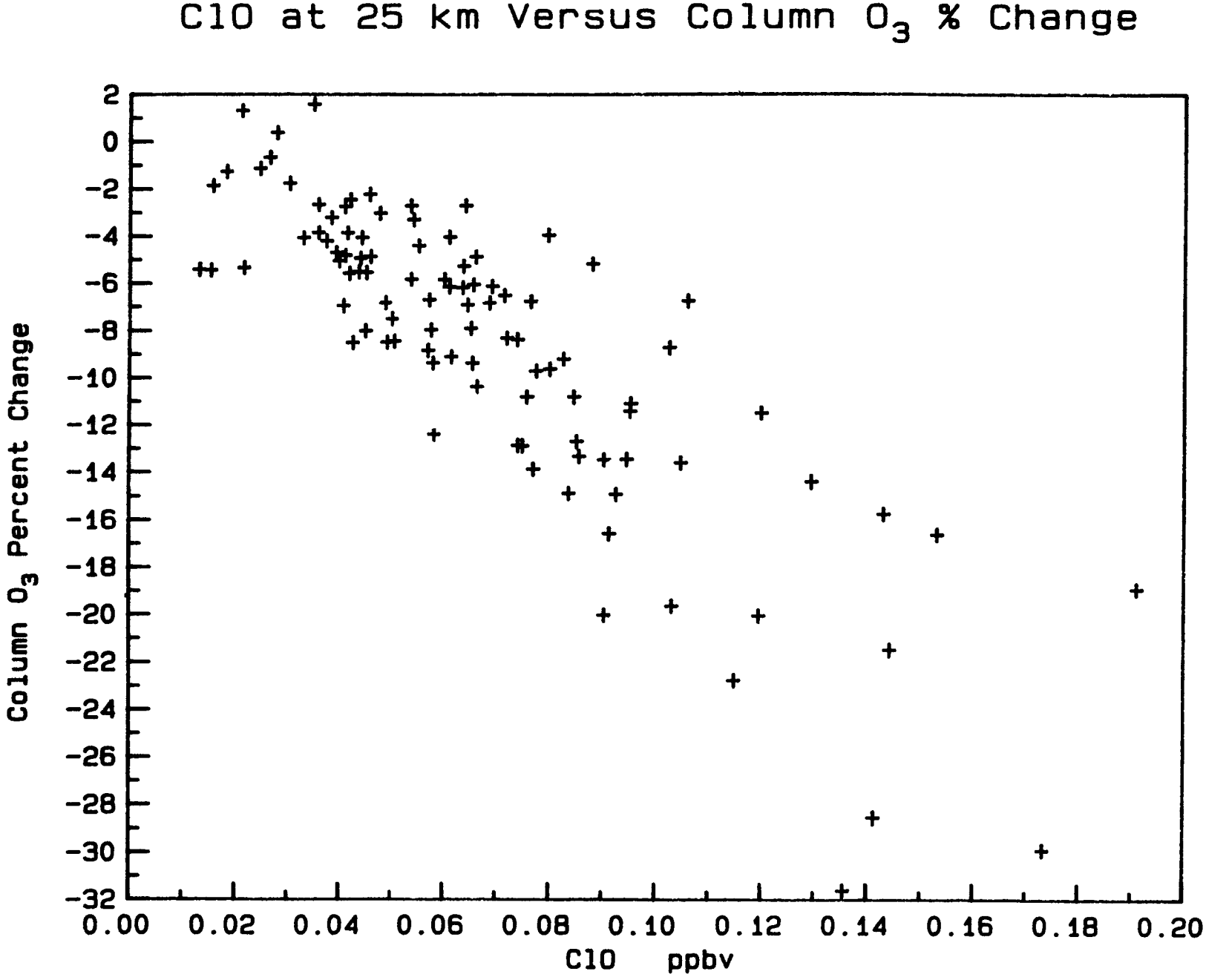
ClO at 25 km Versus Column O_3 % Change
Column O_3 Percent Change
2
0
-2
-4
-6
-8
-10
-12
-14
-16
-18
-20
-22
-24
-26
-28
-30
-32
0.00
0.02
0.04
0.06
0.08
0.10
0.12
0.14
0.16
0.18
0.20
ClO ppbv

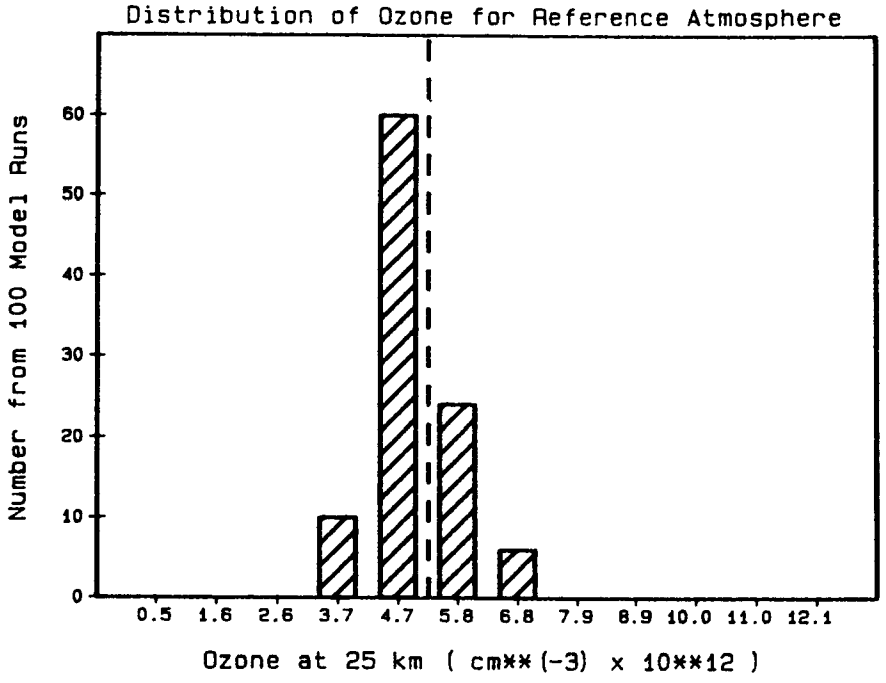

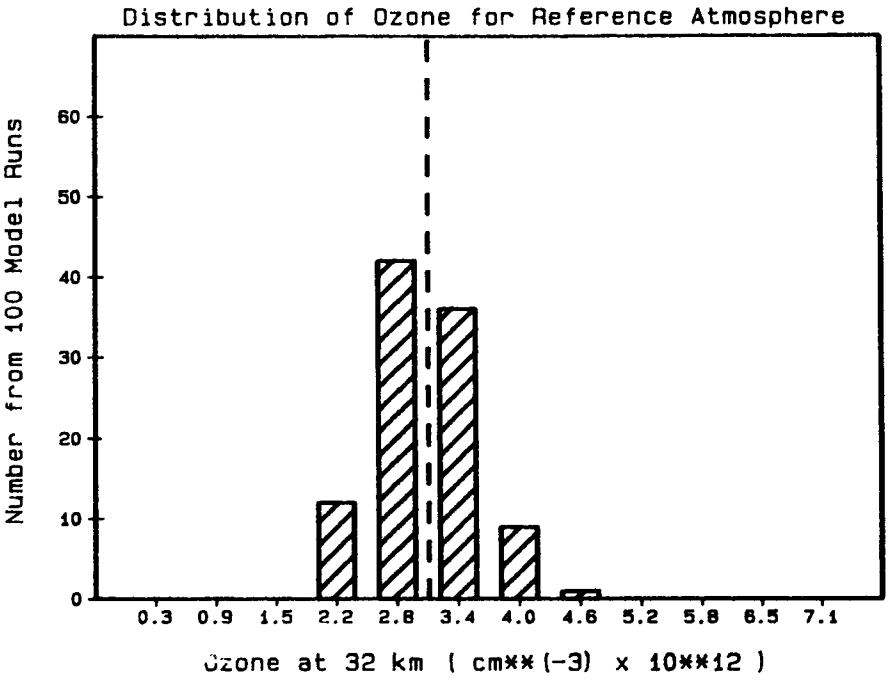

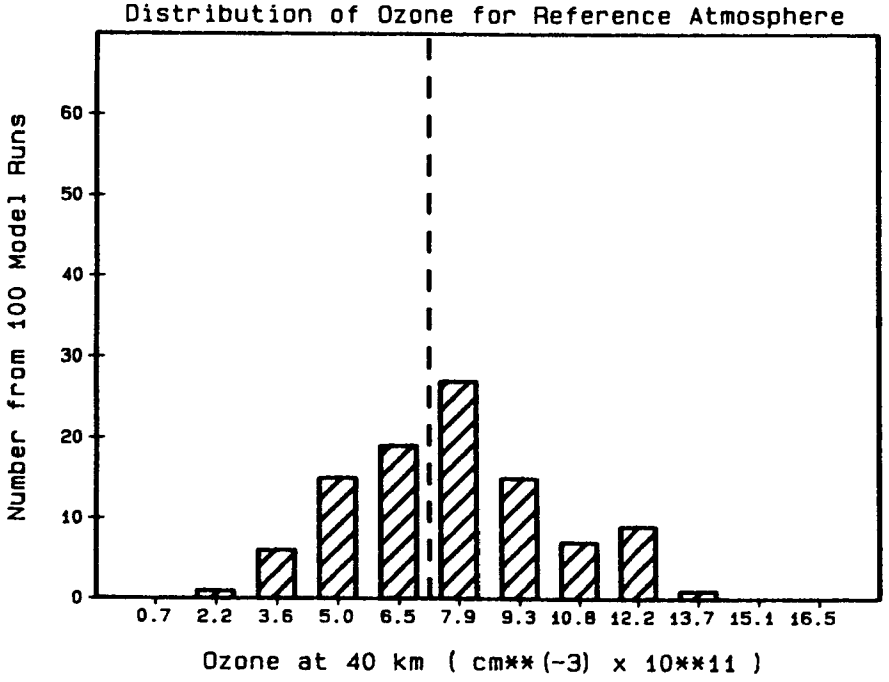

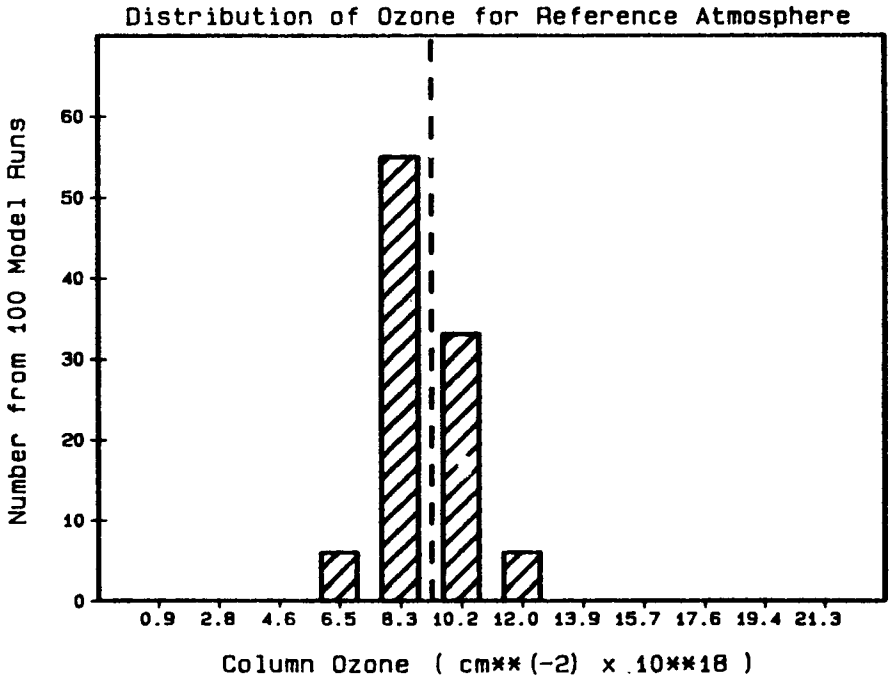

Fernbar 1.1 - 1 April 1986: Plotted: 04/01/1986 10:21:46

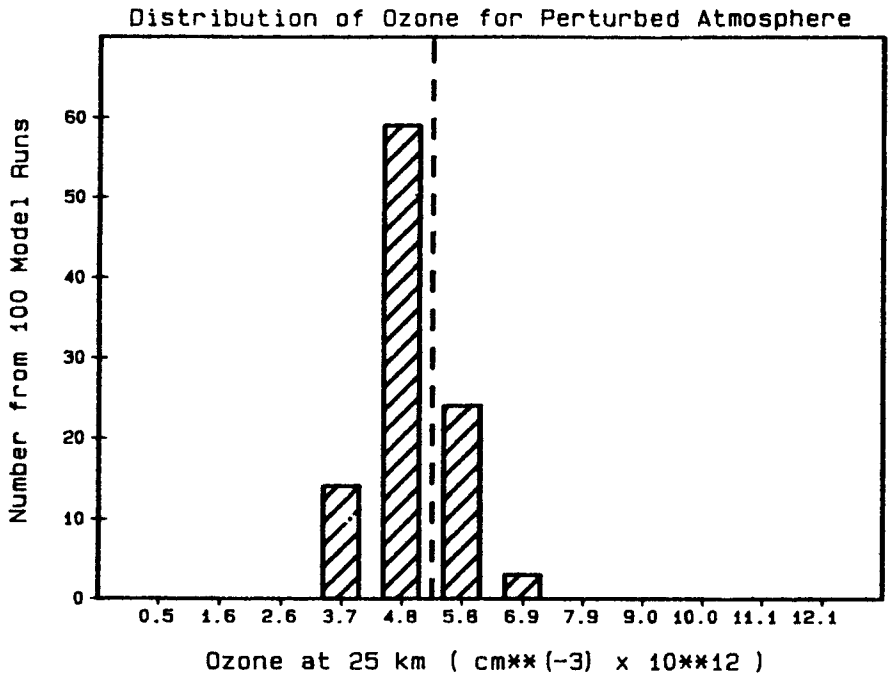

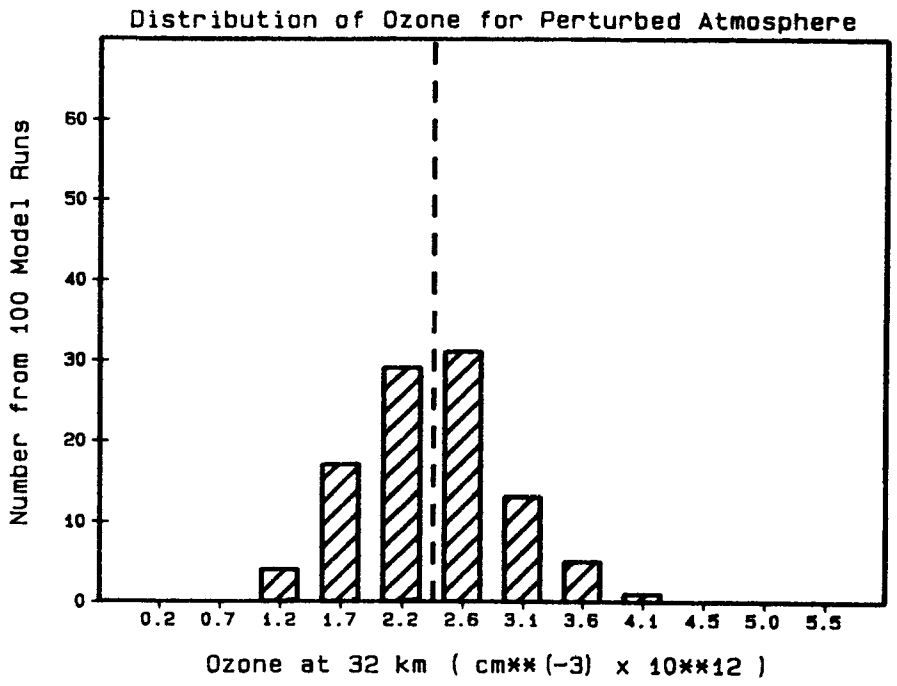

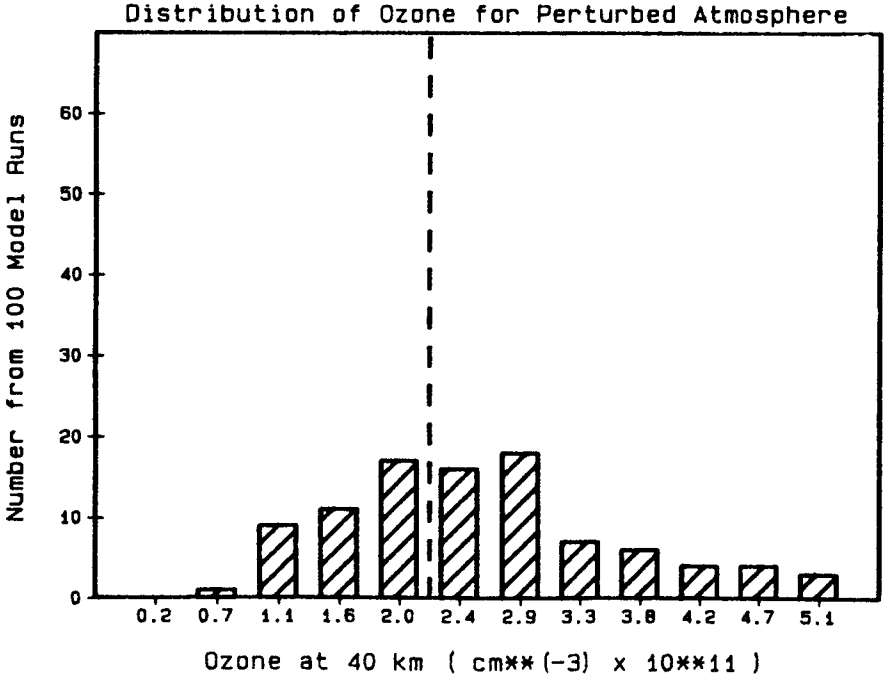

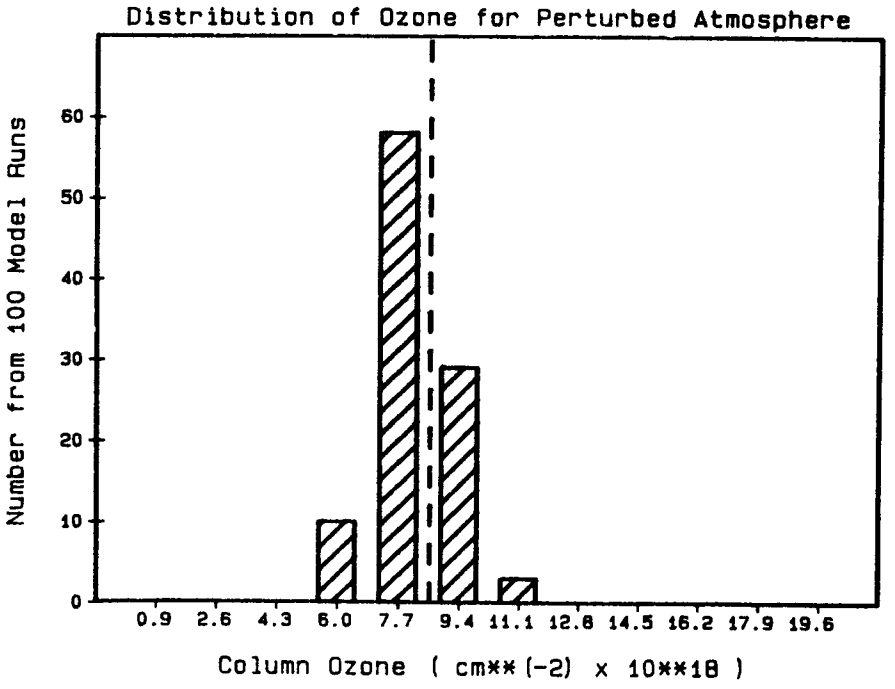

Fernber 1.1 - 1 April 1988: Plotted: 04/01/1988 10:31:31

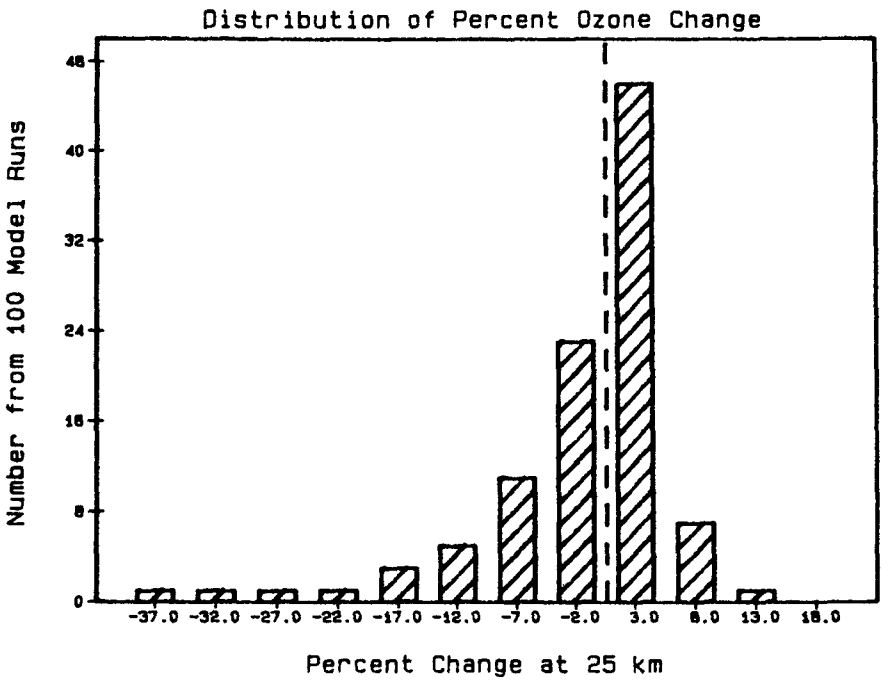
Distribution of Percent Ozone Change
Number from 100 Model Runs
0
8
16
24
32
40
48
-37.0 -32.0 -27.0 -22.0 -17.0 -12.0 -7.0 -2.0 3.0 8.0 13.0 18.0
Percent Change at 25 km

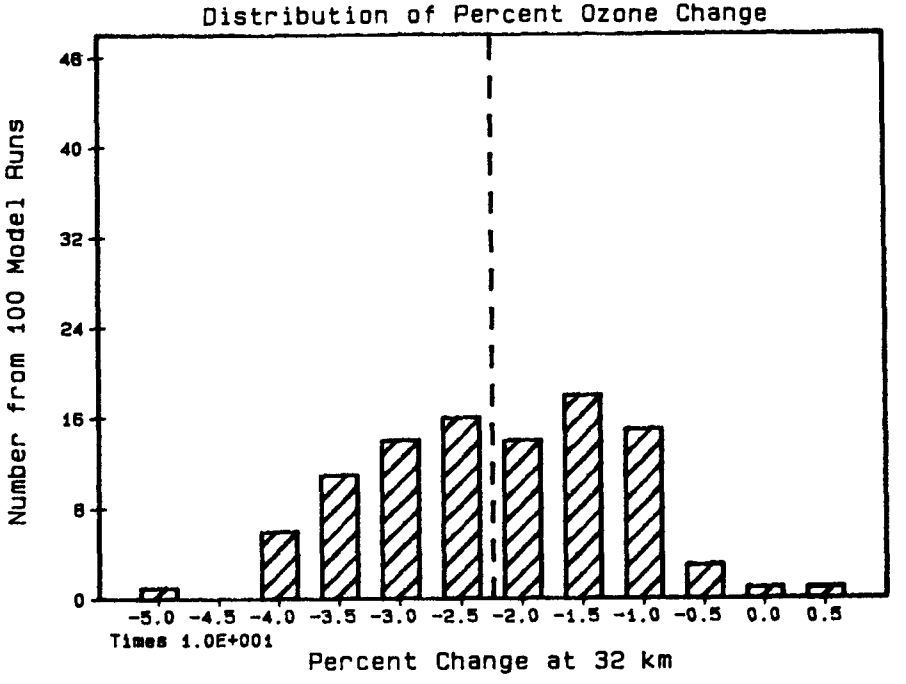
Distribution of Percent Ozone Change
Number from 100 Model Runs
0
8
16
24
32
40
48
-5.0 -4.5 -4.0 -3.5 -3.0 -2.5 -2.0 -1.5 -1.0 -0.5 0.0 0.5
Times 1.0E+001
Percent Change at 32 km

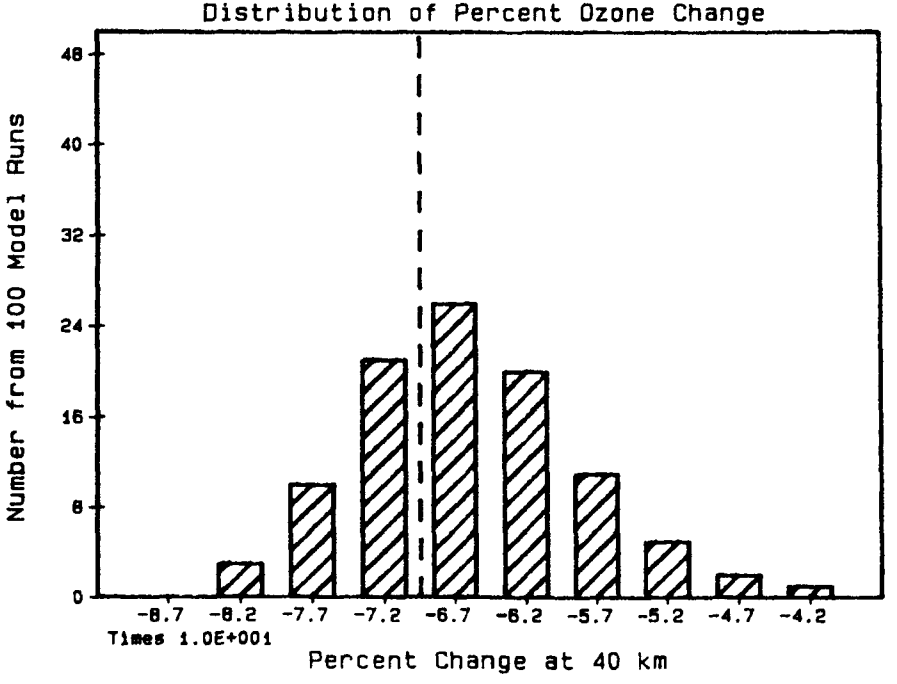
Distribution of Percent Ozone Change
Number from 100 Model Runs
0
8
16
24
32
40
48
-8.7 -8.2 -7.7 -7.2 -6.7 -6.2 -5.7 -5.2 -4.7 -4.2
Times 1.0E+001
Percent Change at 40 km

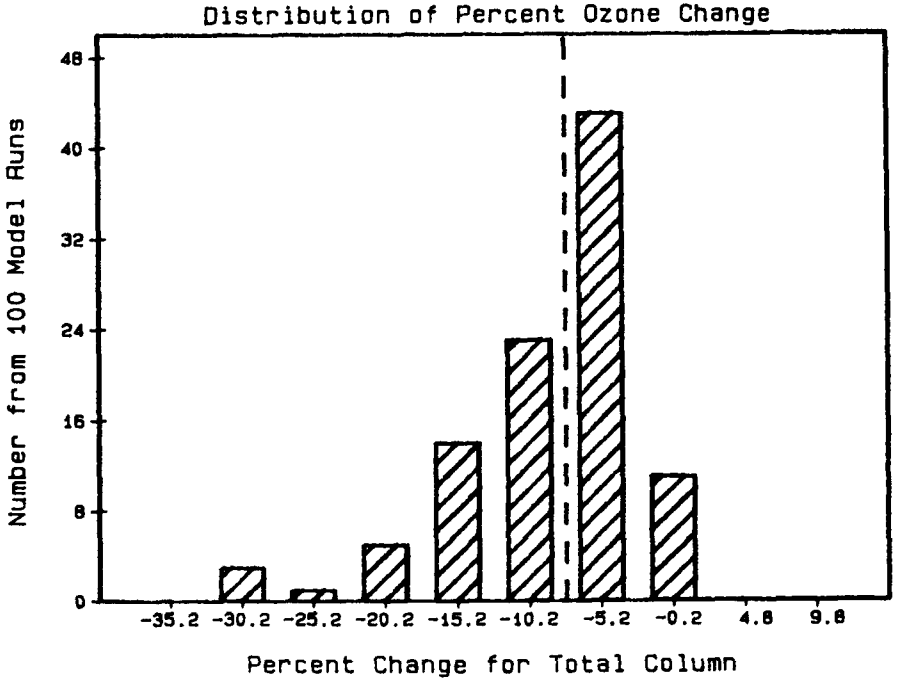
Distribution of Percent Ozone Change
Number from 100 Model Runs
0
8
16
24
32
40
48
-35.2 -30.2 -25.2 -20.2 -15.2 -10.2 -5.2 -0.2 4.8 9.8
Percent Change for Total Column
Fernbar 1.1 - 1 April 1988: Plotted: 04/01/1988 10:11:51

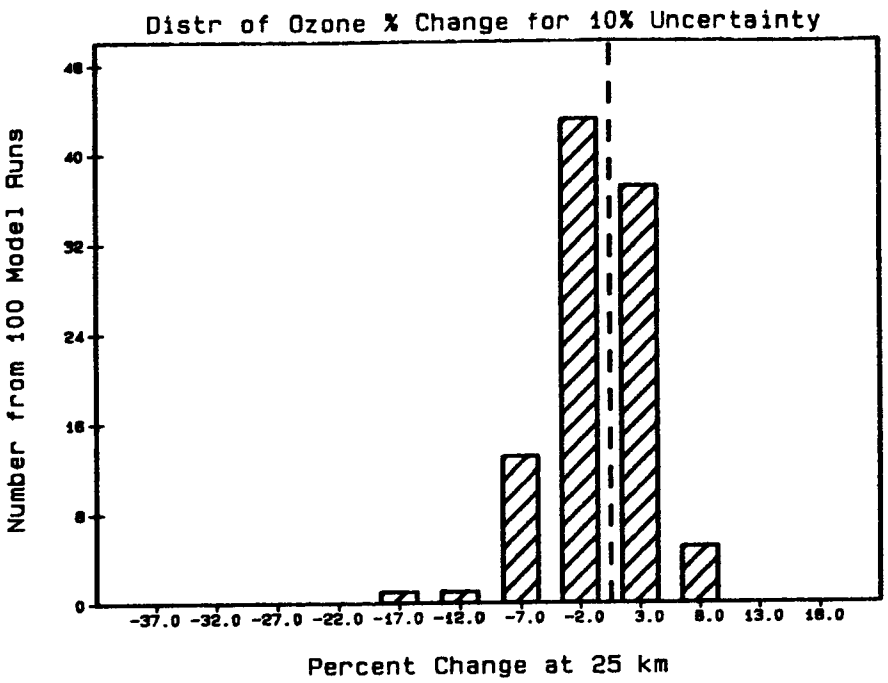

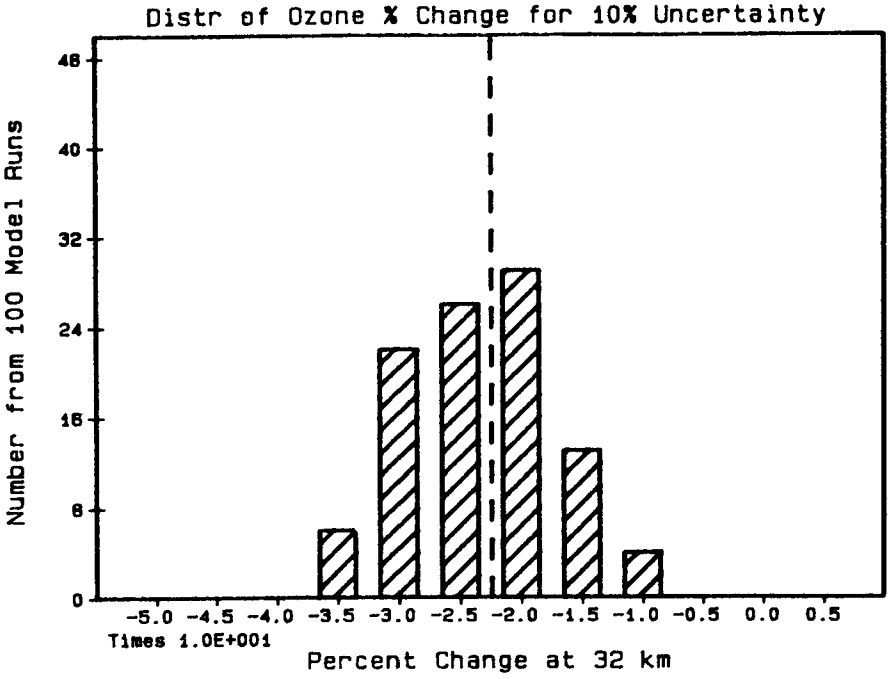

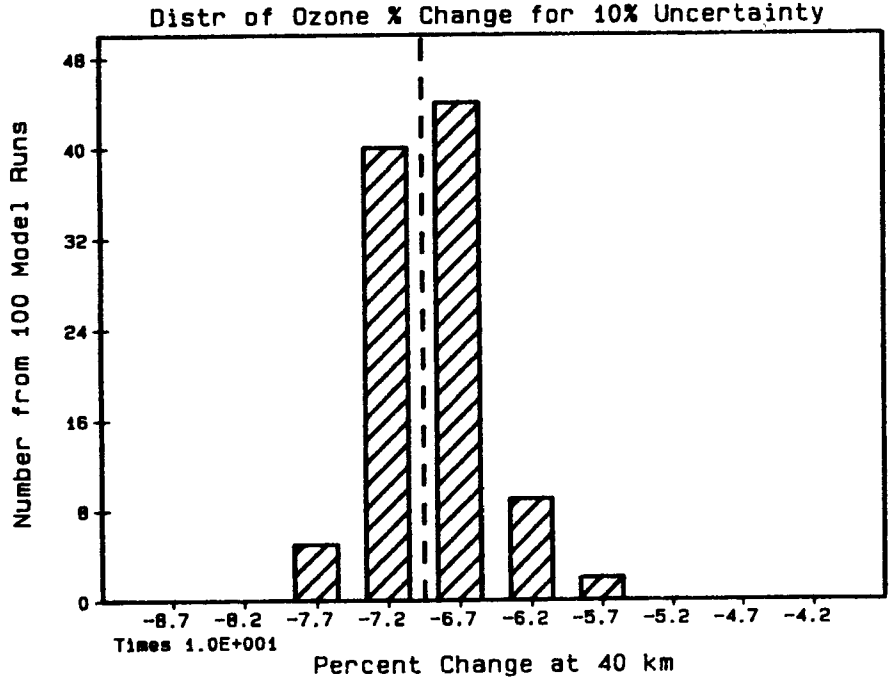

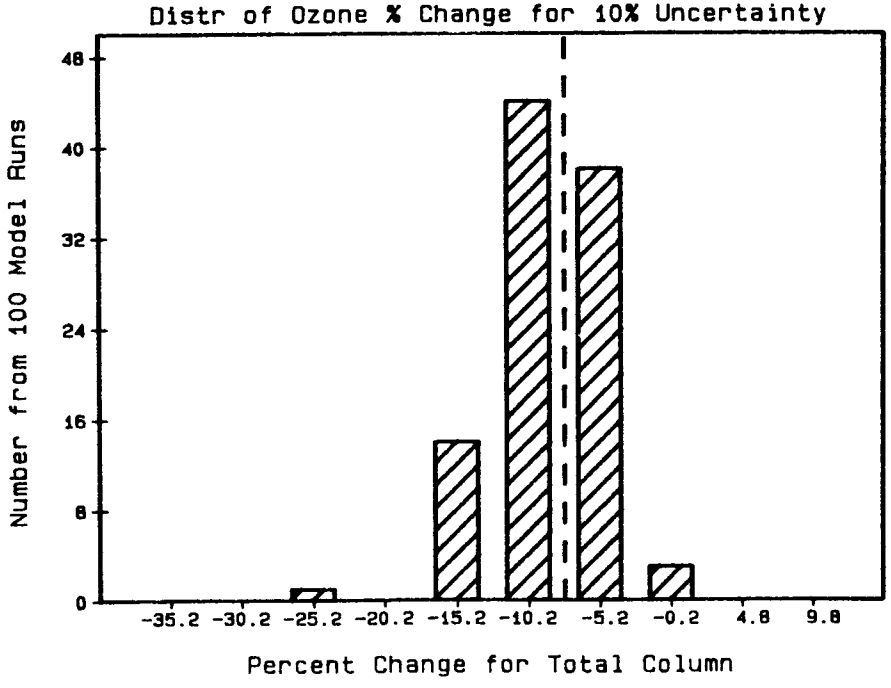

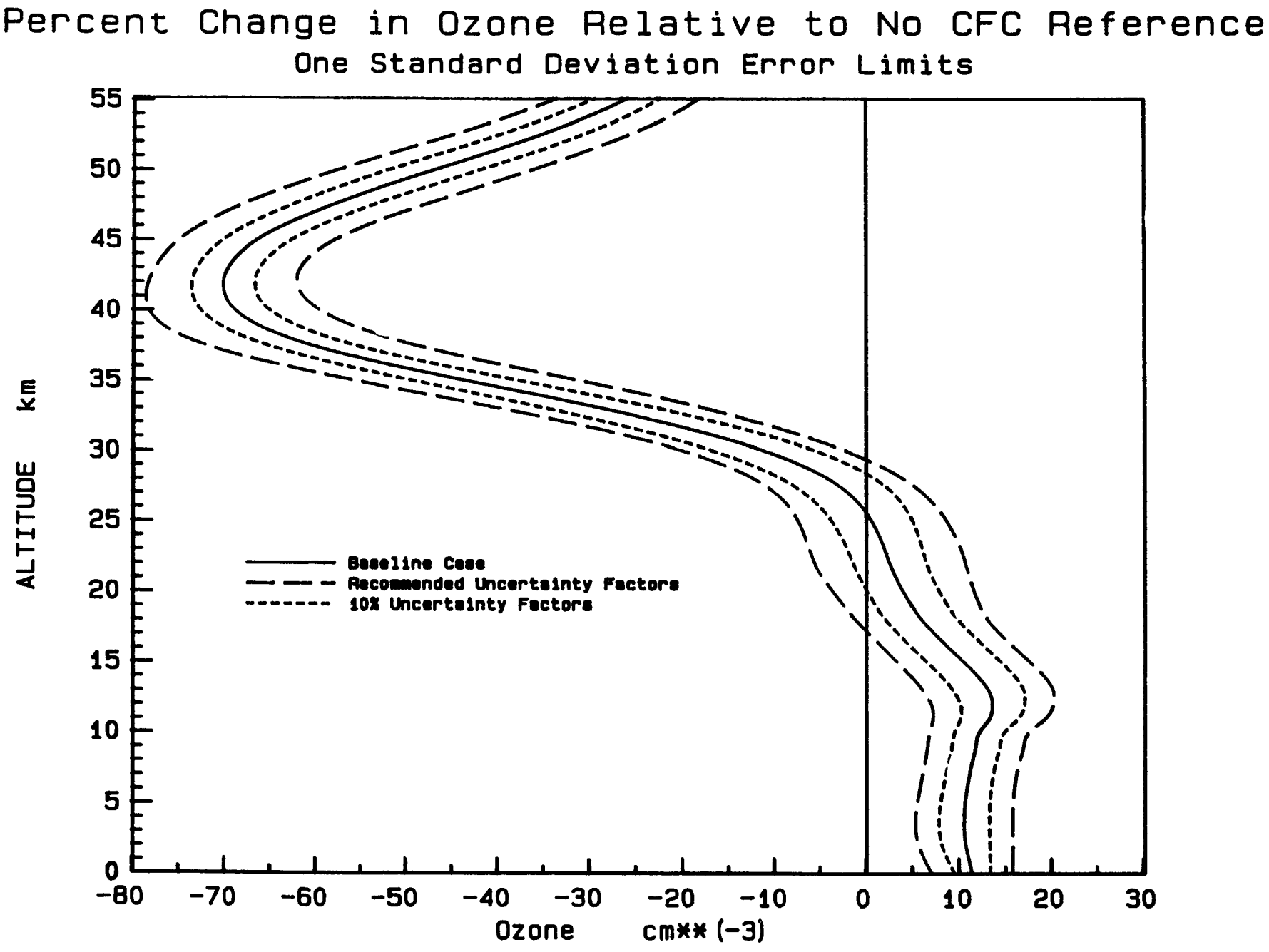
Percent Change in Ozone Relative to No CFC Reference
One Standard Deviation Error Limits
ALTITUDE km
55
50
45
40
35
30
25
20
15
10
5
0
-80
-70
-60
-50
-40
-30
-20
-10
0
10
20
30
Ozone cm** (-3)
Baseline Case
Recommended Uncertainty Factors
10% Uncertainty Factors

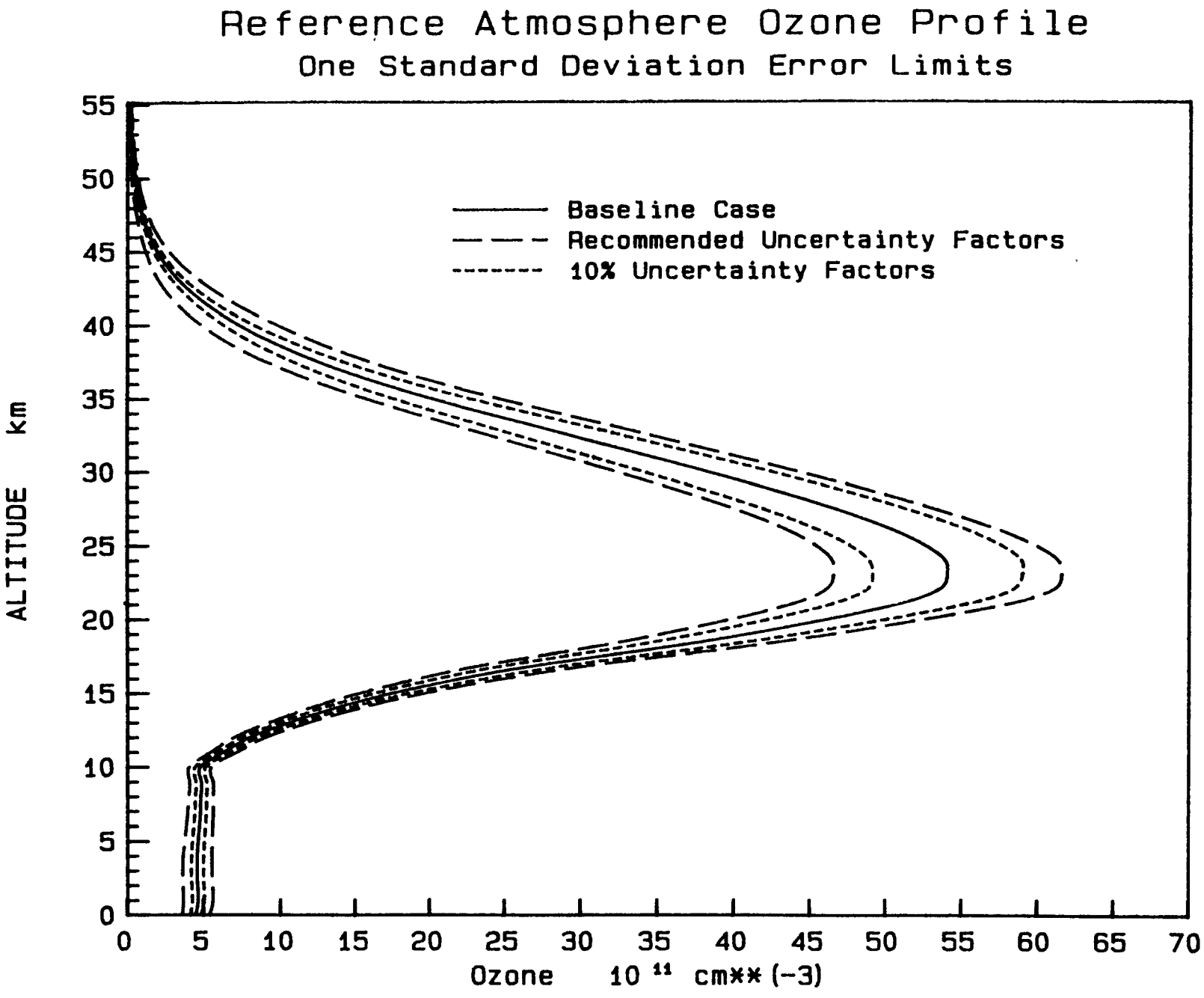
Reference Atmosphere Ozone Profile
One Standard Deviation Error Limits
Baseline Case
Recommended Uncertainty Factors
10% Uncertainty Factors
ALTITUDE km
0
5
10
15
20
25
30
35
40
45
50
55
0
5
10
15
20
25
30
35
40
45
50
55
60
65
70
Ozone 10 11 cm** (-3)

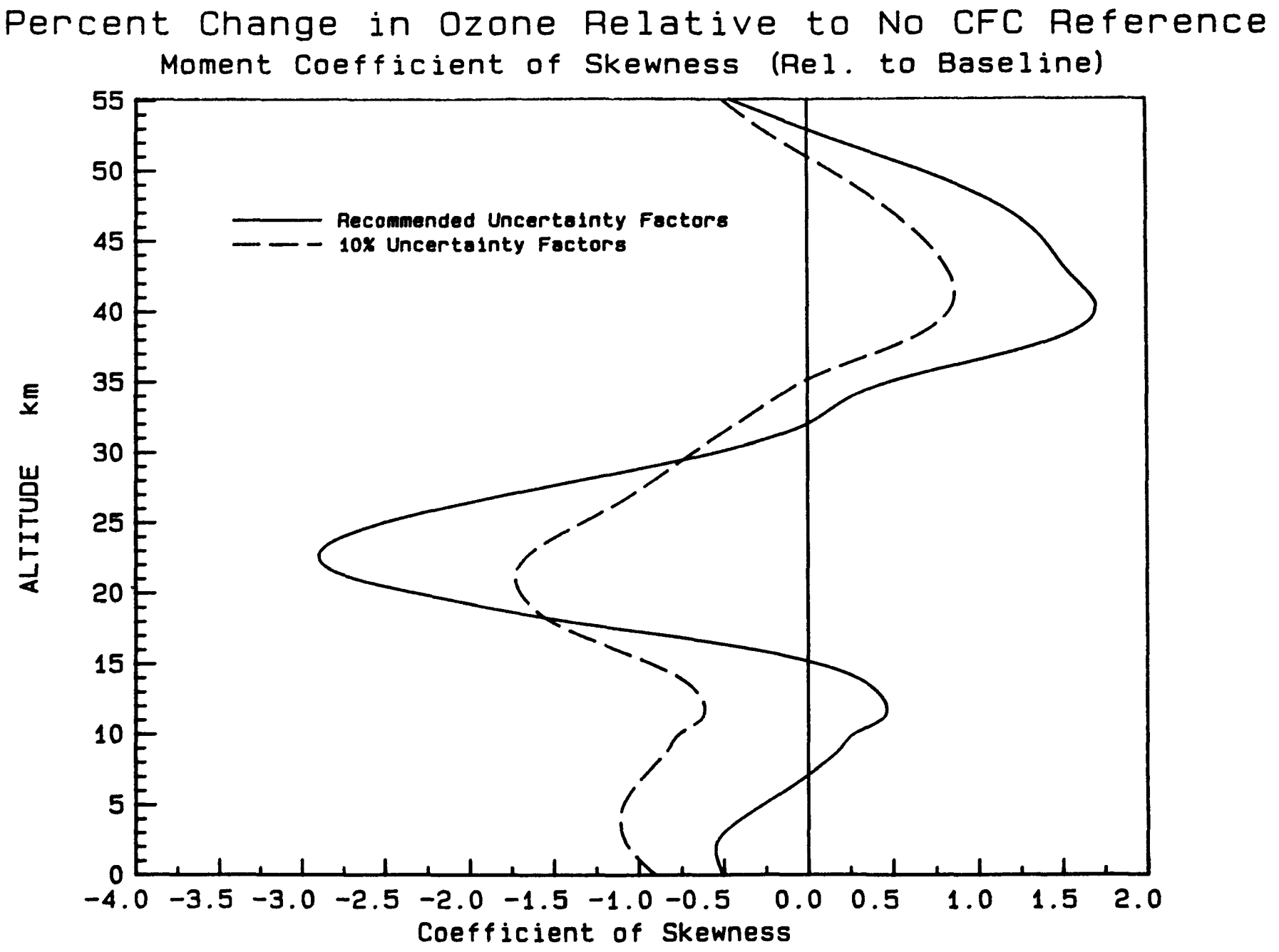
Percent Change in Ozone Relative to No CFC Reference
Moment Coefficient of Skewness (Rel. to Baseline)
Recommended Uncertainty Factors
10% Uncertainty Factors
ALTITUDE km
55
50
45
40
35
30
25
20
15
10
5
0
-4.0 -3.5 -3.0 -2.5 -2.0 -1.5 -1.0 -0.5 0.0 0.5 1.0 1.5 2.0
Coefficient of Skewness

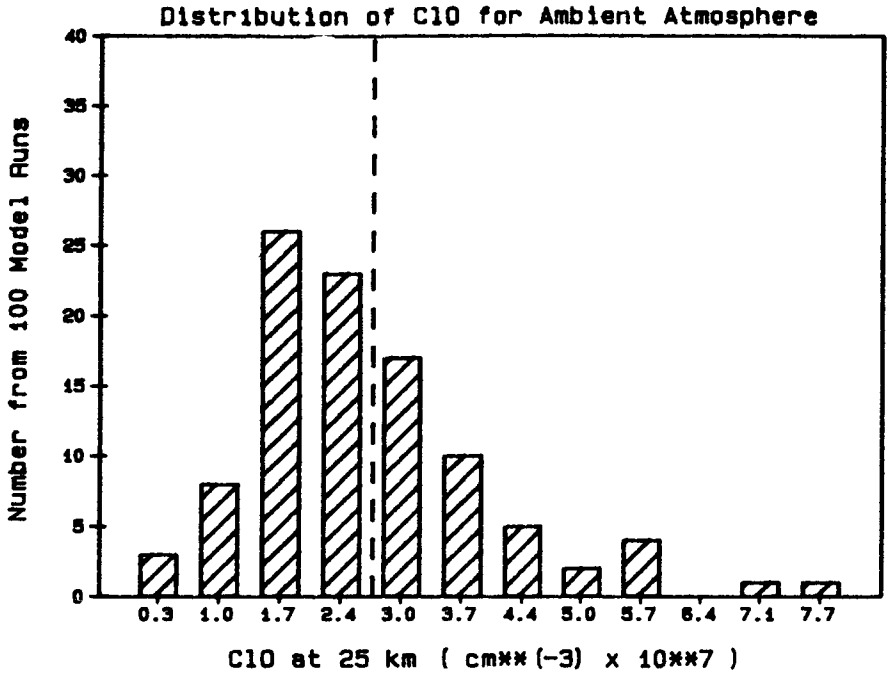

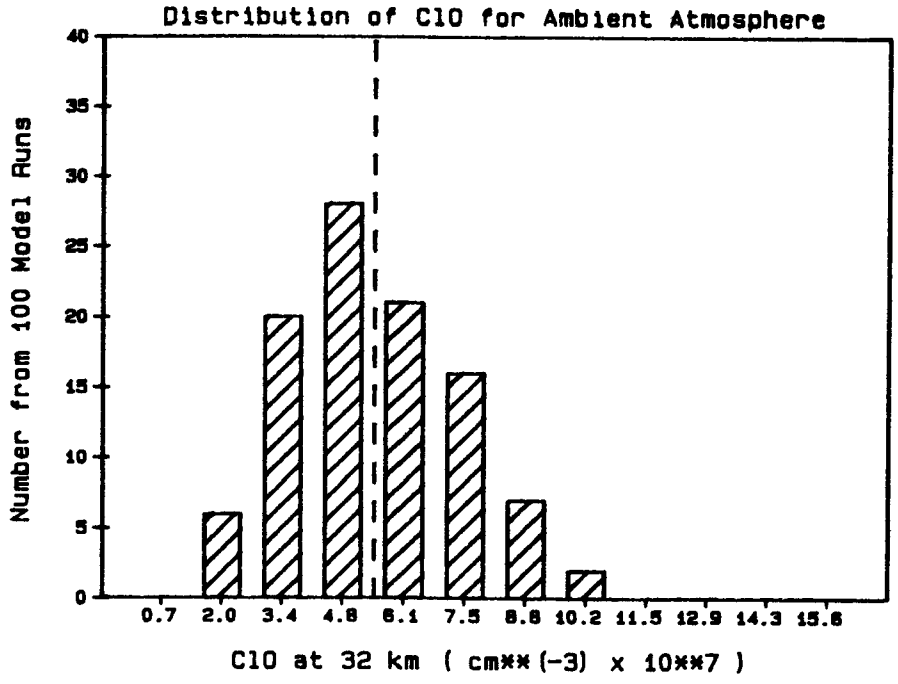

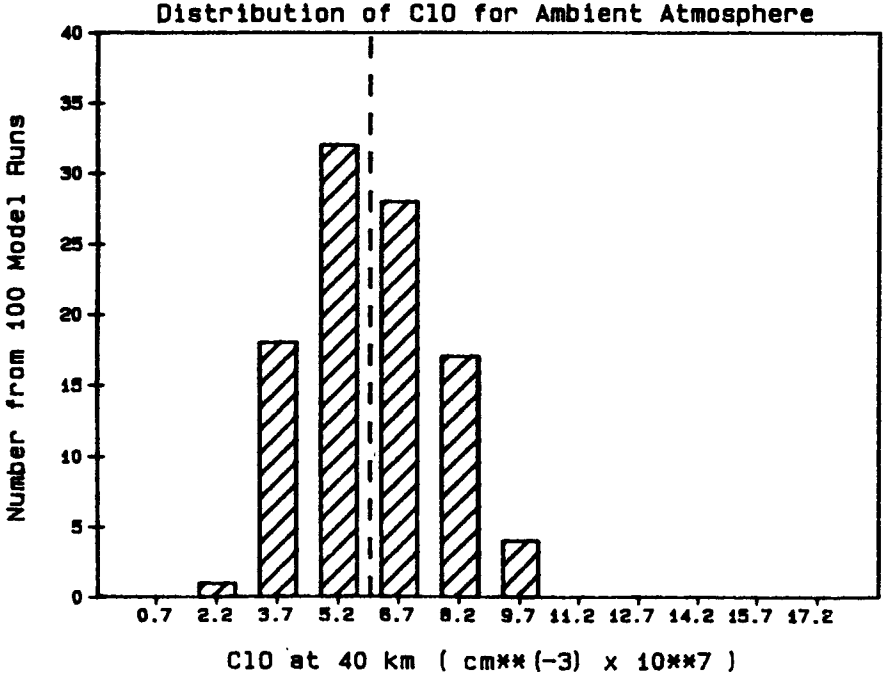

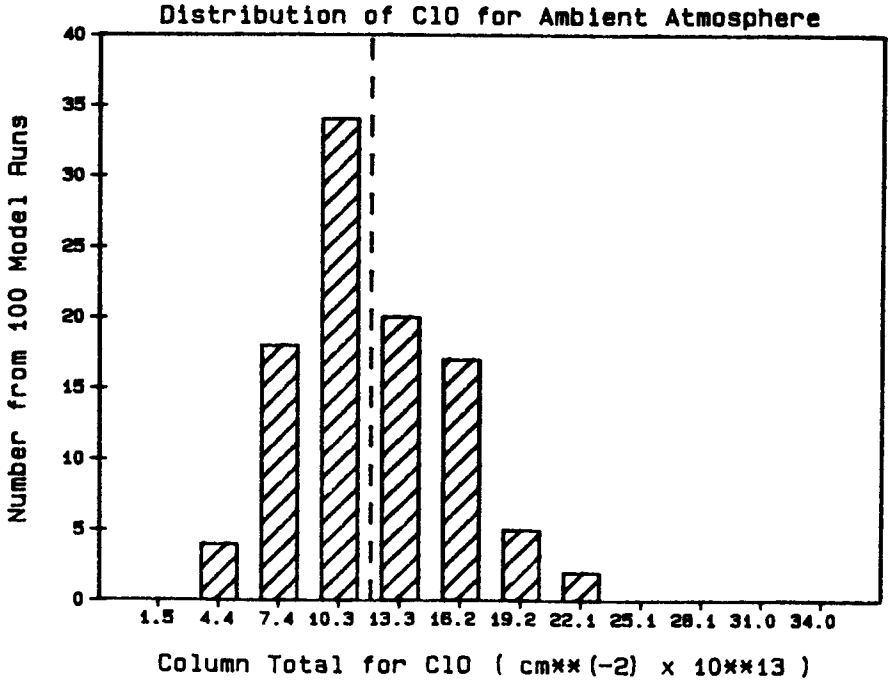

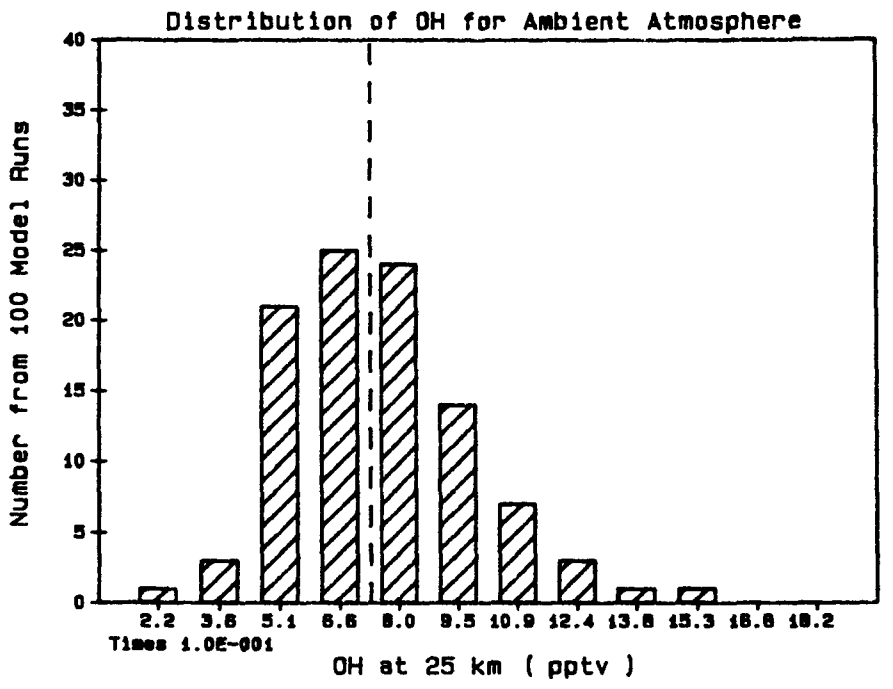
Distribution of OH for Ambient Atmosphere
Number from 100 Model Runs
0
5
10
15
20
25
30
35
40
2.2 3.6 5.1 6.6 8.0 9.5 10.9 12.4 13.8 15.3 16.8 18.2
Times 1.0E-001
OH at 25 km (pptv)

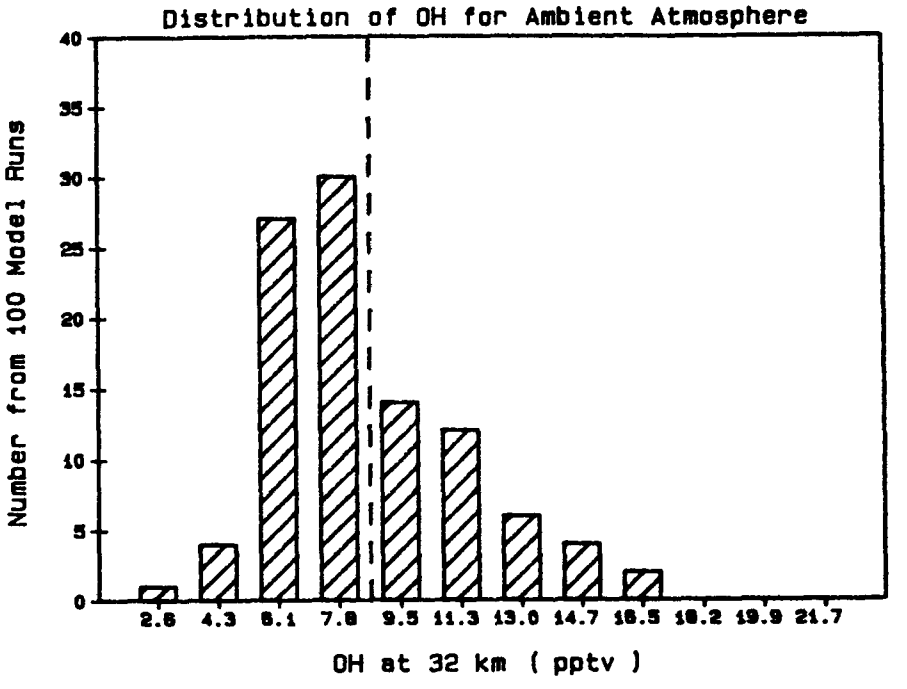
Distribution of OH for Ambient Atmosphere
Number from 100 Model Runs
0
5
10
15
20
25
30
35
40
2.6 4.3 6.1 7.8 9.5 11.3 13.0 14.7 16.5 18.2 19.9 21.7
OH at 32 km (pptv)

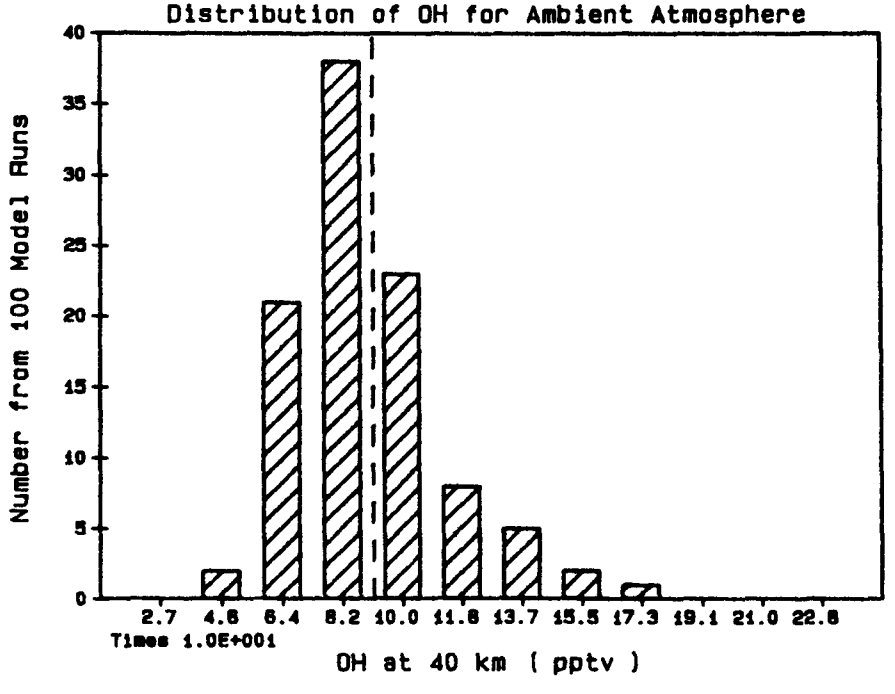
Distribution of OH for Ambient Atmosphere
Number from 100 Model Runs
0
5
10
15
20
25
30
35
40
2.7 4.6 6.4 8.2 10.0 11.8 13.7 15.5 17.3 19.1 21.0 22.8
Times 1.0E+001
OH at 40 km (pptv)

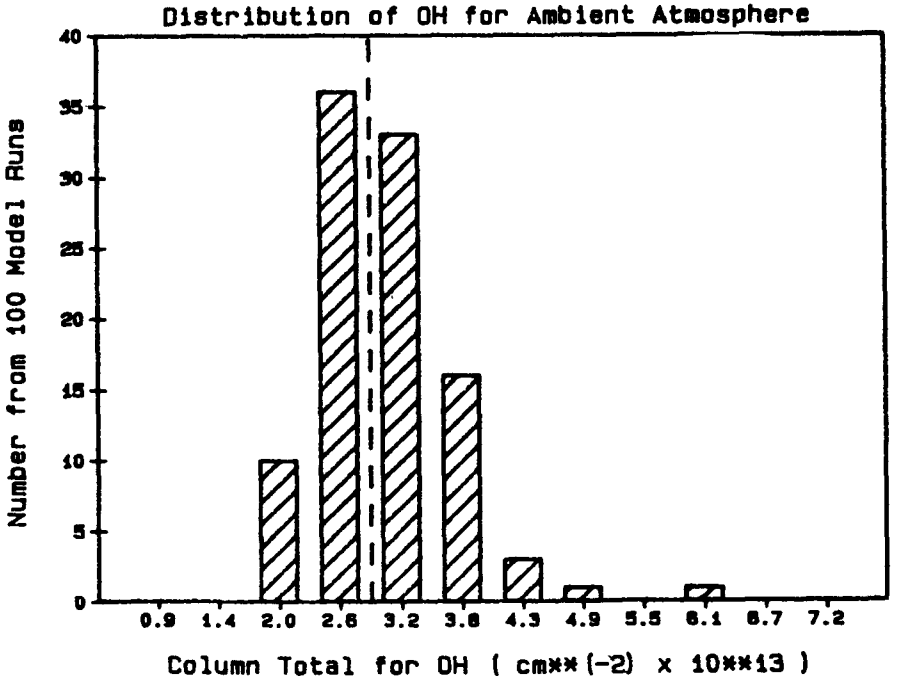
Distribution of OH for Ambient Atmosphere
Number from 100 Model Runs
0
5
10
15
20
25
30
35
40
0.9 1.4 2.0 2.6 3.2 3.8 4.3 4.9 5.5 6.1 6.7 7.2
Column Total for OH (cm**(-2) x 10**13)

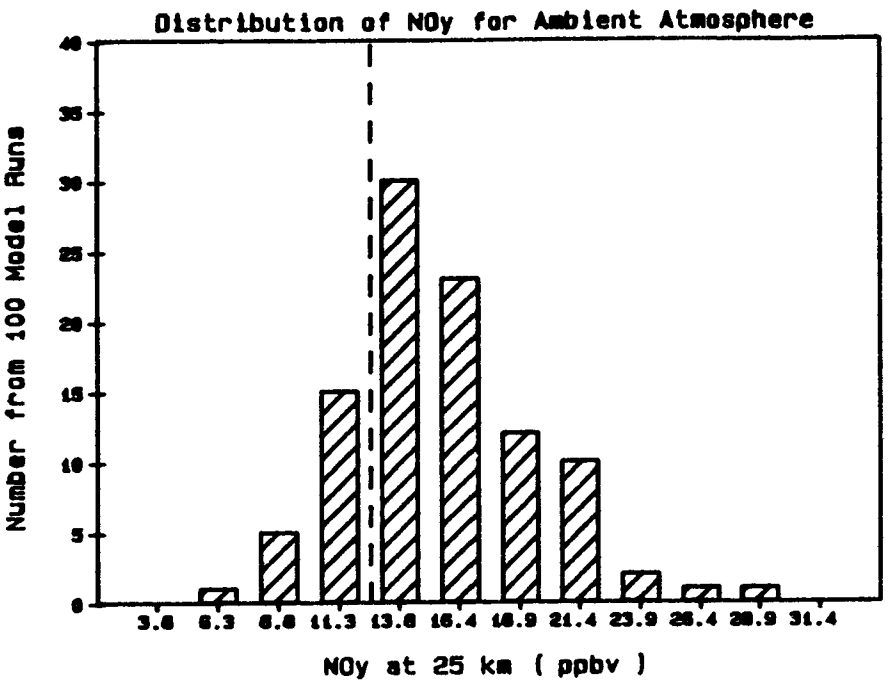

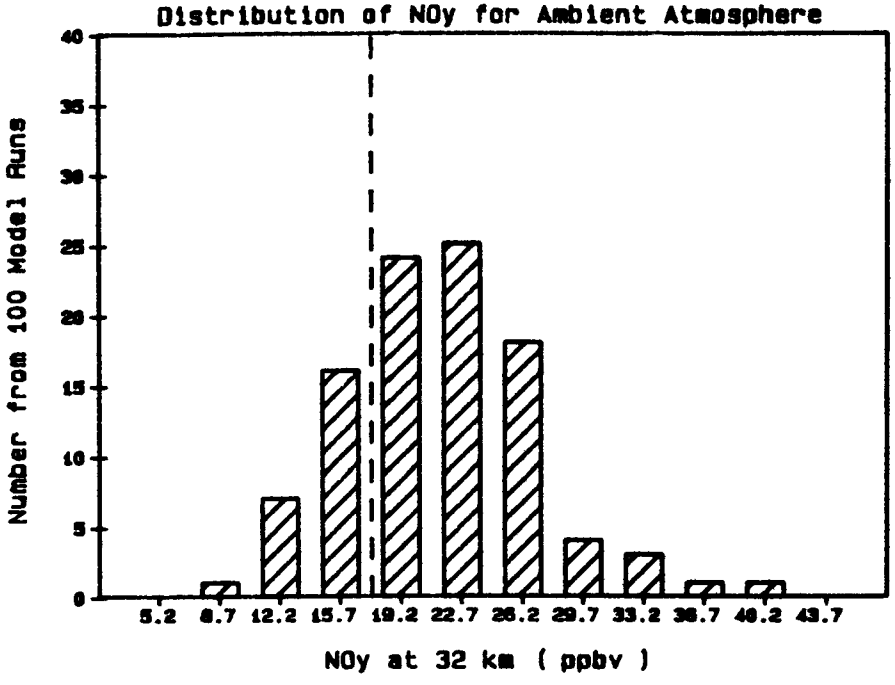

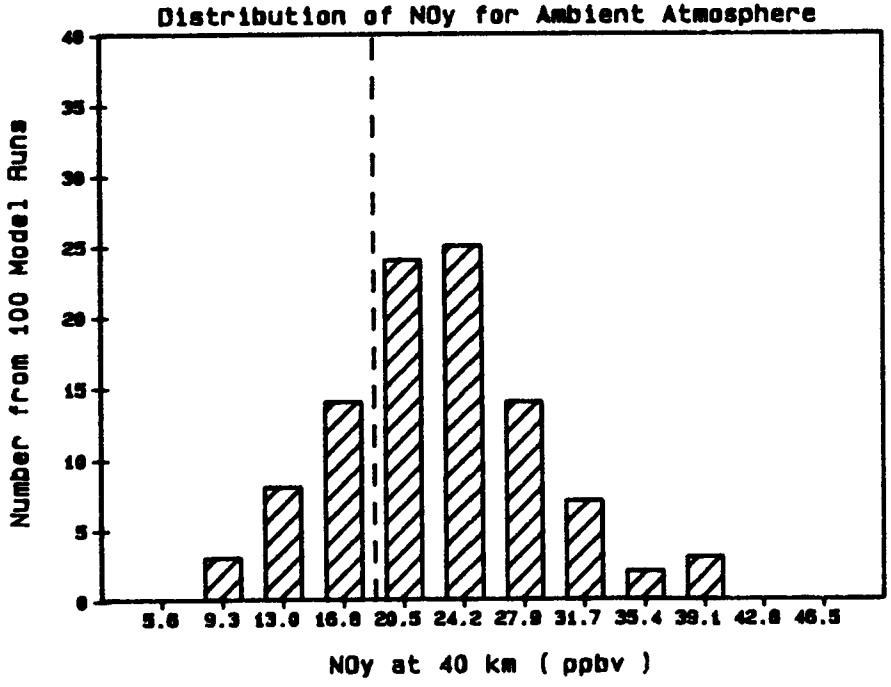

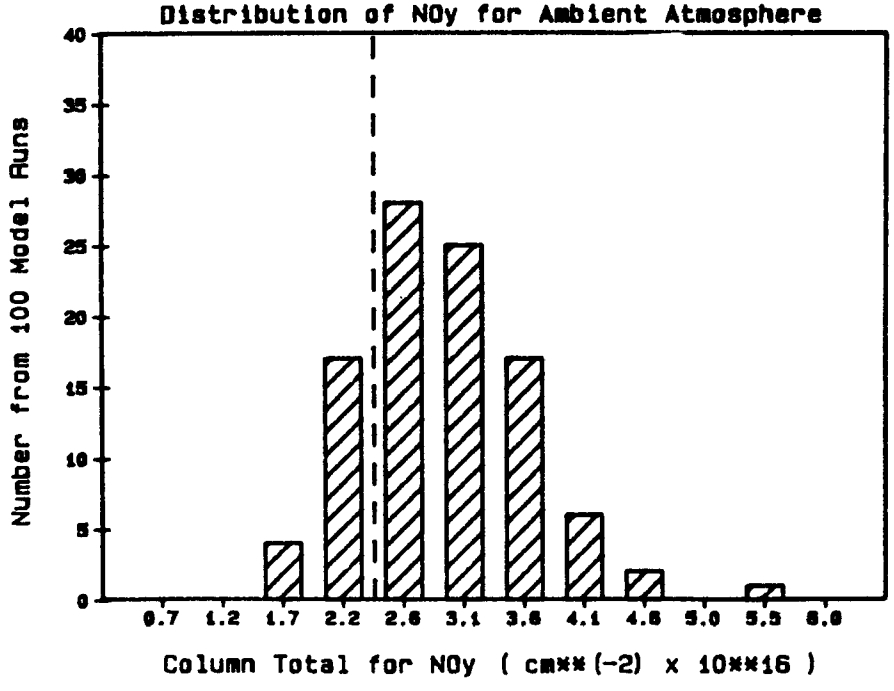

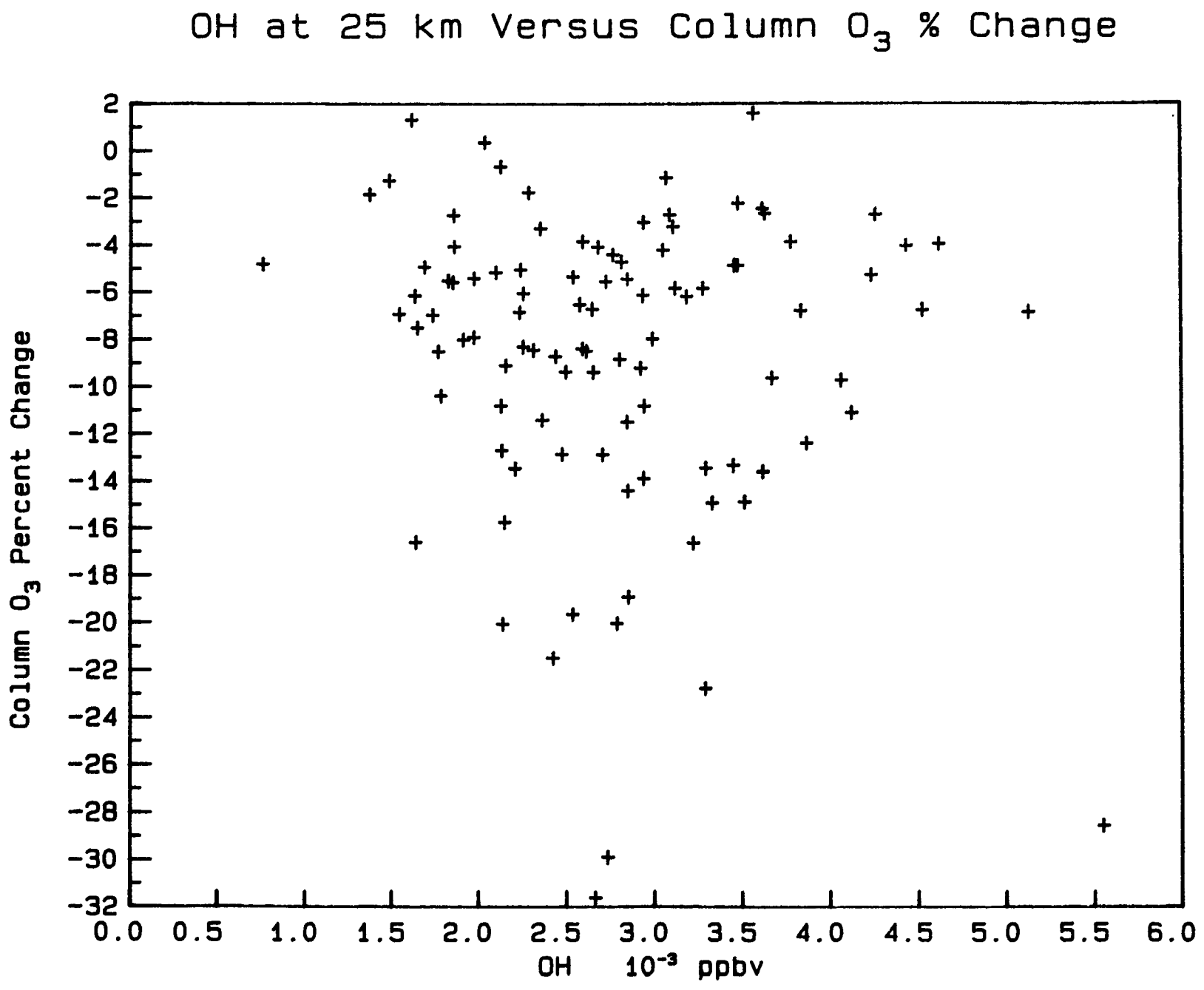
OH at 25 km Versus Column O_3 % Change
Column O_3 Percent Change
2
0
-2
-4
-6
-8
-10
-12
-14
-16
-18
-20
-22
-24
-26
-28
-30
-32
0.0
0.5
1.0
1.5
2.0
2.5
3.0
3.5
4.0
4.5
5.0
5.5
6.0
OH 10^{-3} ppbv

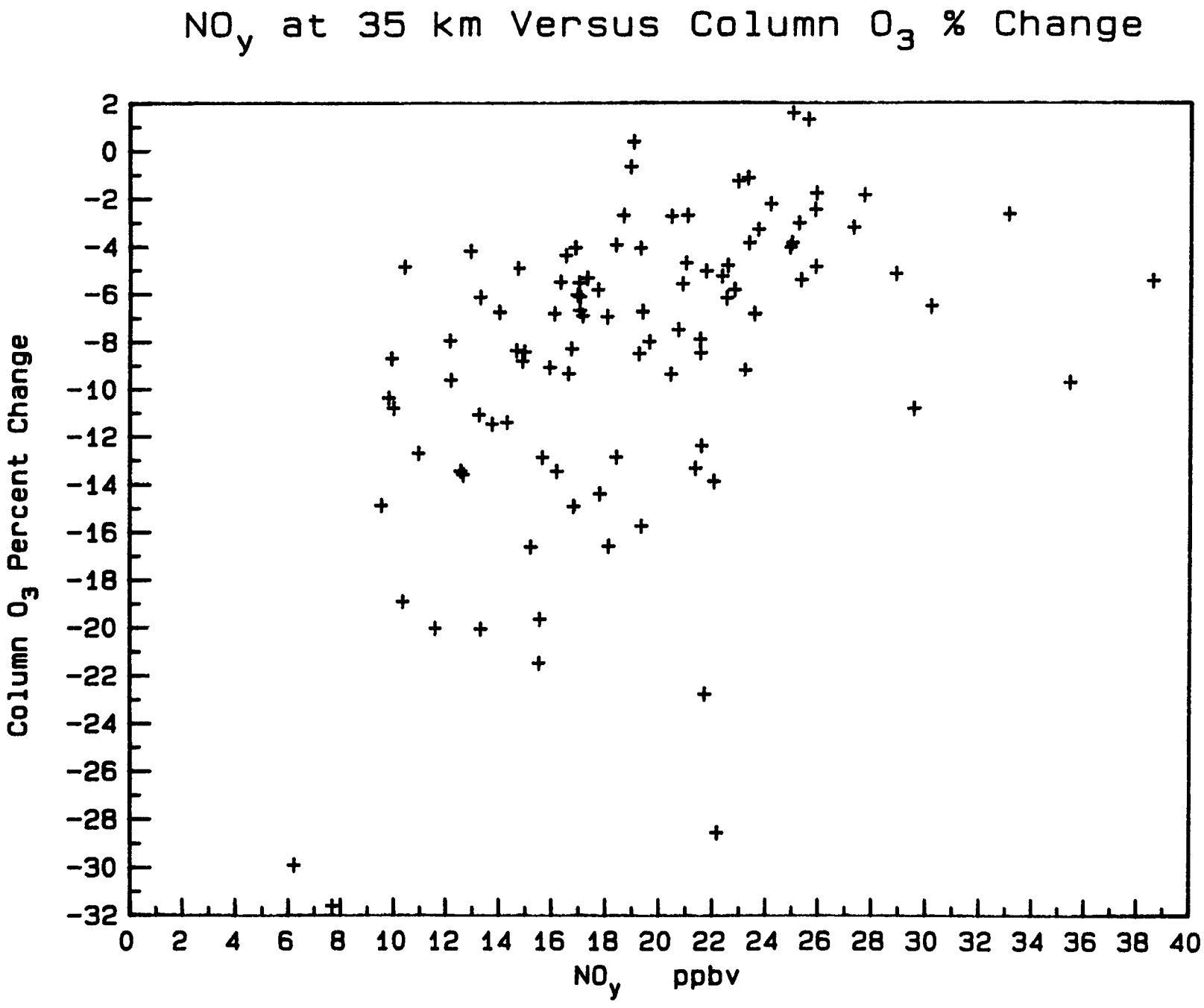
NOy at 35 km Versus Column O3 % Change
Column O3 Percent Change
2
0
-2
-4
-6
-8
-10
-12
-14
-16
-18
-20
-22
-24
-26
-28
-30
-32
0 2 4 6 8 10 12 14 16 18 20 22 24 26 28 30 32 34 36 38 40
NOy ppbv

A PARAMETERIZED NUMERICAL FIT TO TOTAL COLUMN OZONE CHANGES CALCULATED BY THE LLNL 1-D MODEL OF THE TROPOSPHERE AND STRATOSPHERE

PETER S. CONNELL

LAWRENCE LIVERMORE NATIONAL LABORATORY
ATMOSPHERIC AND GEOPHYSICAL SCIENCES DIVISION

NOVEMBER, 1986

ABSTRACT

Economic analysis of the costs and benefits of regulation of chlorofluorocarbon emissions with respect to changes in the total atmospheric ozone column abundance depends on the availability of an accurate means to predict future ozone change as a function of CFC emissions and trends in other atmospheric species. Over about the last decade, these predictive calculations have been made chiefly with one-dimensional numerical models of the stratosphere. Although these models, run time-dependently, are substantially more computationally efficient than the more desirable multi-dimensional models, they remain expensive from the viewpoint of the requirements of cost/benefit analysis.

In this note we present a numerical parameterization of the results of the LLNL one-dimensional model for total column ozone change in terms of surface emissions or abundances of the various source species. Previous versions of the LLNL model have been used in earlier studies to evaluate time-dependent scenarios of future trends in the emissions or atmospheric abundances of CFC-11, CFC-12, CFC-22, CFC-113, CCl_4, CH_3CCl_3, CO_2, CH_4, N_2O, Halon-1301 and Halon-1211. The numerical fit reported here produces calculated ozone changes within about 2% (column ozone change relative to the 1985 model atmosphere) of the current LLNL 1-D model results, for a range of scenarios and ozone changes. It therefore can approximately represent the actual 1-D model for the purposes of economic analysis of regulatory strategies.

It is, however, crucial to note that the 1-D model results, and consequently this parameterization, are subject to substantial uncertainties. Future improvements in our knowledge of atmospheric photochemical kinetics and transport in the troposphere and stratosphere should be expected to modify these current results in unpredictable directions.

1. INTRODUCTION

We have recently reported the results of an extensive model study (Connell and Wuebbles, 1986, hereafter CW) of the sensitivity of stratospheric ozone to various assumed simultaneous trends in emissions or abundances of several long-lived source species; chlorofluorocarbons, Halons romochlorofluorocarbons), carbon dioxide (CO_2), methane (CH_4) and nitrous oxide (N_2O). The model used was the LLNL one-dimensional time-dependent numerical representation of transport and photochemistry in the troposphere and stratosphere. The stratospheric temperature profile was calculated interactively based on the assumption of local radiative equilibrium. The study showed that a wide range of outcomes for change in the total column ozone abundance results from the uncertainty in trend projections for source species and that the effects of projected trends in individual species on ozone are strongly coupled. The conclusions in CW (1986) and WMO (1986) emphasized the uncertainties in predicting the behavior of ozone subject to significant perturbations from current levels of the various source species. Uncertainties arise in specifying photochemical-kinetic parameters, -in interpreting the results of a single-dimensional (vertical) model and in the choice of trend prescriptions for the source species.

An addendum to the CW study, in which the currently available recommendations on kinetic and spectral parameters (JPL, 1985) were implemented in the model, showed that remaining laboratory kinetic uncertainties can produce a substantial impact on the quantitative results of ozone perturbations from the envisioned scenarios of future emissions. All

of these conclusions have significant implications in the consideration of regulatory actions and the accompanying cost-benefit analysis of controlling CFC emissions.

An underlying consideration in studying the effects of CFC emission controls is that the effect of CFC regulation on the total column of ozone also depends strongly on changing abundances of several other natural and anthropogenic trace atmospheric species. Determining the nonlinear ozone response to changes in many species practically requires the use of computationally intensive complete atmospheric model calculations. However, the extensive exercise of current models that would be required in cost-benefit analysis may not be justified in view of continuing progress in understanding and modelling of the stratosphere and its photochemistry. Consequently, we present here a parameterization of the results of the complete 1-D model cited above, for total column ozone depletion in terms of emissions or abundances of the source species. This is intended as a tool for preliminary economic and regulatory investigations with the recognition that both the quantitative specifics and the form of the parameterization, as well as the 1-D model on which they are based, may be quickly superseded by the increase of knowledge. Additionally, it should be recognized that this parameterization will be a less accurate indicator of the effects of trace gas emissions on ozone than the actual model calculations on which it is based.

A brief description of the numerical fit and its basis is given below, followed by application to a few cases of multi-species scenario results from the LLNL 1-D model.

2. DESCRIPTION OF PARAMETERIZATION

The intent is to approximate the predicted total column ozone changes calculated by the LLNL time-dependent temperature-coupled one-dimensional transport-kinetics model of the troposphere and stratosphere, for specified changing fluxes of several trace constituents projected over the period of 90 years from 1985. The general inadequacies of such an approach should be emphasized again. The highly coupled nature of the stratospheric photochemistry and the many parameters being simultaneously varied in the EPA scenarios result in a complicated nonlinear multidimensional ozone response surface. The full domain of response can really only be adequately mapped by a large number of model runs. Consequently, any simple set of fitting equations may be inadequate when applied away from areas actually investigated with the complete model. In addition, changes in kinetic parameters, as have occurred in the past, may radically change the shape of the ozone response surface in unpredictable ways. Problems of linearity of response are exacerbated by the very large ozone depletions encountered in higher CFC flux scenarios (e.g., annual relative increases exceeding 1–2% per year).

With this in mind, some features of the problem enhance the possibility of fitting the model-calculated ozone depletion as a function of the many input parameters in these CFC-dominated scenarios. The atmospheric decomposition lifetimes of the important CFC's are much greater than the maximum relevant ozone photochemical lifetime and characteristic transport times in the model. Additionally, the time scale of interest, several decades to 90 years, is also much longer than these model timescales. This means that, at any given time, the family of species including the CFC's and their Cl-containing decomposition products is essentially well-mixed in the atmosphere. In addition, the ozone profile (and thus the total column abundance of interest here) responds essentially instantaneously

(i.e., on the order of a model year) to changing abundance of stratospheric inorganic chlorine-containing compounds and other trace stratospheric species. The first step in the parameterization, then, is to calculate the expected changes in stratospheric inorganic Cl (and Br) abundance as a function of time from projected CFC (and Halon) emissions. From this value the combined ozone perturbation may be estimated, given assumptions of future abundances of CO_2, N_2O and CH_4 and their corresponding sensitivity coefficients for ozone column change, which can be estimated from 1-D model runs.

The trends assumed for CH_4, N_2O and CO_2 are projected for changes in surface abundance or mixing ratio, not source emissions, as the independent variables in the parameterization equation. The currently observed increases in the atmospheric abundances of N_2O and CH_4 presumably indicate that the respective source strengths exceed the atmospheric sinks and the observed abundances are therefore functions of the emission histories over a period of a few of their respective atmospheric lifetimes ($>$ 100 years for N_2O). By specifying abundances rather than source strengths, the effects of N_2O and CH_4 at a given time are made essentially independent of their emission history and the parameterized representation of results is greatly simplified. The drawback to this choice is that feedback processes in the troposphere, which are important in determining the methane abundance given a source strength, are not included.

The parameterization procedure uses time-dependent historical and projected emission fluxes (base year 1985) for the individual CFC and Halon compounds considered and specifications for the abundances of CO_2, N_2O and CH_4, usually relative to the current (1985) ambient value. The change in the abundance of upper stratospheric total inorganic chlorine-containing species ($\Delta\,[Cl_z] = \Delta\,([Cl]+[ClO]+[ClONO_2]+[ClNO_2]+[HOCl]+[HCl])$) is the principal variable controlling change in the total ozone column. The $\Delta\,Cl_z$ value is derived from integrating the time history of CFC emissions, taking into account the model-derived atmospheric lifetimes of each CFC compound. An ozone column depletion can be associated with the calculated $\Delta\,Cl_z$, based on a curve representing the complete model's response to CFC perturbations. Changes in the abundances of CH_4 and N_2O can alter this nonlinear relationship. CO_2, CH_4, N_2O and bromine emissions also have direct effects, both positive and negative, on the ozone column change, which are taken to be additive to the primary CFC perturbation.

2.1. Projected Abundance of Inorganic Stratospheric Cl

The CFC perturbation dominates in most of the scenarios discussed in CW (1986) and is the principal variable in this parameterization. The impact on ozone of increasing Cl species abundance occurs first and largely in the upper stratosphere, so the quantity of interest is the abundance of total inorganic Cl around 35 km. Vertical profiles of the abundance of the CFC's of interest here show an essentially constant mole fraction throughout the troposphere, that is, the CFC's are well-mixed in the bulk of the atmosphere. Vertical mixing in the lower and mid stratosphere is, however, slow enough that at some altitude, the increasing flux of solar radiation of the wavelength necessary to induce CFC photodecomposition causes a relatively rapid decline in the CFC mole fraction. The position and steepness of the fall-off of the CFC mole fraction is controlled mostly by the number of Cl atoms in the CFC species. For CFC's containing three or more Cl (CFC-11, CFC-113, CCl_4, and CH_3CCl_3) most of the photodecomposition occurs below 35 km. CFC-12

and CFC-22 contain only two and one Cl, respectively, and show a slower decrease with altitude.

The total abundance of a given CFC in the atmosphere is determined by its emission history and atmospheric lifetime. Here we define lifetime, τ, as the total atmospheric burden divided by the CFC source strength at equilibrium. This 'replacement' time is equivalent in a single box model of the atmosphere to the exponential decay lifetime of the atmospheric abundance of the CFC following cessation of emissions. From the CFC abundances and the knowledge that most of the CFC's are substantially photodecomposed at 35 km, the stratospheric abundance of inorganic Cl can be directly estimated from the assumption of partial (CFC-12 and CFC-22) or complete (CFC-11, CFC-113, CCl_4 and CH_3CCl_3) liberation of Cl. The CFC lifetimes in the model depend on short wavelength solar uv flux, singlet atomic oxygen abundance ($O(^1D)$), and hydroxyl radical abundance in the case of CH_3CCl_3 and CFC-22. These quantities all depend directly on the ozone profile, so that the instantaneous CFC lifetimes will change as ozone is perturbed.

The following input is needed to calculate the expected stratospheric inorganic chlorine abundance at 35 km as a function of time:

— Annual emissions for chlorine-containing species with lifetimes longer than about 10 years (for example, units of 10^6 kg),

— Conversion factors from 10^6 kg to ppb Cl for each CFC species (based on molecular weight, number of Cl atoms and mass of atmosphere),

and

— Equilibrium atmospheric lifetimes for the Cl source species.

The factor converting mass of emission to ppb emitted Cl is simply given by the product of the number of Cl atoms in the CFC molecule and Avogadro's number, divided by the CFC molecular weight, the column number density of the atmosphere and the surface area of the earth. With appropriate conversions for units, the individual CFC conversion factors are given by

$$\text{Conversion Factor} = (5.477E-3) * \#\ (\text{Cl})/\text{Molecular Weight (g)} \qquad (1)$$

The ranges of CFC lifetimes were evaluated from a series of 1-D model runs in which constant source fluxes of each CFC were integrated over model times in excess of three lifetimes for the CFC considered. The lower limit of the lifetime ranges corresponds to runs with total column ozone depletions around 10% between an atmosphere in equilibrium with a constant specified emission and an atmosphere free of the respective CFC. The model-derived lifetimes and CFC conversion factors are listed in Table 1. Cunnold et al (1986) have reported observed lifetimes for CFC-11 and CFC-12 based on analysis of data from the Atmospheric Lifetime Experiment. Their results, appropriate to January 1, 1981, are 74(+31 -17) years for CFC-11 and 111(+222 -44) years for CFC-12.

TABLE 1

Cl Source Species	Lifetime (years)	Conversion Factor
CFC-11 ($CFCl_3$)	76-84	1.196E-4
CFC-12 (CF_2Cl_2)	139-150	9.06E-5
CCl_4	67-75	1.424E-4
$CH_3\ CCl_3$	8.3-12	1.232E-4
CFC-113 ($CFCl_2CF_2Cl$)	92-100	8.91E-5
CFC-22 (CHF_2Cl)	22-33	6.33E-5

Two additional factors must be included in the estimation of stratospheric inorganic Cl abundance. Both the model and the real atmosphere have a time constant for mixing a surface-released tracer completely in the troposphere and stratosphere. The approximate mixing time in the model is 3.5 years. Second, the incomplete dissociation of CFC-22 and CFC-12 at 35 km must be taken into account. Multiplicative factors of 0.53 for CFC-22 and 0.93 for CFC-12 are included to account for the incomplete photodissociation of these CFC's within the altitude region of greatest effect on the ozone abundance.

The contribution of a given year's emissions to stratospheric inorganic chlorine will decay exponentially according to the particular CFC species lifetime. For example, total inorganic chlorine arising from 1985 emissions of CFC-11 decay according to the expression,

$$\Delta Cl_z{}^{CFC-11}(t) = 1.196E-4 * (1985\ CFC-11\ \text{emissions}) * e^{-(t-1985)/76.5} * \left(1 - e^{-(t-1985)/3.5(\text{mixing time})}\right). \quad (2)$$

Summing over all CFC species and all years of emissions,

$$\Delta Cl_z(t) = \Delta Cl_z(\text{emissions prior to } t_o) + \sum_{j=CFC's} \{\text{conversion factor } (j) * \sum_{i=t_o}^{t} \text{emissions } (j,i) * e^{-(t-i)/\tau(j)} * \left(1 - e^{(t-i)/3.5}\right)\} \quad (3)$$

2.2. Estimating Ozone Sensitivity To Changes in Stratospheric Cl

In summing Cl emissions from the various CFC species we make the assumption that the effects on ozone will not depend on the particular mix of CFC emissions that results in a given stratospheric inorganic Cl species increase. Differing relative efficiencies, based on mass of emissions, of individual CFC's for perturbing the total integrated vertical ozone column have been discussed previously (Wuebbles, 1983). Values quoted ranged from 0.05 (CFC-22) to 1.11 (CCl_4) relative to CFC-11 as unity, at steady state with constant emissions. Relative efficiencies using the current chemistry calculated by mass of emission, by mole of Cl emitted both unweighted and weighted by atmospheric lifetime

and by inorganic Cl produced at 35 km, are given in Table 2. These were calculated from 1-D model results for constant emissions of a single CFC species to steady state, with emissions adjusted to produce an ozone depletion of around 7.5%. Most of the spread in relative efficiencies by mass results from differences in the number of Cl atoms per molecule, molecular weight and atmospheric lifetime.

TABLE 2

Compound	Relative Efficiencies Mass	Mole Cl	Mole Cl^+	$[Cl_z]$ @ 35 km
CFC-11 ($CFCl_3$)	1.0	1.0	1.0	1.0
CFC-12 (CF_2Cl_2)	1.0	1.32	0.73	0.73
CFC-113 ($CF_2ClCFCl_2$)	0.78	1.05	0.88	0.90
CFC-22 (CHF_2Cl)	0.05	0.08	0.30	0.68
CCl_4	1.06	0.89	1.01	1.14
CH_3CCl_3	0.10	0.10	0.91	0.94

+ Normalized by lifetime.

Vertical profiles of local ozone change, normalized to 7.5% total column ozone depletion, for the six CFC's considered are shown in Figure 1. The profiles for CFC-11, CFC-113, CCl_4 and CH_3CCl_3 are similar, while the profiles for CFC-12 and CFC-22 show an ozone increase in the lower stratosphere and larger ozone depletions around 35 km than the other CFC's. Since photodecomposition occurs at higher altitudes for CFC-12 and CFC-22 than for the other species, the lower stratosphere contains relatively smaller inorganic chlorine abundances. The ozone increase for CFC-12 and CFC-22 results from the interference of ClO with the NO_x catalytic cycle dominant in the lower stratosphere. This interference has been saturated by the larger inorganic Cl abundance in the lower stratosphere for the other CFC's. Comparison of vertical profiles of local ozone change from model results with smaller specified individual CFC emissions (normalized to a 2% total column ozone decrease) show positive ozone changes in the lower stratosphere for CFC-11 and CFC-113 as well (Figure 2).

Figure 3 shows local ozone change profiles normalized to equal abundance of inorganic Cl at 35 km for the steady state individual CFC emission model runs. On the basis of inorganic Cl abundance at 35 km the upper stratospheric ozone decrease is now very similar for all CFC's. Differences remain in the lower stratosphere for CFC-12 and CFC-22, resulting from the lower inorganic Cl abundance around 20-25 km. But in multi-CFC scenarios in which the inorganic Cl abundance grows sufficiently large, Cl contributed by CFC's other than CFC-12 and CFC-22 would be expected to contribute to saturating the ClO interference with the NO_x catalytic cycle and lead to ozone decreases even in the lower stratosphere. The relative efficiencies for CFC-12 and CFC-22 would thus be enhanced compared to the single CFC steady state calculations. Based on the CFC-11 low emission level results, the sign of ozone change in the lower stratosphere reverses when the inorganic Cl abundance reaches about 3.8 ppb in the upper stratosphere, somewhat higher

than observed current levels but much smaller than most predictions for Cl levels in the next century.

Contributions to the total Cl abundance by the individual CFC's in a multi-CFC scenario, with respect to column ozone depletion and based on the evidence above, can be assumed additive and the change in ozone column can be functionally related to the total upper stratospheric inorganic Cl species abundance. This assumption will produce errors in estimation for scenarios with relatively small emissions including contributions largely from CFC-22 or CFC-12, only.

Figure 4 shows the model-calculated total column ozone response to increasing stratospheric inorganic Cl abundance from a multi-CFC run in which other trace species (CO_2, CH_4, N_2O and Halons) were held fixed. The response is nonlinear, showing three regimes. In the first regime, with total column ozone depletion less than roughly 20%, the total column ozone change is composed of local decrease in the upper stratosphere and either local increases in the lower stratosphere or decreases mitigated by the interaction of increasing ClO with the dominant NO_x catalytic ozone destruction cycle. When stratospheric inorganic Cl has increased to about 20 ppb and total column ozone depletion has reached about 25%, the slope of the sensitivity curve steepens as the mitigating interaction of ClO with NO_x is saturated and the ClO_x catalytic loss cycle for ozone becomes dominant throughout the stratosphere. The tail of the sensitivity curve at very large ozone depletion again becomes less steep. The shape of this curve is the primary representation of the behavior of the 1-D model with respect to column ozone depletion caused by increases in stratospheric inorganic chlorine. Interactions of the chlorine-ozone photochemistry with changes in N_2O and CH_4, which will be discussed in slightly more detail below, are treated as modifications to this curve.

The inverse hyperbolic sine function provides a convenient basis function with the necessary S-curve shape. An approximate unweighted nonlinear least-squares fit to the curve in Figure 4 gives the expression

$$\Delta O_3(\%) = 14.64\{\text{asinh}\,[0.337(20.82 - \Delta Cl_z) - \text{asinh}\,[0.337 * 20.82]\}, \qquad \Delta Cl_z \text{in ppb.} \tag{4}$$

Note that the expression is simply a numerical interpolation of the model-derived curve, with no theoretical basis for its form. Although it is defined for all values of Cl_z, it is applicable only within the limits of the validity of the 1-D model. Clearly the expression fails for very large increases in Δ Cl_z since it is unbounded negative for arbitrarily large Δ Cl_z. The complete 1-D model should also be expected to be incorrect for very large ozone depletions (say > 30%), to the extent that the structure of the atmosphere, implicit in the specified eddy diffusion coefficient profile, changes as the stratospheric heating (through ozone solar absorption) changes.

2.3. Effects of CH_4 and N_2O on O_3 Response to Cl Increases

Both N_2O and CH_4 affect ozone through indirect as well as direct processes. The direct effects (e.g. ozone catalytic depletion and photochemical ozone production, respectively) are discussed below. The principal indirect effects result from interaction with the ClO_x (= Cl + ClO) catalytic cycles. The formation of chlorine nitrate ($ClONO_2$) in the reaction

$$ClO + NO_2 + M = ClONO_2 + M$$

reduces the efficiency of both NO_x and ClO_x odd oxygen depletion cycles. Past the point at which all available NO_x is effectively converted to $ClONO_2$, additional increase in ClO_x is significantly more effective in reducing ozone. Increases in N_2O, the precursor of stratospheric NO_x, would tie up ClO_x as $ClONO_2$ and extend to higher levels of stratospheric inorganic chlorine abundance the transition from smaller to larger ClO_x sensitivity.

The reaction of atomic chlorine with methane

$$Cl + CH_4 = HCl + CH_3$$

is a major sink for the reactive ClO_x radicals, Cl and ClO. For higher projected methane abundances, a smaller fraction of the available inorganic chlorine is present in the active radical forms and the impact on ozone is diminished. Several of the pertinent reactions for methane photochemistry have significant activation energies, so that the inclusion of stratospheric temperature feedback has a significant effect on the sensitivity of ozone perturbations to CH_4 increases.

In equation 4, the interaction of N_2O with the effect on ozone of inorganic chlorine increases should appear as a change in the coefficient representing the position of the inflection point on the abscissa in Figure 4. A methane change, which affects the ClO_x/(total Cl) ratio, should appear in equation 4 as a scaling factor for the inorganic Cl abundance term. From the results of runs (Figure 5) that included either N_2O or CH_4 changes coupled with the CFC perturbation depicted in Figure 4, the following expressions were determined

$$\Delta O_3(\%) = 14.64 \{ \text{asinh} [0.337 (20.82 R_{N_2O} - \Delta Cl_z) - \text{asinh} [0.337 * 20.82 R_{N_2O}] \} \quad (5)$$

and

$$\Delta O_3(\%) = 14.64 \{ \text{asinh} [0.337 (20.82 - \Delta Cl_z exp(-0.2 (R_{CH_4} - 1))] - \text{asinh} [0.337 * 20.82] \} \quad (6)$$

where

$$R_{N_2O} = N_2O(t)/N_2O(1985)$$

and (7)

$$R_{CH_4} = CH_4(t)/CH_4(1985).$$

The differences between the solid and dashed lines represent the direct effects of N_2O and CH_4 on ozone, which will be accounted for below.

Methane increases also affect the abundance distribution among the nitrogen oxide species (NO, NO_2, NO_3, N_2O5, HNO_3, HNO_4, HNO_2), so that the effects of CH_4 and N_2O increases are coupled directly, as well as through photochemistry involving Cl species. The magnitude of this coupling can be estimated from combined multiple species scenario model runs (taking into account the small direct effects on ozone of the various trends discussed below). The following expression appears to work fairly well for a range of CFC scenarios:

$$\Delta 0_3\ (\%) = 14.64\ \{\text{asinh}\ [0.337\ (20.82\ (1 + \frac{R_{N_2O} - 1}{R^2_{CH_4}}) - \Delta Cl_z * \ exp\ (-0.2\ (R_{CH_4} - 1))] - \text{asinh}\ [0.337 * 20.82\ (1 + \frac{R_{N_2O} - 1}{R^2_{CH_4}})]\} \quad (8)$$

One aspect of CFC-related ozone perturbation that is not directly included in the expression above is sensitivity of the result to the model's ambient stratospheric abundance of nitrogen oxide species. If the ambient level were actually higher (lower) than the model value, the onset of the steeper portion of the inorganic Cl/O_3 sensitivity curve would be pushed to higher (lower) abundances of stratospheric inorganic chlorine. However, since the total nitrogen oxide abundance is not an external variable in the model but is a derived quantity, we will here consider changes in this value only if they result from change in the N_2O source emission.

A slightly different implementation of equations (3) and (8) has been used in the draft EPA document, "An Assessement of the Risks of Stratospheric Modification" (Hoffman, ed., 1986). The calculated 1-D total column ozone changes in the single CFC steady state runs were compared to the ozone change predicted by equation (8a), a variant of equation (8) using total inorganic chlorine abundance at the top of the model atmosphere. Total dissociation of all CFC compounds, including CFC-22 and CFC-12, was assumed.

$$\Delta 0_3\ (\%) = 14.58\ \{\text{asinh}\ [0.332\ (21.05\ (1 + \frac{R_{N_2O} - 1}{R^2_{CH_4}}) - \Delta Cl_z * \ exp\ (-0.15(R_{CH_4} - 1))] - \text{asinh}\ [0.332 * 21.05\ (1 + \frac{R_{N_2O} - 1}{R^2_{CH_4}})]\} \quad (8a)$$

Efficiencies for perturbing the ozone column were thus produced for the various CFC compunds relative to the parameterization result. These relative efficiencies were than used as multiplicative corrections in equation (3), where they can be subsumed into the conversion factors. These alternatives to the values given in Table 1 are given in Table 1a below.

Table 1a

Cl Source Species	Lifetime (years)	Relative Efficiency	Conversion Factor
CFC-11	76.5	1.14	1.363E- 4
CFC-12	138.8	0.84	7.61E- 5
CCl_4	67.1	1.20	1.719E- 4
CH_3CCl_3	8.26	1.19	1.46E- 4
CFC-113	91.7	1.06	3.44E- 5
CFC-22	22.	0.45	2.05E- 5

2.4. Estimating Direct Ozone Sensitivities to Non-CFC Species

While the scenarios of interest can involve order of magnitude increases in the total stratospheric inorganic chlorine abundance over the next 90 years, increases in other trace species over this period, currently projected, are usually less than a factor of two. The direct effects on the total ozone column of these increases, individually, are on the order of a few per cent, compared to the tens of per cent changes possible for large CFC increases. These smaller direct effects of the other trace species are treated additively in this note.

2.4.1. Carbon dioxide (CO_2)

Changes in CO_2 affect the ozone abundance through the decrease in stratospheric temperature that accompanies increased infrared emission to space by CO_2. The rates of many kinetic processes in the stratosphere are sensitive to temperature, so that CO_2 increases affect most of the ozone-controlling photochemical processes to some degree. Atmospheric CO_2 may as much as double over the next century, but for changes of this magnitude or smaller, the effects of CO_2 on ozone are small enough to be considered additive to the ozone perturbations of CFC's and other source species. The expression

$$\Delta O_3^{CO_2}\ (\%) \ = \ 3.6 \ln [CO_2(t)/CO_2(1985)]. \qquad (9)$$

adequately explains the differences among multiple scenario 1-D model runs with CO_2 trends varying from zero trend to a doubling of 1985 abundance in 2077, as well as step function increases of 10 and 100% in the CW (1986) 1-D model representation of the current atmosphere.

2.4.2. Methane (CH_4)

The direct effect on ozone of methane increase arises from the oxidation of CH_4 by hydroxyl radical in the presence of NO, in a process analogous to photochemical oxidant (smog) production in urban areas. Fitting the ozone change in multiple-species scenario model runs as a linear additive term to the CFC-caused ozone perturbation gives a sensitivity of about 3.75. The expression is

$$\Delta O_3^{CH_4}\ (\%) \ = \ 3.75\ (R_{CH_4} - 1). \qquad (10)$$

2.4.3. Nitrous oxide (N_2O)

The direct effect of N_2O increases on ozone results from increasing the NO_x abundance and the rate of odd oxygen loss through NO_x catalytic cycles in the mid stratosphere. Thus the direct effect of N_2O increases is reduction in ozone while the indirect effect through the ClO_x interaction is opposing the chlorine-caused ozone reduction. From the results of the CFC/N_2O 1-D model run and other scenario runs, the direct ozone/N_2O sensitivity in the linear regime of small changes is about 7. The corresponding expression is

$$\Delta O_3^{N_2O}\ (\%) \ = \ -7.\ (\mathrm{R}_{\mathrm{N_2O}} - 1). \tag{11}$$

2.4.4. Halons (bromocarbons)

Although the bromine-catalyzed stratospheric odd-oxygen loss processes are substantially more efficient per atomic bromine input than the ClO_x cycles, the bromine perturbations at currently envisioned emission rates remain relatively small. The stratospheric abundance of the various inorganic bromine-containing species can be estimated in the same way as that outlined for stratospheric inorganic Cl above, ignoring in the case of Halons the very small pre-1985 historical emissions.

$$\Delta Br_z\ ^{1301}(t) = .0368\ \{\ (1301\ \text{emissions}\ (i))\ e^{-(t-i)/101}\ (1 - e^{-(t-i)/3.5})\}$$

$$\Delta Br_z\ ^{1211}\ (t) = .0331\ \{(1211\ \text{emissions}\ (i))\ e^{-(t-i)/12.9}\ (1 - e^{-(t-i)/3.5})\}, \tag{12}$$

$$\text{emissions in } 10^6 \text{ kg/year}, \Delta Br_z \text{ in ppt.}$$

The 101 year model-derived atmospheric lifetime for Halon 1301 is in reasonable agreement with the value of 110 years estimated by Prather et al. (1984). For Halon 1211, the LLNL 1-D model-derived atmospheric lifetime, for a run during which ozone decreased about 10%, is 12.9 years, or about half the 25 years lifetime estimated by Prather and coworkers. For the expected small stratospheric abundances, direct catalysis of ozone loss should dominate the effects of any ClO_x-like interaction with NO_x photochemistry. Based on individual runs containing either 1301 or 1211 emissions and on the difference between multiple scenarios runs (using mid-range CFC emissions) with and without increasing emissions of 1301 and 1211, a linear expression of the relationship of stratospheric bromine increase and column ozone decrease is given by the expression

$$\Delta O_3\ ^{Br_z}\ (\%) = -0.0302\ \Delta Br_z\ (1301) - 0.0618\ \Delta Br_z\ (1211). \tag{13}$$

2.5 Summary

The sum of the total column ozone perturbation values calculated in equations (8) through (11) and (13) is the parameterized approximation to the total column ozone depletion that would be calculated by the actual 1-D model run.

3. APPLICATION OF PARAMETERIZATION

The contributions of historical (pre-1986) CFC emissions to the future change in stratospheric inorganic Cl abundance have been calculated using expression (2) (to=1911 with no prior emissions) and historical emission data taken from Wuebbles et al. (1984). The data tabulated below (Table 3) for 5-year intervals from 1985 are also plotted in Figure 6. These changes must be added to the Cl_z introduced by the projected future emissions.

TABLE 3

YEAR	Cl_z ppb	Cl_z ppb
1985	2.259	0.000
1990	2.304	0.045
1995	2.180	-0.079
2000	2.053	-0.206
2005	1.943	-0.316
2010	1.848	-0.411
2015	1.764	-0.495
2020	1.688	-0.571
2025	1.618	-0.641
2030	1.553	-0.706
2035	1.492	-0.767
2040	1.436	-0.823
2045	1.383	-0.876
2050	1.333	-0.926
2055	1.286	-0.973
2060	1.242	-1.017
2065	1.200	-1.059
2070	1.161	-1.098
2075	1.124	-1.135

The calculated changes in total stratospheric inorganic Cl from equation (3) for three CFC scenarios are compared below (Table 4) to the 1-D model calculated abundance changes (t_o=1985).

TABLE 4

	LOW		MID		HIGH	
YEAR	1-D	Fit	1-D	Fit	1-D	Fit
1985	0.	0.	0.	0.	0.	0.
1995	1.04	0.96	1.05	1.01	1.36	1.54
2000	2.22	2.11	2.41	2.59	4.27	4.96
2015	3.53	3.38	4.33	4.62	11.5	14.1
2025	4.97	4.75	6.78	7.07	32.5	38.0
2035	6.52	6.21	9.71	9.94		
2045	8.22	7.82	13.2	13.3		
2055	10.07	9.57	17.2	17.2		
2065	12.09	11.52	21.7	21.6		
2075	14.34	13.67	26.8	26.8		

The method works reasonably well when the upper limits of calculated lifetimes are used in the low emission case and the lower limits in the middle and high emission cases, in which ozone depletion was substantial. Total inorganic chlorine abundance is somewhat underestimated in the low case and overestimated in the high case, as a result of the dependence of CFC lifetime on the ozone profile.

The CO_2, N_2O, CH_4 and total Br abundances at 10 year intervals from 1985 in the low, mid and high case scenarios are listed in Table 5.

TABLE 5

YEAR	CO_2 (ppm)	N_2O (ppb)	CH_4 (ppm)	Br (ppt)	Br (low case)
1985	344.5	303.1	1.756	0.0	0.0
1995	362.0	310.8	1.939	3.8	1.9
2005	382.8	318.6	2.142	10.9	5.4
2015	407.4	326.7	2.366	22.1	11.1
2025	436.4	334.9	2.614	36.7	18.3
2035	470.3	343.4	2.887	53.8	26.9
2045	509.9	352.1	3.189	72.8	36.4
2055	555.9	361.0	3.523	93.9	46.9
2065	609.1	370.1	3.892	117.7	58.8
2075	670.7	379.5	4.299	144.3	72.2

Applying equations (4) and (5), using the change in total inorganic Cl abundance calculated above with the prescribed changes in CH_4 and N_2O gives the following estimated CFC contributions to total column ozone depletion (Table 6):

TABLE 6

	O3 % (Equation 8)		
YEAR	LOW	MID	HIGH
1985	0.0	0.0	0.0
1995	-0.69	-0.75	-1.13
2005	-1.48	-1.87	-3.71
2015	-2.32	-3.29	-13.4
2025	-3.21	-5.08	-39.8 (@2020)
2035	-4.17	-7.38	
2045	-5.25	-10.5	
2055	-6.43	-14.7	
2065	-7.75	-21.0	
2075	-9.20	-31.5	

The estimated magnitudes of the direct effect of the other trace species are (Table 7):

TABLE 7

YEAR	CO_2	N_2O	CH_4	Br	Br (low)
1985	0.	0.	0.	0.	0.
1995	0.18	-0.18	0.39	-0.15	- 0.08
2005	0.38	-0.36	0.83	-0.44	- 0.22
2015	0.60	-0.54	1.30	-0.88	- 0.44
2025	0.85	-0.74	1.83	-1.47	- 0.73
2035	1.12	-0.93	2.42	-2.15	- 1.08
2045	1.41	-1.13	3.06	-2.91	- 1.46
2055	1.72	-1.34	3.78	-3.76	- 1.38
2065	2.05	-1.55	4.56	-4.71	- 2.35
2075	2.40	-1.76	5.43	-5.77	- 2.38

The calculated time profiles of the total column ozone change are the sums of Table 6 and Table 7 and are given in Table 8.

TABLE 8

Total Column Ozone Change in per cent

	LOW		MID		HIGH	
YEAR	PAR	1-D	PAR	1-D	PAR	1-D
1985	0.0	0.0	0.0	0.0	0.0	0.0
1995	-0.37	-0.34	-0.51	-0.37	- 0.89	-0.66
2005	-0.85	-0.78	-1.46	-1.06	- 3.30	-2.80
2015	-1.40	-1.32	-2.82	-2.32	- 12.9	-10.9
2025	-1.99	-1.95	-4.60	-4.18	- 39.4	-29.5 @2020
2035	-2.64	-2.69	-6.92	-6.70		
2045	-3.36	-3.57	-10.02	-9.99		
2055	-4.15	-4.59	-14.3	-14.4		
2065	-5.04	-5.81	-20.7	-20.8		
2075	-6.02	-7.28	-31.3	-31.8		

The time profiles of total column ozone change calculated from the expressions developed here are also plotted in Figure 7. The parameterization in the mid-range case has an absolute rms deviation over 90 years from the full 1-D model calculation of .41% and the differences are always within about 0.5% in absolute calculated ozone column depletion relative to 1985. Differences between the parameterization and the full 1-D model in the other cases are generally less than 2% except at very large ozone depletions. Figure 8 shows the comparison of the alternative implementation of equation (8a) and Table 1a to the 1-D model results. Agreement between the parameterization (dashed line) and 1-D model (solid line) is about the same. It is not possible, however, to assume that differences over the whole surface of ozone column change as a function of source species scenarios will remain within these limits. We want to reiterate that these expressions simply provide a means of estimating the 1-D model behavior to allow preliminary investigations of possible regulatory efforts. We do not claim that the column ozone changes calculated from these expressions are accurate or reliable indications of what could actually arise in the atmosphere over the next 90 years.

4. CONCLUSIONS

We have shown here that it is possible to predict the 1-D model-derived total inorganic stratospheric Cl abundance that would arise from a given CFC emission projection in the LLNL 1-D model. In the absence of changes in other species and for total chlorine increases less than about 20 ppb, it is also fairly straightforward to parameterize the resulting ozone column depletions calculated in the 1-D model. Properly treating the effects of coupling substantial changes in methane with major CFC increases or accounting for the possibility of greater or lesser NO_z abundance is more difficult.

The parameterization of the ozone column sensitivity of a 1-D model presented here can be used to estimate within about 2% in units of total column ozone change from t_0=1985 the values that would be calculated by the updated CW 1-D model. But continuing improvement in our understanding and numerical representations of the troposphere and stratosphere may well be expected quickly to supersede the quantitative details of this study.

BIBLIOGRAPHY

Connell, P.S. and D.J. Wuebbles, "Ozone perturbations in the LLNL one-dimensional model - Calculated effects of projected trends in CFC's, CH_4, CO_2, N_2O and Halons over 90 years," UCRL-95548, 1986.

Cunnold, D.M., R.G. Prinn, R.A. Rasmussen, P.G. Simmonds, F.N. Alyea, C.A. Cardelino, A.J. Crawford, P.J. Fraser and R.D. Rosen, "Atmospheric lifetime and annual release estimates for $CFCl_3$ and CF_2Cl_2 from 5 years of ALE data," J. Geophys. Res., 91, 10797–10817, 1986.

EPA, "An Assessment of the Risks of Stratospheric Modification," J.S. Hoffman, ed., U.S. EPA, October, 1986.

JPL (Jet Propulsion Laboratory) Publication 83–62, Chemical Kinetics and Photochemical Data for Use in Stratospheric Modeling, W.B. DeMore, ed., Pasadena, California, 1983.

JPL (Jet Propulsion Laboratory) Publication 85–37, Chemical Kinetics and Photochemical Data for Use in Stratospheric Modeling, W.B. DeMore, ed., Pasadena, California, 1985.

Quinn, T.H., K.A. Wolf, W.E. Mooz, J.K. Hammitt, T.W. Chesnutt and S. Sarma, "Projected use, emissions, and banks of potential ozone-depleting substances, RAND Note N-2282-EPA, 1986.

Prather, M.J., M.B. McElroy and S.C. Wofsy, "Reductions in ozone at high concentrations of stratospheric halogens," Nature, 312, 227–231, 1984.

WMO (World Meteorological Organization), "Atmospheric Ozone 1985: Assessment of Our Understanding of the Processes Controlling its Present Distribution and Change", Global Ozone Research and Monitoring Project — Report No. 16, 1986.

Wuebbles, D.J., "Chlorocarbon emission scenarios: Potential impact on stratospheric ozone," J. Geophys. Res., 88, 1433–1443, 1983.

Wuebbles, D.J., M.C. MacCracken and F.M. Luther, "A proposed reference set of scenarios for radiatively active atmospheric constituents," U.S. Dept. of Energy Carbon Dioxide Research Division Technical Report DOE/NBB- 0066, 1984.

FIGURE CAPTIONS

1. Vertical profiles of ozone abundance change at steady state for a series of 1-D model runs with fixed constant emissions of individual CFC compounds. Total column ozone change normalized to −7.5%.
2. Vertical profiles of ozone abundance change at steady state for a series of 1-D model runs with fixed constant emissions of individual CFC compounds. Total column ozone change normalized to −2.0%.
3. Vertical profiles of ozone abundance change at steady state for a series of 1-D model runs with fixed constant emissions of individual CFC compounds. Profiles normalized to equal increase in startospheric inorganic Cl abundance at 35 km.
4. Total column ozone change in per cent as a function of change in stratospheric inorganic chlorine mixing ratio for the CFC-only reference scenario. Solid line is updated CW (1986) model, dashed line is parameterization fit.
5. Total column ozone change in per cent as a function of change in stratospheric inorganic chlorine mixing ratio for combined CFC/CH_4 and CFC/N_2O scenarios. Solid lines are updated CW (1986) model, dashed line are parameterization fit.
6. Contribution of historical (pre-1985) CFC emissions to future stratospheric inorganic Cl mole fraction.
7. Total column ozone change in per cent as a function of time. Solid lines are time-dependent 1-D multiple scenario calculations (CFC emissions as in Figure 4, N_2O @0.25%/year, CH_4 @0.5%/year, CO_2 mid-range scenario from Wuebbles et al. (1984)). Long dash lines are parameterization fit using 1-D calculated changes in stratospheric inorganic Cl, short dash lines are parameterization fit using stratospheric Cl estimated from CFC emissions.
8. Total column ozone changes in per cent as a function of time for alternative formulation (equation 8a and Table 1a).

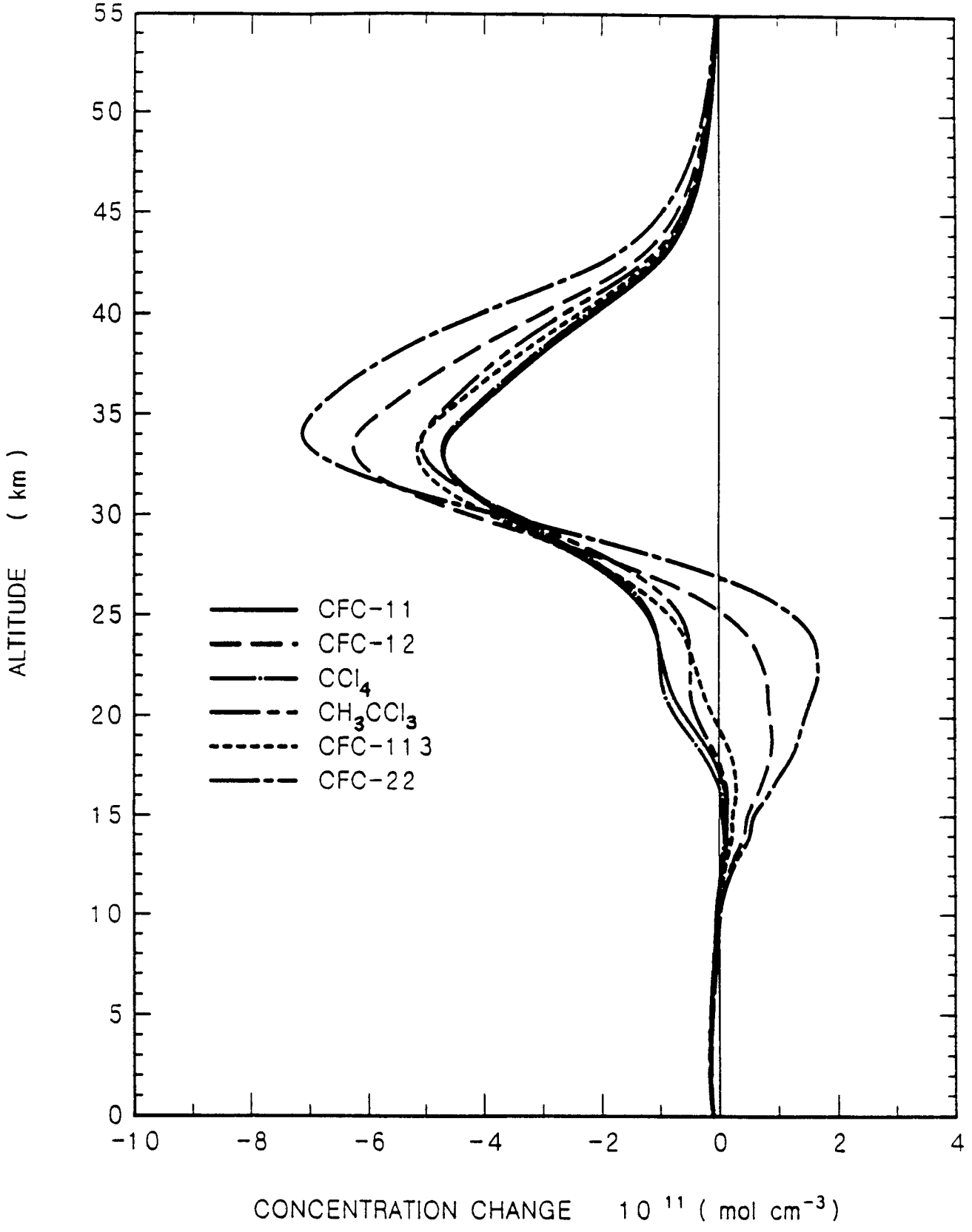
55
50
45
40
35
30
25
20
15
10
5
0
ALTITUDE (km)
-10
-8
-6
-4
-2
0
2
4
CONCENTRATION CHANGE 10 11 (mol cm-3)
CFC-11
CFC-12
CCl4
CH3CCl3
CFC-113
CFC-22

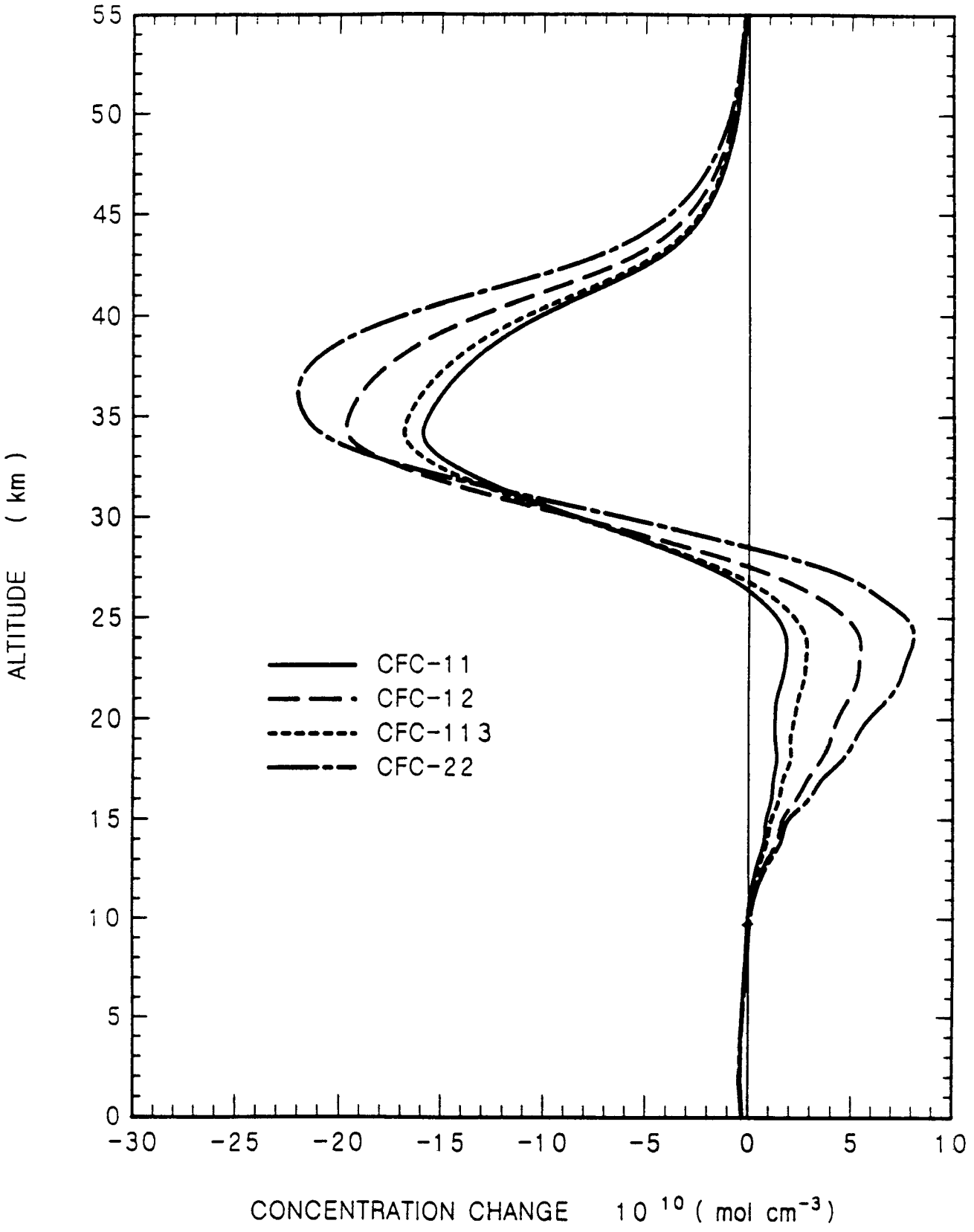
55
50
45
40
35
30
25
20
15
10
5
0
ALTITUDE (km)
CFC-11
CFC-12
CFC-113
CFC-22
-30
-25
-20
-15
-10
-5
0
5
10
CONCENTRATION CHANGE 10 10 (mol cm-3)

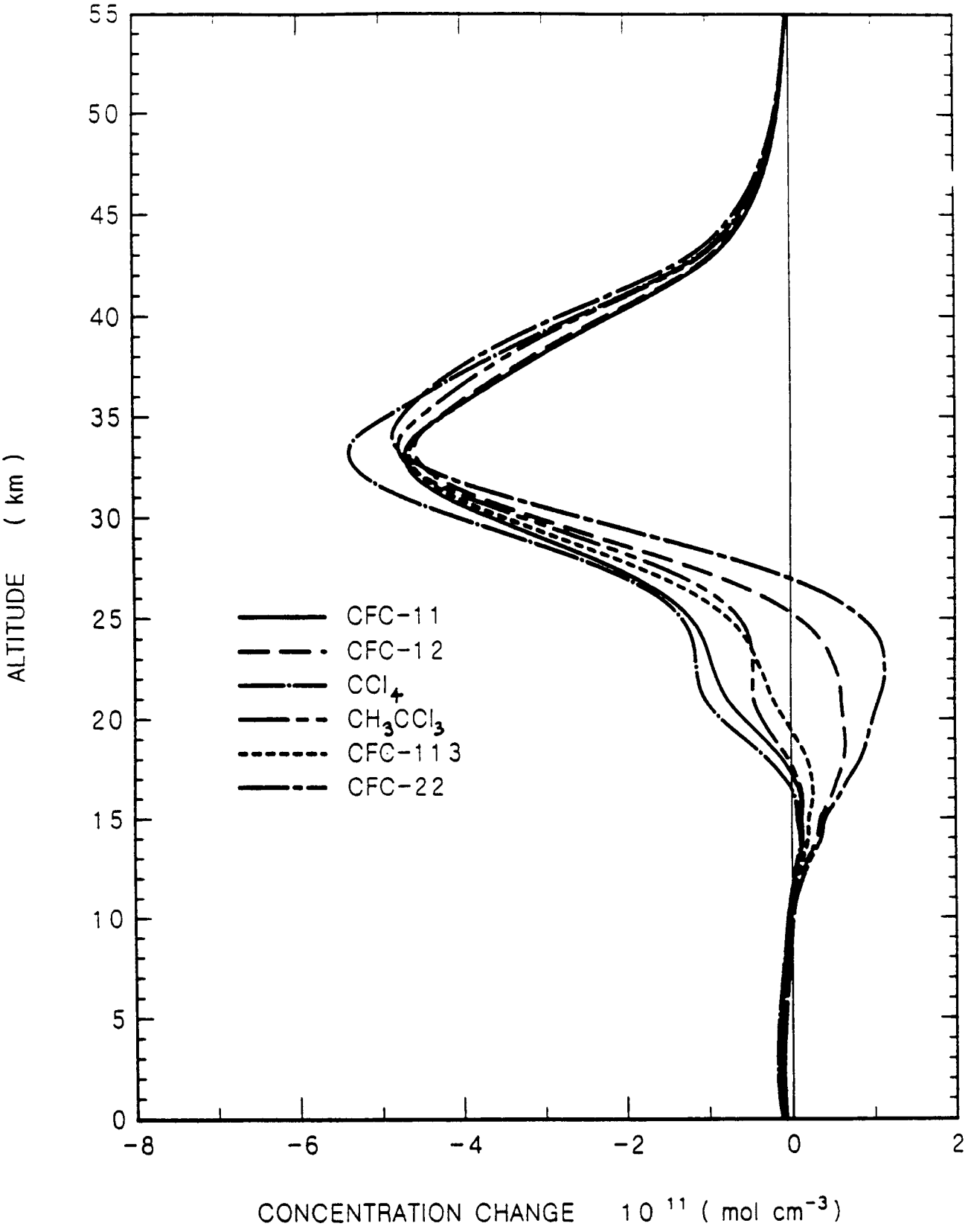
ALTITUDE (km)
55
50
45
40
35
30
25
20
15
10
5
0
-8
-6
-4
-2
0
2
CFC-11
CFC-12
CCl4
CH3CCl3
CFC-113
CFC-22
CONCENTRATION CHANGE 10 11 (mol cm-3)

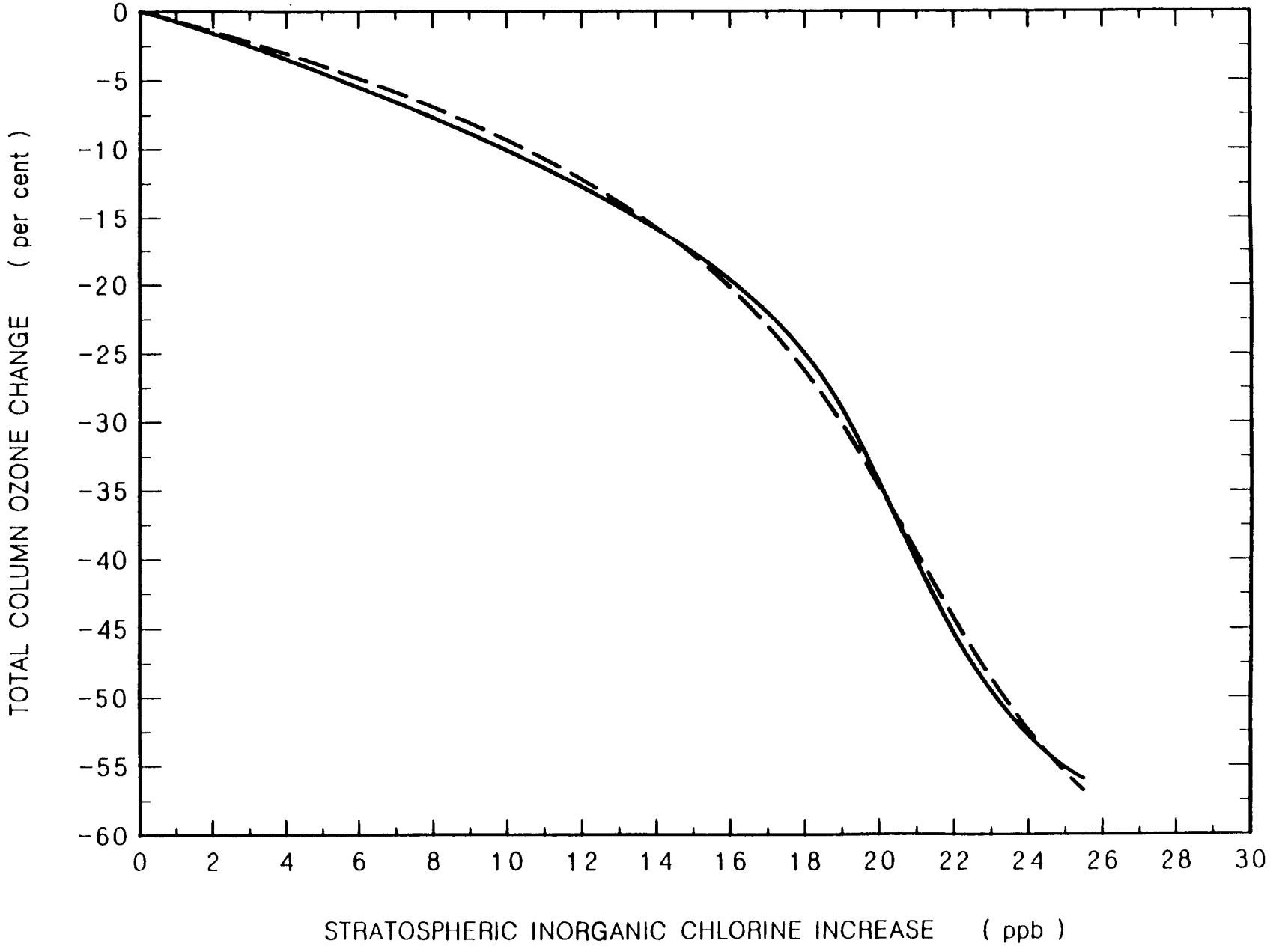
TOTAL COLUMN OZONE CHANGE (per cent)
0
-5
-10
-15
-20
-25
-30
-35
-40
-45
-50
-55
-60
0
2
4
6
8
10
12
14
16
18
20
22
24
26
28
30
STRATOSPHERIC INORGANIC CHLORINE INCREASE (ppb)

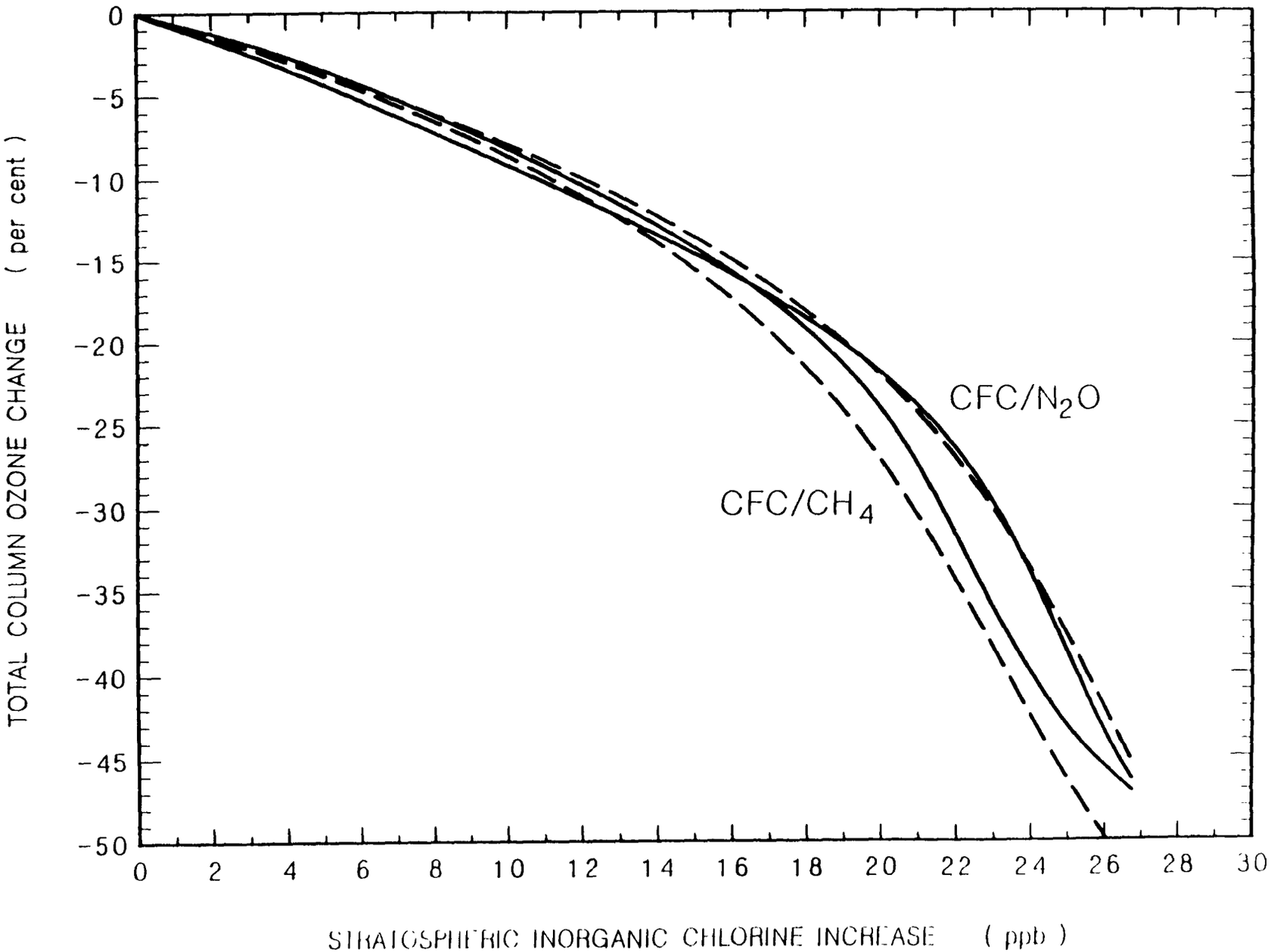
TOTAL COLUMN OZONE CHANGE (per cent)
0
-5
-10
-15
-20
-25
-30
-35
-40
-45
-50
0
2
4
6
8
10
12
14
16
18
20
22
24
26
28
30
CFC/N2O
CFC/CH4
STRATOSPHERIC INORGANIC CHLORINE INCREASE (ppb)

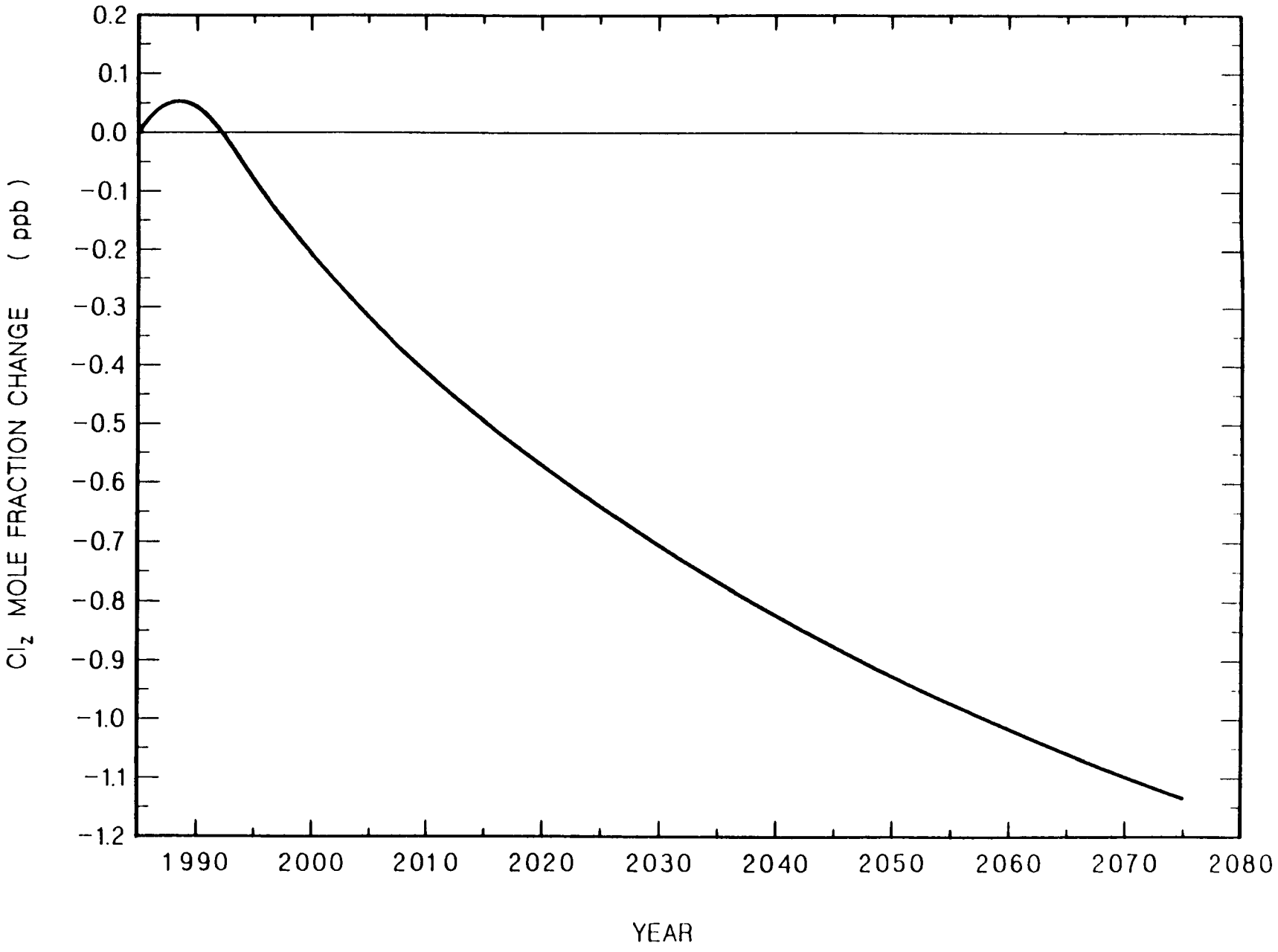
0.2
0.1
0.0
−0.1
−0.2
−0.3
−0.4
−0.5
−0.6
−0.7
−0.8
−0.9
−1.0
−1.1
−1.2
Cl_z MOLE FRACTION CHANGE (ppb)
1990
2000
2010
2020
2030
2040
2050
2060
2070
2080
YEAR

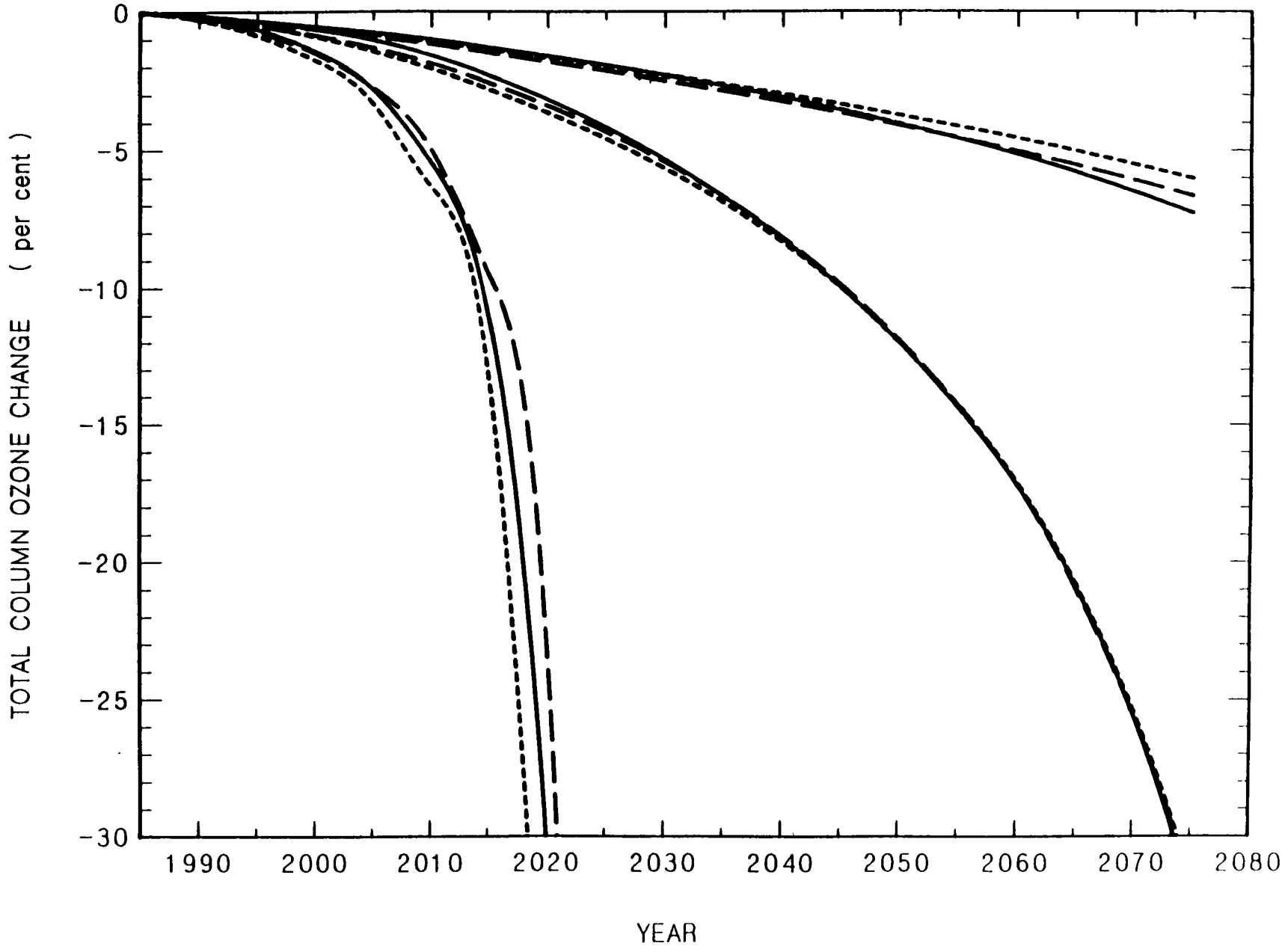
0
-5
-10
-15
-20
-25
-30
TOTAL COLUMN OZONE CHANGE (per cent)
1990
2000
2010
2020
2030
2040
2050
2060
2070
2080
YEAR

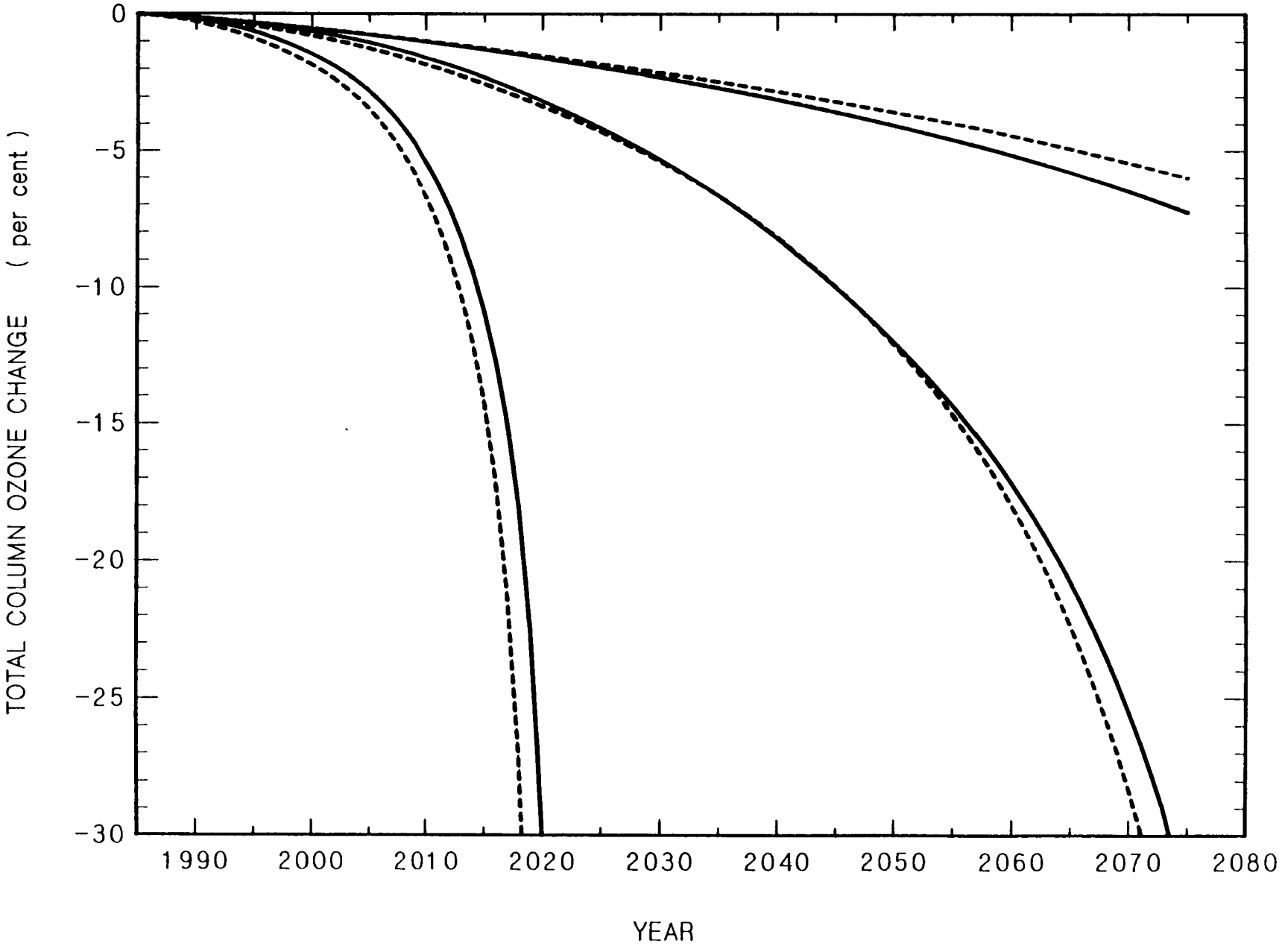
0
-5
-10
-15
-20
-25
-30
TOTAL COLUMN OZONE CHANGE (per cent)
1990
2000
2010
2020
2030
2040
2050
2060
2070
2080
YEAR

GLOBAL MODELING OF THE ULTRAVIOLET SOLAR FLUX INCIDENT ON THE BIOSPHERE

George N. Serafino

Applied Research Corporation

8201 Corporate Drive

Landover, Maryland 20785

and

John E. Frederick

Department of the Geophysical Sciences

The University of Chicago

5734 South Ellis Avenue

Chicago, Illinois 60637

Abstract

This report summarizes an algorithm designed to estimate the ultraviolet solar flux that reaches the Earth's surface at any location on the globe and time of year. Inputs consist of global ozone abundances, terrain height, the distribution of cloudcover, and the albedos of clouds and the underlying surface. Intended users of the algorithm include atmospheric scientists, the photobiology community, and environmental policymakers.

I. Introduction

The interaction of solar radiation with the Earth and its atmosphere is closely coupled to the planet's ability to support life. Ultraviolet solar radiation likely initiated the chemical processes which led to formation of the first organic molecules on the primitive Earth (eg. Ponnamperuma, 1981), while the development of a substantial ozone layer created a surface environment where complex self-replicating molecules could evolve. The decreases shown by both the absorption cross section of ozone and the DNA action spectrum at wavelengths between 280 and 320 nm provide persuasive evidence of the coupling that has existed between the geophysical and biological realms which ultimately provided for the evolution of higher life forms.

Issues of more immediate practical concern center on the observation that the incidence of various skin cancers shows latitudinal variations. This appears related to the biologically active ultraviolet flux reaching the surface of the Earth. While this fact alone is of great significance, couplings of a more subtle nature apparently exist between the radiation environment and biological systems. A prime example is the work by DeFabo and Noonan (1983) which indicates a link between ultraviolet radiation dosage and suppression of the immune system in laboratory mice. Photobiologists have adopted the term UV-A to refer to radiation over the wavelength range 320-400 nm, while UV-B

denotes the region 280-320 nm. Absorption by ozone and atmospheric scattering reduce the solar UV-B flux at the surface of the Earth to a small fraction of what would otherwise exist. The UV-A, being outside the range of strong absorption by ozone, experiences much less attenuation.

This report describes the conceptual formulation of an algorithm designed to predict the UV-B and UV-A radiation fluxes as functions of wavelength at any point on the Earth for any time of year. Papers which summarize the mathematical methods used in the code already exist in the published literature. We make reference to these rather than presenting details here. The algorithm utilizes global scale ozone measurements obtained by the Solar Backscattered Ultraviolet (SBUV) Spectral Radiometer carried on the Nimbus 7 satellite. We combine this data set with additional information on cloudcover and cloud transmission obtained from independent sources. While the development of the algorithm is an exercise in radiative transfer and atmospheric science, we intend the final product to be a tool for use by the photobiology community and environmental policymakers.

II. The Radiative Transfer Formulation

We divide the atmosphere into two parts, (1) the clear atmosphere above any cloudtops and (2) the cloud layer, the atmosphere beneath the cloud (the "sub-cloud layer"), and the ground. In the absence of clouds only case 1 is required. When clouds are present we merge a model of this portion of the atmosphere onto the base of the clear sky calculation. We assume that the lower boundary of the clear atmosphere, being cloudtops or ground, is a Lambertian surface of known albedo. A radiative transfer calculation which includes all orders of multiple scattering and absorption by ozone then gives the direct and diffuse components of solar flux incident on the cloudtops or, for clear skies, on the ground.

The downward diffuse flux, $F^{\downarrow}(\lambda,\theta,\tau)$, for a wavelength λ, solar zenith angle θ, and optical depth τ, can be expressed as the sum of an atmospheric scattering component $F_a^{\downarrow}(\lambda,\theta,\tau)$ and a contribution arising from downward scattering of radiation that has already been reflected from the lower boundary (Dave and Furukawa, 1966).

$$F^{\downarrow}(\lambda,\theta,\tau) = F_a^{\downarrow}(\lambda,\theta,\tau) + Q(\lambda,R,\tau^*)F_g^{\downarrow}(\lambda,\theta,\tau) \qquad (1)$$

where:

$$Q(\lambda,R,\tau^*) = R \,/\, [1-RS(\lambda,\tau^*)] \qquad (2)$$

Here τ^* is the atmospheric optical depth above the reflecting surface (ground or cloudtop) of albedo R, $S(\lambda, \tau^*)$ represents the backscattering power of the atmosphere, and $F_g^{\downarrow}(\lambda, \theta, \tau)$ measures the contribution from flux that has already reflected from the lower boundary and is then scattered back into the lower hemisphere. The advantage of the formulation in equations 1 and 2 is that the quantities $F_a^{\downarrow}$, $F_g^{\downarrow}$, and S can be computed without knowledge of the surface albedo. In practice, we calculate these terms using the Herman and Browning (1965) clear sky, multiple Rayleigh scattering model.

For clear sky conditions the formulation summarized above produces the UV-B and UV-A flux at the ground as a function of wavelength, solar zenith angle (local time), and ozone amount. Under cloudy sky conditions, however, we must define the transmission and reflectivity of the cloud-subcloud-ground layer. For this we use a two stream radiative transfer model coupled with the "adding method" for a multi-layer atmosphere developed by Lacis and Hansen (1974). This approach divides the atmosphere into a series of homogeneous layers where each layer has a known reflectivity and transmission. Clouds occupy the uppermost layers, while the bottom layer is the ground with a transmission of zero. The composite reflectivity and transmission of the multilayer system is determined by combining the reflectivities and transmissions of the individual layers with proper account taken of multiple

reflections of upward and downward directed fluxes. Lacis and Hansen (1974) have presented quantitative details of the technique. The model adopts fractional cloudcover as a function of latitude from Hughes (1984). We assume a mixture of thick low clouds, with an optical depth for scattering of 30, and middle level clouds of optical depth 15 (Stephens, 1978). We assume cloud drops to be non-absorbing in the UV-B and UV-A. However, absorption of radiation still occurs in the clouds owing to the tropospheric ozone amount included in the model. The calculations assume that 85 percent of the downward radiation incident at the cloudtops is scattered into the lower hemisphere. The derived transmission of the cloud-subcloud system multiplied by the total (direct plus diffuse) flux incident on the cloudtops from equation 1 gives the flux at the ground. Note that we assume all radiation transmitted through the cloud to be isotropic over the lower hemisphere, consistent with a large optical depth for scattering.

The reflectivity and transmission of atmospheric layers beneath the cloud deck are defined by expressions for a two stream model as given by Coakley and Chylek (1975) and Joseph et al. (1976). Each layer has a known optical depth and an ozone amount based on climatology supplied with the SBUV data set. To obtain the flux at the ground for a climatological fractional cloudcover, we simply combine values derived separately for clear and cloudy skies using

the weights 1-f and f respectively, where f is the fractional cloudcover at the latitude of interest.

In principle one could compute the UV-B and UV-A fluxes at the ground using a complete radiative transfer calculation for any combination of wavelength, ozone abundance, cloudcover, solar zenith angle, and ground reflectivity. In practice this is not necessary. Instead we generated three sets of flux tables, one with the base of the clear atmosphere at 1000 mb, another at 700 mb, and the last with the base at 400 mb. Each table contains the radiative transfer quantities of equations 1 and 2 for 23 wavelength bands which span the wavelength range 290 to 400 nm, 9 total column ozone amounts, and 13 solar zenith angles. Surface reflectivities corresponding to the ground or cloudtops need not enter the tables in view of the form of equation 1. Each table allows interpolation to obtain surface fluxes for any ozone value and local time, while a combination of all three tables provides fluxes for varying terrain heights and cloudcover conditions. This flexibility allows the algorithm to predict the ultraviolet radiation environment at any location on the globe for any time of year by interpolation based on precomputed radiation tables. Surface fluxes may refer to specific local times or to averages over the daylight period at any location and date.

III. The Input Data Sets

The SBUV instrument provides the total column ozone and vertical ozone profiles needed to evaluate terms in the radiative transfer calculations. We use SBUV column ozone amounts averaged over one month time intervals and over all longitudes in 10 degree wide latitude bands. We associate these means with the center of each month and latitude bin. Interpolation in latitude and time then provides the ozone amount for a specific location and day of the year. Figure 1 illustrates the behavior of column ozone as a function of latitude and month derived from SBUV. We note that a very recent revision in the SBUV data set uses improved absorption cross sections and yields values approximately 6% greater than those shown in Figure 1. The current version of the global radiation algorithm uses the updated ozone results. The extraterrestrial solar irradiance, ozone absorption cross sections, and Rayleigh scattering cross sections used in the calculations are from Chapter 7 of WMO/NASA (1986).

IV. Algorithm Operation and Sample Results

The algorithm allows the user a high degree of flexibility in selecting parameters for a given calculation. Mandatory inputs supplied by the user are: (1) latitude and longitude, (2) day number of the year, 1 through 365, and (3) local time. As an alternative to local time the user can choose to compute mean fluxes over the daylight portion of a 24 hour period. Given these inputs the algorithm chooses a zonal mean ozone value based on the SBUV data set, a terrain elevation and ground albedo from Kalnay et al. (1983), and zonal mean fractional cloudcover from Hughes (1984). The ultraviolet flux at the ground as a function of wavelength is then obtained by interpolation from the precomputed tables for clear and cloudcovered conditions. The user can also circumvent the data sets built into the algorithm and enter a total column ozone value, terrain elevation, ground albedo, and fractional cloudcover suited to any location of interest.

As an illustration of the algorithm's capability, Figure 2 presents the latitudinal and monthly distribution of UV-B radiation at the surface of the Earth for clear sky conditions. Contours in the figure are in watts per square meter and are based on the ozone values of Figure 1. All values refer to a local time of 10:00 A.M. and represent the sum of all radiation at wavelengths between 290 and 320 nm. In practice, radiation at wavelengths less than 290-295 nm makes a negligible contribution to the total UV-B. The

largest fluxes, 4 watts per square meter, reach the ground in the tropics because the sun is most nearly overhead here, and the atmospheric ozone amounts are relatively small. The major feature of Figure 2 is the large variation in radiation flux with latitude, especially during the winter season. In the Northern Hemisphere for December and January the flux decreases by a factor of 10 between the equator and 50 degrees latitude. During summer the latitudinal gradients are much less pronounced than in winter, and one must move from the tropics to 60 degrees to experience a factor of two decrease in flux at the ground. There is very little change in the 10:00 A.M. fluxes in the tropics over the course of a year. At middle latitudes, however, the seasonal cycle can range between a factor of two and ten depending on location.

A calculation analogous to that in Figure 2 could be done for the UV-A spectral region. Although the contours would be similar in shape, the gradients would be much less pronounced because of the greatly reduced absorption by ozone at wavelengths longward of 320 nm. Figure 3 illustrates this behavior by giving contours of the ratio of UV-B to UV-A fluxes as a function of latitude and month at a local time of 10:00 A.M. Clearly, the UV-B flux is much smaller than the UV-A, with the ratio ranging from 2 to 7.5%. The most significant information in Figure 3 is the differing latitudinal and seasonal gradients shown by the UV-B and UV-A. As one moves from the tropics to 60 degrees

latitude in winter, the UV-B flux decreases more rapidly than the UV-A by a factor of three to four. In summer the relative variation is much less than a factor of two.

The examples presented above illustrate latitudinal and seasonal variations. Future updates of the algorithm for use in truly global studies should include longitudinal variations in both fractional cloudcover and ozone. For many applications, however, the focus is on the radiation environment at a specific location as well as on changes in dose rates with parameters such as the ozone amount and fractional cloudcover. A separate report by H. Pitcher and J. Scotto now in preparation will describe such studies, including the comparison of model predictions with ground-based measurements from Robertson-Berger meters.

References

Coakley, J. A., Jr., and P. Chylek, 1975: The two-stream approximation in radiative transfer: Including the angle of incident radiation, J. Atmos. Sci., 32, 409-418.

Dave, J. V., and P. M. Furukawa, 1966: Scattered Radiation in the Ozone Absorption Bands at Selected Levels of a Terrestrial Rayleigh Atmosphere, Meteor. Monogr., Vol. 7, No. 29.

DeFabo, E. C., and F. M. Noonan, 1983: Mechanism of immune suppression by ultraviolet radiation in vivo I. Evidence for the existence of a unique photoreceptor in skin and its role in photoimmunnology, J. Exp. Med., 157, 84-98.

Herman, B. M., and S. R. Browning, 1965: A numerical solution to the equation of radiative transfer, J. Atmos. Sci., 22, 559-566.

Hughes, N. A., 1984: Global cloud climatologies: A historical review, J. Climate Appl. Meteor., 23, 724-751.

Joseph, J. H., W. J. Wiscombe, and J. A. Weinman, 1976: The delta-Eddington approximation for radiative flux transfer, J. Atmos. Sci., 33, 175-204.

Kalnay, E., et al., 1983: Documentation of the GLAS Fourth Order GCM. Volume I: Model Documentation, internal report, Laboratory for Atmospheric Sciences, NASA/Goddard Space Flight Center, Greenbelt, MD. 20771.

Lacis, A. A., and J. E. Hansen, 1974: A parameterization for the absorption of solar radiation in the earth's atmosphere, J. Atmos. Sci., 31, 118-133.

Ponnamperuma, C., 1981: The quickening of life, in Fire of Life, Smithsonian Exposition Books, W. W. Norton and Company, New York, 118-125.

Stephens, G. L., 1978: Radiative properties of extended water clouds: Part II, J. Atmos. Sci., 35, 2111-2132.

WMO/NASA, 1986: Atmospheric Ozone 1985, World Meteorological Organization, Geneva, Global Ozone Research and Monitoring Project, Report Number 16.

List of Figures

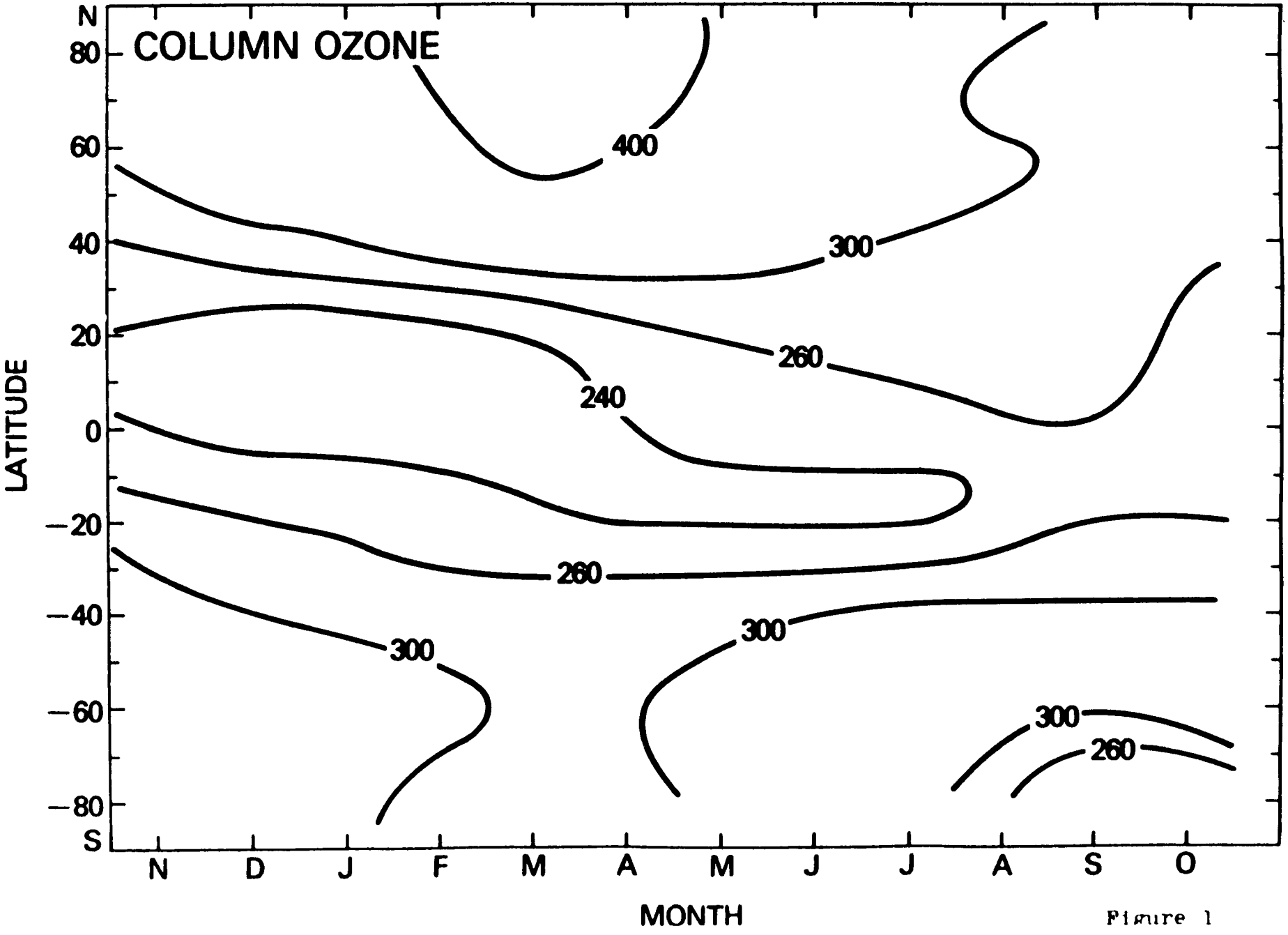
COLUMN OZONE
N
80
60
40
20
0
−20
−40
−60
−80
S
LATITUDE
400
300
260
240
260
300
300
300
260
N
D
J
F
M
A
M
J
J
A
S
O
MONTH

Figure 1

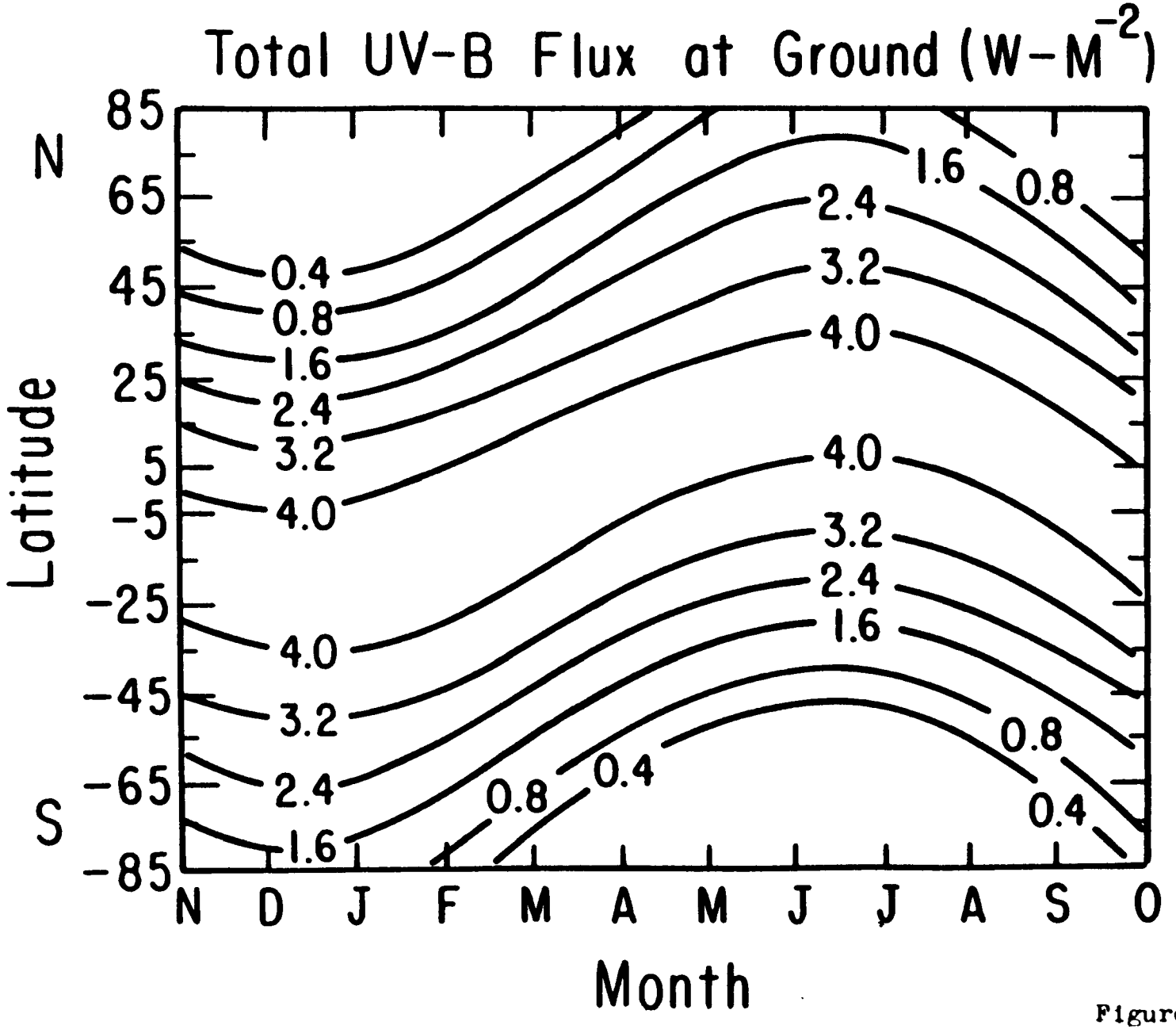
Total UV-B Flux at Ground (W-M^{-2})
N
S
Latitude
85
65
45
25
5
-5
-25
-45
-65
-85
0.4
0.8
1.6
2.4
3.2
4.0
4.0
3.2
2.4
1.6
0.8
0.4
4.0
3.2
2.4
1.6
0.8
0.4
N D J F M A M J J A S O
Month

Figure 2

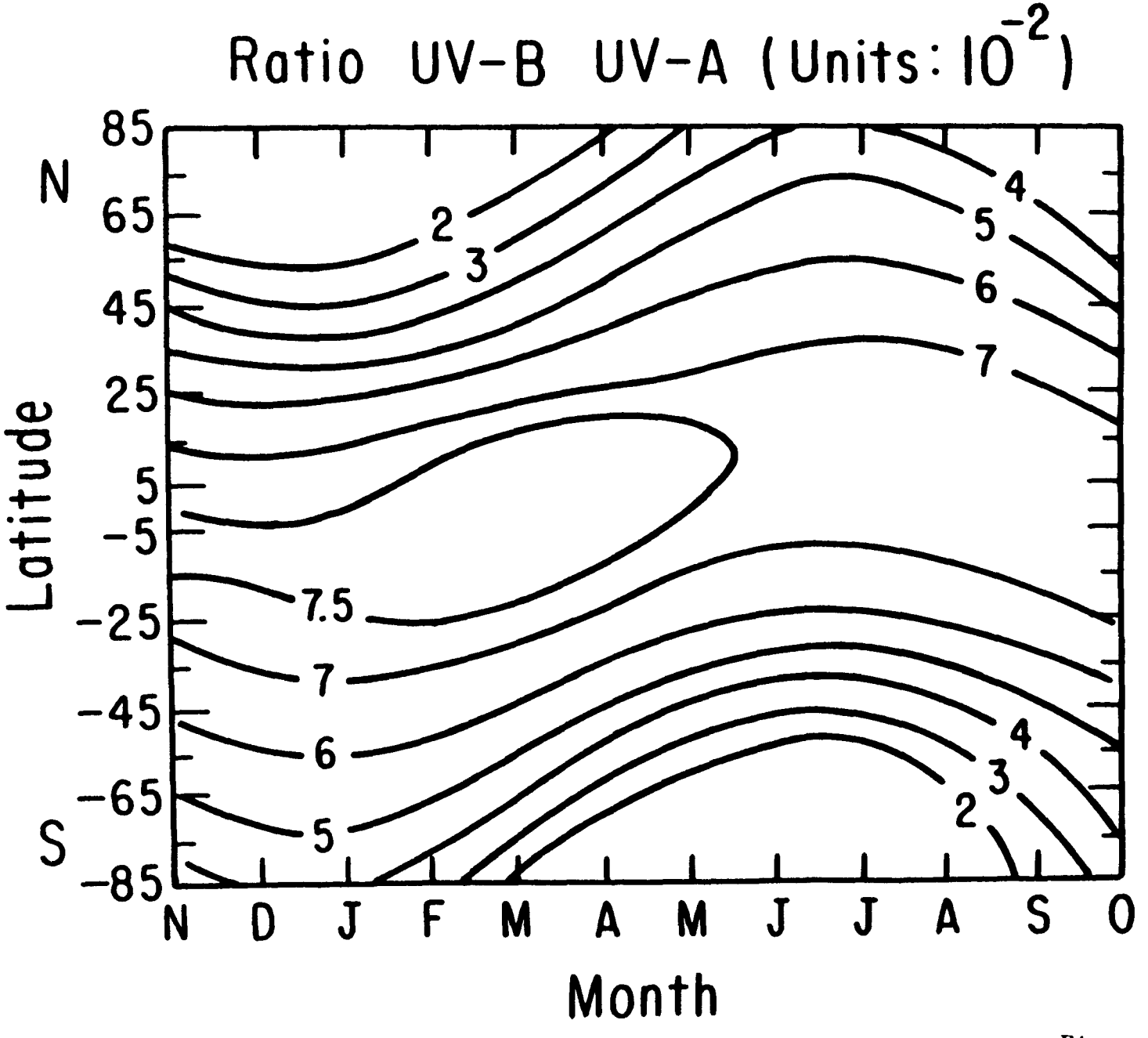
Ratio UV-B UV-A (Units: 10^{-2})
Latitude
N
S
85
65
45
25
5
-5
-25
-45
-65
-85
2
3
4
5
6
7
7.5
7
6
5
4
3
2
N D J F M A M J J A S O
Month

Figure 3